THE
PHYSICAL REVIEW
A Journal of Experimental and Theoretical Physics Established by E. L. Nichols in 1893
VOL. 59, NO. 11 JUNE 1, 1941 SECOND SERIES

The Rest Mass of the Mesotron

PAUL WEISZ
Bartol Research Foundation of the Franklin Institute, Swarthmore, Pennsylvania
(Received April 2, 1941)

The experimentally found values for the lifetime at rest of the cosmic-ray mesotron, from recent reliable investigations by various authors, are directly compared after recalculating them on the basis of the same assumed rest mass. The thus corrected values for the lifetime still disagree, but are shown to be a function of the average path length of the radiation employed in each experiment. When, instead of the existence of only one possible value for the rest mass for which we have no experimental evidence, a distribution in rest masses is assumed, the described phenomenon can be accounted for regardless of what form the mass distribution may have. The same assumption leads to explanations of other experimental findings, and predicts an actual lifetime τ_0 much smaller than any measured value, strongly indicating that upon correcting the measured results on the basis of the existence of a mass distribution, a value of the order of Yukawa's original prediction $\tau_0=5\times10^{-7}$ sec. is obtained.

IT must be admitted that a few cloud-chamber photographs of tracks of slowest observable mesotrons in a strong magnetic field constitute the whole basis of our present knowledge of the rest mass of the mesotron. These records have yielded estimates of the rest mass of from about 100 (Auger[1]) to as high as 540 (Williams and Pickup[2]) times the electron rest mass, values from 150 to 200 times m_e (mass of electron) having been observed most frequently. Thus, one may, at present, merely state that a value of, say, $180m_e$ is *most probable*, and even here we should allow for an error of, say, $\pm 20m_e$.

On the other hand, the determination of the time of decay τ_0 of the mesotron has been subject to numerous and comparatively accurate experimental investigations, although any determination thus made is at least as inaccurate as our knowledge of the rest mass. For in general we have, as regards loss by my mean life considerations alone,

$$-(1/\Delta n)(d\Delta n/dx)=(Mm_e/\tau_0 p), \qquad (1)$$

where Δn is the number of particles per square centimeter per second per unit solid angle falling within a small momentum range dp in the neighborhood of the momentum p appropriate to a group of particles, where x is the path traversed, τ_0 is the lifetime at rest, and M is the ratio of the rest mass of the particle to the electron's rest mass (m_e).

The momentum p is approximately determined by the energy of the particle, so that for a method of measurement which confines itself to a group of particles which, at the top of the atmosphere, have energy lying between E_0, and E_0+dE_0, it is obvious that the value obtained for τ_0 is intimately bound up with the value assumed for M.

[1] P. Auger, Comptes rendus **206**, 346 (1938).
[2] E. J. Williams and E. Pickup, Nature **141**, 684 (1938).

In considering formula (1) as applied to the aforesaid group of particles defined by E_0 and E_0+dE_0, we must suppose that a procedure the equivalent of the following is adopted: For any value of x representative of a distance measured in the atmosphere, the beam of cosmic rays to be measured is suitably defined by a telescopic arrangement and measurements are made below a thickness of lead which, in conjunction with the air path length x, permits passage only of rays of initial energy greater than E_0. Each measurement of this kind is then accompanied by another measurement with an additional thickness of lead such that the total path length in air and lead permits observation of only those rays which initially had energy greater than E_0+dE_0. The difference between corresponding measurements gives the number of rays which initially had an energy between E_0 and E_0+dE_0 and which have survived death by mean life considerations. If a new value of x be now chosen, either by inclining the telescopic system or by altering the altitude, we must suppose that the corresponding lead thicknesses are readjusted to maintain the same equivalent mass absorption thicknesses for combined lead and air path as before.

In work of this kind it has been customary for the most part to assume that the energies concerned are sufficiently high to permit the assumption

$$p=E/c.$$

It has further been customary to neglect the variation of p and so of E along the air path insofar as (1) is concerned, so that with these assumptions, (1) integrates to the form

$$\Delta n_x=\Delta n_0 e^{-kxM}, \tag{2}$$

where
$$k=cm_e/\tau_0 E_0. \tag{3}$$

Thus

$$\Delta n_1/\Delta n_2=\exp[-kM(x_1-x_2)]. \tag{4}$$

From the known data for n_1/n_2, E_0, x_2 and x_1 and an assumption regarding M, τ_0 is determined.

A number of investigators have employed this method generally, although under differing conditions, and with differing apparatus, and these more recent determinations leave no doubt regarding their experimental accuracy. Despite this fact, the disagreement among these individual results exceeds the experimental accuracy.

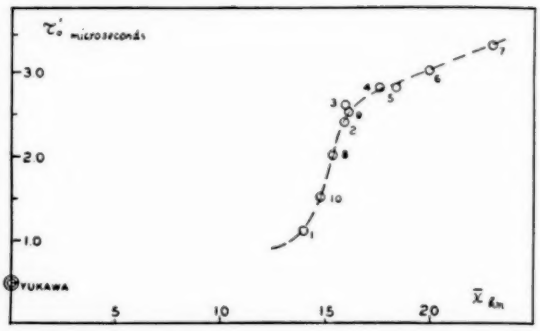

FIG. 1. Relation between measured "pseudo" lifetime at rest for the cosmic-ray mesotrons, by various authors, and the average path length $\bar{x}$ of the radiation in each experiment. (1) P. Auger (two altitudes and angles), see B. Rossi, Rev. Mod. Phys. **11**, 296 (1939). (2) S. de Benedetti (two angles), see B. Rossi, reference 1. (3) W. Kolhoerster and I. Matthes (atmospheric expansion), Physik. Zeits. **40**, 142 (1939). This is the only measurement using the barometric expansion of the atmosphere known to the author to be independent of a knowledge of the pure absorption coefficient, and of any influence of the electron or other component which is not subject to disintegration. The average momentum should be taken for sea level without absorber. (4) Bernardini and Bocciarelli (two angles), see reference 1. (5) H. V. Neher and H. G. Stever (two altitudes, with ionization chambers), Phys. Rev. **58**, 766 (1940). (6) M. A. Pomerantz (two angles), Phys. Rev. **57**, 3 (1940). (7) T. H. Johnson and M. A. Pomerantz (two angles), Phys. Rev. **55**, 104 (1939) see also B. Rossi, reference 1. (8) B. Rossi, N. Hilberry, and J. B. Hoag (two angles and altitudes), Phys. Rev. **57**, 461 (1940). (9) and (10) N. N. Das Gupta and P. C. Bhattacharya, Proc. Nat. Inst. Sci. India **6**, 713 (1940).

On the basis of early and rather inaccurate measurements of the angular distribution of the hard component, it was pointed out[3] that discrepancies arising relative to calculations on the basis of the disintegration theory may be due to our limited knowledge of the mesotron rest mass.

The above-mentioned determinations of various authors were used in a direct comparison by reconsidering the experimental results in each case on the basis of the same assumptions and, in particular, on the assumption of the same rest mass of $160m_e$, used by Rossi in connection with some of these measurements.[4] Upon careful consideration, the values thus obtained for the lifetime are not scattered "at random" but, as is shown in Fig. 1, show a marked relationship to the average path length $\bar{x}$, which was determined from the information of the various investigators on their experimental conditions.

[3] P. Weisz, Phys. Rev. **55**, 1266 (1939).
[4] B. Rossi, Rev. Mod. Phys. **11**, 149 (1939).

In addition to calling attention to the foregoing matters and to elucidating the dependence of *measured* mean life upon average path length in the experiments, the purpose of this paper is to show that the apparent paradox involved in this dependence may be resolved by assuming that for each energy there is a distribution of rest mass among the mesotrons.

Let us suppose that μ is the rest mass of a particle, m_e is the electronic mass, and M the ratio defined by

$$M=\mu/m_e.$$

Let us further suppose that, at the top of the atmosphere, there is, for the energy range E_0 to E_0+dE_0, a spectral distribution formula of the type

$$\delta(\Delta n_0)=\Delta n_0\varphi(M)dM, \tag{5}$$

where Δn_0 corresponds to the range dE_0 at the top of the atmosphere, and the form of $\varphi(M)$ may depend upon the energy, although, for reasons to be given presently, it appears that φ is the same for all energies, If we assume the lowest mass to be the electron mass, $\varphi(M)$, of course, satisfies the condition

$$\int_1^\infty \varphi(M)dM=1. \tag{6}$$

If $\delta(\Delta n)$ is the number of the group $\delta(\Delta n_0)$ which have survived mean life considerations after describing the path length x, we have

$$-\frac{d}{dx}[\delta(\Delta n)]=\frac{Mm_e}{\tau_0 p}[\delta(\Delta n)]. \tag{7}$$

It is possible to express the momentum p in terms of the energy E by the elimination of $\beta(=v/c)$ between the equations

$$E=Mm_ec^2[(1-\beta^2)^{-\frac{1}{2}}-1], \tag{8}$$

$$p=Mm_ec\beta/(1-\beta^2)^{\frac{1}{2}}, \tag{9}$$

where v is the velocity of the particle.

Through use of the Bloch formula, it is then possible to express E in terms of E_0 and x, and so realize an appropriate right-hand side for (7) as a function of x.

If, however, we stay within the limits of approximation which have been customary in this work, we may write the results of (8) and (9) in the form $p=E/c$. Moreover, we may write approximately, in place of the Bloch formula

$$E=E_0-\alpha h, \tag{10}$$

where α is a constant and h is the water equivalent of the path x. These approximations still leave the right-hand side of (7) a function of x through h. Thus (7) becomes

$$\frac{-1}{[\delta(\Delta n)]}\frac{d}{dx}[\delta(\Delta n)]=\frac{Mm_ec}{\tau_0(E_0-\alpha h)}. \tag{11}$$

Thus, considering as above any group of particles characterized by E_0 and the range dE_0, and by M and the range dM, we see that since $(E_0-\alpha h)$ is independent of M, the right-hand side of (11) is always greater the greater M. Hence, at each point of the path of the particles of range M to $M+dM$, the percentage loss of particles per unit path is greater the greater M. The result of this is that *the average rest mass of the particles decreases with increase of path traversed.*

Applying these ideas more specifically to the type of experiments which have been performed, we realize from (2) and (3) that the ordinary determination of mean life may be regarded as leading to a quantity which we shall call τ_0' defined by

$$\tau_0'=(x_1-x_2)(m_e\bar{M}c/E_0)/\log_e(\Delta n_1/\Delta n_2), \tag{12}$$

where $\bar{M}$ refers to the value of M used in the calculations, while Δn_1 and Δn_2 refer to the numbers of particles for the distances x_1 and x_2 corresponding to the two experiments, in which it will be recalled that the water equivalent path length for each is made the same by choice of suitable thicknesses of lead.

On the basis of acceptance of a mass distribution implied by (5) and with neglect of energy loss along the path our formula (11) leads to

$$\delta(\Delta n)=\delta(\Delta n_0)e^{-kMx} \tag{13}$$

or, in view of (5),

$$\delta(\Delta n)=\Delta n_0 e^{-kMx}\varphi(M)dM, \tag{14}$$

where Δn_0 refers to the top of the atmosphere and k has the value given by (3). Equation (14) leads to

$$\Delta n=\Delta n_0\int_1^\infty \varphi(M)e^{-kMx}dM. \tag{15}$$

It is our purpose to express the pseudo τ_0', which depends upon the average path length of the measurements, in terms of the true τ_0 which is independent of this path length. Writing $\bar{x}$ as the average path length, and Δx as the difference in path length for the two experiments, we have, from (12) and (15)

$$\tau_0' = \frac{m_e \bar{M} c \Delta x}{E_0} \Big/ \log_e \left[\frac{\int_1^\infty \varphi(M) \exp[-kM(\bar{x}-\Delta x)]dM}{\int_1^\infty \varphi(M) \exp[-kM(\bar{x}+\Delta x)]dM} \right], \tag{16}$$

so that

$$\frac{1}{(\tau_0')^2} \frac{d\tau_0'}{d\bar{x}} = \frac{1}{\tau_0 \bar{M} \Delta x} \left[\frac{\int_1^\infty M\varphi(M) \exp[-kM(\bar{x}-\Delta x)]dM}{\int_1^\infty \varphi(M) \exp[-kM(\bar{x}-\Delta x)]dM} - \frac{\int_1^\infty M\varphi(M) \exp[-kM(\bar{x}-\Delta x)]dM}{\int_1^\infty \varphi(M) \exp[-kM(\bar{x}+\Delta x)]dM} \right]. \tag{17}$$

In other words, having due regard to the meanings of the integrals, we see that $d\tau_0'/d\bar{x}$ is proportional to

(average mass at $\bar{x}-\Delta x$)
$-$(average mass at $\bar{x}+\Delta x$).

Since, as already shown, the average mass decreases with $\bar{x}$, we conclude that $d\tau_0'/d\bar{x}$ is positive. In other words, it is to be expected that the pseudo lifetime, calculated on the basis of neglect of the mass distribution law, should increase with average path length. This is exactly the conclusion represented by the experimental data shown in Fig. 1, which are consequently in harmony with the idea here proposed as to the existence of a spectral distribution in the rest masses of the mesotrons.

The departure of τ_0' from τ_0 is obviously a function of the form of $\varphi(M)$. Now Pomerantz,[5] in the course of very accurate measurements, has recently shown that the lifetime measured under the same conditions, but for different absorber thicknesses, i.e., different momenta, is the same, as the slight discrepancy which existed could be accounted for quantitatively as well as in character by transition effects and scattering, according to Pomerantz and Johnson.[6] Also, using Bruins' data and method,[7] i.e., the comparison of the vertical intensity (counter arrangement) with the "all-around" intensities (ionization chamber) underground one finds the same values of the lifetime at different thicknesses of dense absorber

If there existed an essential variation of the mass distribution $\varphi(M)$ with energy, this would result in the determination of different values for τ_0 if in the same kind of experiment, i.e., the same average path length, radiation of different initial energy E_0 is dealt with, and if the variation in $\varphi(M)$ stays unconsidered, as is the case when a constant value is assumed.

Therefore, we may conclude from the quoted measurements[5-7] that there exists no essential variation of the form of $\varphi(M)$, at least not in the region of high energies where these experiments were performed. Hence, there should be no objection to comparing directly the values for the lifetime as measured by different authors for components of the cosmic radiation which had different initial energies in the various experiments.

It seems worth mentioning that on account of the phenomenon of decreasing average rest mass with path length, the real lifetime τ_0 is smaller than any measured pseudo lifetime, unless we had some means of making the measurement at or very close to the origin of the radiation ($x=0$). On roughly extrapolating the relation in Fig. 1, found for the pseudo lifetime τ_0' with path length $\bar{x}$ towards $\bar{x}=0$, one may actually obtain a value of τ_0 corresponding to a value of about

[5] M. A. Pomerantz, Phys. Rev. **57**, 3 (1940).
[6] M. A. Pomerantz and T. H. Johnson, Phys. Rev. **59**, 143 (1941).
[7] E. M. Bruins, Proc. Ned. Akad. Wet. **18**, 75 (1940).

$\tau_0 = 5 \times 10^{-7}$ sec., which is Yukawa's original estimate of the mesotron's lifetime.

There are a great number of consequences, of course, which follow from the assumption of a distribution in rest mass, a few of which will be discussed in brief.

Recent investigations[8] have revealed that cloud-chamber photographs of highly ionizing particles are obtained more frequently at high than at low altitudes in the atmosphere, contradictory to the present knowledge concerning the number of slow mesotrons in the atmosphere. As has already been explained, the average mass of all mesotrons must decrease with path length, i.e., it will increase with altitude in the atmosphere, and this could explain the increasing frequency of heavy ionized tracks. For the rest mass goes in as a parameter in the Bloch formula, where it becomes of great importance at low energies.

This expresses itself in measurements of the energy loss of low energy particles ($<10^9$ ev electron energy) when traversing an absorber, such as Anderson and Neddermeyer have carried out, and which were used as part of their original evidence for the existence of a rest mass greater than that of the electron. Their improved experimental data,[9] indeed show a considerable parameter "scattering" of the experimental points attributed to the "heavy particles." For we can estimate the natural fluctuations including experimental error, statistics, etc., from their data for ordinary electrons to be smaller than 100 Mev while the heavy particle data are scattered over a parameter of as much as 300 Mev and more.

In all phenomena described above, the particular shape of the distribution function $\varphi(M)$ is essentially unimportant. However, there are a number of other phenomena for which this will be of particular interest. In this connection, W. F. G. Swann[10] has pointed out the possibility of an explanation of the secondary peak in the Rossi curve on the basis of different mesotron rest masses. Other effects, as for example a fine structure of the angular distribution, may find their explanation on the same grounds.

It is a pleasure to me to take this opportunity to thank Dr. W. F. G. Swann for his interest and his steady guidance in the mathematical formulation of the problem.

Note added in proof: The variation of energy along the path of the radiation due to ionization loss was neglected when showing theoretically that a distribution in rest masses tends to increase the measured lifetime at rest with increasing average path traversed. It was not clearly expressed, however, that the values for the measured lifetime at rest at various average path lengths from determinations of different authors were calculated, and *the increase of the measured pseudo lifetime with average path length (presented in Fig. 1) was thus found due consideration being given to the variation of energy along the path of the mesotrons.*

[8] G. Herzog, Phys. Rev. **59**, 117 (1941); G. Herzog and W. H. Bostick, Phys. Rev. **59**, 122 (1941).

[9] S. H. Neddermeyer and C. D. Anderson, Rev. Mod. Phys. **11**, 196 (1939).

[10] W. F. G. Swann, paper read before the American Philosophical Society at Philadelphia, on November 22, 1940.

An Investigation of the Properties of Proportional Counters. I*

M. E. Rose and S. A. Korff
Bartol Research Foundation of the Franklin Institute, Swarthmore, Pennsylvania

(Received April 2, 1941)

A theoretical and experimental investigation of the amplification properties of proportional counters has been made. On the basis of a discharge mechanism in which the amplification is due to electron avalanches the theory has been developed with the following primary assumptions: (1) All secondaries are produced by electron impact with no photon emission in the counter gas and thus no photoelectric emission at the cathode; (2) fluctuations in energy loss and specific ionization are neglected. The analysis involves the determination of the average number of ionizing collisions per unit distance (average energy) as a function of position in the counter, and the spatial extent of the ionization region near the wire anode. The former quantity is calculated explicitly in terms of the constants of the counter and the latter is shown to be simply related to the threshold voltage for proportional amplification, and is most suitably determined from the measurements. The gas fillers used in the measurements of the amplification factor were, for the most part, methane-argon mixtures of various relative concentrations and total pressures. In addition, other polyatomic mixtures, illuminating gas, BF_3-A and ether-A were used. Comparison of theory and experiment gives quite satisfactory agreement in all cases but two: large A concentration (50 percent or more at a total pressure of 10 cm Hg) and low total pressure (5 cm, or less, with a mixture containing 90 percent CH_4). In the anomalous cases the measured amplification factor rises extremely rapidly and such mixtures are therefore somewhat undesirable for stability reasons. This unstable behavior is characteristic of gas mixtures of the monatomic and/or diatomic type. An explanation of the difference in amplification properties of the polyatomic and simpler type gases is proposed. It is shown that while photon emission in the ultraviolet and subsequent contributions to the avalanche by photoelectric emission at the cathode is to be expected for the simpler gases, polyatomic gases should effectively quench such photon emission by virtue of greater energy loss of the slower electrons in exciting molecular vibrations and rotations. Moreover, appreciable emission of ultraviolet light by polyatomic molecules under electron bombardment is not to be expected. This explanation receives confirmation from cathode tests which were performed: measurements of pulse size, or amplification factor, for solid and perforated, oxidized and non-oxidized Cu cathodes. Further support of these arguments is found in experiments of other investigators: energy loss and mean free path measurements, electron bombardment of gases in a photo-cell. Finally, specific recommendations as to desirable pressure and concentration in the CH_4-A mixture are given.

I. Introduction

ALTHOUGH counters are extremely useful instruments and have been used extensively as sensitive detectors for all types of radiations, the investigation and clarification of the physical phenomena taking place in the counter has until recently been neglected.[1] In the case of counters operated in the sub-threshold region our understanding of the discharge mechanism, of the procedures to be followed and of the limits within which useful results may be obtained has been particularly limited with the result that the use of these counters has been somewhat restricted. Aside from the intrinsic interest in the sub-threshold discharge phenomena, a more thorough understanding of them and the way in which they affect counter behavior, or even a complete set of empirical rules regarding counter properties, would contribute to a more efficient use and a wider application of these counters to new types of measurements.

From previous investigations[2] it has been established that, for voltages well below the Geiger threshold, and over most of the sub-threshold region, the pulse size on the central system will be proportional to the initial ionization produced by the primary particles (discriminatory property of the proportional counter).

* This is a report of a preliminary survey of proportional counter properties dealing with the questions of discharge mechanism and the effect of the nature of the gas on counter amplification. A subsequent paper will provide more complete data on amplification and other proportional properties.

[1] A discussion of the mechanism of the discharge in Geiger-Mueller counters has been given by C. G. Montgomery and D. D. Montgomery, Phys. Rev. **57**, 1030 (1940). Attention may be called to the definition of the Geiger threshold adopted by these authors, which we follow, as that voltage above which all pulse sizes are independent of the initial ionization produced in the counter.

[2] H. Geiger and O. Klemperer, Zeits. f. Physik **49**, 753 (1928); S. A. Korff, Rev. Mod. Phys. **11**, 211 (1939); Rev. Sci. Inst. **12**, 94 (1941); G. Brubaker and E. Pollard, Rev. Sci. Inst. **8**, 255 (1937); C. G. Montgomery and D. D. Montgomery, Rev. Sci. Inst. **11**, 237 (1940).

In addition, in using the proportional counter one is interested in the following two questions: First, the more qualitative question as to what type of gas fillers should be used and secondly, the quantitative dependence of counter properties on gas pressure, relative concentration in the case of a mixture and on geometry (cathode, anode sizes). Here we shall be mainly interested in the first of these questions although some results are presented (Section IV) to show the effect of the other variables. In the following section the theoretical treatment of the discharge process is presented.

II. Theoretical

The properties of the proportional counter are most suitably defined by the characteristic curve or the dependence on counter voltage of the pulse size produced by amplification of the initial ionization. By virtue of the proportionality property we may define the amplification factor in a general way as the ratio of charge collected by the central wire anode to the amount of charge formed by the primary particle. In general, it is desirable that the counter have a large amplification factor so as to minimize the necessity for vacuum tube amplification; or, when portability and weight are important considerations, as in cosmic-ray balloon flights, it is economical to use counters with large amplification so as to allow the use of smaller voltage sources. On the other hand, counters whose amplification does not vary too sensitively with voltage would be more desirable for the minimization of errors due to voltage fluctuations.

The analysis of the proportional discharge requires first the postulation of some mechanism whereby the primary ionization is amplified. This primary ionization, whether it is direct ionization by charged particles, γ-ray secondaries or due to recoil nuclei produced by neutrons, will take place in the immediate vicinity of the path of the primary particle. This also applies to the ionization produced by such secondary electrons as are formed with energies above the ionization potential of the counter gas. Excluding the very rare case that the primary particle passes very near the wire (within a diameter, say) the initial energy of the secondary electrons is rapidly expended in various types of inelastic impacts and there will be no further ionization until the electrons are in the immediate vicinity of the wire where, by virtue of the strong field there prevailing, their energy becomes sufficiently great and increases sufficiently rapidly to produce sustained ionization. If the distance from the wire at which this ionization starts is several mean free paths a large multiplication of the charge density will take place by the successive and cumulative ionizations. In short, an electron avalanche is formed.

This discharge mechanism obviously implies the assumption that all secondaries are produced by electron impact and that all of them reach the wire. Explicitly we assume that:

1. (a) The emission of ultraviolet light and the consequent photoelectric effect at the (Cu) cathode is negligible. This is the most interesting assumption since evidence to be presented below (Sections IV and V) indicates that photoeffects are indeed negligible in polyatomic gases but not in simpler gases, monatomic and diatomic. (b) Secondary electron emission by positive ions at the cathode is neglected. This assumption should be well justified below the Geiger threshold where no effects of positive ion space charge are evident.

2. Recombination and electron attachment to neutral molecules can be neglected. Recombination will be very unimportant under the conditions of high field and low pressure usual in counters. Electron attachment will be appreciable for only a few gases (O_2, air and certain other gases not usually used in counters).[3]

Even in this picture the amplification process is of such complexity that it is necessary to make a further assumption:

3. We neglect fluctuations in energy loss and in specific ionization. While it is difficult to justify this assumption on *a priori* grounds the comparison of theory and experiment (Section IV) would seem to indicate that fluctuations do not play an important role.

We now consider a single electron arising from the initial ionization and calculate the amplification factor as the number arriving at the wire. Denoting the number of electrons at a distance r

[3] An effect on pulse size of the distance of the primary particles from the wire has been noted by Brubaker and Pollard (reference 2), and this is attributed to electron capture. However, under usual conditions of operation the primary particles are not very well collimated or are scattered by the counter walls so that no capture effects should be observed. In any case the capture introduces only a time lag ($\sim 10^{-5}$ sec.), because of the small mobility of the negative ions formed, and the time constant of the counter wire system can always be made longer than this.

from the center of the wire by $N(r)$ we have for the increase of $N(r)$ when r decreases by dr,

$$-dN=N(r)dr\int_0^{\epsilon_m}\frac{n(\epsilon,r)}{l(\epsilon)}d\epsilon. \tag{1}$$

Here we denote by ϵ the excess of the electron energy over the (average) ionization potential of the gas (or gas mixture) in the counter. For the sake of brevity we shall refer to the excess energy ϵ as the *energy*, whereas the actual energy is unitalicized. In (1) $n(\epsilon, r)d\epsilon$ is the fraction of the total number of electrons at r with *energy* between ϵ and $\epsilon+d\epsilon$, that is, the *energy* distribution normalized to unity. $l(\epsilon)$ is the mean free path for ionization and ϵ_m is the maximum *energy* of the electrons at r. The integral in (1) is thus simply the average number of ionizing collisions per unit distance which we shall denote by $\kappa(r)$, so that we have from (1)

$$N(r)=\exp\int_r^{r_0}\kappa(r)dr. \tag{2}$$

In (2) we have introduced r_0 as the distance from the center of the wire at which the avalanche-producing ionization starts.

The amplification factor A is then given by $N(r_1)$ where r_1 is the radius of the wire:

$$A=N(r_1)=\exp\int_{r_1}^{r_0}\kappa(r)dr. \tag{3}$$

It is seen, as may have been anticipated, that the main task of the theory is the calculation of the average number of ionizing collisions per unit distance $\kappa(r)$ and the spatial extent of the ionization region r_0. Considering the former quantity it is clear that in principle a knowledge of the *energy* distribution at each point r is involved although all that is eventually required is the average value of a known function of the *energy, viz.:*

$$\kappa(r)=(1/l(\epsilon))_{Av}. \tag{4}$$

In order to specify the *energy* dependence of the mean free path we recognize the fact that the electrons attain an energy of the order of the ionization potential ($\sim$15 volts) at a point very near the wire and that the energy gain in the region of ionization is sufficiently slow so that the electron energy at the wire is only a few times the ionization potential. The maximum energy may, in fact, be computed (cf. Eq. (10) below), and is generally 30–50 volts for counter voltages of as much as 1000 volts, the inelastic collisions being almost sufficient to overcome the effect of the accelerating field. Therefore the energy region pertinent to our considerations is such that the ionization cross section increases linearly with energy.[4] We write for the cross section

$$\sigma(\epsilon)=a\epsilon, \tag{5}$$

where a is a constant depending on the nature of the gas (cf. Table I below); and for the mean free path

$$l(\epsilon)=1/aN_m\epsilon, \tag{5a}$$

where N_m is the number of molecules (or atoms) per unit volume (see also Eq. (15)). Thus we have

$$\kappa(r)=aN_m\epsilon_{Av} \tag{6}$$

and we are concerned with the determination of the average *energy*, ϵ_{Av}.

In order to obtain the average *energy* we first consider the manner in which the *energy* distribution arises. The distribution, according to the present scheme (no fluctuations), arises from the fact that electrons at r have different points of origin r' and the *energy* at r is given by the average *energy* gain in traversing the distance from r' to r. The average *energy* gain is determined by[5]

$$-d\epsilon/dr=(cV_0/r)-\gamma(\epsilon). \tag{7}$$

Equation (7) determines ϵ for those electrons at r which have started from r', as a function of r and r' subject to the initial condition

$$\epsilon(r=r')=0. \tag{7a}$$

Here $\gamma(\epsilon)$ is the energy loss per unit distance due to all energetically possible inelastic processes, V_0 is the voltage across the counter and $1/c$

[4] Cf. for instance, K. T. Compton and I. Langmuir, Rev. Mod. Phys. **2**, 127 (1930).

[5] The average *energy* determined from the integration of (7) is, of course, to be distinguished from the true average *energy* referred to above. The former $\epsilon(r, r')$ is the average *energy* of an electron at r when it has started from a given point r', while the true average is $\epsilon(r, r')$ averaged over all points of formation with the appropriate weight factor, *viz.* the number of electrons formed at r'. (In Eq. (7) we have omitted the electronic charge so that all energies are measured in the same units as the counter voltage.)

$=\log(r_2/r_1)$ so that $\frac{1}{2}c$ is the capacity per unit length of the counter, with r_2 the cylinder (cathode) radius.

According to the above, the number of electrons at r having an *energy* between ϵ and $\epsilon+d\epsilon$ is just the number which were formed at a distance between r' and $r'+dr'$ where $dr'=(dr'/d\epsilon)d\epsilon$ and r' is given in terms of ϵ and r by (7). Thus the *energy* distribution at r depends on the distribution at r' and is accordingly given by the following integral equation:

$$N(r)n(\epsilon, r)d\epsilon = dr'N(r')\int_0^{\epsilon_m'} \frac{n(\epsilon', r')}{l(\epsilon')}d\epsilon'. \quad (8)$$

Here ϵ_m' is the maximum *energy* at r', and we have introduced the actual number of electrons with *energy* between ϵ and $\epsilon+d\epsilon$, namely $N(r)n(\epsilon, r)d\epsilon$.

An exact solution of this integral equation, and the determination of the distribution function itself, appears to be out of the question. Instead we proceed directly to the average *energy* which may be obtained by the following approximate method. First we put the average *energy* in evidence by noting that $n(\epsilon, r)$ has the dimensions of (energy)$^{-1}$ and hence can be written quite generally as

$$n(\epsilon, r) = (1/\epsilon_{Av})\varphi(\epsilon/\epsilon_{Av}), \quad (9)$$

where φ is a dimensionless function of the indicated dimensionless argument and the dependence on r is contained in $\epsilon_{Av}(r)$. Then the essential approximation consists in the fulfillment of the integral equation only for those *energies* for which the number of electrons is greatest. Since most of the electrons at r, more than half, were formed in the last mean free path and since the more remote the point of origin (i.e., the greater the *energy*) the fewer the number of corresponding electrons, the *energy* distribution will be monotonically decreasing with the most important *energy* region at $\epsilon=0$. Thus we may set $r'=r$, $\epsilon=0$ and $d\epsilon/dr'=-d\epsilon/dr=cV_0/r$. Then the average *energy* is obtained at once from (8) with the help of (5a), (6) and (9). We find

$$\epsilon_{Av}(r) = \left(\frac{\varphi(0)}{aN_m}\frac{cV_0}{r}\right)^{\frac{1}{2}}. \quad (10)$$

Thus we see that the average *energy*, and the width of the *energy* distribution which will be proportional to ϵ_{Av}, both increase as the electrons approach the wire, as was to be expected. From (6) the average number of ionizing collisions per unit distance follows immediately.[6]

$$\kappa(r) = (\varphi(0)aN_m cV_0/r)^{\frac{1}{2}}. \quad (11)$$

TABLE I. *Rate of increase of the ionization cross section with energy.*

GAS	$a(10^{17}$ CM^2/VOLT)	REFERENCE
A	1.81	*
Ne	0.14	*
He	0.11	*
H_2	0.46	†
O_2	0.66	†
N_2	0.70	†
NO	0.74	†
CO	0.83	†
C_2H_2	1.91	†
CH_4	1.24	**

* P. T. Smith, Phys. Rev. **36**, 1293 (1930).
† J. T. Tate and P. T. Smith, Phys. Rev. **39**, 270 (1932).
** A. Ll. Hughes and E. Klein, Phys. Rev. **23**, 450 (1924).

[6] The quantity $\varphi(0)$ which occurs in these results, and which is essentially the number of slowest electrons, cannot be evaluated uniquely without knowing the actual form of the distribution function. However the function φ is sufficiently restricted so that $\varphi(0)$ cannot, in general, vary over wide limits. In addition to the requirement that φ shall be a monotonically decreasing function of its argument, there are two further conditions to be imposed on this function. With $x=\epsilon/\epsilon_{Av}$ we have from the normalization condition,

$$\int_0^\infty \varphi(x)dx = 1$$

and from the definition of x,

$$\int_0^\infty x\varphi(x)dx = 1.$$

Various functional forms for φ may be assumed and after the above conditions have been imposed $\varphi(0)$ may be calculated. For a great variety of functions we find $\varphi(0)$ is between $\frac{1}{2}$ and 2 with by far the great majority of the values lying near unity. Accordingly, in the numerical applications to follow we have taken $\varphi(0)=1$. It may be noted that the dependence of the average number of ionizing collisions per unit distance on r is a direct consequence of the cylindrical geometry. The result (11) may at once be generalized for any geometry by replacing cV_0/r by the electric field $\mathcal{E}$. (There will also be a slight geometry dependence of $\varphi(0)$ but this can be neglected in first approximation.) In the case of plane parallel electrodes we may compare our result with the measurements of the first Townsend ionization coefficient, generally denoted in the literature by α. For field strengths comparable to those near the counter wire and for the usual counter pressures ($\sim$100 mm Hg) the ratio $\mathcal{E}/p$ is of order 1000 volts/mm. For such values of $\mathcal{E}/p$ the observations show that $\alpha/p \equiv \kappa/p$ is proportional to $(\mathcal{E}/p)^{\frac{1}{2}}$ in exact conformity with the result predicted by (11). Fairly good quantitative agreement is also found. Cf. L. B. Loeb, *Fundamental Processes of Electrical Discharge in Gases* (John Wiley and Sons, 1939), p. 360.

The final step in the calculation is the consideration of r_0. According to the way in which this quantity was introduced (see Eq. (2)) it is the distance from the wire at which the avalanche starts, and at this point one may expect fluctuations to play a more important role. Therefore we may not expect any reasonably accurate calculation of r_0 in terms of the physical constants of the counter without a much more refined and greatly complicated theory. However, it may be shown that r_0 is related in a simple way to another constant of the counter which could be directly measured and which is of considerably greater interest in defining the properties of the proportional counter. To see this we introduce a critical *energy* ϵ_0 which is the average *energy* at the point where ionization starts. According to (10) ϵ_0 is given by

$$\epsilon_0=\left(\frac{\varphi(0)}{aN_m}\frac{cV_0}{r_0}\right)^{\frac{1}{2}}. \tag{12}$$

The critical *energy* ϵ_0 for the onset of the avalanche will be determined by the nature of the gas (ionization potentials and cross section) but should not depend on the counter voltage or on geometrical factors. It then follows from (12) that r_0 increases linearly with counter voltage. In particular there will be some counter voltage for which ionization does not begin until the electrons reach the wire, i.e., $r_0=r_1$. At this voltage, the threshold voltage for the proportional region, the amplification factor becomes unity and below this voltage the counter acts as an ionization chamber. Denoting the proportional threshold by V_t we have

$$r_0=r_1V_0/V_t. \tag{13}$$

Thus r_0 may be defined in terms of the directly measurable voltages and wire radius.

With (13) and (11) the final result for the amplification factor follows readily from (3):

$$A=\exp 2(aN_mcr_1\varphi(0)V_0)^{\frac{1}{2}}[(V_0/V_t)^{\frac{1}{2}}-1] \tag{14}$$

in which, as was mentioned above, $\varphi(0)$ is to be set equal to unity and V_t is to be determined from the measurements. The quantity a in (14), that is, the rate of change of the ionization cross section for energies just above the ionization potential, is given in Table I for those gases for which measurements exist. For the quantity aN_m in the case of a mixture of gases, we obviously have

$$aN_m=\sum_i a_iN_{mi}, \tag{15}$$

where N_{mi} is the particle density of molecules of the ith constituent of the mixture.

III. Apparatus

The amplification factor for the several counters used in the experiments was determined by measuring the counter voltage corresponding to a previously determined pulse size. The pulse sizes were measured by using a variable-gain amplifier and a thyratron recorder. The amplifier consisted of a conventional resistance-coupled circuit, employing one or alternatively three stages, with tubes of type 6J7. The gain of each stage could be controlled. For any given bias setting a certain minimum pulse size was necessary to record. Calibration of the gain settings was accomplished by the use of a simple pulse-generator. This consisted of a resistance potential divider across a battery, equipped with a key and capacitatively coupled to the input.

The potential applied to the counter was produced by a modified Street-Johnson type of voltage regulator. The counter voltage remained independent of the fluctuations in the a.c. line, and could be controlled and kept stable in the range between 200 and 1600 volts. The output voltage was read on a microammeter in series with a standard resistance and was believed to be accurate to within 2 percent.

The various counters were attached to a manifold connected to a vacuum system. Gas-supply bulbs were attached so that the kind and amount of each gas could be changed at will, and the pressure in the system and in all the counters could be read on a mercury manometer. Many of the runs were repeated in random order to insure reproducibility.

In each case the maximum pulse size due to Po α-particles passing down the length of the counter was measured. Therefore the initial ionization is that due to α-particles with a residual range equal to the length of the sensitive part of the counter. This ionization may then be obtained from the integrated Bragg curve,[7] re-

[7] For specific ionization data see, for example, M. G. Holloway and M. S. Livingston, Phys. Rev. **54**, 18 (1938).

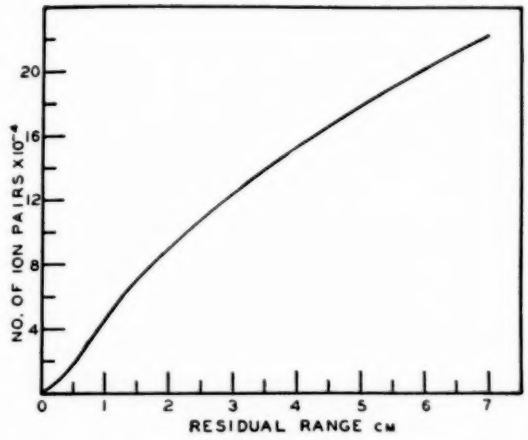

FIG. 1. Total ionization of alpha-particles in air at 0°C and 76 cm Hg as a function of residual range.

produced in Fig. 1 for convenience, and for gases other than air the conversion factors as given by Gurney[8] were used. The amplification factor is then $A = CP/en$, where C is the capacity of the central system, P the pulse size, n the initial ionization and e the electronic charge.

IV. Comparison of Theory and Experiment

In addition to providing a test of the theory the present measurements were designed to furnish a first orientation with regard to proportional counter properties. In fact the limitations as to measurable pulse size of the amplifier used allowed measurements to be made only for the higher voltages (roughly the upper half of the proportional region); since this is the region of large amplification, it is, to be sure, the more important region from a practical point of view. However, the proportional threshold voltages were therefore not measured directly but were obtained by fitting the theoretical curves at one experimental point.[9]

[8] R. W. Gurney, Proc. Roy. Soc. **A107**, 332 (1925). Although no measurements exist for CH_4, used in the experiments described below, the specific ionization may be taken equal to that in Ne, with very little error, because of the similarity of electron structure.

[9] Measurements down to the ionization chamber region of voltage would require a more elaborate amplifier or the use of a balanced pliotron circuit with a counter carefully shielded by guard rings. Using the latter apparatus such measurements are now being conducted in this laboratory. In addition to providing a complete exploration of the proportional region a direct measurement of the proportional threshold as well as the amplification factor is then possible.

For the most part the measurements were carried out with methane-argon mixtures which were found to be a suitable gas filler for the counters. We have investigated the effect of the relative concentration of the constituents of this mixture and the results are shown in Fig. 2. The relative concentrations were 100, 90, 75 and 50 percent methane. In each case the highest voltage measured marks approximately the limit of the proportional region. With the amplification factor plotted on a logarithmic scale the theoretical curves over the measured range of voltages are, in appearance, virtually straight lines. For the three methane-rich mixtures the agreement between theory and experiment is seen to be very satisfactory, the deviations of the measured points lying within the experimental error. The threshold voltages as determined by fitting at each experimental point showed an extreme variation of only 5 percent or less. These threshold voltages, which with the maximum voltages measured give the approximate breadth of the proportional region, are listed in the second column of Table II.

The results for the 50 percent concentration are anomalous in the sense that it is not possible to fit a theoretical curve to the observed points. The measured amplification factor rises too rapidly with voltage. This case requires special consideration which is reserved for the next section.

Figure 3 shows the experimental points for the amplification factor and the corresponding theoretical curves for mixtures of 90 percent methane and 10 percent argon for total pressures of 5, 10, 20, 30 and 40 cm. Again, in the case of all but the lowest pressure good agreement between theory and experiment is obtained. The threshold voltage as a function of pressure is given in the last column of Table II. It is interesting to note that these four threshold voltages show a linear increase with pressure so that the amplification factor (from Eq. (14)) decreases essentially exponentially with increasing pressure. The same sort of anomalous behavior as noted before is found for the lowest pressure (cf. Section V).

The experimental points and theoretical amplification-voltage curves for some widely used mixtures are shown in Fig. 4. The CH_4-H_2 mixture was actually illuminating gas whose heterogeneous composition was known—except

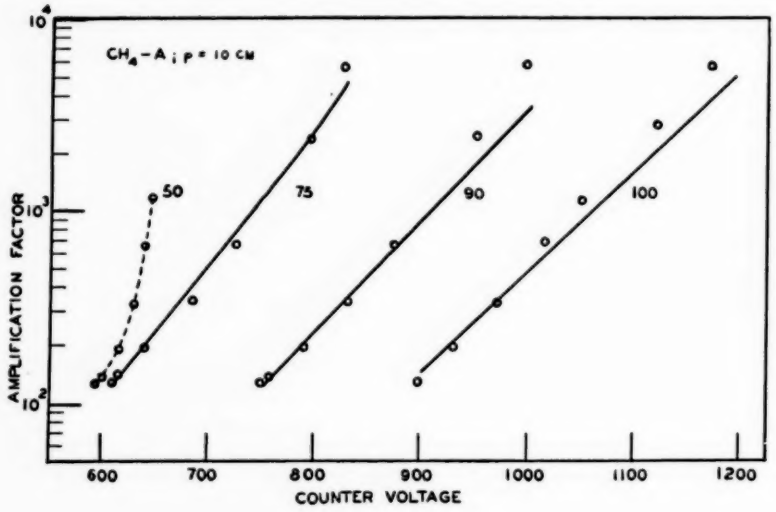

FIG. 2. The amplification factor (logarithmic scale) plotted against counter voltage for various relative concentrations in CH_4-A mixtures at 10-cm pressure. The points are experimental and the full curves are theoretical with one point adjusted (see Eq. (14)). The numbers affixed to the curves give the relative concentration of CH_4 in percent. The dimensions of the counter were: wire diameter 0.075 mm; Cu cylinder, diameter 1 cm and length 3 cm.

for a small amount of CO_2 the mixture is composed of gases whose ionization at low energies has been measured (Table I). The BF_3-A counter was of the type used in neutron measurements. (In obtaining the theoretical curves for this and the A-ether counter the ionization in BF_3 and in ether was obtained by fitting at a second point. The ionization coefficient a obtained for ether was then in agreement—within 5 percent—with the value to be expected with the assumption of additivity of cross sections and from the data listed in Table I for H_2, O_2 and CO, *viz.* $a=6.2\times10^{-17}$ cm²/volt). The main point of interest in connection with these measurements is that in each case the mixtures contained a polyatomic constituent of rather large concentration: 31 percent CH_4 in the illuminating gas, 47 percent ether in the ether-A mixture and 82 percent BF_3 in the BF_3-A mixture. The total pressures were 3.5, 17 and 11 cm, respectively. The threshold voltages for the three counters were determined to be 450, 470 and 955 volts, respectively.

Finally, the effect of geometry, which is of course mainly dependent on wire diameter, was investigated. As is to be expected, and as is predicted by the theoretical formula (Eq. (14)), the amplification factor increases as the wire diameter is made smaller. The counters were filled with the 75 percent CH_4-A mixture at a total pressure of 10 cm. The results for the wire diameter of 0.075 mm have already been given, Fig. 2. Decreasing the wire diameter to 0.025 mm shifts the amplification curve by about 100 volts in the direction of lower voltages. This corresponds to an increase in the amplification by a factor of 5. Increasing the wire diameter to 0.125 mm shifts the amplification curve towards higher voltages by about 40 volts, as compared to the curve of Fig. 2. This is equivalent to a reduction in the amplification factor by 50 percent. As in the case of the intermediate wire size, the measurements for the 0.025 and 0.125-mm wires may be satisfactorily fitted by a theoretical curve. Thus, with the exception of the anomalous cases noted above, the theory is in agreement with the data for concentration, pressure and geometry dependence.

V. Comparison of Discharge in Polyatomic and Simple Gases

The anomalously rapid rise of the amplification factor, at least in the case of the mixture with relatively large argon concentration, is not surprising. It had been previously observed that the amplification in counters filled with A, A-O_2, A-H_2, Ne-H_2 or H_2 will increase by a factor of as

TABLE II. *Threshold voltages for proportional counter discharge.*

Pressure 10 cm Hg Conc. CH_4 (%)	V_t volts	0.90 CH_4–0.10A Total Pressure cm Hg	V_t volts
100	430	40	1090
90	350	30	840
75	270	20	610
		10	350

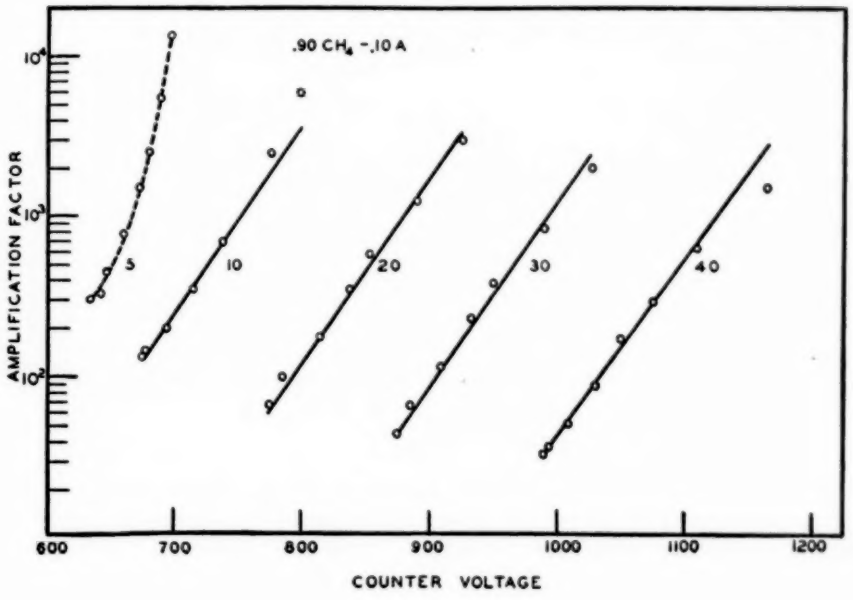

FIG. 3. The amplification factor (logarithmic scale) against counter voltage for a 90 percent CH_4 concentration in CH_4-A mixtures at pressures (in cm Hg) given by the numbers affixed to the curves. Points are experimental, full curves theoretical. Counter dimensions as in Fig. 2.

much as 100 when the counter voltage is increased by only 2–5 volts.[10] On the other hand such mixtures as CCl_4-A, BF_3-A and illuminating gas were observed to give a much more slowly rising amplification. We have also used A and H_2 and for each gas have verified the extremely rapid rise of the amplification with voltage. In no case can the theory (based on the assumptions of Section II) account for this behavior.

This rather striking difference in the amplification of counters filled with simple gases and with polyatomic gases may be explained in terms of a fundamental difference in the discharge mechanism in the two cases. In view of the agreement obtained between theory and experiment (Section IV) the discharge mechanism postulated in Section II may be regarded as correct for polyatomic gases. For the simpler gases it is most probable that the first assumption regarding the absence of photoelectric emission no longer holds. Indeed, it is easier to account for the presence of photons capable of emitting photoelectrons than it is to explain their absence. Since the electrons attain sufficient energy to ionize they must also cause excitation of electronic levels with the subsequent emission of ultraviolet radiation. The emission of photoelectrons at the cathode then initiates a new avalanche and the process may be repeated several times. The rapid rise of the amplification is then readily understandable. To account for the presumable absence of such photons in the mixtures relatively rich in a polyatomic constituent we recognize the fact that over the greatest part of the path of the electrons their energy is insufficient for electronic excitation in the gas molecules. By far most of the inelastic collisions may therefore excite only vibrational and rotational energy so that, except near the wire, only infra-red radiation could be emitted. In the case of polyatomic molecules, as contrasted to the simpler molecules, the much greater number of degrees of freedom for the molecular motions may be expected to enhance the excitation of low energy vibrations. Moreover, because of the great number of collisions taking place in the "infra-red" region of the counter, even a small increase in the probability of vibrational excitation would have an important effect. Hence, in a gas with fairly large concentration of polyatomic molecules, the energy of the electrons would rise more slowly than in the simpler gases and the spatial extent of the "ultraviolet" region, near the wire, would become considerably smaller. This would then mean a smaller intensity of the higher energy photons.

In addition, emission of ultraviolet radiation from the polyatomic molecules excited by electron bombardment would not be expected as a general rule. For methane, as an example, no

[10] S. A. Korff, Rev. Mod. Phys. **11**, 213 (1939).

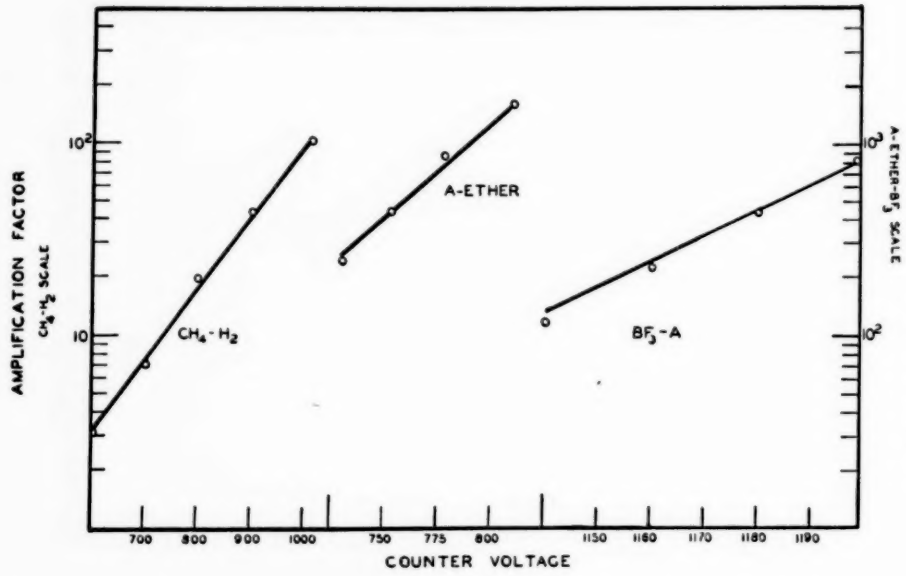

FIG. 4. The amplification factor (logarithmic scale) against counter voltage for various polyatomic gas mixtures. Note change in voltage scale for each curve. The scale for the amplification factor in the case of CH_4-H_2 is on the left, the scale for the other two mixtures is on the right. Points are experimental, curves theoretical. Counter dimensions: CH_4-H_2 and BF_3-A counters, wire diameter 0.075 mm, cylinder diameter 1.8 cm and length 20 cm; ether-A counter, same as in Fig. 2.

absorption in the ultraviolet is obtained until 1600A (at 10-cm pressure) and then the appearance of the absorption bands indicates predissociation of the molecule.[11] In general it may be expected that the absorption of radiation of 7–8 volts or more, or bombardment with electrons of such energies, would lead to dissociation rather than light emission. Thus, the binding energy of the H_2 molecule in methane is 3.7 volts and the binding energy of the H atom is 4.5 volts so that with 1600A radiation dissociation could take place leaving some 3 or 4 volts as kinetic energy of the products.[12] Thus the methane in CH_4-A mixtures, and presumably other polyatomic molecules, would appear effectively to quench the emission of ultraviolet by providing a more probable mode of energy loss for the lower energy electrons and by failing to contribute to such emission even when the excitation of electronic levels is energetically possible.

As a test of the above hypothesis we have performed the following experiments. Three counters were simultaneously attached to the manifold so that they could be filled with the same gas at exactly the same pressure. The counters themselves were identical in all but one respect: One had a non-oxidized Cu cathode as usual, another had a similarly clean cathode made of Cu screening so that the cathode area was reduced by nearly 50 percent and the third was constructed of the same screening but was oxidized to CuO. The counters were otherwise the same as those used with the CH_4-A mixtures, (Figs. 2 and 3). The amplification curves with hydrogen in the counters are shown in Fig. 5. It is seen that at the higher voltages there is a very definite cathode effect. The reduction of pulse sizes by oxidation of the cathode (2nd and 3rd counters) shows that the very small change in electric field due to the substitution of screening for solid Cu is not responsible for the reduction in pulse size upon perforation of the cathode (1st and 2nd counters). These results are most plausibly interpreted in terms of avalanche production by photoelectrons.[13] At the lower voltages inappreciable photon emission is indicated as could be expected from intensity considerations (much smaller number of electrons in the initial avalanche). With argon in the counters similar results were obtained. When the same experiments were repeated with only methane in the counters the results shown in Fig. 6 were found. Here it is seen that even at the highest voltages

[11] Cf. for instance, A. Rose, Zeits. f. Physik **81**, 751 (1933).

[12] L. G. Smith, Phys. Rev. **51**, 263 (1937).

[13] Unfortunately the comparison of pulse sizes with Cu and CuO cathodes cannot be checked with photoelectric data. Such measurements as exist show that from the photoelectric thresholds to 1800A Cu gives a greater yield of photoelectrons, R. Fleischmann, Ann. d. Physik **5**, 73 (1930). However, the cathode tests with H_2 may be taken as an indication that this is also true at 1000A.

there is no evidence for a cathode effect. A similar absence of cathode effect was obtained with the other polyatomic gas mixtures (Fig. 4). On the other hand the two CH_4-A mixtures whose amplification factor rose too rapidly, Figs. 2 and 3, showed a cathode effect only slightly less pronounced than that shown in Fig. 5 for H_2. These results therefore justify the assumption (1) on which the theory was based and form a strong argument for the essential correctness of the proposed hypothesis as to the role of photons in simple gases as contrasted with the "quenching" action of the polyatomic gases.

Further support for the arguments presented in the above may be obtained from other experiments. Thus, Bailey and Duncanson[14] have measured energy losses and mean free paths for slow electrons in various gases and have found that certain polyatomic gases of the hydrocarbon type and triatomic gases (NH_3, H_2O vapor and CO_2) have smaller mean free paths and larger fractional energy losses at less than 1 volt, where only infra-red may be excited, than at higher energies. On the other hand, inert gases and several of the diatomic variety were shown to have the largest energy losses and smallest mean free paths at the higher energies where visible and ultraviolet light may be excited. More direct experiments, from the present point of view, were carried out by Glocker[15] who found that electrons

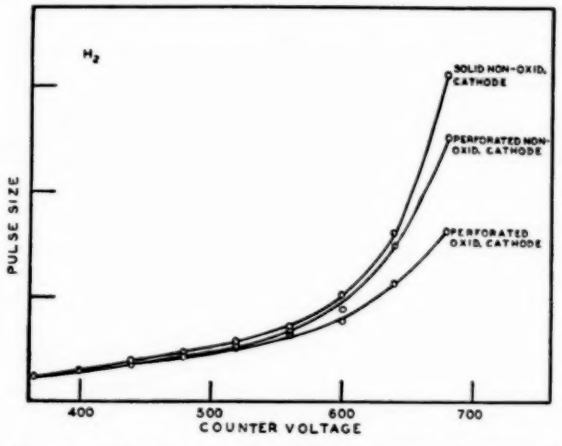

FIG. 5. Pulse size, or amplification factor (linear scale, arbitrary units), against counter voltage for the three cathodes described in the figure. Counter was filled with H_2 at 7.3-cm pressure. Counter dimensions as in Fig. 2.

[14] V. A. Bailey and W. E. Duncanson, Phil. Mag. **10**, 145 (1930).

[15] G. Glocker, Proc. Nat. Acad. Sci. **11**, 74 (1925).

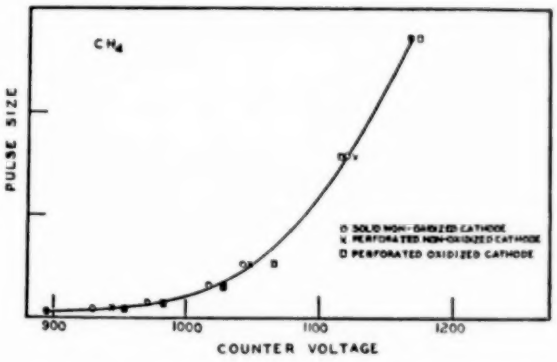

FIG. 6. Pulse size, or amplification factor (linear scale, arbitrary units), against counter voltage for the three cathodes described. Counter was filled with CH_4 at 7.3 cm pressure. Counter dimensions as in Fig. 2.

with energies up to 17 volts bombarding methane in a photoelectric cell gave no measurable photoelectric currents. However, with hydrogen in the photo-cell photoelectric currents were obtained for electron energies above 13 volts which is slightly larger than the energy of the first excited state in H_2.

These experiments have shown that for effective photon quenching and consequent stability not only must the relative concentration of the polyatomic gas be greater than a certain critical value but in addition the absolute amount of this gas must not be too small. While the existence of a critical concentration is easily understood in the light of the foregoing qualitative considerations, the existence of a critical pressure could be understood only on the basis of a more quantitative treatment of the photon emission and photoelectric effect in the counter. However, this pressure effect may be accepted as an empirical fact to be used as a guide in the determination of the most suitable conditions for counter operation.[16] Thus, if it is desired to operate the counter so as to obtain large *and* stable amplification, the gas mixture should contain polyatomic as well as simpler type constituents with pressure and concentration conditions near the critical limits. With CH_4-A mixtures, for example, a relative concentration of 75 percent CH_4 at a total pressure of 10 cm would be close to optimum conditions.

[16] Cf. S. C. Curran and J. E. Strothers, Proc. Camb. Phil. Soc. **35**, 654 (1939) where a similar effect is observed for counters filled with argon-alcohol mixtures above the Geiger threshold.

Temperature Diffuse Scattering of a Simple Cubic Lattice

W. H. ZACHARIASEN
Ryerson Physical Laboratory, University of Chicago, Chicago, Illinois
(Received April 3, 1941)

The rigorous calculation of the temperature diffuse scattering pattern of a crystal presupposes a knowledge of the propagation velocities and of the polarization directions. It is shown how these quantities can be found for a simple cubic lattice of the Born-Kármán type. When the elastic constants satisfy the condition $c_{11}=3c_{12}$ the formula for the intensity distribution in the diffraction maxima is particularly simple and this case is therefore treated in some detail. Expressions for the positions and half-widths of the intensity maxima have been developed. Also the case $c_{11}\gg 3c_{12}$ has received special attention. For lattices of this type the diffuse diffraction maxima have a complex structure, each maximum consisting in the general case of three peaks. Formulae are given for the position and intensity of these peaks. Under proper conditions only one or two of the three peaks composing a maximum will be observable. An intensity expression for very small scattering angles has been developed. According to theory there is no diffuse halo around the forward beam. Such a halo has been reported by some experimenters, and it is suggested that the observed diffuse ring is not connected with the temperature diffuse scattering, but is due to continuous radiation in the incident beam and scattering from the air.

IN a recent article[1] this writer gave a new theoretical treatment of the diffuse scattering of x-rays by crystals. The derivation led to a new intensity formula for the temperature diffuse scattering, i.e., for that part of the diffuse scattering which is due to the heat motion of the crystal lattice. When the direction of the incident x-rays is such that the Laue-Bragg scattering is negligible the intensity formula becomes (compare Eq. (17) of reference 1)

$$J_2=\frac{NI_a}{4\pi^2 m_a \tau_0^2}\sum_j \frac{(\mathbf{s}\cdot\mathbf{A}_j)^2}{v_j^2}Q_j. \qquad (1)$$

In this equation τ_0 is the wave vector of a vibrational mode defined by

$$\mathbf{k}-\mathbf{k}_0+\tau_0=\mathbf{B}_H. \qquad (2)$$

The various symbols occurring in these two equations have the following meaning: N is the number of atoms doing the scattering; I_a is the intensity of coherent scattering from a single atom; m_a is the atomic mass; $\mathbf{B}_H$ is a reciprocal lattice vector; $\mathbf{k}_0$ is the wave vector of the incident x-rays; $\mathbf{k}$ is the wave vector of the scattered x-rays; $\mathbf{s}=2\pi(\mathbf{k}-\mathbf{k}_0)$; $\mathbf{A}_j$ $(j=1, 2, 3)$ is the jth polarization direction associated with the wave vector τ_0; v_j is the propagation velocity corresponding to the jth polarization direction; $Q_j=kT(x/(\exp x-1)+x/2)$, where $x=hv_j\tau_0/kT$, is the familiar quantum factor.

The propagation velocities v_j and the polarization directions $\mathbf{A}_j$ are functions of the wave vector τ_0—both of its magnitude (i.e., of the wave number) and of its direction. Even for cubic crystals this functional relationship is quite complicated and little is known about it. In order to calculate accurately the intensity distribution of the temperature diffuse scattering pattern it accordingly becomes necessary first to make a detailed study of the lattice vibrations.

In the earlier communication[1] the main features of the diffraction pattern were studied by means of the admittedly crude approximation of setting $v_1=v_2=v_3=$ a constant. This approximation led to a considerable simplification in the intensity formula (compare Eq. (18) of reference 1) and expressions for the positions of the intensity maxima and for the intensity distribution in the immediate neighborhood of a maximum were readily obtained. In view of the crude assumption upon which the simplified intensity formula is based one cannot expect it faithfully to reproduce the details of the diffraction pattern. The results which are obtained in the following sections do indeed show that the simplified formula cannot be used for the interpretation of experimental data which have some measure of accuracy.

[1] W. H. Zachariasen, Phys. Rev. **57**, 597 (1940). See also the earlier work: H. Faxén, Zeits. f. Physik **17**, 266 (1923); I. Waller, Zeits. f. Physik **17**, 398 (1923), Dissertation, Uppsala (1925).

In this article we will study the vibrations and the temperature diffuse scattering pattern of a simple cubic lattice.

The Vibrations of a Simple Cubic Lattice

The normal vibrations of a lattice correspond to standing elastic waves. If an atom is assumed to vibrate as a single particle, a wave of the type

$$\mathbf{A}\exp i(\omega t+2\pi\boldsymbol{\tau}\cdot\mathbf{r}) \tag{3}$$

has physical significance only at the lattice points and wave vectors $\boldsymbol{\tau}$ and $\boldsymbol{\tau}+\mathbf{B}_H$ consequently represent the same vibrational mode. The wave vectors $\boldsymbol{\tau}$ may therefore be subjected to the condition

$$\boldsymbol{\tau}\leq|\boldsymbol{\tau}+\mathbf{B}_H|, \tag{4}$$

which restricts the vectors $\boldsymbol{\tau}$ to lie within a polyhedron—the Brillouin zone. The Brillouin zone has the same volume as the unit cell of the reciprocal lattice and if the lattice is orthogonal it has also the same shape. The upper limit τ_m to the wave number will in general be different for different propagation directions since the Brillouin zone is a polyhedron rather than a sphere. The Brillouin zone of a simple cubic lattice is evidently a cube of edge $1/a_0$ where a_0 is the grating constant. In this case τ_m is $1/2a_0$ for waves propagating along the cube axes, while it is $3^{\frac{1}{2}}/2a_0$ for waves advancing along the cube diagonals.

The equations of motion of a simple cubic lattice which take into account the interaction between nearest and next nearest neighbors have been given by Born and Kármán.[2] By trial with the plane wave solution given in Eq. (3), the equations of motion are found to lead to the familiar set of linear and homogeneous equations for the determination of frequency and polarization direction. For the purpose of discussions to be given later it is convenient to write this homogeneous system in the form

$$[\boldsymbol{\phi}(\boldsymbol{\tau})-v^2\mathbf{1}]\cdot\mathbf{A}=0. \tag{5}$$

The symbol $\mathbf{1}$ represents the unit tensor, i.e., $\mathbf{1}\equiv\begin{pmatrix}1&0&0\\0&1&0\\0&0&1\end{pmatrix}$. The components of the symmetrical tensor $\boldsymbol{\phi}$ in the Cartesian system which has its coordinate axes along the cube edges are of the type

$$\phi_{11}=\frac{a+2b-[a+b(\cos2\pi\tau_2+\cos2\pi\tau_3)]\cos2\pi\tau_1}{\tau^2},$$
$$\phi_{12}=\frac{b\sin2\pi\tau_1\sin2\pi\tau_2}{\tau^2}. \tag{6}$$

In these expressions τ_1, τ_2, τ_3 are the components of $\boldsymbol{\tau}$ in the reciprocal lattice, i.e., $\boldsymbol{\tau}=\sum\tau_j\mathbf{b}_j$, so that $\tau^2=(\tau_1^2+\tau_2^2+\tau_3^3)/a_0^2$ while the Brillouin zone is given by the condition $-\frac{1}{2}\leq\tau_j\leq+\frac{1}{2}$. The constants a and b are

$$a=\alpha/2\pi^2m_a,\quad b=\gamma/\pi^2m_a, \tag{7}$$

where α and γ are the force constants for nearest and next nearest neighbors, respectively, (compare reference 2). The secular equation

$$|\boldsymbol{\phi}-v^2\mathbf{1}|=0 \tag{8}$$

has three real roots v_j^2 while the corresponding polarization directions are obtained from Eq. (5). It is useful to note that the polarization directions $\mathbf{A}_j$ coincide with the principal axes of the tensor $\boldsymbol{\phi}$ and that v_j^2 are the components of $\boldsymbol{\phi}$ referred to these axes. None of the three polarization directions will, in general, coincide with the propagation direction. Thus none of the three waves is, in general, purely longitudinal. Indeed, for arbitrary propagation direction there is no purely transverse wave either.

The three velocities of propagation depend, in general, both upon the magnitude and upon the direction of the wave vector $\boldsymbol{\tau}$. For given propagation direction the velocities decrease with increasing wave number. It is seen from Eqs. (6) that this dispersion is negligible only in the range for which the approximations $\sin2\pi\tau_i\approx2\pi\tau_i$ can be used. This range is, however, of particular importance in connection with the temperature diffuse scattering since such small values of the wave vector $\boldsymbol{\tau}$ correspond to the intensity maxima of the diffraction pattern. We will therefore treat the case of small vibrational wave numbers separately.

[2] M. Born and Th. v. Kármán, Physik. Zeits. **13**, 297 (1912). See also M. Blackman, Proc. Roy. Soc. **148**, 365, 384 (1935); **159**, 416 (1937).

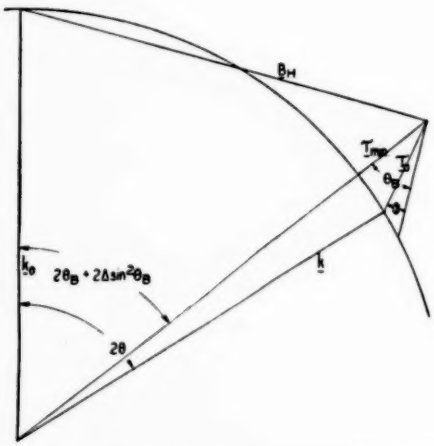

FIG. 1. This shows the familiar reciprocal lattice construction of Eq. (2) (compare Fig. 1 of reference 1). It is to be imagined that the terminus of $\mathbf{B}_H$ lies very much closer to the sphere of reflection than indicated in the drawing. The angle between $\boldsymbol{\tau}_{\min}$ and the normal to $\mathbf{B}_H$ is truly $\theta_B - \Delta\cos 2\theta_B$, but the second term has been neglected since Δ is assumed to be small. The figure corresponds to a negative value of Δ.

THE INTENSITY MAXIMA OF THE TEMPERATURE DIFFUSE SCATTERING

When the vibrational wave number is so small that we may set $\sin 2\pi\tau_i \approx 2\pi\tau_i$ and $\cos 2\pi\tau_i \approx 1-2\pi^2\tau_i^2$ the tensor may be written in the form

$$\phi = 2\pi^2 a_0^2 b[1+2\mathbf{nn}] + 2\pi^2 a_0^2(a-b)\begin{pmatrix}\alpha_1^2 & 0 & 0\\ 0 & \alpha_2^2 & 0\\ 0 & 0 & \alpha_3^2\end{pmatrix}. \quad (9)$$

In this equation $\mathbf{n}$ is the unit vector along the propagation direction (i.e., $\boldsymbol{\tau} = \tau\mathbf{n}$) while $\alpha_1, \alpha_2, \alpha_3$ are the direction cosines of $\mathbf{n}$ relative to the cube edges. Born and Kármán[2] showed that the force constants α and γ can be expressed in terms of the elastic constants, namely

$$\alpha = a_0(c_{11}-c_{12}-c_{44}), \qquad 4\gamma = a_0(c_{12}+c_{44}). \quad (10)$$

Assuming the Cauchy relation to hold (i.e., $c_{12}=c_{44}$) we have therefore

$$2\pi^2 a_0^2 b = c_{12}V/m_a, \qquad 2\pi^2 a_0^2(a-b) = (c_{11}-3c_{12})V/m_a, \quad (11)$$

where $V=a_0^3$ is the volume of the unit cell.

The first term on the right side of Eq. (9) is a tensor with rotational symmetry about the propagation direction $\mathbf{n}$. In other words if $c_{11}=3c_{12}$ the three waves correspond to one purely longitudinal and to two purely transverse waves. The propagation velocities are, furthermore, constants, independent of the propagation direction, but the longitudinal velocity is $3^{\frac{1}{2}}$ times as great as the transverse velocities.

In the other extreme case when the first term of Eq. (9) is negligible compared to the second term (i.e., c_{12} negligible in comparison to c_{11}) the polarization directions are along the cube edges and the propagation velocities are proportional to the direction cosines of the wave vector.

In the following we shall discuss Eq. (1) for these two extreme cases. Since τ is assumed to be small (so that it is justifiable to neglect the dispersion) this discussion is necessarily restricted to cases in which the actual glancing angle of incidence θ_i is near the Bragg glancing angle θ_B. We require in other words that $\theta_i - \theta_B \equiv \Delta$ is small compared to θ_B. Unless the temperature T is very small compared to the characteristic temperature of the crystal we may set $Q_j = kT$. (This approximation is clearly valid if $\tau/\tau_m < T/\Theta$ where Θ is the characteristic temperature.)

Case I. $c_{11}-3c_{12}\approx 0$.

Introducing the approximations mentioned above we find the intensity formula of Eq. (1) becomes

$$J_2 \approx \frac{4I_a kT\sin^2\theta_B}{3V^2 c_{12}} \frac{1+2\cos^2\varphi}{(\lambda\tau_0)^2}\delta V, \quad (12)$$

where δV is the volume of the scattering crystal and where $\frac{1}{2}\pi-\varphi$ is the angle between vectors $\boldsymbol{\tau}_0$ and $\mathbf{s}$.[3] It is readily seen from Eq. (12) that the intensity of scattering is symmetrical with respect to the plane of incidence and we will therefore limit our considerations to this plane. As shown in Fig. 1 we may set $\lambda\tau_{\min} = \lambda\tau_0\cos(\theta_B-\varphi)$ where $\lambda\tau_{\min} = -\Delta\sin 2\theta_B$ (compare Eq. (21) of reference 1). Hence we obtain the following expression for the intensity of scattering at a scattering angle 2θ in the plane of

[3] Compare this result with the nearly identical Eq. (11) of Faxén's article, reference 1.

incidence

$$J_2(2\theta)=K\frac{\cos^2(\theta_B-\varphi)[1+2\cos^2\varphi]}{(\Delta\sin 2\theta_B)^2}, \quad (13)$$

where

$$K=\frac{4I_a kT\sin^2\theta_B}{3V^2c_{12}}\delta V$$

and where $2\theta=2\theta_B+2\Delta/(1+\cot\theta_B\cot\varphi)$. In Fig. 2 Eq. (13) is plotted as function of the scattering angle. The intensity maximum can be shown to correspond to the value

$$\varphi_m\approx 0.600\theta_B+0.017\theta_B^4. \quad (14)$$

The scattering angle for the intensity maximum, $2\theta_m$, is thus (when $\theta_B<1$ rad. so that the second term in Eq. (14) may be neglected)

$$2\theta_m=2\theta_B+2\Delta/(1+\cot\theta_B\cot(0.6\theta_B)). \quad (15)$$

The deviation from the Bragg scattering angle (i.e., $2\theta_m-2\theta_B$) for different values of θ_B is shown in Fig. 3 as function of Δ, while Fig. 4 shows the corresponding variation in the half-width of the diffraction maximum.

It is of interest to compare our results with those obtained from the simplified intensity formula (given as Eq. (18) of reference 1). The simplified formula gave $2\theta_m\approx 2\theta_B+2\Delta\sin^2\theta_B=2\theta_B+2\Delta/(1+\cot^2\theta_B)$ and a half-width value of $|\Delta|\sin 2\theta_B$, (compare Eqs. (23) and (25) of reference 1). Thus the rigorous treatment of the lattice model under consideration leads to a somewhat smaller displacement from the Bragg position and to a somewhat smaller half-width than the simplified formula.

It is clear from Eq. (9) that the results which we have just obtained are valid for simple cubic crystals for which $(c_{11}-3c_{12})/5c_{12}\ll 1$. The alkali halides are usually considered fair approximations to simple cubic lattices, particularly if cation and anion do not differ greatly in mass. The elastic coefficients are known for both KCl and NaCl and the Cauchy relation $c_{12}=c_{44}$ holds with great accuracy.[4] The ratio $(c_{11}-3c_{12})/5c_{12}$ has the value 0.58 for KCl and 0.12 for NaCl. The formulas deduced for Case I, accordingly, ought to hold fairly well for NaCl while we are not justified in applying these equations to observations made with KCl. Measurements of the half-widths of the diffuse maxima of NaCl[5] gave distinctly smaller values than were demanded by the simplified formula, but agree with the results obtained above. No really reliable measurements are as yet available for the positions of the diffuse maxima in the case of NaCl.[6] The shift from the Bragg position seems to be definitely established, but the measurements are not sufficiently accurate to justify a detailed comparison with theory. It should be emphasized that the results obtained for Case I are only approximately valid for NaCl. For more accurate results also the second term of Eq. (9) must be considered.

Case II. $c_{11}\gg 3c_{12}$.

When the second term of Eq. (9) is large compared to the first term the following approximation may be used

$$J_2\approx K\frac{3[\sum\alpha_j\beta_j]^2}{(\Delta\sin 2\theta_B)^2\sum H_j^2}\sum_i\frac{H_i^2}{1+(g-1)\alpha_i^2}. \quad (16)$$

The quantity K has the same meaning as in Eq. (13), H_1, H_2, H_3 are the Miller indices of the

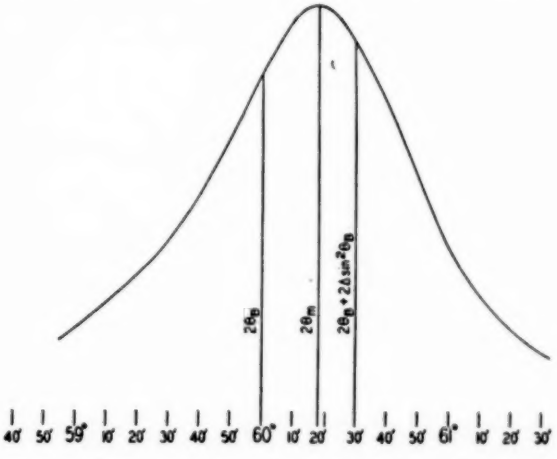

FIG. 2. Diffuse maximum calculated according to Eq. (13). The numerical values $\theta_B=30°$ and $\Delta=1°$ were used. The three vertical lines represent the Bragg scattering angle (60°00′), the location of the diffuse maximum according to Eq. (13) (60°18′) and the position of the maximum according to the simplified intensity formula (60°30′).

[4] W. Voigt, *Lehrbuch der Kristallphysik* (Leipzig, 1910). K. Försterling, Zeits. f. Physik **2**, 172 (1920).

[5] Stanley Siegel and W. H. Zachariasen, Phys. Rev. **57**, 795 (1940).

[6] C. V. Raman and P. Nilakantan, Proc. Ind. Acad. Sci. **12**, 141 (1940); W. H. Zachariasen, Phys. Rev. **59**, 207 (1941); R. Q. Gregg and N. S. Gingrich, Phys. Rev. **59**, 619 (1941).

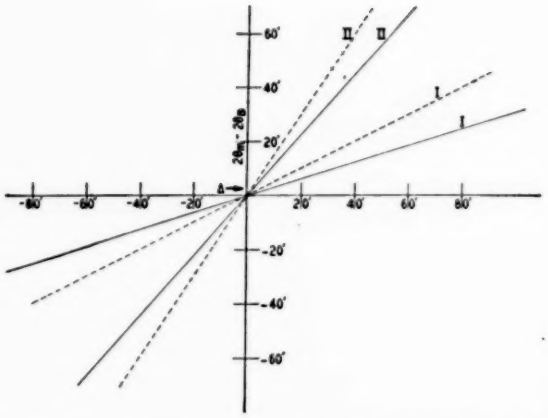

FIG. 3. Deviation from the Bragg scattering angle as function of Δ. Curves *I* are calculated for $\theta_B=30°$, curves *II* for $\theta_B=60°$. The fully drawn lines represent the shift according to Eq. (15), while the dotted lines are obtained from the simplified intensity formula.

lattice plane for which the Bragg equation is nearly satisfied and β_1, β_2, β_3 are the direction cosines of the vector $\lambda\tau_{\min}$. The constant g represents the ratio c_{11}/c_{12}.

It is seen from Eq. (16) that the diffuse maximum in the general case (i.e., when H_1, H_2, H_3 are all different from zero) is composed of three peaks which are connected by saddle-shaped ridges. The α_1, α_2, α_3 values corresponding to the three peaks are approximately 1,0,0, 0,1,0 and 0,0,1. Accordingly we have the following approximate expression for the intensity of scattering at the three peaks, J_A, J_B, J_C

$$J_A\approx\frac{3K\beta_1^2}{(\Delta\sin2\theta_B)^2\sum H_j^2}(H_1^2/g+H_2^2+H_3^2),$$

$$J_B\approx\frac{3K\beta_2^2}{(\Delta\sin2\theta_B)^2\sum H_j^2}(H_1^2+H_2^2/g+H_3^2), \quad (17)$$

$$J_C\approx\frac{3K\beta_3^2}{(\Delta\sin2\theta_B)^2\sum H_j^2}(H_1^2+H_2^2+H_3^2/g).$$

Unless it coincides with a symmetry plane of the crystal, none of the three peaks will lie in the plane of incidence. The positions of the three peaks may be expressed as follows

$$\begin{aligned}\mathbf{u}_m^A&\approx\mathbf{u}_m^0+\Delta\sin2\theta_B[(1/\beta_1-\beta_1)\mathbf{i}-\beta_2\mathbf{j}-\beta_3\mathbf{k}]\\ \mathbf{u}_m^B&\approx\mathbf{u}_m^0+\Delta\sin2\theta_B\\ &\quad\times[-\beta_1\mathbf{i}+(1/\beta_2-\beta_2)\mathbf{j}-\beta_3\mathbf{k}] \quad (18)\\ \mathbf{u}_m^C&\approx\mathbf{u}_m^0+\Delta\sin2\theta_B\\ &\quad\times[-\beta_1\mathbf{i}-\beta_2\mathbf{j}+(1/\beta_3-\beta_3)\mathbf{k}].\end{aligned}$$

In this equation $\mathbf{u}_m^0$ is a unit vector in the plane of incidence corresponding to a scattering angle of $2\theta_B+2\Delta\sin^2\theta_B$, while $\mathbf{u}_m^A$, $\mathbf{u}_m^B$ and $\mathbf{u}_m^C$ represent the scattering directions of the three peaks. The three unit vectors along the cube edges are denoted by **i**, **j**, **k**. It is interesting to consider the variation of the relative intensities and positions of the three peaks as β_1, β_2, β_3 are allowed to change. (β_1, β_2, β_3—we recall—may be set equal to the direction cosines of the scattering direction.) Thus only two peaks come into consideration when the scattering direction lies in a cube face, and only one peak if the scattering direction coincides with a cube edge.

If the reflecting lattice plane has Miller indices (H_1H_20) and if we further assume the plane of incidence to coincide with a cube face (i.e., $\beta_3=0$) and restrict our considerations to this plane then Eq. (16) may be written in the form

$$J_2=\frac{3K\cos^2(\psi-\varphi)}{(\Delta\sin2\theta_B)^2(H_1^2+H_2^2)}\times\left\{\frac{H_1^2}{1+(g-1)\sin^2\varphi}+\frac{H_2^2}{1+(g-1)\cos^2\varphi}\right\}, \quad (19)$$

where $\alpha_1=\sin\varphi$, $\beta_1=\sin\psi$ and thus

$$\psi=\theta_B+\tan^{-1}(H_2/H_1).$$

If we reflect from a cube face (i.e., H_1, 0, 0) the equation simplifies still further and becomes

$$J_2\approx\frac{3K\cos^2(\theta_B-\varphi)}{(\Delta\sin2\theta_B)^2[1+(g-1)\sin^2\varphi]}. \quad (20)$$

Many interesting conclusions can be drawn from the equations given above, but since they are obtained with ease there is no need to enumerate them.

There are, as yet, few observations by means of which the formulae for Case II may be tested. Some data for the diffuse maximum associated with the (111) lattice plane of diamond have been published.[7] The diamond lattice does not—it is true—correspond to a simple cubic lattice. In addition to the three acoustical frequency branches of our lattice model there are in the diamond lattice three optical branches. However,

[7] C. V. Raman and P. Nilakantan, Proc. Ind. Acad. Sci. 11, 389, 398 (1940).

TABLE I. *Observed and calculated scattering angles for the diffuse maxima of diamond.*

θ_i	RADIATION	Δ	$2\theta_m{}^A$ OBSERVED	$2\theta_m{}^A$ CALCULATED
17°11′	α	−4°47′	41°44′	41°49′
	β	−2°34′	38°11′	38°28′
17°48′	α	−4°10′	42°12′	42° 5′
	β	−1°57′	38°48′	38°43′
18°41′	α	−3°17′	42°31′	42°29′
	β	−1° 4′	38°59′	39° 4′
19°53′	α	−2° 5′	43° 5′	43° 1′
20°10′	α	−1°48′	43°12′	43° 8′
20°40′	α	−1°18′	43°23′	43°21′
20°49′	α	−1° 9′	43°32′	43°25′
	β	+1° 4′	40°00′	39°56′
21° 4′	β	+1°19′	40°10′	40° 2′

as far as the diffuse scattering is concerned the three acoustical branches are the important ones and we may therefore with some confidence use the equations for Case II to interpret the observations obtained for diamond. In the experiments of Raman and Nilakantan the incident x-ray beam is approximately parallel to a threefold symmetry axis. Since Cu K radiation was used the actual glancing angle of incidence on three sets of (111) planes differs but little (i.e., by a few degrees) from the Bragg angle. One of the three direction cosines β_1, β_2, β_3 is clearly very much larger than the two others which are approximately equal. Setting $\beta_1 \gg \beta_2 = \beta_3$ we see from Eqs. (17) and (18) that only one of the three peaks, namely J_A, can be observed and this peak will lie in the plane of incidence. We pointed out above that the three peaks are connected by saddle-shaped ridges corresponding, respectively, to $\alpha_1=0$, $\alpha_2=0$, $\alpha_3=0$. Obviously these ridges will appear as diffuse streamers on the photographic plate. The two streamers associated with the peak J_A correspond to $\alpha_2=0$ and to $\alpha_3=0$ and were observed by Raman and Nilakantan who could not explain them. According to Eq. (18) the scattering angle for the peak J_A becomes $2\theta_m{}^A \approx 2\theta_B + \Delta(\tan\theta_B + \tan\chi)\sin 2\theta_B$ where χ is the angle between $\boldsymbol{\tau}_{\min}$ and the unit vector $\mathbf{i}$. With good approximation we may take $\boldsymbol{\tau}_{\min}$ parallel to the direction of scattering for the Laue-Bragg case (i.e., $\chi = \tan^{-1}(3^{-\frac{1}{2}}) - \theta_B$). Consequently we arrive at the following formulae

$$\begin{aligned} &\text{Cu } K\alpha \text{ radiation: } 2\theta_m{}^A \approx 43°\,56' + 0.444\Delta \\ &\text{Cu } K\beta \text{ radiation: } 2\theta_m{}^A \approx 39°\,30' + 0.405\Delta. \end{aligned} \tag{21}$$

The first four columns of Table I contain the experimental data taken from the article by Raman and Nilakantan while the last column contains the theoretical scattering angles calculated by means of Eq. (21). The quantitative agreement is seen to be excellent.

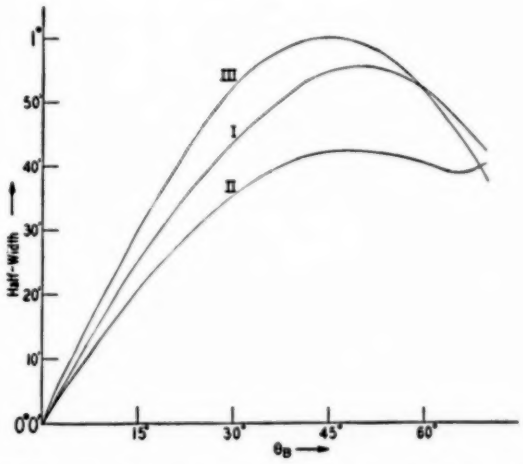

FIG. 4. The half-width of the diffuse maximum as function of θ_B on the assumption $\Delta=1°$. Curves *I* and *II* are obtained from Eq. (13). There are two curves since the diffuse maximum is asymmetrical. Curve *I* represents the half-width on the small angle, curve *II* the half-width on the large angle side of the peak. The half-width as calculated from the simplified intensity formula is shown as curve *III*.

When the direction of the incident x-rays is so chosen that $\beta_1=\beta_2=\beta_3$ the three peaks J_A, J_B, J_C will appear with equal intensity and form an equilateral triangle about the direction $\mathbf{u}_m{}^0$ (compare Eqs. (17) and (18)). Experiments corresponding to this case have recently been reported by Jahn and Lonsdale.[8]

Although we have given a detailed discussion of the temperature diffuse scattering maxima only for two particular cases our treatment demonstrates clearly that a rigorous calculation of the intensity distribution becomes a complicated problem even for crystal lattices of the very simplest types. We have seen that the intensity maxima have a detailed structure which cannot be interpreted in terms of the simplified intensity formula. If the elastic constants are known the intensity distribution in the maxima can be calculated (using Eqs. (5) and (9)) by straightforward methods although extensive numerical computations are involved. Conversely, accurate experimental data will give valuable

[8] H. A. Jahn and K. Lonsdale, Nature **147**, 88 (1941).

information about the elastic constants in cases where these are not already known.

The Temperature Diffuse Scattering Pattern

For most scattering directions the wave vector is so large in magnitude that the approximation given in Eq. (9) cannot be used. In this case the calculations must be based on the general expression for the tensor ϕ given in Eq. (6), and the numerical computations become even more laborious. It is readily seen that the propagation velocities (for given propagation direction) decrease as the wave number increases towards its maximum value. Since the intensity of scattering is inversely proportional to the square of the propagation velocity the effect of the dispersion is to increase the intensity near the minima of the scattering pattern beyond the value calculated from the simplified intensity formula. Of particular interest is the intensity of scattering for very small scattering angles. Raman and Nilakantan[7] claim to have observed a diffuse halo around the forward beam. However, these writers made their observations with mixed continuous and characteristic radiation and it is not clear from their article if care was taken to eliminate air scattering.

When the scattered wave vector $\mathbf{k}$ is so near the incident wave vector $\mathbf{k}_0$ that $\mathbf{k}-\mathbf{k}_0$ lies within the Brillouin zone then vector $\mathbf{B}_H$ of Eq. (2) is zero. For the sake of convenience let the incident x-ray beam be normal to a cube face (i.e., $\mathbf{k}_0 \| \mathbf{j}$) and let us make the observations in another cube face (say in the plane containing vectors $\mathbf{i}$ and $\mathbf{j}$). Let us further assume $a_0 \gg \lambda$, and let $T > \Theta$ so that $Q_j \approx kT$. For scattering angles $2\theta \leq \lambda/2a_0$ we may accordingly set

$$J_2 \approx \frac{I_e kT}{V^2 c_{11}} \frac{2\pi^2 \tau_1^2}{1-\cos 2\pi\tau_1} \delta V, \tag{22}$$

where $2\theta \approx \lambda\tau_1/a_0$. The intensity of scattering is thus constant when τ_1 is very small and increases to more than twice this initial value as τ_1 approaches its maximum value of $\frac{1}{2}$. If the calculations are extended beyond the limiting angle $2\theta = \lambda/2a_0$ one must set $\mathbf{k}-\mathbf{k}_0+\boldsymbol{\tau}_0 = \mathbf{a}_1$ so that Eq. (22) is no longer valid. A simple consideration shows, however, that the intensity of scattering steadily increases with increasing scattering angle until it reaches the maximum value associated with the lattice plane $\mathbf{B}_H = \mathbf{a}_1$. There is thus no intensity maximum associated with the sector $\mathbf{B}_H = 0$ (compare Section 2 of reference 1) and hence theory predicts no halo around the forward beam. Another explanation must therefore be sought for the diffuse ring described by Raman and Nilakantan, and their experiments ought to be repeated with monochromatic radiation and with an evacuated film camera to eliminate effects due to continuous radiation and scattering from the air.

It should be pointed out that accurate intensity measurements for small scattering angles are of special theoretical importance. Measurements of this kind may clearly be used to determine experimentally the dispersion curve and hence the whole frequency spectrum.

In future articles we shall report on detailed calculations for specific crystals in connection with the interpretation of experimental data.

Electron Emission of Metals in Electric Fields

II. Field Dependence of the Surface Photo-Effect

EUGENE GUTH AND CHARLES J. MULLIN
University of Notre Dame, Notre Dame, Indiana

(Received February 27, 1941)

The photoelectric current emitted under the influence of an applied electric field is found to contain a term analogous to the Schottky term for thermionic emission and also a term periodic in the field intensity similar to that recently found and explained for thermionic emission. If frequencies near the threshold are used, then for fields of 3×10^5 volts cm^{-1} the periodic term has a magnitude of about four percent of the nonperiodic part of the current. If the photoelectric threshold frequency for zero field is used to eject the electrons, the resultant plot of the nonperiodic part of the photo-current against the field is a straight line for high field intensities. This line gives the most convenient reference system for observing the periodic term; in addition, the use of the zero field threshold gives the fractional magnitude of the periodic term a relatively large value.

I. INTRODUCTION

IN a recent paper[1] the observed[2,3] periodic deviations from the Schottky line are explained as due to a periodic dependency of the transmission coefficient upon the intensity of the applied field. This periodic behavior of the transmission coefficient may be interpreted as the result of interference of the electron waves reflected from the potential barrier at the surface of the metal. Since this same potential barrier is used in the theory of the surface photoelectric effect, and since the transmission coefficient enters the expression for the photo-current in the same way, a periodic dependence of the photo-current on the applied field, similar to the dependence of the thermionic current, is to be expected. In the present paper the influence of an applied field upon the emitted photo-current is investigated, and an expression for the current is derived. It is found that the current contains the expected periodic term, the fractional magnitude being even larger than with thermionic emission. The effect should be most easily observable for frequencies very near the threshold, for then the fraction of the current due to the periodic term has its largest value.

Some indications of the results to be expected for the field dependence of a photo-current may be seen by considering briefly the analogous problem of thermionic emission. In this case one has

$$i=A_0\bar{D}(F)T^2e^{-\chi/kT}$$

or

$$\log\frac{i(F)}{i(0)}=\frac{e^{\frac{1}{2}}}{kT}F^{\frac{1}{2}}+\log\frac{\bar{D}(F)}{\bar{D}(0)}, \qquad (1)$$

where A_0 is the emission constant $=120$ amp./cm^2; $\bar{D}(F)$ is the transmission coefficient summed over all electron energies greater than that necessary for an electron to escape from the metal; $i(F)$ is the thermionic current at field F and temperature T°K; χ is the thermionic work function at field F. One usually plots $\log i+$const. against $F^{\frac{1}{2}}$. Then, neglecting the variation of $\bar{D}(F)$ with F, one has the result that the plot should be a straight line, known as the Schottky line. The increase of current with field is due to the fact that increasing the field decreases the maximum height of the potential barrier at the metal surface and therefore makes a larger number of electrons available for emission. However, it has been found that the transmission coefficient $\bar{D}(F)$ also varies with F, i.e., with the shape of the barrier; hence, $\bar{D}(F)/\bar{D}(0)\neq1$ and one does not obtain a perfectly straight line from the plot of Eq. (1). Rather, $\bar{D}(F)$ varies periodically with F, so that the plot yields periodic deviations from a straight line. In the theory of photo-emission a similar

[1] E. Guth and C. J. Mullin, Phys. Rev. **59**, 575 (1941).
[2] R. L. E. Seifert and T. E. Phipps, Phys. Rev. **56**, 652 (1939).
[3] D. Turnbull and T. E. Phipps, Phys. Rev. **56**, 663 (1939). Cf. also W. B. Nottingham, Phys. Rev. **57**, 935 (1940).

periodic fluctuation in the photo-current as one changes the intensity of the applied field is to be expected. Experimental data on the field dependence of photo-currents[4] are rather meager and have not as yet disclosed this periodic behavior; in fact, even the photoelectric analog to the Schottky effect does not seem to have been thoroughly investigated.

It is here assumed that the potential traversed by the escaping electron is the usual image+applied field potential which has been so successful in the explanation of thermionic emission; i.e.,

$$V = W_a - (e^2/4x) - eFx. \tag{2}$$

Here W_a is the difference in the potential energy of the electron in the metal and at infinity when $F=0$; x is the distance of the escaping electron from the metal surface; F is the intensity of the applied field; W_a' is the maximum barrier height when the field intensity is F. (We do not consider patch effects which come in for fields from 0 to about 5000 volts or higher, depending upon the wire specimen used.) This potential is shown in Fig. 1 of reference 1. It may now be assumed that the current is given by the expression

$$i \propto \int_{W_a'}^{\infty} N(W)P(W, \nu)D(W, F)dW$$

or

$$i \propto \int_{0}^{\infty} N(\epsilon)P(\epsilon, \nu)D(\epsilon, F)d\epsilon, \tag{3}$$

where W is the normal energy[5] of the electron before it absorbs a photon; $\epsilon = W - W_a' + h\nu$ is the excess of the electron's normal energy $W+h\nu$ (after the electron has absorbed a quantum $h\nu$) over the maximum height of the potential barrier at the emitting surface; $P(\nu, \epsilon)$ is the probability that an electron with normal energy W will absorb a quantum $h\nu$ and become a potential photoelectron; $D(\epsilon, F)$ is the probability that an electron with excess normal energy ϵ over the barrier will escape through the metal surface under the influence of an applied field of intensity F. A particular case of Eq. (3) which is obtained by considering only $F=0$ and assuming that $D(\epsilon, 0)=1$ forms the basis of Fowler's[6] well-known theory of the photoelectric effect which is valid for frequencies in the neighborhood of the threshold. *A priori* reasons do not completely justify Eq. (3); however, Mitchell[7] calculated the current by applying the standard perturbation theory and found that Fowler's procedure, and hence (3) also, gives a good approximation in the neighborhood of the threshold frequency.

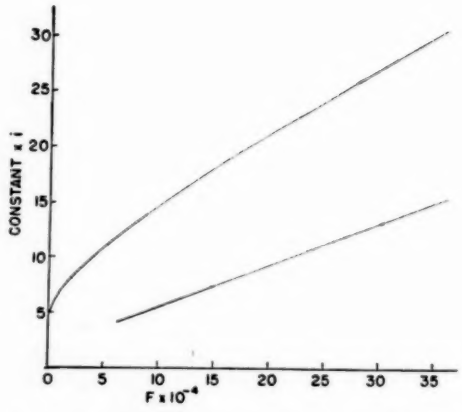

FIG. 1. The photo-current as a function of the applied field. The field intensities F are in volts per cm. The upper curve is for $h\nu - h\nu_0 = 0.1$ ev, the lower for $h\nu - h\nu_0 = 0$. Both curves are plotted with $T = 500°$K.

In Section II of the present paper Fowler's evaluation of the integral in (3) is generalized to include the application of a field. $D(\epsilon, F)$ is taken as unity and the current increase due to the lowering of the potential barrier because of the applied field F is obtained; this is the photoelectric analog to the Schottky effect. In Section III the variation of $D(\epsilon, F)$ with ϵ and F is considered and the resulting expression (17) is found to contain the expected periodic term.

II. Photoelectric Analog of the Schottky Effect

In the first approximation one may assume that all electrons for which $W+h\nu-W_a'>0$ escape from the metal, i.e., $D(\epsilon, F)=1$ for these electrons; furthermore, if one considers values of

[4] The work of E. O. Lawrence and L. B. Linford [Phys. Rev. **36**, 482 (1930)] was an attempt in this direction. Also Dr. R. J. Cashman has informed us that he is investigating the field dependence of the photo-current experimentally.

[5] Here and in what follows we use the expression "normal energy" to mean the part of the energy corresponding to the normal velocity component of the electron.

[6] R. H. Fowler, Phys. Rev. **38**, 45 (1931); or cf. R. H. Fowler, *Statistical Mechanics* (Cambridge University Press and Macmillan, 1936), second edition, pp. 358 ff.

[7] K. Mitchell, Proc. Roy. Soc. **A146**, 442 (1934), and Proc. Camb. Phil. Soc. **31**, 416 (1935).

ν near the threshold value ν_0, then the probability $P(\nu, \epsilon)$ that an electron will absorb a quantum $h\nu$ and become a photoelectron should be independent of the normal energy W of the electron. With such assumptions Fowler[6] has derived an expression for the photo-current emitted at temperature T and frequency ν. His result is

$$i \propto \frac{4\pi mk^2T^2}{h^3}\left\{\frac{\pi^2}{6}+\frac{1}{2}\delta^2 - \left[e^{-\delta}-\frac{e^{-2\delta}}{2^2}+\frac{e^{-3\delta}}{3^2}-\cdots\right]\right\}, \quad \delta \geqslant 0$$

and (4)

$$i \propto \frac{4\pi mk^2T^2}{h^3}\left[e^{-\delta}-\frac{e^{-2\delta}}{2^2}+\frac{e^{-3\delta}}{3^2}-\cdots\right], \quad \delta \leqslant 0$$

where

$$\delta = h(\nu-\nu_0)/kT.$$

If an electric field is applied to the emitting surface, Eq. (4) should again be valid if the zero field threshold ν_0 is replaced by a field dependent threshold ν_0', whose dependence upon the field is given by the relation

$$h\nu_0' = h\nu_0 - e^{\frac{1}{2}}F^{\frac{1}{2}},$$

i.e., we replace δ by

$$\delta' = (h\nu - h\nu_0 + e^{\frac{1}{2}}F^{\frac{1}{2}})/kT. \tag{5}$$

This shift in the threshold frequency arises from the lowering of the potential barrier by the applied field; this corresponds exactly to the decrease of the thermionic work function when the applied field is increased. Since decreasing the barrier height makes more electrons available for emission, an increase in current is expected; this is the analog to the Schottky effect in thermionic emission. There is, however, one essential difference: The number of electrons made available by lowering the barrier is considerably different in the two cases; the thermionic electrons have energies so large that their energy distribution (which determines the number made available by lowering the barrier) is Maxwellian, while on the other hand, the potential photoelectrons have much smaller energies, so that they have a Fermi-Dirac energy distribution. Hence, for photo-currents the current increase observed because of the decrease in the maximum barrier height with increasing field is not expected to be equal to that produced when the same field is applied under similar circumstances to a thermionic filament.

A particularly simple case of the field dependence of the current occurs when

$$\delta' = (h\nu - h\nu_0 + e^{\frac{1}{2}}F^{\frac{1}{2}})/kT \gg 0, \tag{6}$$

so that the bracket term of (4) may be neglected. This condition may be fulfilled for large fields even for values of ν less than ν_0. If this condition is fulfilled, then

$$i \propto \tfrac{1}{6}\pi^2(kT)^2 + \tfrac{1}{2}[h(\nu-\nu_0)]^2 + h(\nu-\nu_0)e^{\frac{1}{2}}F^{\frac{1}{2}} + \tfrac{1}{2}e^3F$$

or

$$i \propto a + bF^{\frac{1}{2}} + cF. \tag{7a}$$

Figure 1 shows the current plotted as a function of F for a particular temperature and for two values of $h(\nu-\nu_0)$. It is to be noted that when $\nu=\nu_0$ the coefficient b in (7a) vanishes, so that the plot of (7a) yields a straight line,

$$i \propto a + cF. \tag{7b}$$

The effect of the field on the current when the condition (6) is not fulfilled may be found by substituting δ' (as given by (5)) for δ in Eq. (4). The expressions (7a) and (7b), and other expressions derived for the field dependency of the current, will hold accurately only for fields above about 10^4 volt/cm, because of the occurrence of patch effects for lower fields.

III. Influence of the Field Dependency of the Transmission Coefficient

If, for convenience, we introduce the following system of atomic units: unit of length $= a = h^2/me^2 = 0.528\text{A} =$ radius of first Bohr orbit in H, unit of energy $= e^2/2a = 13.54$ ev $=$ ionization potential of H, the equation (2) for the potential becomes

$$V = W_a - \frac{1}{2x} - \frac{x}{2x_0^2}. \tag{8}$$

The maximum height of the barrier is then

$$W_a' = W_a - (1/x_0), \tag{9}$$

the term $1/x_0$ being the amount the barrier is lowered by the applied field. The quantity x_0, the

position of the potential maximum, is here used as a variable in place of the field F. The relation between x_0 and F is established by the equation

$$x_0=\tfrac{1}{2}(300e/F)^{\frac{1}{2}}10^8a/0.528, \qquad (10)$$

where F is in volts cm^{-1}. For the field intensities of interest the number of electrons which tunnel through the barrier may be neglected; the photocurrent arises from the electrons which surmount the barrier. Thus, in order that an electron with normal energy W be emitted after absorbing a quantum $h\nu$, it is at least necessary that

$$W+h\nu \geqslant W_a'=W_a-(1/x_0).$$

Hence, according to Eq. (3)

$$i \propto \int_0^\infty N(\epsilon)P(\nu,\epsilon)D(\epsilon,F)d\epsilon$$

with W_a' given by (9).

The value of $N(\epsilon)$ is given by the Fermi-Dirac distribution,[8] and the value of $D(\epsilon, F)$ has been worked out[1] for the barrier of Fig. 1 of reference 1. We give only the results here.

$$N(\epsilon)=\frac{4\pi mkT}{h^3}\log[1+\exp(-[\epsilon+h(\nu_0'-\nu)]/kT)], \qquad (11)$$

$$D(\epsilon,F)=\frac{1}{1+\exp[-2\pi(x_0^3/2)^{\frac{1}{2}}\epsilon]}-\frac{\sqrt{W_a}}{2}\cdot\frac{\exp[-\pi(x_0^3/2)^{\frac{1}{2}}\epsilon]}{(1+\exp[-2\pi(x_0^3/2)^{\frac{1}{2}}\epsilon)^{\frac{1}{2}}]}\cdot\cos v$$

$$-\frac{W_a^4}{16(\epsilon+W_a')^3}\cdot\frac{1}{(1+\exp[-2\pi(x_0^3/2)^{\frac{1}{2}}\epsilon]^2)^2}, \qquad (12)$$

with

$$v=\frac{4\sqrt{2}}{3}x_0^{\frac{1}{2}}-\frac{2}{\sqrt{W_a}}+\tan^{-1}\frac{\sqrt{W_a}}{4}-(\gamma+2\log 2)\left(\frac{x_0^3}{2}\right)^{\frac{1}{2}}\epsilon,$$

where ν_0' is the threshold frequency at field F and is related to the zero field threshold ν_0 by the relation $h\nu_0'=h\nu_0-(1/x_0)$; and $\gamma=$ Euler's constant $=0.5772$.

Thus the only unknown quantity in the expression (4) for the current is the transition probability $P(\nu,\epsilon)$. The work of Mitchell shows that near the threshold the transition probability is independent of the electron energy. Hence, the emitted current is given by the relation

$$i \propto \frac{4\pi mkT}{h^3}\int_0^\infty D(\epsilon,F)\log[1+\exp(-[\epsilon+h(\nu_0'-\nu)]/kT)]d\epsilon \qquad (13)$$

with $D(\epsilon, F)$ given by (12).

We may expand the log into the following forms

$$\log[1+\exp(-[\epsilon+h(\nu_0'-\nu)]/kT)]=\sum_{n=1}^{\infty}\frac{(-1)^{n+1}}{n}\exp(-n[\epsilon+h(\nu_0'-\nu)]/kT) \quad \text{if} \quad \begin{matrix}\nu_0' \geqslant \nu \\ 0 \leqslant \epsilon \leqslant \infty\end{matrix}$$

$$\log[1+\exp(-[\epsilon+h(\nu_0'-\nu)]/kT)]=-\frac{\epsilon}{kT}+\frac{h(\nu-\nu_0')}{kT}+\sum_{n=1}^{\infty}\frac{(-1)^{n+1}}{n}\exp(n[\epsilon-h(\nu-\nu_0')]/kT)$$

$$\text{if} \quad \begin{matrix}\nu \geqslant \nu_0' \\ 0 \leqslant \epsilon \leqslant h(\nu-\nu_0')\end{matrix} \qquad (14)$$

$$\log[1+\exp(-[\epsilon+h(\nu_0'-\nu)]/kT)]=\sum_{n=1}^{\infty}\frac{(-1)^{n+1}}{n}\exp(-n[\epsilon-h(\nu-\nu_0')]/kT) \quad \text{if} \quad \begin{matrix}\nu \geqslant \nu_0' \\ h(\nu-\nu_0') \leqslant \epsilon < \infty.\end{matrix}$$

[8] Cf. R. H. Fowler, *Statistical Mechanics*, (second edition), pp. 341 ff.

We then have the following expressions for the current

$$i \propto \frac{4\pi mkT}{h^3}\left\{\int_0^{h(\nu-\nu_0')} D(\epsilon, F)\left(\frac{h\nu-h\nu_0'-\epsilon}{kT}\right)d\epsilon+\int_0^{h(\nu-\nu_0')} D(\epsilon, F)\sum_{n=1}^{\infty}\frac{(-1)^{n+1}}{n}\exp(n[\epsilon-h(\nu-\nu_0')]/kT)d\epsilon\right.$$

$$\left.+\int_{h(\nu-\nu_0')}^{\infty} D(\epsilon, F)\sum_{n=1}^{\infty}\frac{(-1)^{n+1}}{n}\exp(-[\epsilon-h(\nu-\nu_0')]/kT)d\epsilon\right\} \quad \nu \geqslant \nu_0' \qquad (15)$$

and

$$i \propto \frac{4\pi mkT}{h^3}\int_0^{\infty} D(\epsilon, F)\sum_{n=1}^{\infty}\frac{(-1)^{n+1}}{n}\exp(-n[\epsilon+h(\nu_0'-\nu)]/kT)d\epsilon \quad \nu \leqslant \nu_0'. \qquad (16)$$

For the purposes of summing over the electron energies we may neglect the term $[W_a^4/16(\epsilon+W_a')^3]$ $\cdot(1+\exp[-2\pi(x_0^3/2)^{\frac{1}{4}}\epsilon])^{-2}$; furthermore, we make the approximation

$$(1+\exp[-2\pi(x_0^3/2)^{\frac{1}{4}}\epsilon])^{-\frac{1}{2}} \sim (1-\tfrac{1}{2}\exp[-2\pi(x_0^3/2)^{\frac{1}{4}}\epsilon])\sum_{n=0}^{\infty}(-1)^n\exp[-2n\pi(x_0^3/2)^{\frac{1}{4}}\epsilon].$$

With these approximations we may write

$$D(\epsilon, F) \sim \sum_{k=0}^{\infty}(-1)^k\exp[-2k\pi(x_0^3/2)^{\frac{1}{4}}\epsilon]-\frac{\sqrt{W_a}}{2}\exp[-\pi(x_0^3/2)^{\frac{1}{4}}\epsilon](1-\tfrac{1}{2}\exp[-2\pi(x_0^3/2)^{\frac{1}{4}}\epsilon])$$

$$\sum_{k=0}^{\infty}(-1)^k\exp[-2k\pi(x_0^3/2)^{\frac{1}{4}}\epsilon]\cdot\cos v.$$

The integrations of (15) and (16) may now be carried through in a straightforward manner. The resulting formulae give particularly simple and interesting results when $h(\nu-\nu_0')/kT \gg 0$ so that the condition $\exp[-h(\nu-\nu_0')/kT] \ll 1$ is fulfilled. Note that even if one takes $\nu=\nu_0$, the threshold at zero field, the condition is fulfilled for all values of the field above some relatively small value (since ν_0' decreases as F is increased). For large values of F the condition may be fulfilled with ν chosen even less than ν_0. In the case that $\exp[-h(\nu-\nu_0')/kT] \ll 1$, the integration of (7) yields with good approximation:

$$i \propto \frac{4\pi mk^2T^2}{h^3}\left\{\frac{\pi^2}{6}+\frac{1}{2}\left[\frac{h(\nu-\nu_0')}{kT}\right]^2-\frac{\sqrt{W_a}}{2}\frac{h(\nu-\nu_0')}{(kT)^2}\cdot\frac{\cos u}{\{[\pi(x_0^3/2)^{\frac{1}{4}}+1/kT]^2+(\gamma+2\log 2)^2x_0^3/2\}^{\frac{1}{4}}}\right\}, \qquad (17)$$

where

$$u=\frac{4\sqrt{2}}{3}x_0^{\frac{1}{4}}-\frac{2}{\sqrt{W_a}}+\tan^{-1}\frac{\sqrt{W_a}}{4}-\tan^{-1}\frac{(\gamma+2\log 2)(x_0^3/2)^{\frac{1}{4}}}{[\pi(x_0^3/2)^{\frac{1}{4}}+1/kT]}.$$

The formula (17) gives the desired expression for the photo-current. An expression for the current when the condition $h(\nu-\nu_0')/kT \gg 0$ is not fulfilled is readily obtained from (11) and (12). However, the resulting expressions are rather lengthy and complicated and hence difficult to analyze. For a study of the field dependence of the photo-current using light of a fixed frequency, an analysis of the simple expression (17) is sufficient. In deriving (17) a small temperature-independent term has been neglected in the coefficient of the cosine. This neglect is justified as long as T is more than a few degrees absolute. However, an examination of (17) shows that if T is allowed to become zero, then the neglected term, which is a function only of the field, must be considered in order that the periodic term should not vanish when $T=0$. Thus, if T is so small that

$$\frac{h(\nu-\nu_0')(\pi(x_0^3/2)^{\frac{1}{4}}+1/kT)}{2\{(\pi(x_0^3/2)^{\frac{1}{4}}+1/kT)^2+(\gamma+2\log 2)^2x_0^3/2\}} \ll \frac{1}{\pi^2x_0^3} \qquad (18)$$

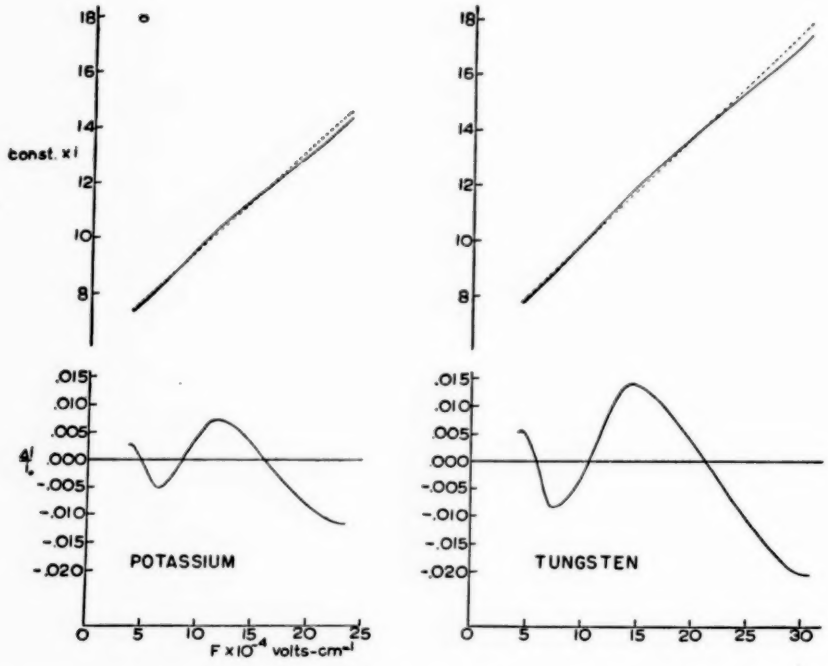

FIG. 2. Field dependence of the photoelectric current. The periodic fluctuation in the current is seen in the upper diagrams. The dotted line shows the nonperiodic part of the current. The lower diagrams show the fractional magnitude of the periodic term, i.e., the periodic term divided by the nonperiodic term. All diagrams are for $\nu=\nu_0$ and $T=300°\text{K}$.

a consideration of the term neglected in (17) gives

$$i\propto\frac{\pi^2}{6}(kT)^2+\frac{1}{2x_0^2}-\frac{\sqrt{W_a}}{\pi^2x_0^3}\cos u. \tag{19}$$

Even for the highest fields considered the inequality (18) is satisfied only if T is very near to the absolute zero.

IV. Discussion of the Results

A comparison of (17), which was obtained by considering the transmission coefficient, and (7), which was obtained by assuming the transmission to be unity, yields the expected result that the change in the transmission coefficient as the shape of the barrier is changed gives rise to a periodic term which causes deviations from the current expected from Eq. (7a). These deviations have values as large as four percent of the total current for fields of 3×10^5 volt/cm. The deviations could be observed most easily in the case where the incident light has a frequency equal to the zero field threshold for the metal; for in this case the equation for the expected current (neglecting the periodic term) has the form

$$i\propto\frac{\pi^2}{6}(kT)^2+\frac{1}{2x_0^2} \tag{20}$$

or since $x_0=\text{const.}\times1/F^{\frac{1}{2}}$

$$i\propto a+cF, \tag{21}$$

where a and c are independent of F. This is the same result as that obtained in Eq. (7b) by assuming that $D(\epsilon, F)=1$. Hence, it is seen that the periodic term arises from the dependence of the transmission probability on energy and field. Equation (21) shows that if $\nu=\nu_0$, a plot of i *versus* F should give a straight line, the simplest reference for observing the deviations. In this case Eq. (17) has the simple form

$$i\propto\frac{\pi^2}{6}(kT)^2+\frac{1}{2x_0^2}-\frac{\sqrt{W_a}}{2x_0}\times\frac{\cos u}{\{(\pi(x_0^3/2)^{\frac{1}{2}}+1/kT]^2+(\gamma+2\log2)^2x_2^3/2\}^{\frac{1}{2}}}. \tag{22}$$

The current, as given by (22) is plotted in Fig. 2 as a function of the field for potassium and tungsten; the dotted portion gives the straight line obtained by neglecting the periodic term. If the periodic term is Δi, and the nonperiodic part of the current i_0, the quantity $\Delta i/i_0$ is then a measure of the fractional deviation from the nonperiodic current; this is also shown in Fig. 2 for potassium and tungsten. It is to be noted that the period of the deviations is the same for

both metals; the positions of the maxima and minima are different because of the difference of W_a values. Both for tungsten and for potassium the W_i values ($W_i = W_a - \chi$ = width of the Fermi band at absolute zero), which are needed to obtain the W_a values, were calculated from the free electron model of a metal, assuming one free electron per atom. This probably gives a good value for potassium, but a value slightly too large for tungsten. The values of χ used were: $\chi = 4.53$ for tungsten, and $\chi = 2.24$ ev for potassium. The quantity $\Delta i/i_0$ is seen to increase as F is increased or as $\nu - \nu_0$ is decreased. Δi itself is nearly independent of temperature, but the temperature dependence of the nonperiodic i_0 makes the fractional deviation $\Delta i/i_0$ dependent on temperature.

Part III of this work on the transition from thermionic to cold emission will appear in the near future.

JUNE 1, 1941 PHYSICAL REVIEW VOLUME 59

Species Classification and Rotational Energy Level Patterns of Non-Linear Triatomic Molecules*

ROBERT S. MULLIKEN
Ryerson Physical Laboratory, University of Chicago, Chicago, Illinois
(Received March 17, 1941)

With the object of making existing knowledge more readily available, the quantized energy levels of symmetrical and asymmetrical tops are discussed from the viewpoint of their classification into species defined by symmetry operations; and simple species nomenclatures are proposed. These are then applied in a discussion of the rotational levels of symmetrical non-linear triatomic molecules AB_2. With SO_2 as an example, the pattern of rotational levels is studied as a function of the apex angle 2α (near-prolate-symmetrical case for large α, oblate or near-oblate case for intermediate α, second near-prolate case for small α). The classification of the *over-all* wave functions with respect to behavior for exchange of equal nuclei and for inversion is then considered. This gives rise to level patterns like those of diatomic and linear molecules in the first near-prolate case, but of interesting unfamiliar types (expected also in molecules such as BCl_3 or NH_3) in the oblate case, and of relatively unfamiliar types (known for the molecule H_2CO) in the second near-prolate case. Rotational-vibrational and rotational-electronic perturbations are discussed in relation to the species classifications. The concept of gyrovibronic species, and a corresponding nomenclature, are introduced. Top selection rules are discussed, using a convenient tabular formulation. Tables are given, for the case of symmetry C_{2v}, showing what types of transitions are allowed by the vibronic selection rules for every type of electronic transition, allowed or forbidden; the use of these tables is illustrated by application to the near-ultraviolet absorption spectrum of formaldehyde. Finally, non-linear ABC molecules are considered.

I. INTRODUCTION

TRIATOMIC molecules AB_2 fall into two types, linear and bent. The quantized rotational and electronic energy levels of *linear* molecules are like those of diatomic molecules, but the vibrational levels introduce new complexities. *Bent* AB_2 molecules rotate like asymmetrical tops, and their rotational levels are arranged and classified accordingly. Often, however, the level patterns are not very different from those of symmetrical-top molecules.

In connection with a program of investigation of electronic spectra and structures of AB_2 molecules, it became desirable to obtain as clear a view as possible of the classification and arrangement of the energy levels as a function of the shape and masses. Although everything necessary is contained either explicitly or implicitly in existing literature,[1,2] these discussions are for the most part not in a form readily available for application. Tables and figures

* Assistance in the preparation of materials was furnished by the personnel of Works Project Administration Official Project No. 665-54-3-387.

[1] See especially D. M. Dennison, Rev. Mod. Phys. **3**, 280 (1931), and references given there.
[2] A. V. Bushkovitch, Phys. Rev. **45**, 545 (1934): bent AB_2 molecules.

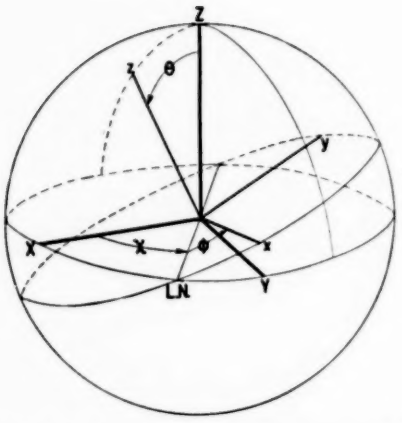

FIG. 1. External and internal top axes, and Eulerian angles. *LN* denotes the positive side of the line of nodes.

showing energy-level patterns and their symmetry properties have therefore been worked out and are presented in this and a subsequent paper. These patterns are in part also applicable to other asymmetrical- and symmetrical-top molecules. The relations between energy levels of linear and bent AB_2 molecules have also been studied (see subsequent paper).

In Fig. 4, the lowest rotational levels for an SO_2 molecule are shown quantitatively as a function of the OSO angle. In another paper to be published shortly, Mr. N. C. Metropolis discusses the structures of electronic bands of SO_2 and similar molecules, as a function of the shape of the molecule in its upper and lower states.

II. WAVE FUNCTIONS OF RIGID TOPS

It will be useful first to go over the subject of symmetrical- and asymmetrical-top molecules in wave mechanics. Let the three principal moments of inertia I be distinguished by symbols a, b, c (small, medium, and large); this represents a slight modification of the set of symbols A, B, C usually used for this purpose. If $I_b=I_a$, the top is oblate-symmetrical; if I_b, I_a, and I_c are all unequal, the top is asymmetrical; if $I_b=I_c$, the top is prolate-symmetrical. The spherical-top case $I_a=I_b=I_c$ will not be specially considered here.

Top wave functions are best written as functions of the three Eulerian angles θ, ϕ, χ which specify the orientation of the principal axes of inertia x, y, z of the top relative to a fixed set of external axes X, Y, Z, both sets of axes having their origin at the center of mass (see Fig. 1). Although various choices are possible, we may best confine ourselves to a right-handed choice of X, Y, Z and to one of a few definite assignments of x, y, z to a, b, c. In this paper we shall use exclusively right-handed assignments with y along b. For symmetrical tops, z will always be taken along the symmetry axis, which is a for the prolate, c for the oblate case. For asymmetrical tops, z will be taken along either a or c.

In group theory nomenclature, all top wave functions belong to representations of the continuous three-dimensional rotation group, or *external rotation group*, corresponding to the infinity of possible rotations of the external axis system X, Y, Z which leave the form of the Schrödinger equation of the top invariant. The external rotation group has infinitely many irreducible representations, one for each J value, with $(2J+1)$-fold degeneracy. J is the familiar quantum number of total angular momentum. Thus we have a species classification according to J values.

Symmetrical-top functions are further classified under the continuous two-dimensional rotation group D_∞ (*internal rotation group* of the symmetrical top). This group has infinitely many representations, one for each K value, except

TABLE I. *Internal species classification for symmetric-top wave functions (point group D_∞). Cf. also E. Bright Wilson, Jr., J. Chem. Phys.* **3**, *282 (1935). The operator C_n^s denotes a rotation around the z axis by an angle $2\pi/n$ ($n=2, 3, 4\cdots\infty$). The operator C_2 refers to a twofold rotation around any axis through the origin and in the x, y plane. The species symbols* Σ, Π, Δ, Φ, $\cdots$ *for $K=0, 1, 2, 3, \cdots$ are taken from the nomenclature for the electronic states of diatomic molecules (symmetry group $C_{\infty v}$ or $D_{\infty h}$, closely related to D_∞); in the diatomic case, K is called* Λ. *The species Σ_1 and Σ_2 occur for even and odd J values, respectively (cf. Table III). In regard to the general arrangement of the table cf. Mulliken, Phys. Rev.* **43**, *288 (1933), except that in the present case the operations have not been completely separated into group theory "classes."*

D_∞	E	∞C_n^s	∞C_2
Σ_1(even J)	1	1	1
Σ_2 (odd J)	1	1	−1
Π	2	$2\cos 2\pi/n$	0
Δ	2	$2\cos 4\pi/n$	0
Φ	2	$2\cos 6\pi/n$	0
.	.	.	.
.	.	.	.
.	.	.	.

that for $K=0$ there are two. The latter are non-degenerate, all others ($K>0$) have twofold degeneracy corresponding to $\pm K$. K is the familiar quantum number associated with the component of angular momentum around the symmetry axis. Table I gives details of the classification and of a convenient species nomenclature.

For the *asymmetrical top*, the internal rotation group is the finite group V composed of four operations, whose four, non-degenerate, representations define four species of wave functions that may conveniently be labeled as in Table II, which is adapted from a table given by Wilson. The labels[3] are the standard ones for group V, except that numerical subscripts for the B representations have been replaced by more descriptive ones, such that any wave function of species B_i is symmetrical for a twofold rotation about the principal inertia axis i ($i=a$, b, or c) but antisymmetrical for a twofold rotation about either of the other two principal axes.

We now turn to the detailed forms of the wave functions. For the symmetric top,[1] the wave functions may be written

$$\psi_{JkM}(\theta, \phi, \chi)=\Theta_{JkM}(\theta)e^{ik\phi}e^{iM\chi}, \qquad (1)$$

where k and M are positive or negative integers, and

$$\Theta_{JkM}(\theta)=N_{JkM}x^{\frac{1}{2}|k-M|}(1-x)^{\frac{1}{2}|k+M|}\sum_0^n a_\nu x^\nu,$$

with

$$n=J-\tfrac{1}{2}|k+M|-\tfrac{1}{2}|k-M|,$$

and $$x=\tfrac{1}{2}(1-\cos\theta). \qquad (2)$$

TABLE II. *Internal species classification for wave functions of rigid asymmetrical top (point group V): cf. Wilson, reference 3. Each operator C_2 refers to a twofold rotation of the internal axis system x, y, z around one of the three principal axes of inertia a, b, c. Each of the axes x, y, z is always directed along one of a, b, c, but the detailed correlation can vary; for the case of AB_2 molecules, cf. Eqs. (18).*

V	E	C_2^c	C_2^b	C_2^a
A	1	1	1	1
B_c	1	1	−1	−1
B_b	1	−1	1	−1
B_a	1	−1	−1	1

[3] E. Bright Wilson, Jr., J. Chem. Phys. **3**, 284 (1935), Table XVIII. Other systems of labels have been used by Casimir (cf. reference 2) and by Dennison (reference 1).

TABLE III. *Classification of symmetric-top wave functions $S_{JKM\gamma}$ of Eqs. (4) under asymmetric-top species. Derived using Tables I, II and Appendix I. The way in which symmetric-top species (first column) transform or split into asymmetric-top species (columns three, four) can also be derived directly from Tables I and II using group theory (cf. e.g. Mulliken, Phys. Rev. **43**, 293–4 (1933)); only the detailed assignment of $S_{JKM\gamma}$'s to asymmetric-top species needs Appendix I.*

Sym.-Top Species	$J+\gamma$ ($\gamma=0$ for $K=0$)	As.-Top Species: Prolate Sym. Top ($z=a$, $K=K_a$)	As.-Top Species: Oblate Sym. Top ($z=c$, $K=K_c$)
Σ_1	even	A	A
Σ_2	odd	B_a	B_c
Π, Φ, etc. (any odd K)	even	B_b	B_b
	odd	B_c	B_a
Δ, Γ, etc. (any even $K>0$)	even	A	A
	odd	B_a	B_c

The ψ's of Eq. (1) exist only for $J\geqq|k|$ and $J\geqq|M|$. In the following it is always to be understood that the positive numerical factor N_{JkM} is such that ψ_{JkM} is normalized, and that the leading term a_0 in the hypergeometric series $\sum_0^n a_\nu x^\nu$ has been taken as $+1$.

Following Van Vleck,[4] we now define, for $k\neq 0$,

$$\overset{\times}{\psi}_{JkM}=(-1)^\beta\psi_{JkM}, \qquad (3)$$

where β is the larger of the two quantities k, M. Let us further define

$$\left.\begin{aligned} S_{JKM}&=2^{-\frac{1}{2}}(\overset{\times}{\psi}_{JKM}+(-1)^\gamma\overset{\times}{\psi}_{J-KM}), \text{ for } K\neq 0,\\ S_{J0M}&=\psi_{J0M} \text{ for } K=0,\end{aligned}\right\} \qquad (4)$$

where $K=|k|$, and γ may be either 0 or 1 (for $K=0$, γ may be regarded as 0). The use of two distinct symbols K and k here helps to clarify the discussion; usually both K and k are denoted by the same symbol K.

If $K=0$, there is one symmetric-top wave function ψ_{J0M} for each value-pair J, M. This belongs to the symmetric-top species Σ_1 or Σ_2 (cf. Table I). If $K>0$ (species II, Δ, and so on), there are two wave functions of equal energy for each value-pair J, M. These may most conveniently be taken either as ψ_{JKM} and ψ_{J-KM} of Eq. (1), or as the two functions S_{JKM} of Eqs. (4).

Every asymmetric-top wave function $A_{J\tau M}$ can be expressed as a linear combination of symmetrical-top functions.[1] These linear combinations become as simple as possible if one builds

[4] Cf. S. C. Wang, Phys. Rev. **34**, 243 (1929).

them from S_{JKM}'s. This is because each S_{JKM} satisfies the requirements for classification under a definite asymmetric-top species, as is not true of the ψ_{JkM}'s. Thus we have

$$A_{J\tau M}=\sum_{K,\gamma} a_{K\gamma}^{JM\tau} S_{JKM\gamma}. \qquad (5)$$

Since any $A_{J\tau M}$ belongs to one of the four species of Table II, only S_{JKM}'s of that particular species have non-vanishing a's in Eq. (5). In general (i.e. for J not very small) there exist several different A_{JM}'s of the same species, characterized by different sets of a's; hence the superscript τ. If two moments of inertia of an asymmetric top approach equality, and if S_{JKM}'s of the nearest symmetric-top case are used in Eq. (5), then one $a^{\tau}_{K\gamma}$ approaches unity and the rest approach zero. Thus for every $A_{J\tau M}$ of a slightly asymmetric top, there is one particular S_{JKM} to which it closely approximates.

More generally, given an asymmetric top with moments of inertia I_a, I_b, I_c, we may imagine the latter to be modified in a continuous manner so that: (a), I_b and I_c both approach $\frac{1}{2}(I_b+I_c)$, leaving I_a unchanged; or (b), so that I_a and I_c both approach $\frac{1}{2}(I_a+I_c)$, leaving I_b; or (c), that I_a and I_b both approach $\frac{1}{2}(I_a+I_b)$, leaving I_c. In case (a) the asymmetric top goes over into a prolate, in case (c) into an oblate symmetric top. In case (b), which, however, is not of practical interest, the asymmetric top may become oblate, prolate, or spherical. A different set of a^{τ}'s is obtained in Eq. (5) according to whether the S_{JKM}'s used correspond to comparison a, b, or c. Omitting comparison b, we then have:

$$A_{J\tau M}=\sum_{K_a,\gamma} a_{K_a\gamma}^{JM\tau} S_{JK_aM\gamma}=\sum_{K_c,\gamma} a_{K_c\gamma}^{JM\tau} S_{JK_cM\gamma}. \qquad (6)$$

The first expansion may be called the prolate expansion, since it is in terms of S's of a prolate symmetric top ($a=z=$symmetry axis; $K=K_a$).

TABLE IV. *Relations among* $(J+\gamma)$, K_a, K_c, *and asymmetrical-top species. (Obtained from last three columns of Table III.)*

SPECIES	$J+\gamma$	K_a	K_c
A	even	even	even
B_b	even	odd	odd
B_a	odd	even	odd
B_c	odd	odd	even

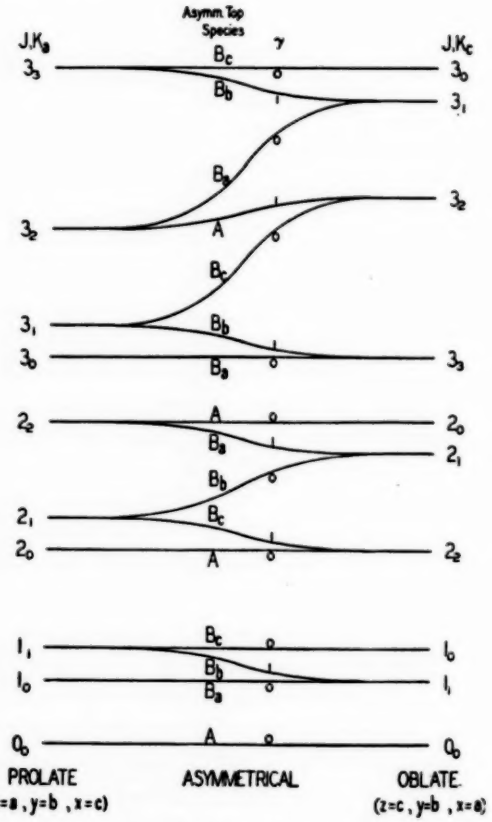

FIG. 2. Species classifications of quantized energy levels of tops, and correlations between prolate-symmetrical, asymmetrical, and oblate-symmetrical levels. The levels are drawn schematically, but for the two symmetrical cases are arranged in qualitative agreement with $BJ(J+1)+CK^2$ (C positive for the prolate, negative for the oblate case). The γ values given are for the S_{JKM} symmetrical-top wave functions (cf. Eqs. (4)) which are used in constructing the asymmetrical-top wave functions as in Eqs. (6). For a given level, γ is the same whether oblate or prolate S_{JKM}'s are used, as can be seen by study of Table IV.

Similarly the second expansion may be called the oblate expansion ($c=z=$symmetry axis; $K=K_c$). The prolate and oblate S's for a given J, K, M are, of course, formally identical but differ in the physical meaning of their Eulerian angles and their K's.

For a *near-prolate* asymmetric top (I_b and I_c much nearer to each other than to I_a), the prolate expansion is of course much the more convergent, while for a *near-oblate* top, the oblate expansion is the more convergent. In both cases, however (and even in the limiting *symmetric*-top cases), either expansion can be used. Often *both* expansions are qualitatively useful for classification purposes (cf. Table IV). For a highly

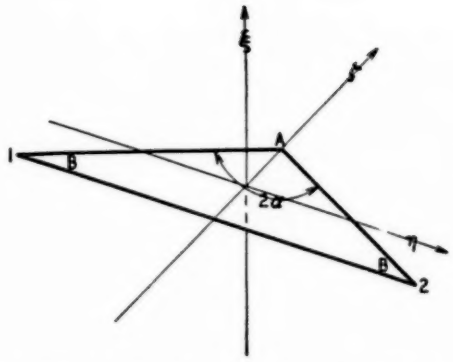

FIG. 3. Fixed internal axes for isosceles AB_2 (cf. Eqs. (7), (18) for relations to top axes). These fixed axes are always to be based on the *equilibrium* configuration of the nuclei shown in the figure, even when the molecule is distorted by vibration.

asymmetrical-top molecule (example, H_2O), there is *in general* little to choose between the two expansions; nevertheless the prolate expansion is then much the more convergent for the highest energy levels of a given J, and the oblate expansion for the lowest.[5]

In expanding according to Eqs. (6), it is necessary to know the classification of any $S_{JKM\gamma}$ according to asymmetric-top species. This can be determined by seeing how the function behaves under the operations of the asymmetric-top group V (see Appendix I); the desired classification can then be made from Table II. The results are given in Table III. They are seen to be independent of M, and to depend only on the evenness or oddness of the quantities $J+\gamma$ and K. Table III shows, however, that, in part, the asymmetric-top species classification of a given $S_{JKM\gamma}$ differs according to whether the K is K_a or K_c.[6]

Table III can be used either to determine what species of asymmetric-top level or levels would result from a symmetric-top level of given species by making the top slightly asymmetrical; or to determine what particular $S_{JKM\gamma}$'s can appear in an expansion like Eqs. (6) for an asymmetric-top function belonging to a given species. For the latter purpose, the content of Table III may more conveniently be rearranged in the form of Table IV.

Table III or IV forms a useful basis for constructing a diagram (Fig. 2) showing how the rotational energy levels of a top must be correlated in passing continuously (with the values of the moments of inertia about the three top axes remaining always in a fixed order) from a prolate through an asymmetric to an oblate case. The asymmetric-top species of each level is of course invariant here to the changes in the moments of inertia. Table IV shows further that, for any given asymmetric-top level, γ in Eqs. (4) and (6) is the same whether the oblate or the prolate expansion is used, so that γ may be regarded as characteristic of the level (cf. Fig. 2).

Finally, Table IV shows how the species classification for an asymmetric-top level is equivalent to a classification according to the evenness or oddness of the K_a and K_c values of the two alternative sets of S_{JKM}'s in terms of which the given asymmetric-top wave function may be expanded. Thus asymmetric-top levels of species A always correspond to K_a, K_c=even, even; species B_b to K_a, K_c=odd, odd; and so on. One may therefore use, instead of the more fundamental definitions of Table II, the evenness or oddness of K_a and K_c to define the four asymmetric-top species.

The possible spectroscopic transitions which can take place for a rigid asymmetrical-top

TABLE V. *Selection-polarization rules for transitions between levels of rigid asymmetrical top. P_c, P_b, P_a mean electric dipole moment along c, b, or a axis; f means forbidden. (Derivation: cf. e.g. R. S. Mulliken, Phys. Rev.* **43**, *290 (1933), noting that P_c, P_b, P_a behave, respectively, according to B_c, B_b, B_a of Table II.)*

	A	B_c	B_b	B_a
A	f	P_c	P_b	P_a
B_c	P_c	f	P_a	P_b
B_b	P_b	P_a	f	P_c
B_a	P_a	P_b	P_c	f

[5] This may be verified by studying the rotational energy level diagram of H_2O as set up by Randall, Dennison, and co-workers (cf. Dennison, Rev. Mod. Phys. **12**, 189 (1940).

[6] This difference has its origin in the fact that the asymmetric-top species are most conveniently classified according to the behavior of the wave functions for rotations of the internal axis system around axes specified by a, b, c (see Table II), while the symmetric-top wave functions must be based on axes in which z is always the symmetry axis, which may coincide with a (prolate case) *or* with c (oblate case). The asymmetric-top species definitions might have been based on rotations around x, y, z (leading to species labels B_x, B_y, B_z), but a given asymmetric-top level would then have two (or more) sets of species labels corresponding to the two (or more) different choices of x, y, z axes for the oblate and prolate expansions. The a, b, c species labels, on the other hand, are unique for a given asymmetric-top level.

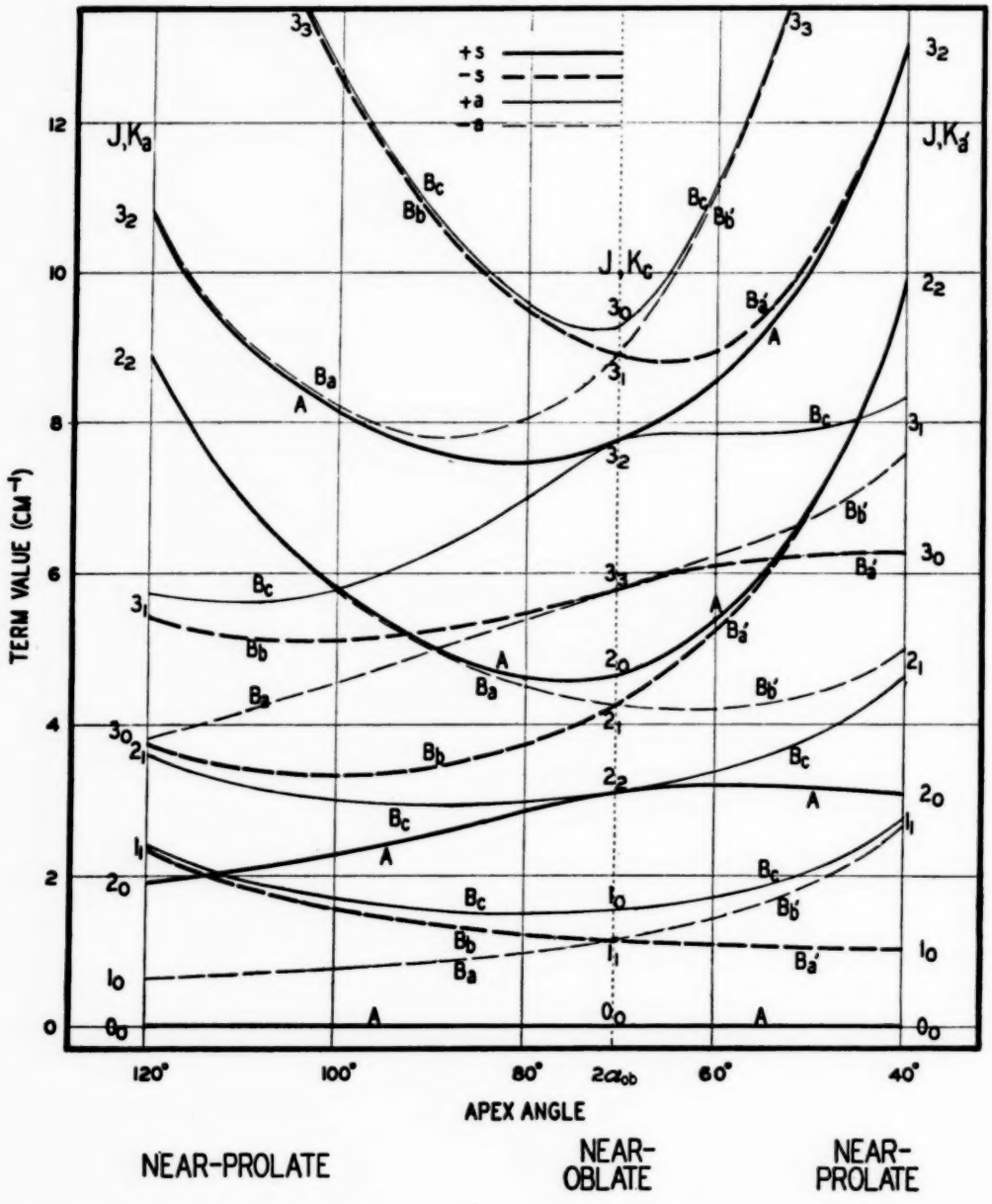

FIG. 4. Rotational energy in cm^{-1} as a function of the apex angle 2α for levels $J=0$ to 3 of an AB_2 molecule. Based on quantitative computations for the molecule SO_2 by Mr. N. C. Metropolis assuming an S—O distance 1.43A for all angles; points on each curve were computed for the angles 120°, 110°, 90°, 72° 32′, 70° 32′, 68° 32′, 50°, and 40°. 70° 32′ is the value of the critical angle $2\alpha_{ob}$ for SO_2. The actual SO_2 molecule has $2\alpha=120°\pm5°$, $r_{SO}=1.434\pm0.02$A according to electron diffraction work (V. Schomaker and D. P. Stevenson, J. Am. Chem. Soc. **62**, 1270 (1940)). Top species labels are given for each curve. Over-all species labels are also indicated by the character of the curves (see legend at top of figure) for the case that the molecule is in a $^1A_1$ vibronic state.

model are subject (for ordinary electric dipole radiation or absorption) to certain well-known polarization and selection rules. These can conveniently be summarized as in Table V. This table has a very simple form because of the way in which the asymmetric-top species have been defined in Table II. In using Table V for actual molecules (cf. Section VII), it must be kept in

mind that, in general, the active dipole moment P for a transition may have components along more than one of the axes a, b, c.

III. Rotational Energy Levels of Bent AB_2 Molecules

The results of Section II can be applied at once to AB_2 molecules in which the two B atoms are equidistant from the A atom. Such molecules rotate like prolate symmetrical tops if the ABA angle 2α is either 0° (hypothetical) or 180° (linear AB_2), and like oblate symmetrical tops for a certain intermediate value of α, say α_{ob}, whose value depends on the masses. For all other values of the apex angle, the molecule rotates like an asymmetric top. A special characteristic of AB_2 molecules, as of other plane molecules, is that $I_c=I_b+I_a$.

In our discussion it will often be necessary to refer to a fixed set of internal axes based on the geometrical symmetry of the molecule in its equilibrium configuration, and independent of α. A suitable right-handed set of axes ξ, η, ζ is shown in Fig. 3. These will be employed directly in connection with the electronic and vibrational wave functions of AB_2, while the sets of top axes needed in connection with the rotational wave functions of AB_2 can all be expressed in terms of ξ, η, ζ.

When the rotational energy levels of an AB_2 molecule are plotted as continuous functions of α, a diagram like Fig. 4 results (the use of various kinds of lines for the curves in Fig. 4 should for the moment be disregarded). Figure 4 has been drawn to scale to correspond to a normal SO_2 molecule, but is typical for bent AB_2 molecules of similar mass distribution. The positions of all levels in the range of J values from 0 to 3 were very kindly computed for this purpose by Mr. N. C. Metropolis from the asymmetrical-top energy equations,[1] for enough different α values to make the forms of the curves quantitatively correct.

Figure 4 is seen to consist of two regions, one to the left and one to the right of the critical angle 70° 32′ ($2\alpha_{ob}$). The left-hand region is qualitatively a replica of Fig. 2, except that the α-scale has been cut off at the left before reaching the true symmetrical-top case at $2\alpha=180°$. If the curves were carried further to the left, all but the lowest would go rapidly upward. Near 180° they would lose all practical meaning, since a strong vibration-rotation interaction sets in which makes it necessary to use a different treatment (cf. subsequent paper).

Inspection of Fig. 4 shows, however, that the arrangement of the rotational levels, even for values of 2α rather far from 180°, approximates closely to the law $BJ(J+1)+CK_a^2$ just as for a true prolate symmetrical top. (B and C of course are functions of α.) This justifies the designation "near-prolate" and the assignment of K_a values as given at the left of the figure. The asymmetry of the near-prolate top is manifested mainly in the splitting into a doublet of each level with $K_a>0$.

The left-hand region of Fig. 4 terminates at its right with the pure oblate case (J, K_c) at $\alpha=\alpha_{ob}$. For α values close to α_{ob} the name "near-oblate" is seen to be appropriate. The figure shows that the near-oblate case covers a much narrower range of α values than the near-prolate case.

In connection with the breadths of the near-prolate and near-oblate ranges, it should be pointed out that Fig. 4, because it is confined to the smallest J values, gives a somewhat deceptive impression. For high J and low K values, these ranges become much narrower (cf., e.g., Fig. 2 of reference 8).

The right-hand region of Fig. 4, like the left-hand region, is qualitatively a replica of Fig. 2, except that the oblate case is at the left and the prolate case at the right. As before, there is a broad near-prolate region but the near-oblate region is narrow.

The two near-prolate cases, i.e. at the left and at the right of Fig. 4, may be distinguished as *obtuse* near-prolate ($2\alpha>90°$) and *acute* near-prolate ($2\alpha<90°$).

Each energy curve in Fig. 4 is labeled according to its asymmetric-top species, assigned on the basis of Table II or IV. It will be noticed, however, that in the right-hand region of the figure, the species B_a and B_b have been labeled $B_{a'}$ and $B_{b'}$, while K_a has been written $K_{a'}$. When a given curve is followed from the left to the right of Fig. 4, the correlation is $A\rightarrow A$, $B_c\rightarrow B_c$, but $B_a\rightarrow B_{b'}$ and $B_b\rightarrow B_{a'}$. The reason

for this and for the use of the primes is that, while the large moment of inertia axis c remains always along ξ of Fig. 3, the small and medium axes of inertia exchange places in passing through α_{ob} ($a \rightarrow b'$, $b \rightarrow a'$). If one had labeled the B species with subscripts ξ, η, ζ in accordance with the axes of Fig. 3, then the $B_\eta(B_a)$ and $B_\xi(B_b)$ curves would have remained B_η and B_ξ, respectively, in going through α_{ob} in Fig. 4.

The doublets which occur when $K_c > 0$ show interesting behavior on passing through $\alpha = \alpha_{ob}$. Doublets consisting of an A and a B_c curve, which occur for even K_c values, make an osculatory contact at $\alpha = \alpha_{ob}$. On the other hand, doublets consisting of a B_a and a B_b curve, which occur for odd K_c values, intersect each other as they pass through α_{ob} and respectively become $B_{b'}$ and $B_{a'}$.

It is now of interest to consider in more detail the rotational wave functions, constructed as linear combinations of symmetric-top S_{JKM}'s. Figure 4 implies the use of four different sets of S_{JKM}'s which, though formally identical, involve four different ways of choosing the Eulerian angles, based on four different sets of internal top axes x, y, z, as follows:

1. Obtuse near-prolate case:
$$z = -\eta,\ y = \zeta,\ x = \xi.$$
2. Near-oblate case with $\alpha > \alpha_{ob}$:
$$z = \xi,\ y = \zeta,\ x = \eta.$$
3. Near-oblate case with $\alpha < \alpha_{ob}$: (7)
$$z = \xi,\ y = -\eta,\ x = \zeta.$$
4. Acute near-prolate case:
$$z = \zeta,\ y = \eta,\ x = \xi.$$

In the pure oblate case ($\alpha = \alpha_{ob}$), either of the choices 2 and 3,—which differ only by a 90° rotation of the axes x and y around z,—is equally valid. One must, however, be careful to note which choice has been made, since ϕ is $\pi/2$ greater in choice 3 than in choice 2 (θ and χ are not affected). A result of this is that γ in Eq. (4) for a given oblate S_{JKM} based on choice 2 is in general altered to, say, γ' if one transforms this S_{JKM} to the basis of choice 3. As has been shown in Section II, the S_{JKM}'s in terms of which any given asymmetric-top wave function can be expanded have a definite γ which is independent of whether the prolate or oblate expansion is used. Applied to bent AB_2 this means that for a definite asymmetric-top energy level curve, γ is identical for choices 1 and 2, and γ' is identical for choices 3 and 4, but γ and γ' may differ.

TABLE VI. *Species of group I. Known as "parity" species.*

I	E	I
+	1	1
−	1	−1

TABLE VII. *Species of group P_2.*

P_2	E	P_2
s	1	1
a	1	−1

IV. Over-All Species Classifications of Rotational Levels of Symmetrical Bent AB_2 and Related Molecules

The wave function ψ of an isosceles bent AB_2 molecule may be expressed as a product of factors, plus small correction terms:

$$\psi = \psi_{evr}\psi_{ns} = [\psi_r\psi_{ev} + \psi'_{evr}]\psi_{ns}. \qquad (8)$$

In Eq. (8), a further factor depending on the coordinates of the center of mass has been omitted. ψ_{ns} represents the nuclear "spin" characteristics. A very small correction term ψ'_{evrns} may be neglected. ψ_r is the rotational wave function, which (except for minor modification to allow for non-rigidity) may be taken in accordance with Eq. (6). The *vibronic* wave function ψ_{ev} is a function of the electronic and vibrational coordinates. ψ'_{evr} is a small correction function which takes care of interactions between the rotational and the other internal degrees of freedom.

The complete ψ of Eq. (8), as well as each of its approximate factors and their sub-factors, is subject to a species classification based on a consideration of the behavior of the wave function under each of a group of operations to which the form of the corresponding Schrödinger equation is invariant. The classification for ψ_r has already been discussed. That for ψ_{ns}, and its consequences, will be assumed known. It will always be assumed in the following that we are dealing with *singlet* electronic states, and that all the wave functions considered are antisymmetrical in the electrons.

Let us consider first the classification of ψ_{evr}. The Schrödinger equation is invariant under (*a*) a three-dimensional rotation group; (*b*) an inversion group I; (*c*) a nuclear permutation group P_2. Group (*a*) consists of all possible rotations of the axis system X, Y, Z about its

origin, and gives rise to the J species classification, which is characteristic equally of ψ_r and ψ_{evr}. Groups (b) and (c) each consist of the identity operation E and one other operation, namely for (b) the inversion I of the axis system X, Y, Z at its origin, i.e. a reversal of the positive directions of all three axes, and for (c) an exchange of labels (P_2) between the two B nuclei. Groups (b) and (c) each give rise to a classification of ψ_{evr} into two species (cf. Tables VI, VII); together, they give a fourfold classification which, with the J classification, constitute the rigorous *over-all* species classification for ψ_{evr}. Commonly we shall use the term "over-all" for the I and P_2 classification alone, the J classification being taken for granted.

The internal ψ_r or *top*-species classifications discussed in Section II are no longer quite rigorous, since ψ_{evr} can be factored only approximately. A similar remark applies to the vibronic classification. Nevertheless, if the top and the vibronic species can be given for any level, then the over-all species is definitely determined. (The converse is not true.)

In general, a complete classification and set of selection rules is obtained by using top and vibronic species. Hence the addition of the over-all species classification and selection rules ($+ \leftrightarrow -$; $s \leftrightarrow s$ and $a \leftrightarrow a$) may seem superfluous. However, the use of the fourfold over-all species classification for AB_2 molecules *instead of* the fourfold asymmetric-top classification has much to recommend it. For one thing, the over-all species have rigorous validity, while the top species do not. Although usually this distinction is unimportant, nevertheless in special cases involving strong vibration-rotation or vibronic-rotation interactions, the top-species classification breaks down. Even in less extreme cases, perturbations can occur between levels alike in their over-all species classification but differing in their top and vibronic species. Further, the classification under P_2 (or under P_n for molecules with n equal nuclei)[7] is necessary in determining the statistical weights of levels.

In current practice, the over-all species classification is used in every band spectrum analysis for diatomic molecules, but is ignored in polyatomic spectra in favor of the top-species classification, plus the partially duplicating P_n classification. In view of what has been said above, it would seem desirable to make the use of the over-all classification and selection rules a standard practice for polyatomic molecules. But a study also of the top-species classification is desirable in understanding the rotational levels and wave functions. And in molecules where there is no P_n classification (e.g. ABC molecules, —cf. Section VI), the over-all species classification cannot completely replace the top-species classification.

In order to determine how over-all are related to top and vibronic classifications for bent AB_2, it is necessary first to analyze the operators I and P_2 each into a product of factors which can act on ψ_r and ψ_{ev} separately. The results (see Appendix II) are as follows:

$$I = C_2^{\xi}\sigma^{\xi}, \quad P_2 = C_2^{\zeta}\Gamma_2^{\zeta}, \tag{9}$$

where $C_2^{\xi} \equiv C_2^{c}$, and $C_2^{\zeta} \equiv C_2^{b}$ (for $\alpha > \alpha_{ob}$) or $C_2^{a'}$ (for $\alpha < \alpha_{ob}$) are two of the twofold rotations of Table II, acting on the top reference axes x, y, z. Further, σ^{ξ} represents a reflection in a plane perpendicular to the ξ axis, i.e. in the plane of the molecule, acting on the vibronic reference axes ξ, η, ζ. Γ_2^{ζ} represents a twofold rotation around the ζ axis. That is, Γ_2^{ζ} is just like C_2^{ζ} except that it acts on the axis system of ψ_{ev} instead of on that of ψ_r.

Thus the first of the two factors of I or P_2 in Eqs. (9) acts on ψ_r, the second on ψ_{ev}. Since all wave functions of bent AB_2 are non-degenerate, —except for the M degeneracy, which does not

TABLE VIII. *Vibrational, electronic, or vibronic species. Cf. R. S. Mulliken, Phys. Rev.* **43**, *288 (1933) for the electronic case and for the selection rules (the axes are there called x, y, z instead of ξ, η, ζ, and Γ_2 is called C_2). The vibrational case is the same except that the operators act on nuclear vibrational displacement coordinates (see Appendix II). In the vibronic case, the operators act simultaneously on electronic position coordinates and nuclear displacement coordinates. In the vibrational case the group, strictly speaking, is C_s (operations E and σ^{η} only), but it can be treated as C_{2v} if the two species which are antisymmetrical to σ^{ξ} are excluded, leaving only A_1 and B_2.*

C_{2v}	E	Γ_2^{ζ}	σ^{ξ}	σ^{η}
A_1	1	1	1	1
A_2	1	1	−1	−1
B_1	1	−1	−1	1
B_2	1	−1	1	−1

[7] Cf. reference 1, Section 3.

trouble us, since the operators under discussion do not change the part of the wave function which contains M,—the effect of every operator (C_2, σ, Γ, or the complete I or P_2) is merely to multiply the wave function on which it acts by either $+$ or -1.

Let us for the moment indicate the effects of the vibronic operators σ^ξ or Γ_2^ζ by $\chi(\sigma)$ or $\chi(\Gamma)$. The effects of the C_2 operators on ψ_r can be immediately determined as functions of J, γ or γ', and K_η, K_ξ, or K_ζ, by using Table I or II with due regard to the choice of top axes which may be appropriate (cf. Eqs. (7) and discussion following). At this point K_η, K_ξ, K_ζ, respectively, have been introduced in place of the equivalent designations K_a, K_c, $K_{a'}$, because of their greater general convenience.

The effect of the operator I or P_2 is obtained by multiplying the effects of its two factors. In this way we obtain

$$\begin{aligned} I\psi_{evr} &= [(-1)^\delta \chi(\sigma^\xi)]\psi_{evr}; \\ P_2\psi_{evr} &= [(-1)^\epsilon \chi(\Gamma_2^\zeta)]\psi_{evr}, \end{aligned} \tag{10}$$

with

$$\left.\begin{aligned} &\delta = J+\gamma+K_\eta \quad \text{for} \quad \alpha > \alpha_{ob}, \\ &\delta = K_\xi = J+\gamma'+K_\zeta \quad \text{for} \quad \alpha < \alpha_{ob}, \\ &\epsilon = J+\gamma \quad \text{for} \quad \alpha > \alpha_{ob}, \\ &\epsilon = J+\gamma'+K_\xi = K_\zeta \quad \text{for} \quad \alpha < \alpha_{ob}. \end{aligned}\right\} \tag{11}$$

For an A_1 (*totally symmetrical*) vibronic state, by definition (cf. Table VIII), χ is $+1$ for σ^ξ and Γ_2^ζ, so that we can drop the χ factors of Eqs. (10). The over-all species classifications of all rotational levels can then be determined by reference to Eqs. (10)–(11) and Tables VI–VII. The results are shown in the energy curves of Fig. 4 by the use of heavy and light, full or dashed lines.

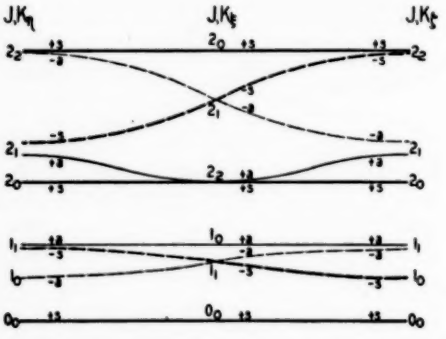

FIG. 5. Schematic simplification of lower levels ($J=0$ to 2) of Fig. 4, with omission of asymmetric-top species labels and addition of over-all species labels. The K subscripts η, ξ, ζ in the J, K headings are based on Fig. 3; they are respectively equivalent to a, c, a' of Fig. 4.

Figure 5 is a schematic simplified version of Fig. 4, with the $J=3$ levels and the top-species labels omitted, but with the over-all species labels ($+s$ etc.) added. It will be noted that energy curves belonging to a given over-all species pass in a continuous manner through the critical angle α_{ob}, each intersecting another curve at α_{ob} if K_ξ is odd, or else making an osculating contact if K_ξ is even and greater than zero.

Of considerable interest is the pattern of over-all species character as a function of J and K. Obtuse near-prolate AB_2 molecules ($K=K_\eta$) are found to show the same kind of pattern as linear AB_2 and diatomic molecules. The I species or "parity" (cf. Table VI) is given for $K=0$ by $(-1)^J$, while for $K>0$ each K doublet consists of one $+$ and one $-$ component. Further, the K doublets (like the analogous Λ doublets of diatomic molecules) consist of pairs $+s$, $-a$ or else $+a$, $-s$.

Acute near-prolate AB_2 molecules ($K=K_\zeta$) show the same patterns as obtuse near-prolate molecules so far as parity is concerned, but are entirely different in respect to P_2 classification. Although in the obtuse case the P_2 species (cf. Table VII) alternates with J for $K=0$ and the K doublets contain one s, one a component for $K>0$, in the acute case the P_2 species depends only on K (s for even, a for odd K_ζ). This difference is important for the appearance of bands, since the P_2 species, in conjunction with ψ_{ns}, determines the location of missing or weak rotational levels and band lines.

SO_2 in its normal state ($2\alpha=120°$) constitutes an example of the obtuse near-prolate case. Since the oxygen nuclear spins are zero, all a levels are missing, and only s levels are present. A well-known molecule which has rotational behavior essentially like that of acute near-prolate AB_2 is the Y-shaped molecule formaldehyde (H_2CO). If axes analogous to those in Fig. 4 are used, the ζ axis (bisecting the HCH angle) is the axis of smallest moment of inertia a, and the line joining the two identical H nuclei is parallel to the η axis. These relations are exactly like those in acute near-prolate AB_2, and the corresponding alternation with K in the

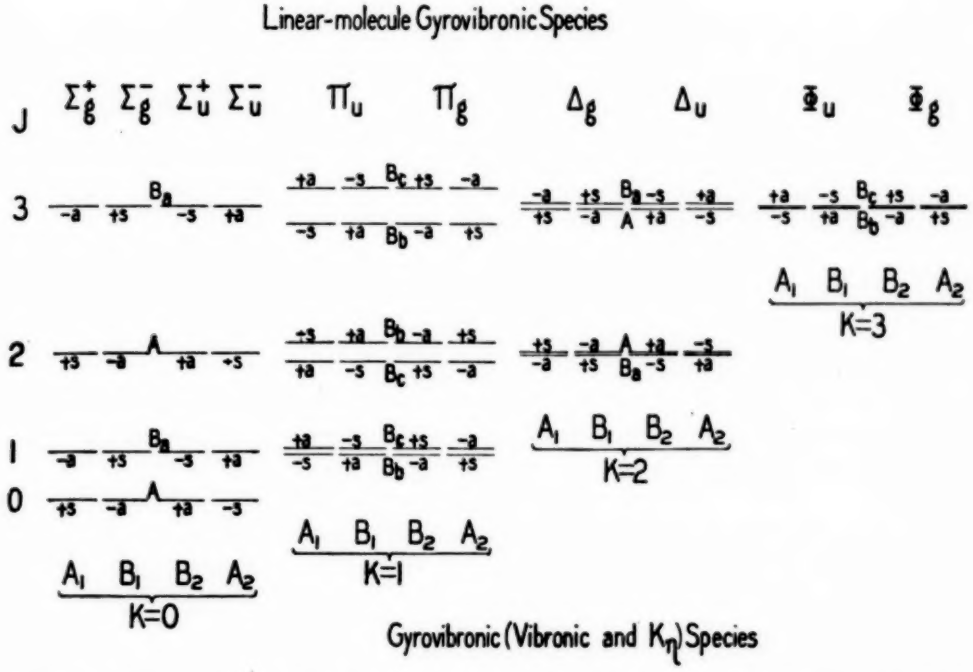

FIG. 6. Arrangement of bent AB_2 rotational levels, with their over-all and asymmetric-top species classifications, for the four vibronic species and for several K_η values (see descriptions at bottom of figure). Each column represents a different gyrovibronic species of near-prolate AB_2. Doublet separations are shown qualitatively correctly for near-prolate AB_2. At the top of each column is given the label for that gyrovibronic species of linear AB_2 which has qualitatively the same pattern of over-all species ($+$, $-$, s, a) as appears in the column in question.

statistical weights of levels and intensities of sub-bands has been used, and verified, in the analysis of the formaldehyde spectrum.[8]

Still a third pattern of over-all species character is found for oblate or near-oblate AB_2 ($K=K_\xi$). Here, unlike both the prolate cases, the parity is independent of J, being given by $(-1)^{K_\xi}$, and both components of a K doublet have the same parity. On the other hand, the components of every K doublet differ in P_2 classification (one s, one a) just as in the obtuse near-prolate case (see Fig. 5). The same behavior must occur also in other oblate-top molecules, for example BCl_3 (plane) or NH_3 (pyramidal). In these molecules the s, a classification, however, is replaced by another. Further, the tunnel effect causes in NH_3 an additional doubling of every level, the upper component of each tunnel doublet being of reversed parity, so that now for each J value there is a $+$ and a $-$ level if $K=0$, two of each if $K>0$.

[8] G. H. Dieke and G. B. Kistiakowsky, Phys. Rev. **45**, 4 (1934); etc.

V. Effect of Vibronic State on Over-All Species Patterns. Gyrovibronic Species. Rotational-Vibrational Perturbations

Figures 4 and 5 and the foregoing discussion apply to totally symmetrical singlet ($^1A_1$) vibronic states. For other singlet states of AB_2 molecules, Figs. 4 and 5 need to be modified only by the reversal, *throughout*, of one or both of the over-all species labels. For molecules such as BCl_3 and NH_3, however, new complications can arise as a result of degeneracy in the vibronic states.

In determining the dependence of over-all species on vibronic species for bent AB_2, we first review the definitions of the four vibronic species (cf. Table VIII). These are based on the

TABLE IX. *Vibronic species for* AB_2 *molecules.*

C_{2v}	$^1A_1$	$^1A_2$	$^1B_1$	$^1B_2$
$^3A_1$	$^{3v}A_1$	$^{3v}A_2$	$^{3v}B_1$	$^{3v}B_2$
$^3B_2$	$^{3v}B_2$	$^{3v}B_1$	$^{3v}A_2$	$^{3v}A_1$

behavior of ψ_{ev} under operations of its symmetry group C_{2v}. Referring to Table VIII, we find that $\chi(\sigma^\xi)=1$ in Eqs. (10) corresponds to A_1 or B_2 vibronic states, $\chi(\sigma^\xi)=-1$ to A_2 or B_1 states. Similarly, $\chi(\Gamma_2^\xi)$ is $+1$ for A_1 and A_2 states and -1 for B_1 and B_2 states.

With this information, the over-all species labels in Fig. 4 or 5 can be modified to correspond to vibronic states other than A_1. The results, for J values from 0 to 3, are shown in Fig. 6 *for the obtuse near-prolate case* ($K=K_\eta$). (The caption and labels at the top of Fig. 6 should for the moment be disregarded.) In Fig. 6, the rotational levels have been sorted out according to K values, so as to display more clearly the over-all species patterns as functions of J and K separately. Similar figures for the oblate and the acute near-prolate cases can be readily constructed, but will not be given here.

In connection with Fig. 6, the concept of *gyrovibronic species* may be introduced. This is conveniently defined so that for near-prolate AB_2 there is a different gyrovibronic species for each different combination of K value and vibronic species, i.e. one gyrovibronic species for each column in Fig. 6.

In using Table VIII and Fig. 6, the vibronic species may first be determined from the electronic and vibrational species, if these are known. We have

$$\psi_{ev}=\psi_e\psi_v+\psi'_{ev}, \qquad (12)$$

with electronic, vibrational and vibronic species all classified as in Table VIII. To distinguish the three cases, prefixes can if necessary be added to the species symbols, e.g. ${}^eA_1$, ${}^vB_2$, ${}^{ev}A_2$.[9] The relations between ψ_e, ψ_v, and ψ_{ev} species (see Table IX) are easily obtained.

It may be appropriate here to remind the reader of the three vibrational modes for bent AB_2,—a symmetrical valence mode ν_s, an antisymmetrical valence mode ν_a, and a deformation (angular variation) mode ν_d. These modes have the same species classification as ψ_v itself. If we use small letters for the modal species,[9] ν_s and ν_d belong to the species a_1, ν_a to b_2. ψ_v then belongs to the species ${}^vA_1$ or ${}^vB_2$ according as an even or an odd number of quanta of ν_a are excited.

Figure 6 is helpful for a better understanding of certain types of perturbations in AB_2 molecules. As an example, consider the ${}^1A_1$ vibronic state with $v_a=v_d=0$, $v_s=1$ and the ${}^1B_2$ vibronic state with $v_a=1$, $v_d=v_s=0$, for the H_2O molecule in its normal (${}^1A_1$) electronic state. These states lie close together, and are known to perturb each other strongly, the perturbation being classed as a rotation-vibration interaction.[10] In Fig. 6, for any J value, consider the levels belonging to an A_1 and a B_2 vibronic state. For $K_\eta=1$ of A_1, we have a $+a$ and a $-s$ level, of top species B_c and B_b, respectively. For $K_\eta=2$ of B_2 we likewise have a $+a$ and a $-s$ level, but now of top species A and B_a, respectively; and for $K_\eta=0$ of B_2 a $+a$, of the top species A. Systematic perturbations can now occur between the $+a$ levels, and between the $-s$ levels, for each J value, even though the top species are different in each such case. A similar discussion can be given for $K_\eta=1$ of B_2, and for other levels. Actually, fairly large perturbations of this kind occur for the H_2O levels mentioned, markedly impairing the top-species classifications.

The H_2O molecule as a top is highly asymmetric, and can be understood almost equally well in terms of the near-oblate or the near-prolate approximation. If one constructs a diagram similar to Fig. 6 but for near-oblate AB_2, it is found that the perturbations just discussed are now between levels of *the same* K (here K_ξ). For instance, for $K_\xi=1$, each J value gives one $-s$ and one $-a$ level, for either an A_1 or a B_2 vibronic state. In the former the $-s$ is B_b, the $-a$ is B_a, in the latter the relation is reversed. The resulting perturbations can be shown to correspond to a partial development of vibrational angular momentum around the ξ axis.[10]

A similar situation is found if, using Fig. 6, we consider two near-by vibronic states of near-prolate AB_2, one of species A_1, the other B_1. This of course requires electronic excitation, since vibration alone cannot give a B_1 state. For $K_\eta=1$ (and any J value), the A_1 state gives a $-s$, B_b and a $+a$, B_c level while the B_1 state gives a $-s$, B_c and a $+a$, B_b level. Systematic

[9] R. S. Mulliken, J. Phys. Chem. **41**, 159 (1937).

[10] E. Bright Wilson, Jr., J. Chem. Phys. **4**, 313 (1936); H. H. Nielsen, J. Chem. Phys. **5**, 818 (1937); W. H. Shaffer and H. H. Nielsen, Phys. Rev. **56**, 188 (1939); B. T. Darling and D. M. Dennison, Phys. Rev. **57**, 128 (1940).

TABLE X. *Top selection rules for bent* ABC *molecules.*

	A, B_c	B_a, B_b
A, B_c	P_c	P_{ab}
B_a, B_b	P_{ab}	P_c

perturbations are thus possible. Here there is an interesting possibility: it can be shown (see subsequent paper mentioned above) that a Π_u electronic state of linear AB_2 splits into an A_1 and a B_1 electronic state of bent AB_2. Conversely, the mutual perturbation between suitable A_1 and B_1 levels of bent AB_2, in the manner discussed above, represents the first step in a transformation of wave functions toward those of a Π_u electronic state of linear AB_2. It can be shown that during the completion of this process, the asymmetric-top species classifications of bent AB_2 are completely destroyed by 50–50 mixing of wave functions of different species, while concomitantly the electronic angular momentum around the η axis appropriate to a Π state is developed.

This leads to an explanation of the caption and symbolism at the top of Fig. 6. As already noted, each column in Fig. 6 belongs to a different gyrovibronic species of near-prolate AB_2. Now on comparing the patterns of over-all species labels as functions of J with patterns for various vibronic species of linear AB_2, it is found that each column shows identically the same pattern as the linear AB_2 vibronic species whose symbol has been placed at the head of the column. In every case, K_η of bent AB_2 is the same as K for the linear AB_2 species with the same pattern. In all cases with $K_\eta > 0$, there are *two* columns (e.g. A_1 and B_1 with $K_\eta = 1$) whose over-all species patterns are qualitatively identical. In bent AB_2 these differ in energy-order of doublets and in asymmetric-top species, but both these differences disappear for linear AB_2, —the latter in the way we have seen, the former because K doubling due to asymmetry is not present for linear AB_2.

As is pointed out in the subsequent paper, the vibronic species labels of linear AB_2 are at the same time gyrovibronic species labels. Thus the two sets of labels at the top and bottom of Fig. 6 correspond to a set of relations between the gyrovibronic species of linear AB_2 and those of obtuse-prolate AB_2.

VI. Rotational Levels of Unsymmetrical Triatomic Molecules

With certain modifications, the whole of the foregoing discussion is applicable to unsymmetrical bent triatomic molecules (ABC or non-isosceles AB_2). In general such molecules are asymmetrical-top rotators, but may fall under near-prolate or near-oblate cases, or under the rigorous oblate case, depending on the masses and the shape of the triangle. Figures 1 and 2 and Table II are applicable without change.

Figure 3 requires modification. The ξ axis remains perpendicular to the molecule plane, but since there is no longer a symmetry axis to define ζ, we can only say that η and ζ must be chosen with one along the a, the other along the b axis of inertia. Of the three angles of the triangle, any one can be taken as the "apex angle" 2α. If, however, there is a "central atom" to which the others are chemically bound, the apex angle can best be taken at this atom.

Whichever angle is taken as apex angle, figures very similar to Figs. 4 and 5 can be constructed, keeping the lengths of two sides of the triangle constant and varying the angle 2α between them. If a definite choice of the axes η and ζ is made at some definite value of α, then Eqs. (7) hold for various possible choices of top axes x, y, z.

In Figs. 4–6, and Eqs. (9)–(11), the over-all species classification based on a group P_2 and giving rise to the labels s, a now disappears. If one considers any two curves in Fig. 4 for symmetrical AB_2 which cross or touch at $\alpha = \alpha_{ob}$, it is seen that these are alike in parity (both $+$, or both $-$), but differ in their P_2 labels. The disappearance of the latter in the unsymmetrical case means that two such curves are now identical in over-all species and, according to a well-known rule of wave mechanics, can no longer touch or cross. Yet it is also seen that the members of every such pair of curves still belong to different top species, and this tends to permit touching or crossing. Avoidance of contact is brought about only because of the lack of rigor in the factoring of ψ_{evr} into $\psi_r \psi_{ev}$ in

TABLE XI. *Directions of polarization (ζ = symmetry axis; f = forbidden) for various possible types of vibrational transitions allowed by vibronic selection rules, for electronic transitions between an ${}^{e}A_1$ state and each of the four species of electronic states. Obtained by determining vibronic states and applying their selection rules (cf. Tables VIII, IX and reference there); for example, ${}^{e}A_1{}^{v}B_2 \rightarrow {}^{e}A_2{}^{v}B_1$ is ${}^{ev}B_2 \rightarrow {}^{ev}B_2$, which in vibronic approximation is allowed with ζ polarization. The bold-faced symbols in the table denote transitions allowed by the electronic as well as the vibronic selection rules; all others are forbidden by the electronic rules.*

C_{2v}		${}^{e}A_1$				${}^{e}A_2$				${}^{e}B_1$				${}^{e}B_2$			
		${}^{v}A_1$	${}^{v}A_2$	${}^{v}B_1$	${}^{v}B_2$	${}^{v}A_1$	${}^{v}A_2$	${}^{v}B_1$	${}^{v}B_2$	${}^{v}A_1$	${}^{v}A_2$	${}^{v}B_1$	${}^{v}B_2$	${}^{v}A_1$	${}^{v}A_2$	${}^{v}B_1$	${}^{v}B_2$
${}^{e}A_1$	${}^{v}A_1$	**ζ**	f	ξ	η	f	ζ	η	ξ	**ξ**	η	ζ	f	**n**	ξ	f	ζ
	${}^{v}A_2$	f	**ζ**	η	ξ	ζ	f	ξ	η	η	**ξ**	f	ζ	ξ	**n**	ζ	f
	${}^{v}B_1$	ξ	η	**ζ**	f	η	ξ	f	ζ	ζ	f	**ξ**	η	f	ζ	**n**	ξ
	${}^{v}B_2$	η	ξ	f	**ζ**	ξ	η	ζ	f	f	ζ	η	**ξ**	ζ	f	ξ	**n**

Eq. (8). Thus in general the members of each pair of curves should approach and almost touch, then separate, the lower or upper curve of each pair on the left of α_{ob} going over continuously into the respectively lower or upper one on the right of α_{ob}.

In Fig. 6, the vibronic state species are reduced to two, under the symmetry group C_s. Species A_1 and B_2 of Fig. 6 become A', species B_1 and A_2 become A''. In addition, the s and a labels disappear. Simultaneously, the g and u subscripts of the linear-molecule gyrovibronic species labels disappear.

VII. Rotational Selection Rules for Triatomic Molecules

In the application of the rotational (i.e. top-species) selection rules of Table V to triatomic molecules, certain questions sometimes arise. In isosceles AB_2 molecules, the dipole moment P of the transition (whether it is the permanent dipole moment as for pure rotation spectra, or whether it comes from an electronic or vibrational transition) is always along one of the three axes ξ, η, ζ of Fig. 3. Since these coincide with principal axes of inertia both before and after the transition, P is definitely P_a, P_b, or P_c and Table V can usually be used directly.

This, however, is not true if the equilibrium apex angle passes through $2\alpha_{ob}$ during the transition, causing a change in the correlation of the ξ, η, ζ to the a, b, c axes. In this event, a convenient procedure is to redefine the asymmetric-top species—make use of their behavior under operations C_2^{ξ}, C_2^{η}, C_2^{ζ}—, as A, B_{ξ}, B_{η}, B_{ζ}, and to use P_{ξ}, P_{η}, P_{ζ} as moment components. Table V then holds after substituting ξ, η, ζ for a, b, c.

In ABC or unsymmetrical AB_2, nothing more can in general be said about the direction of P for a transition than that it is either in the molecule plane (P_{ab}), or perpendicular to it (P_c). The top species B_a and B_b of Tables II and V now become indistinguishable so far as polarization-selection rules are concerned; similarly with the species A and B_c. Table V may then be reduced to the form of Table X.

In conclusion, it may be well to remind the reader again that top selection rules are in general less rigorous than over-all selection rules, and, in particular, lose force when strong systematic perturbations occur like those discussed near the end of Section V.

VIII. Vibronic Selection Rules for Molecules of Symmetry C_{2v}

Although in principle the electronic, vibrational, and vibronic selection rules for bent AB_2 and other molecules of symmetry C_{2v} are well known, experience indicates that it is very convenient to have at hand a table showing all the allowed types of *vibronic transitions* compatible with each type of electronic transition,

TABLE XII. *Same as Table XI, but vibrational species A_1 and B_2 only, as for AB_2 molecules. Axes ξ, η, ζ as in Fig. 3.*

C_{2v}		${}^{e}A_1$		${}^{e}A_2$		${}^{e}B_1$		${}^{e}B_2$	
		${}^{v}A_1$	${}^{v}B_2$	${}^{v}A_1$	${}^{v}B_2$	${}^{v}A_1$	${}^{v}B_2$	${}^{v}A_1$	${}^{v}B_2$
${}^{e}A_1$	${}^{v}A_1$	**ζ**	η	f	ξ	**ξ**	f	**n**	ζ
	${}^{v}B_2$	η	**ζ**	ξ	f	f	**ξ**	ζ	**n**

TABLE XIII. *Completion of Table XI or XII for transitions between any two electronic state-species. The first two lines of Table XIII are meant to represent the same thing as the whole of Table XI or XII, and the four letters a, b, c, d in Table XIII are meant to be identified with the content of the four squares of Table XI or XII.*

C_{2v}	${}^{e}A_1$	${}^{e}A_2$	${}^{e}B_1$	${}^{e}B_2$
${}^{e}A_1$	a	b	c	d
${}^{e}A_2$	b	a	d	c
${}^{e}B_1$	c	d	a	b
${}^{e}B_2$	d	c	b	a

allowed or forbidden. This is particularly true because in practice forbidden electronic transitions, and forbidden components in allowed electronic transitions, have proved quite commonly to be of observable intensity. This is really not surprising in view of the considerable magnitude to be expected[11] in many instances for the term ψ'_{ev} in Eq. (12) if ψ_e is written corresponding to nuclei arranged with their equilibrium symmetry, as is necessary here since the electronic transitions we are talking about are "allowed" or "forbidden" only with respect to electronic selection rules for this symmetry.

Tables XI and XIII together give the desired information for any molecule of symmetry C_{2v}. Table XII is a simplified version of Table XI, applicable to the special case of AB_2 molecules, where the only vibrational species are A_1 and B_2; here Tables XII and XIII are to be used together. As an example of the use of the tables, consider the λ2900 absorption band system of formaldehyde. This is most probably[12] an ${}^1A_2-{}^1A_1$ transition, forbidden by the electronic selection rules. Table XI shows, however, that the vibronic rules permit transitions from any lower vibrational state to each of three different species of upper vibrational states, in each case with a different type of polarization and hence of band structure. According to Dieke and Kistiakowsky's analysis,[8] the main bands of the system have η polarization, but other weaker bands are observed with ζ polarization. One may predict that still other weak bands should also be present with ξ polarization. If a vibrationless (${}^1A_1$) lower state is assumed, the η bands must have a ${}^1B_1$ upper state, which can be accounted for very reasonably by one quantum of the out-of-plane bending vibration, of species b_1. The ζ bands may perhaps have a ${}^1B_1$ lower and a ${}^1B_2$ upper state. From this example, the usefulness of the tables in surveying possible interpretations of a given spectrum can be seen.

The writer is indebted to Dr. W. H. Shaffer, Dr. A. Sayvetz, and Mr. N. C. Metropolis for helpful discussions and cooperation in connection with the preparation of this paper.

Appendix I. Derivation of Tables III and IV

To obtain Tables III and IV, it is necessary to examine the behavior of any S_{JKM} of Eqs. (4) under C_2^z, C_2^y, and C_2^z of group V of Table II. [The axes x, y, z here are related in some unique way in any given case to a, b, c of Table II; cf. Eqs. (7).] It is readily determined, from Fig. 1 (and cf. reference 1), that the new internal axes induced by C_2^z, C_2^y, C_2^z lead to new Eulerian angles which, for a given orientation of the top, are related to the old angles θ, ϕ, χ as follows:

$$\left.\begin{array}{ll} C_2^z: & \theta'=\theta, \quad \phi'=\phi-\pi, \quad \chi'=\chi \\ C_2^y: & \theta''=\pi-\theta, \quad \phi''=-\phi, \quad \chi''=\chi-\pi. \end{array}\right\} \tag{13}$$

The relations for C_2^z and the corresponding θ''', ϕ''', χ''' follow from those for C_2^z and C_2^y, since $C_2^z=C_2^yC_2^z$ (similarly, $C_2^y=C_2^zC_2^z$, etc.).

We now seek to determine the coefficients a (all are $+1$ or -1) in transformations such as

$$\begin{aligned} S_{JKM}(C_2^y\theta, C_2^y\phi, C_2^y\chi) &\equiv S_{JKM}(\theta'', \phi'', \chi'') \\ &= U_{JKM}(\theta, \phi, \chi)=a''S_{JKM}(\theta, \phi, \chi). \end{aligned} \tag{14}$$

From such relations as $e^{ik\phi''}=e^{-ik\phi}$, $e^{iM\chi''}=(-1)^Me^{iM\chi}$, together with the relation[13]

$$\Theta_{JKM}(\pi-\theta)=(-1)^n\Theta_{J-KM}(\theta), \tag{15}$$

with n as in Eq. (2) above, and making use of Eqs. (3) and (4), we can obtain the following results, independent of M:

$$\left.\begin{array}{lll} \text{Operation } C_2^z: & S_{JKM}(\theta', \phi', \chi')=(-1)^KS_{JKM}(\theta, \phi, \chi), \\ C_2^y: & S_{JKM}(\theta'', \phi'', \chi'')=(-1)^{J+\gamma}S_{JKM}(\theta, \phi, \chi), \\ C_2^z: & S_{JKM}(\theta''', \phi''', \chi''')=(-1)^{J+K+\gamma}S_{JKM}(\theta, \phi, \chi). \end{array}\right\} \tag{16}$$

It should be mentioned here that the introduction of Van Vleck's factor $(-1)^\beta$ in Eq. (3) has served to remove a complicating factor $(-1)^{M+\frac{1}{2}|K+M|+\frac{1}{2}|K-M|}$ which otherwise would have appeared, for $K>0$, in the coefficients for both of the operations C_2^y and C_2^z.

In order to use Eqs. (16) in classifying any

[11] G. Herzberg and E. Teller, Zeits. f. physik. Chemie **B21**, 410 (1933).

[12] H. L. McMurry and R. S. Mulliken, Proc. Nat. Acad. **26**, 312 (1940) and references given there.

[13] H. Rademacher and F. Reiche, Zeits. f. Physik **41**, 461 (1927), Eq. (21).

given S_{JKM}, the axes x, y, z must be correlated with a, b, c of Table II. The correlation, which is different for prolate and oblate S_{JKM}'s, may be made in accordance with choices 1 and 2 (*or*, 3 and 4) of Eqs. (7), as follows:

$$\left.\begin{aligned} z_{pr} &= \pm x_{ob} = a \\ y_{pr} &= \pm y_{ob} = b \\ x_{pr} &= z_{ob} = c. \end{aligned}\right\} \tag{17}$$

Thus C_2^z becomes C_2^a for the prolate case, C_2^c for the oblate case; and so on. Using Eqs. (16) in connection with Tables I and II, and putting $K=K_a$ for the prolate, $K=K_c$ for the oblate case, we obtain Tables III and IV.

Appendix II. Factoring of the Operators I and P_2

Species classifications are in general based on a study of all groups of operations which leave the form of the Schrödinger equation invariant. The operations in question are such as to generate coordinate-transformations (corresponding to axis-transformations or to permutations of the labels of identical particles). The classifications are then based on a consideration of the different possible sets of transformation matrices $a^R{}_{ij}$ in transformation equations

$$\psi_i(q^R) = \bar{\psi}_i(q) = \sum_j a^R{}_{ij}\psi_j(q), \tag{18}$$

where q refers to the coordinates expressed in the original system, q^R to the coordinates in the new system generated by operation (or operator) R. ψ represents a definite *functional form*, and $\bar{\psi}$ another form obtained by transforming $\psi(q^R)$ back from q^R to q.

The complete ψ_{evr} Schrödinger equation of bent AB_2 is a function of coordinates which are best chosen in accordance with the approximate factoring of ψ_{evr} into $\psi_r(\theta, \phi, \chi)\,\psi_{ev}(\xi_i, \eta_i, \zeta_i,$ electron spins), the ξ_i, η_i, ζ_i being a system of electronic coordinates based on the axes shown in Fig. 3, together with coordinates, based on sets of axes parallel to ξ, η, ζ, which measure the *displacements* of the nuclei from their equilibrium locations. The nuclear displacements are, of course, confined to the plane of the molecule, and their coordinates can be replaced by the usual normal coordinates.

It can be shown generally that the same matrices $a^R{}_{ij}$ generated by a coordinate or axis transformation R can also be obtained by consideration of a related position transformation R^{-1}. For consider any point O in coordinate space described by the set of coordinates q_O in the original coordinate system and by another set of values $q_O{}^R$ in the new system generated by R. There is then another point P, with coordinates q_P in the original system, such that $q_O{}^R = q_P$; further, the operations R which leave the form of the Schrödinger equation invariant are always of such a nature that the positions P and O have the relation $P = R^{-1}O$. It then follows for the values of the functions ψ that

$$\psi_i(q_O{}^R) = \psi_i(q_P).$$

Hence, using Eq. (18), we have

$$\psi_i(q_P) = \sum_j a^R{}_{ij}\psi_j(q_O). \tag{19}$$

Hence a consideration of the position transformation R^{-1} yields precisely the same matrices $a^R{}_{ij}$ as the desired coordinate transformation (18). As a corollary, if we are considering operators R acting on the complete wave function (here ψ_{evr}), and wish to factor them into operators acting on the factors (here ψ_e, ψ_v, ψ_r), we see that we can get equally correct results by factoring the corresponding position-transformation operators.

In the present application to the operators I and P_2 of ψ_{evr} of bent AB_2, the matrices of Eq. (19) are one-dimensional, that is,

$$\psi_i(q_P) = a^R\psi_i(q_O), \tag{20}$$

with $a^R = \pm 1$ (cf. Tables VI, VII). Also, $R^{-1} \equiv R$, for both I and P_2. In order to obtain the factoring of I and P_2 as given in Eqs. (9), the reader may imagine the AB_2 triangle, with axes and numbering of the B atoms as in Fig. 3, to be set into Fig. 1. We now think of the position transformation corresponding to inversion. This moves the three nuclei and all the electrons from their initial locations X_i, Y_i, Z_i (referred to the external axis system X, Y, Z) to $-X_i$, $-Y_i$, $-Z_i$. One sees that this could be accomplished by a combination of two operations: (a), a rotation (C_2^ξ) of the entire molecule top around its ξ axis; (b), a reflection (σ^ξ), in the molecule plane, of the locations of the electrons and nuclei. (Really,

σ^ξ affects only the electrons, since the nuclei determine the molecule plane.)

Operation I is not possible for a rigid top and so does not belong to the operation group of ψ_r; it is nevertheless possible for the actual molecule because we can combine operation (a) acting on ψ_r with operation (b) acting on ψ_{ev}. Operation (b), considered as a position transformation, consists essentially in reversing the internal electronic structure by reflection in a plane, so that the top changes from a left-handed to a right-handed one, or vice versa.

The coordinate transformation P_2 exchanges labels between the B nuclei 1 and 2; the position-transformation P_2 exchanges their positions (say $X_1Y_1Z_1 \rightarrow X_2Y_2Z_2$ and vice versa), without moving atom A or the electrons. In verifying the factoring of P_2 as given in Eqs. (9), one may conveniently start by picturing the AB_2 triangle distorted as by vibration, add a sample electron in an arbitrary initial location, and see what happens under the action of each of the position-transformation factors.

JUNE 1, 1941 PHYSICAL REVIEW VOLUME 59

On the Thermodynamic Interpretation of Certain Thermionic and Thermoelectric Phenomena

CONYERS HERRING
University of Missouri, Columbia, Missouri

(Received April 2, 1941)

It is well known that steady-state thermionic phenomena can be described only approximately in terms of the thermodynamic functions of equilibrium states of the metal concerned. These phenomena can, however, be related to the thermoelectric properties of the metal, and in this paper this relationship is developed for a metal of arbitrary crystalline symmetry. Application is made to the interpretation of experiments which measure the contact potential difference between metal surfaces at different temperatures, and to experiments which measure the cooling effect accompanying thermionic emission. Among other things it is shown that in spite of the high accuracy with which measurements of the latter type can be made, it is not possible at present to draw conclusions from them concerning the temperature coefficient of the work function. This would be true even for a single crystal surface because of the uncertainty in the value of the Thomson coefficient at high temperatures; for polycrystalline surfaces an equal or greater uncertainty is introduced by patch effects, which are discussed in detail.

1. INTRODUCTION

THE thermodynamic theory of thermionic emission and related phenomena has been treated by many authors over several decades, and in most respects the results are quite unambiguous and satisfactory.[1] Schottky and Rothe have pointed out,[2] however, that the cooling effect[3] which occurs when saturation current is drawn from an emitting cathode depends in part on the nature of the electron transport process inside the metal. This part of the cooling effect, though small, cannot be calculated, as can the rest of the effect, from the thermodynamic potentials of equilibrium states of the metal. One of the objects of this paper will be to derive an exact expression for this cooling effect, i.e., for

[1] For expositions of the thermodynamic theory see: P. W. Bridgman, *Thermodynamics of Electrical Phenomena in Metals* (Macmillan, 1934); W. Schottky and H. Rothe, *Handbuch der Experimentalphysik* (Leipzig, 1928), XIII, 2; H. Rukop, W. Schottky, and R. Suhrmann, Die Physik **3**, 133 (1935) (supplementary to the article of Schottky and Rothe).

[2] W. Schottky and H. Rothe, reference 1, Chapter VI, Section 8.

[3] Measurements which have been made of the cooling effect for pure metal surfaces include: C. Davisson and L. H. Germer, Phys. Rev. **20**, 300 (1922) (W); F. Krüger and G. Stabenow, Ann. d. Physik **22**, 713 (1935) (Ta, W, Mo); G. M. Fleming and J. E. Henderson, Phys. Rev. **58**, 887 (1940) (W).

the heat l_{sat} which must be supplied to an ideal surface, per electron emitted, in order to keep it at constant temperature. An approximate expression is known[2] to be

$$l_{sat} \approx e\phi + 2kT, \tag{1}$$

where ϕ is the "true work function" defined by (4) or (5) below. The chief approximation consists in the neglect of heat convected to the surface by the current from the interior of the metal.

A related question concerns the interpretation of measurements of the contact potential difference V_{12} between two wires of the same material at different temperatures T_1 and T_2.[4] The experimenters have usually assumed that

$$V_{12} = \phi(T_1) - \phi(T_2). \tag{2}$$

This will only be true, however, if the electrochemical potentials defined by (3) below are the same for the electrons in the two wires; however since the wires are not at the same temperature, the condition for their equilibrium when connected together is not equality of electrochemical potentials, as it would be if the temperatures were the same, but involves instead the rate of migration of electrons in thermal conduction. The second object of this paper is to calculate the correction which must be applied to (2); this correction, though of course small, is appreciable in the interpretation of the most accurate experiments.

Sections 2 to 5 are theoretical, while in Section 6 the interpretation of several recent thermionic experiments is discussed.

2. Definitions and Preliminary Remarks

The most concise way of treating the thermodynamics of thermionic phenomena involves the use of chemical or electrochemical potentials.[5] Consider first a metal block of volume v at uniform temperature T. If U, S represent, respectively, the energy and entropy of the block, and if n is the number of moles of electrons it contains, the electrochemical potential of the electrons in the metal is defined as

$$\bar{\mu} = \left[\frac{\partial}{\partial n}(U - TS)\right]_{v,\,T}. \tag{3}$$

More explicitly stated, $-\bar{\mu}$ is the change in the free energy of the system (metal + vapor) when a mole of electrons is evaporated isothermally and removed to infinity, minus the free energy of the mole of electron vapor; in evaluating the latter it is to be assumed that at sufficiently low densities the energy of the mole of vapor becomes $3RT/2$, and its entropy approaches the value calculated for a perfect gas from the quantum statistics.

The electrochemical potential of the electrons in a small sample of free electron gas is defined by an expression of the same form as (3), and can be expressed in terms of the temperature and pressure of the gas, if the latter is assumed perfect. If we have a free electron vapor in equilibrium with the metal, the electrochemical potentials of the electrons in the two phases must be equal. Thus the equilibrium vapor pressure can be expressed in terms of the $\bar{\mu}$ of the metal, and by the use of the familiar relation between vapor pressure and saturation current density j one can obtain the Richardson equation:[6]

$$j = A(1-\bar{r})T^2 \exp[-e\phi/kT], \tag{4}$$

where $A = 4\pi mk^2e/h^3 = 120$ amp./cm^2 deg.^{2}, $\bar{r}$ is the reflection coefficient of the metal surface, averaged over a Maxwellian distribution, and where

$$\phi = -\Phi_0 - (\bar{\mu}/Ne), \tag{5}$$

in which Φ_0 is the electrostatic potential a small distance outside the metal surface, and N is the

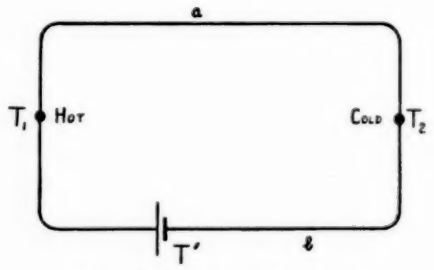

Fig. 1. Thermoelectric circuit.

[4] Recent contact potential measurements of this sort include: D. B. Langmuir, Phys. Rev. **49**, 428 (1936) (thoriated W); A. L. Reimann, Proc. Roy. Soc. **A163**, 499 (1937) (thoriated W); J. G. Potter, Phys. Rev. **58**, 623 (1940) (W).

[5] This treatment is the one used by Schottky and Rothe, reference 1. The notation and terminology chosen for the present paper are those used by E. A. Guggenheim, *Modern Thermodynamics by the Methods of Willard Gibbs* (Methuen, 1933), Chapter X.

[6] W. Schottky and H. Rothe, reference 1, Chapter IV.

Avogadro number. The quantity ϕ defined by (5) will be referred to as the "true work function" of the metal; it may of course vary with the temperature. This ϕ refers, of course, to a homogeneous single crystal surface, and it may be expected to be different for different crystal faces. The "apparent work function," obtained from the slope of a Richardson plot, involves $d\phi/dT$ and, if the emitting filament is polycrystalline, involves a complicated average over the different crystal faces.[7] This will be taken up in detail in Section 6.

If two blocks a, b, of different metals *at the same temperature*, are connected together by a wire, their $\bar{\mu}$'s will become equal. This implies, according to (5), that the contact potential difference between 1 and 2 is

$$V_{ab}=\Phi_{gb}-\Phi_{ga}=\phi_a-\phi_b. \tag{6}$$

If the temperatures are different, it is not necessary that $\bar{\mu}_1=\bar{\mu}_2$ in the steady state. A very simple argument can be constructed to show that $\bar{\mu}$ must change as we go along a temperature gradient in a wire. Consider the thermoelectric circuit shown in Fig. 1, containing a battery or potentiometer at temperature T' in the b part of the circuit. If the e.m.f. of the battery is chosen equal and opposite to the e.m.f. E_{ba} of the thermoelectric circuit, no current will flow. In this state the difference between the $\bar{\mu}$'s of the electrons in metal b just to the right and just to the left of the battery will be $-NeE_{ba}$. Since $\bar{\mu}_b=\bar{\mu}_a$ at each junction we may write

$$\int_{T'}^{T_2}\frac{d\bar{\mu}_b}{dT}dT+\int_{T_2}^{T_1}\frac{d\bar{\mu}_a}{dT}dT+\int_{T_1}^{T'}\frac{d\bar{\mu}_b}{dT}dT=-NeE_{ba}$$

or, differentiating[8] with respect to T_1, we find

$$\frac{d\bar{\mu}_a}{dT_1}-\frac{d\bar{\mu}_b}{dT_1}=-Ne\frac{dE_{ba}}{dT_1}=Ne\int_0^{T_1}\left(\frac{\sigma_a}{T}-\frac{\sigma_b}{T}\right)dT, \tag{7}$$

where σ_a, σ_b, are the Thomson coefficients of the two metals, which in the usual thermodynamic theory[9] are related as indicated to the thermoelectric power. It will be shown below that (7) can be replaced by the relations (19) for the two metals separately.

One more concept must be introduced. When electrons are taken from or added to the metal block, it acquires a surface charge. Because of this change in the state of the surface of the metal, the quantity $\bar{\mu}$ just defined depends on the properties of the surface, and could be changed, for example, by depositing a layer of impurity atoms on the surface. It will, therefore, be convenient to define another quantity which depends only on the state of the interior of the metal. To do this we shall imagine that it is possible to introduce a continuous distribution of charge into the interior of the metal, whose density ρ_c varies appreciably only in distances large compared with atomic dimensions. The various states of the metal block which could be brought about if it were possible to manipulate a continuous non-electronic charge of this sort can be described by using as thermodynamic coordinates the quantities T, v (or more generally, state of strain), $c=(Ne)^{-1}\iiint\rho_c d\tau$, and $n'=n-n_0-c$, where n_0 is the number of moles of electrons in the block when neutral. Thus n' is a measure of the total charge, electronic and continuous together, inside the surface of the block. Define

$$\mu=\left[\frac{\partial}{\partial c}(U-TS)\right]_{n',\,v,\,T}. \tag{8}$$

The definition (3) is equivalent to

$$\bar{\mu}=\left[\frac{\partial}{\partial n'}(U-TS)\right]_{c,\,v,\,T}=\mu-Ne\Phi_m, \tag{9}$$

where Φ_m is the space average of the electrostatic potential in the interior of the metal, and thus includes the effect of any double layer which may exist at the surface. The quantity μ, which is independent of the state of the surface, is usually called the chemical potential.

3. Convection of Entropy

A clear and elegant formulation of the thermodynamic theory of thermoelectric phenomena in crystalline metals has been given by Ehrenfest and Rutgers.[10] From two assumptions these

[7] The nature of this average is discussed in detail by M. H. Nichols, Phys. Rev., to appear soon.

[8] For another derivation of (7) see P. W. Bridgman, reference 1, Chapter IV.

[9] See for example W. Meissner, *Handbuch der Experimentalphysik* (Leipzig, 1935), Vol. XI, No. 2, p. 400.

[10] P. Ehrenfest and A. J. Rutgers, Proc. Amst. Acad. **32**, 698 (1929).

authors deduce all these phenomena (Seebeck, Peltier, Thomson, and Bridgman effects, etc.), and the relations between them. These assumptions, briefly stated, are that the thermoelectric effects are reversible, and that the rate at which heat must be added or taken out reversibly at each point of a metal in which a steady-state current distribution flows, is a linear function of the current density and its first derivatives. In the analysis to follow, this reversibility and linearity will be postulated for arbitrary current distributions, whether they are divergenceless or not; this extension is a rather slight one, however, and there can be little doubt of its validity whenever the steady-state postulates of Ehrenfest and Rutgers are true.

Let us consider an unevenly heated metal block, not necessarily of homogeneous composition, and define: $\mathbf{j}$ = electronic current density; s = entropy density; Q = heat added per unit time per unit volume; during any process (we shall suppose that heat reservoirs can be placed in thermal contact with all parts of the interior of the metal); $q=\frac{1}{2}[Q(\mathbf{j}, \partial T/\partial t, \cdots)-Q(-\mathbf{j}, -\partial T/\partial t, \cdots)]$, i.e., half the difference between the Q's of a given process and the reverse process; q_0 = value of q for any process in which the temperature distribution and state of strain throughout the metal remain constant. Our assumptions may now be stated as follows. For an arbitrary current distribution, which we may imagine to be produced by suitably varying a magnetic field and shifting a hypothetical continuous charge distribution ρ_c, we have

(I) Reversibility:[11] $$\iiint \frac{\partial s}{\partial t} d\tau = \iiint \frac{q}{T} d\tau$$

(II) Linearity: $$q_0 = A_\alpha j_\alpha + B_{\alpha\beta} \frac{\partial j_\alpha}{\partial x_\beta}.$$

(Here and in the following the summation convention will be used for repeated Greek suffixes, which run from 1 to 3.)

[11] It has been suggested by P. W. Bridgman (reference 1, Chapter II) that such irreversible processes as heat conduction and Joulean heating are always accompanied by a characteristic increase of entropy, regardless of what other processes may be occurring at the same time. If this were true, the reversibility relation (*I*) would follow. This suggested law might be a very general one, but would have to be subjected to certain restrictions: for example, starting from the usual statistical theory of electrons in metals, J. Meixner has shown (Ann. d. Physik **35**, 701 (1939)) that the thermoelectric effects are not reversible in a magnetic field.

Let us consider an arbitrary current distribution which vanishes at the boundary of the metal block, and let us suppose the temperature distribution and state of strain to be held constant in the course of time. For our unevenly heated block we may define μ at each point by an equation analogous to (8), and we have

$$\frac{\partial s}{\partial t} = \left(\frac{\partial s}{\partial \rho_c}\right)_{n', v, T} \frac{\partial j_\alpha}{\partial x_\alpha} = -\frac{1}{Ne}\left(\frac{\partial \mu}{\partial T}\right)_{v, n'} \frac{\partial j_\alpha}{\partial x_\alpha}, \quad (10)$$

where v, n', refer to a small neighborhood of the point at which s and μ are measured. Inserting this and (II) into (I) and integrating by parts, there results

$$\iiint \left[\frac{1}{Ne}\frac{\partial}{\partial x_\alpha}\left(\frac{\partial \mu}{\partial T}\right) - \frac{A_\alpha}{T} + \frac{\partial}{\partial x_\beta}\left(\frac{B_{\alpha\beta}}{T}\right)\right] j_\alpha d\tau = 0$$

and since the current distribution is arbitrary, the quantity in brackets must vanish at every point of the metal. Solving the resultant equation for A_α and placing this in (II) we obtain

$$\frac{q_0}{T} = \frac{\partial}{\partial x_\beta}(j_\alpha S_{\alpha\beta}) + \frac{\partial s}{\partial t}, \quad (11)$$

where

$$S_{\alpha\beta} = \frac{B_{\alpha\beta}}{T} + \frac{\delta_{\alpha\beta}}{Ne}\frac{\partial \mu}{\partial T}. \quad (12)$$

The meaning of (11) is that the vector $j_\alpha S_{\alpha\beta}$ represents an entropy flux carried by the electronic current.

We may now use the third law of thermodynamics to express $S_{\alpha\beta}$ in terms of the Thomson coefficients, which, from (11) and their definition, are

$$\sigma_{\alpha\beta} = T\partial S_{\alpha\beta}/\partial T. \quad (13)$$

We assume that $S_{\alpha\beta}$ depends on temperature and composition, but not on the magnitude of the temperature gradient, an assumption which is permissible for the small temperature gradients experimentally realizable. If we apply the third law and (11) to a process taking place at constant

uniform temperature, with arbitrary current distribution, we see that

$$S_{\alpha\beta}\to 0 \quad \text{as} \quad T\to 0, \tag{14}$$

and so from (13)

$$S_{\alpha\beta}=\int_0^T \frac{\sigma_{\alpha\beta}}{T}dT. \tag{15}$$

4. Variation of $\bar{\mu}$ Inside a Non-Uniformly Heated Metal

We have yet to apply the first law of thermodynamics. Let a steady state be established for the metal block in which $\mathbf{j}=0$ everywhere, and $\rho_c=0$. If the block is not of homogeneous composition, or if it is a crystal of lower than cubic symmetry, it may be necessary to apply a solenoidal electric field $\mathbf{E}'$ from external sources, in order to prevent thermoelectric currents from flowing. Let Φ be the potential due to the charge distribution in the metal in this state. Now let an arbitrary current distribution be set up by changing the applied magnetic field and bringing in a continuous charge distribution ρ_c of net charge zero, the temperature distribution and state of strain being held fixed. In this process the distribution of electronic plus continuous charge will remain unchanged, so that the change in total energy of the system metal plus continuous charge will equal the change in the non-electrostatic part of this energy. Now if u represents the density of the non-electrostatic part of the energy, we have from (8)

$$\iiint \frac{\partial u}{\partial \rho_c}\frac{\partial \rho_c}{\partial t}d\tau = \frac{1}{Ne}\iiint\left(\mu - T\frac{\partial \mu}{\partial T}\right)\frac{\partial j_\alpha}{\partial x_\alpha}d\tau. \tag{16}$$

The "reversible part" of the work done per unit time, i.e., the half difference between the rate of working in this process and the rate in a process in which the currents are reversed, is

$$\iiint\left(E'_\alpha j_\alpha+\Phi\frac{\partial \rho_c}{\partial t}\right)d\tau. \tag{17}$$

Equating (16) to (17) plus T times (11) and using (10) we obtain

$$\frac{1}{Ne}\iiint\left(\mu - T\frac{\partial \mu}{\partial T}\right)\frac{\partial j_\alpha}{\partial x_\alpha}d\tau = \iiint\left[E'_\alpha j_\alpha+\Phi\frac{\partial j_\alpha}{\partial x_\alpha}+T\frac{\partial}{\partial x_\beta}(j_\alpha S_{\alpha\beta}) - \frac{T}{Ne}\frac{\partial \mu}{\partial T}\frac{\partial j_\alpha}{\partial x_\alpha}\right]d\tau.$$

Integrating by parts and remembering that $\mathbf{j}$ is arbitrary we have

$$\frac{\partial(\mu - Ne\Phi)}{\partial x_\alpha}=Ne\left(S_{\alpha\beta}\frac{\partial T}{\partial x_\beta}-E'_\alpha\right). \tag{18}$$

It will be noticed that for crystals of lower than cubic symmetry, temperature gradients can be set up for which the curl of the first term on the right of (18) will not vanish, so that $\mathbf{E}'$ cannot vanish. This means that in the absence of an externally imposed field thermoelectric currents will flow even in a single crystal.

For a cubic crystal or a polycrystalline substance, of homogeneous composition, we may set $\mathbf{E}'=0$ and replace $\mu - Ne\Phi$ by $\bar{\mu}$. Equation (18) becomes, after using (15) with $\sigma_{\alpha\beta}=\sigma\delta_{\alpha\beta}$,

$$\frac{d\bar{\mu}}{dT}=Ne\int_0^T\frac{\sigma}{T}dT. \tag{19}$$

This equation, which applies to the current-free state of the metal, is the extension of (7).

5. Heat Loss in Thermionic Emission

The calculation of the heat loss l_{sat} per emitted electron is most conveniently made in two stages. The first step is to calculate the heat loss l_{slow} for a quasi-static vaporization of electrons, from the principle that the entropy fed in per unit time at the surface in such a steady-state vaporization must equal the difference between the entropy fluxes in the vapor and the metal. The second step is to calculate the difference $(l_{\text{sat}}-l_{\text{slow}})$ from energy considerations.

In the steady-state quasi-static vaporization, the entropy flux across any plane drawn through the vapor, parallel to the metal surface, is equal to the electron flux times the entropy per electron

of the vapor. For a perfect gas of electrons at the density prescribed by equilibrium with the metal, the Sackur-Tetrode expression for the entropy per electron becomes $e\phi/T+5k/2$. This is most easily shown from (5) by using for the vapor phase the relation

$$\bar{\mu}=\left[\frac{\partial}{\partial n}(U-TS+pv)\right]_{p,t}.$$

which is equivalent to (3). Thus the entropy which must be fed in at the surface, per unit time, by conduction or independent heating, is

$$\frac{l_{\text{slow}}}{T}=\frac{e\phi}{T}+\frac{5}{2}k+eS_{11}, \tag{20}$$

where the coordinate direction 1 is taken normal to the emitting surface.

The difference $(l_{\text{sat}}-l_{\text{slow}})$ must be equal to the difference, between saturation and quasi-static conditions, in the average kinetic energy per electron crossing a plane parallel to the metal surface. For quasi-static conditions this average energy can be evaluated from the Maxwell-Boltzmann distribution law, and is $5kT/2$. For saturation conditions the ratio will depend upon the variation of the reflection coefficient r of the metal surface with normal energy. If r is constant, as is usually assumed, the saturation electrons will have a Maxwellian distribution and the ratio in question can be evaluated[12] to $2kT$. For this case we have from (20) and (15)

$$l_{\text{sat}}=e\phi+2kT+eT\int_0^T\frac{\sigma_{11}}{T}dT, \tag{21}$$

where σ_{11} is the Thomson coefficient for current and temperature gradient normal to the surface.

6. Discussion of Experiments

In the interpretation of the experiments listed in references 3 and 4 we encounter the difficulty, already mentioned in Section 2, that all the surfaces used have been polycrystalline, whereas all the preceding analysis has been made for a uniform surface. For such a uniform surface, a Richardson plot yields the "apparent work function"

$$\phi^*=\frac{kT^2}{e}\frac{d}{dT}\left(\log\frac{j}{T^2}\right),$$

which, if the temperature dependence of $\bar{r}$ in (4) is neglected, is

$$\phi^*=\phi-T(d\phi/dT), \tag{22}$$

and an "apparent emission constant" A^*, which for temperature-independent $\bar{r}$ is

$$A^*=A(1-\bar{r})\exp\left[-\frac{e}{k}\frac{d\phi}{dT}\right]. \tag{23}$$

The relation of the quantities obtained from a Richardson plot for a polycrystalline sample to the quantities A_i^*, ϕ_i^*, for the different crystal faces i, can be shown[7] to depend on the strength of the collecting field. For the strong fields usually used in thermionic experiments, the quantities obtained from the Richardson plot after correction for Schottky effect may be designated by $\bar{\phi}^*$ and A_e. It can be shown that

$$\bar{\phi}^*=\sum w_i\phi_i^*, \tag{24}$$

where w_i is the fraction of the total current which comes from the ith kind of crystal face. It is also easy to show that if all the A_i^* are equal, the "effective emission constant" A_e has the property

$$A_e<A_i^*. \tag{25}$$

The physical meaning of (24) and (25) is that if there are appreciable differences in work function between different crystal faces, most of the emission comes from low work function facets, so that A_e is roughly A^* times the ratio of the area occupied by the low work function faces to the total area.

In cooling experiments on polycrystalline specimens, it can likewise be shown that the quantity measured is

$$\bar{l}_{\text{sat}}=\sum w_i l_{\text{sat}\,i}, \tag{26}$$

provided again that the collecting field is sufficiently large. Since the average in (26) involves the same weight factors as that in (24) we can obtain from (22) and (21) the relation, valid for cubic metals,

$$e\bar{\phi}^*=\bar{l}_{\text{sat}}-T\frac{d\bar{l}_{\text{sat}}}{dT}+eT\sum\phi_i\frac{dw_i}{dT}+e\sigma T. \tag{27}$$

[12] A. L. Reimann, *Thermionic Emission* (Chapman and Hall, 1934), p. 52.

The third term of (27) is positive and at 2500°K it may amount to $\frac{1}{10}$ ev or more, if the differences between the work functions of different crystal faces are a little larger than kT, as is known to be the case for W.[13] The value of σ in the last term is not known with certainty for any metal at high temperatures, since the existing measurements of thermoelectric powers and Thomson and Peltier coefficients are not at all consistent with one another. However, it is likely that the absolute magnitude of this term at 2500°K is of the order of 1/20 electron volt for some of the metals used in thermionics.

The quantity $d\phi/dT$ occurring in (23) can, in principle, be calculated from cooling effect measurements if it is assumed that $d\phi/dT$ is the same for all crystal faces. For we have from (21) and (26)

$$e\left\langle\frac{d\phi}{dT}\right\rangle_{wAv}=\frac{dl_{sat}}{dT}-2k-e\sum\phi_i\frac{dw_i}{dT}-e\int_0^T\frac{\sigma}{T}dT-e\sigma. \quad (28)$$

Finally, the quantity measured as the contact potential of a polycrystalline metal involves an average $\langle\phi_i\rangle_{Av}$ of the true work functions ϕ_i, each weighted according to the fraction f_i of the surface area made up by the ith kind of face. From this and (19) we see that the contact potential V_{12} measured in the experiments of reference 4 is given by

$$V_{12}=\langle\phi_i\rangle_{Av}(T_1)-\langle\phi_i\rangle_{Av}(T_2)-\int_{T_1}^{T_2}\int_0^T\frac{\sigma}{T'}dT'dT. \quad (29)$$

Potter[4] has measured the quantity (29) for W, between 300° and 935°K. Neglecting the last term on the right of (29), he obtained $d\langle\varphi_i\rangle_{Av}/dT=6.3\times10^{-5}$ volt/deg. He also obtained evidence that $d\phi_i/dT$ has this same value for all individual crystal faces i. If this conclusion is accepted, (23) and (25) demand that

$$A_e<A^*<A\exp\left[-\frac{e}{k}\frac{d\phi}{dT}\right]=58\text{ amp./cm}^2/\text{deg.}^2.$$

This value 58 is very close to the best experimental values of A_e for polycrystalline W. But Nottingham[14] has justly pointed out that the "patch effect" inequality (25) would alone suffice to make A_e smaller than A^* by a factor of the order of two, and that reflection might make A^* appreciably below the value calculated from $d\phi/dT$.

This apparent contradiction is only slightly alleviated by inclusion of the last term of (29). This term can be evaluated by combining (a) measurements of the "absolute thermoelectric power" $\int_0^T(\sigma/T)dT$ for a silver alloy at low temperatures[15,16] with (b) measurements of the thermoelectric power of Cu against silver alloy and W against Cu[16] and (c) direct measurements of σ for Cu above room temperature.[16] This new reduction of Potter's observations gives $d\langle\varphi_i\rangle_{Av}/dT=5.2\times10^{-5}$ volt/deg. The difference between this and Potter's original value is of the same order as the probable error claimed for the latter. It should be remembered, of course, that the temperature derivative of the work function need not have the same value in the thermionic range which it has at lower temperatures. In fact, the third law of thermodynamics requires that $d\phi/dT\to0$ as $T\to0$.

Krüger and Stabenow[3] have made accurate measurements of the cooling effect for W and Ta at a number of different temperatures between 2000° and 2700°K, and for Mo at temperatures near 2100°K. Using only the first two terms of (28), they found $\langle d\phi/dT\rangle_{wAv}=6\times10^{-5}$ volt/deg. for both Ta and W, the probable error in this figure being estimated at 20–30 percent. Using only the first two terms of (27) they found $\bar{\phi}^*=4.44$ volts for W and 4.08 volts for Ta. The values obtained from Richardson plots are, respectively, about 4.52 and 4.10 volts.[17] Krüger and Stabenow did not measure the emission currents from their specimens, so there may be some uncertainty as to whether the conditions of their surfaces were the same as those of reference 17. In any case, however, the uncertainty in the magnitude of the

[13] M. H. Nichols, Phys. Rev. **57**, 297 (1940).

[14] W. B. Nottingham, Phys. Rev. **58**, 927 (1940).

[15] G. Borelius, W. H. Keesom, C. H. Johannson and J. O. Linde, Proc. Amst. Acad. **35**, 10 (1932).

[16] Summarized by W. Meissner, reference 9.

[17] S. Dushman, Rev. Mod. Phys. **2**, 394 (1930); A. B. Cardwell, Phys. Rev. **47**, 628 (1935) (Ta); P. Freitag and F. Krüger, Am. d. Physik **21**, 697 (1935) (W).

last two terms of (27) is of the same order as the difference between the emission current and the calorimetric values, and larger than the uncertainty in either of these. For an accurate comparison of the two work functions both the surface structure of the emitter and its Thomson coefficient will have to be known. And because of the uncertainty in the last three terms of (28), any attempt to calculate A^* from the cooling effect for a polycrystalline metal is at present even more hopeless.[18]

For the sake of simplicity, all the equations of this section have been derived neglecting any possible variation of the mean reflection coefficient $\bar{r}$ with temperature. It is easily shown that if there is a reflection coefficient for an electron with normal momentum p_x, given by

$$r=\exp[-p_x^2/2m\omega],$$

as has been proposed by Nottingham,[19] a term $\omega^2kT/(\omega+kT)^2$ should be added to the right of (27), and a term $-k\omega^2/(\omega+kT)^2$ should be added to the right of (28). If $\omega=0.2$ ev, as proposed by Nottingham,[19] the former correction is 0.05 ev at 2320°K and the latter is -2.2×10^{-5} ev/deg. These values are undoubtedly much too large to represent the reflection effect, since Nottingham's "reflection coefficient" includes the effects of patch fields in addition to true reflection.

[18] Using an incorrect formula, Krüger and Stabenow obtained from their data the low value 0.66 amp./cm² deg.² for A*.

[19] W. B. Nottingham, Phys. Rev. **49**, 78 (1936.)

JUNE 1, 1941 PHYSICAL REVIEW VOLUME 59

On the Measurement of Observables in Relativistic Quantum Mechanics

O. HALPERN AND M. H. JOHNSON
New York University, University Heights, New York
(Received October 19, 1940)

The paper discusses the question how far observables in quantum theory permit accurate measurement if *no assumptions* are made about the values of conjugate variables. The physical connection between the uncertainty principle and the commutation relations is briefly discussed. A treatment of the γ-ray microscope makes it appear that even with small-angle diffraction no great improvement beyond the Compton wave-length can be obtained. An analysis of an ideal arrangement to measure electric field strengths leads to the result that, admitting the existence of arbitrarily constituted test bodies, the accuracy of the measurement still cannot exceed certain limits which are mainly defined by the wave-length of the field and the spatial and temporal domain of measurement. These restrictions are due to the properties of the "vacuum," which are changed as a consequence of the possibility of pair production.

1. INTRODUCTION

IT may perhaps be said to be a distinctive feature of the mathematical theory of quantum mechanics that quantities of physical significance are assumed to be measurable individually with arbitrary accuracy, at least in principle. This feature is expressed mathematically by the assumption that it is possible to transform any single arbitrary function of the dynamical variables to its principle axes. Restrictions on the simultaneous measurement of two or more observables occur if their mathematical representations do not commute.

The discussions of the many ideal experiments which have been carried through, mainly for the verification of the uncertainty relations in special cases, are thus important in testing general postulates in particular cases. They derive their power of conviction that other methods might not lead to different results primarily from the fact that on the one hand they conform to the general principles of the theory, and on the other that the experimental arrangements employed are usually of so general a nature that imagination fails to provide us with suggestions leading to experiments based on different principles.

In *relativistic quantum mechanics* important conceptual difficulties arise from the fact that into every description of a measurement there enters a statement concerning the time at which the measurement is carried out. Interpreting the relativistic commutation relations rigidly we might feel inclined to say that the three components of momentum of a free electron should be measurable independently of the time interval allowed, while there should exist restrictions on the accurate measurement of the energy within an arbitrarily short time interval. But the knowledge of the three momentum components of a free particle would immediately yield that of its energy. On the other hand also, we know from the discussion of ideal experiments that a momentum component is not measurable with unlimited accuracy in an indefinitely short time.

These well-known facts seem sufficient to shatter confidence in the direct and unambiguous connection between commutation relations and experimentally verifiable uncertainty relations. The solution of this apparent paradox, as it is probably accepted by many physicists at present, can be seen in the fact that the proper use of the Dirac equation prevents the treatment of the electron as a one-body problem. The large number of complications in the properties of the vacuum due to the phenomenon of pair production as postulated by every relativistic theory, prevents the simple application of the rules and postulates found valid in nonrelativistic quantum mechanics.

We intend to show in the next paragraph how the change in electrodynamics necessitated by relativistic quantum mechanics tends to destroy the possibility of an arbitrarily accurate determination of the position of an electron with the gamma-ray microscope. Although this line of reasoning, if valid, can only make futile the special arrangement used, we feel inclined to generalize the result on the basis of the experience gained from the previous discussions of ideal experiments and the uncertainty relations.

Our result will probably be accepted as confirmation of views or expectations now held by many physicists with reference to the properties of the Dirac electron. On the other hand, the investigation of paragraph three will refer to a case in which no large velocities need occur. Nevertheless, the properties of the vacuum seem to invalidate the concept of observable in a field in which it has generally been supposed to apply without restriction.[1] We refer to the measurability of an electric field strength in an electromagnetic field variable in space and time. This problem has been given its most comprehensive treatment by Bohr and Rosenfeld,[2] who have arrived at the result that the average value of a field strength over an indefinitely large space-time domain can be measured with unlimited accuracy provided no atomistic restrictions are imposed on the test body used in the ideal experiment. But they did not take into account the later discovered properties of the vacuum due to pair production.[3] In our opinion the measurement of an individual component of a field strength is not possible if the newly discovered properties of the vacuum are taken into account even in the most qualitative manner. It goes without saying that these new facts gain importance only when the space-time domain over which we average is sufficiently small; no objection can be raised against the asymptotic approach of the quantum theoretical concepts towards the classical concepts of field strength in large world domains.

2. A Gamma-Ray Microscope for Measurements of Arbitrarily High Accuracy

It has been pointed out in previous discussions that in the measurement of the position of an electron by means of the gamma-ray microscope, a natural limitation seems to occur due to the Compton shift of the scattered radiation. The wave-length of a ray scattered through an angle ϑ is given by the relation

$$\lambda=\lambda_0+(2h/mc)\,\sin^2\tfrac{1}{2}\theta \qquad (1)$$

[1] Through the discussion of an ideal experiment Cox and Myers (Nature **142**, 394 (1938)) arrive at the result that the electron's spin (magnetic moment) cannot be measured *even if the electron is bound*. This thesis cannot be maintained but is due to an error in the physical discussion leading to it.

[2] N. Bohr and Rosenfeld, Proc. Dan. Acad. Sci., Copenhagen, 1933.

[3] The phenomenon of pair production is mentioned in this paper as the most characteristic consequence of any relativistic quantum theory and also because it plays the most important part in the experiments analyzed by us. The possibility should be kept in mind that in the case of other ideal experiments, other relativistic features become more important while pair production may remain latent.

with the usual symbols. On the other hand, since the inaccuracy Δx of a measurement of position is limited by the relation

$$\Delta x \sim \lambda/\epsilon \tag{2}$$

in which the numerical aperture $\epsilon \ll 1$ is connected with the *maximum* angle of scattering ϑ_0 by $\epsilon = 2\vartheta_0$, many authors have assumed that an accuracy in the neighborhood of the Compton wave-length would be the limit for the gamma-ray microscope.

Now a closer discussion of frequency conditions and resolving power for scattering under small angles leads to a different result. It seems that the gamma-ray microscope should allow a position measurement with *arbitrarily high accuracy* in spite of the fact that a frequency shift due to the Compton recoil must be taken into account. This statement becomes incorrect, and therefore the position not accurately measurable, when we consider the changes in the theory due to the phenomena associated with pair production.[3]

To prove this statement we first observe that the shift in wave-length for *small angle* scattering is *quadratic* in the scattering angle

$$\lambda = \lambda_0 + \tfrac{1}{2}\Lambda\vartheta^2 \qquad (\Lambda = h/mc). \tag{3}$$

Suppose now that we use as a primary wave-length

$$\lambda_0 = \Lambda\epsilon\delta, \tag{4}$$

where δ is a pure number to be specified later. The spread in wave-lengths over the opening of the microscope according to Eq. (3) is smaller than $\Lambda\epsilon^2/8$. By Eq. (2) the accuracy obtainable is given by the relation

$$\Delta x \sim \lambda/\epsilon \sim (\lambda_0 + \tfrac{1}{2}\Lambda\vartheta_0^2)/\epsilon \sim \Lambda(\delta + \tfrac{1}{8}\epsilon). \tag{5}$$

Since for small angles the scattered intensity varies as $(1+\Lambda\epsilon^2/2\lambda_0)^{-3}$ we must take $\delta \gg \epsilon$ in order to make full use of the aperture. For example we can choose $\delta = \epsilon^{\frac{1}{2}}$. We then note from Eq. (5) that the accuracy of measurement can be made an arbitrarily small fraction of the Compton wave-length provided that the aperture, and with it the primary wave-length, be made sufficiently small.

By this reasoning the possibility of an arbitrarily accurate measurement of a position coordinate seems established provided the phenomena are described correctly by the theory of optics as it was accepted before pair production was discovered. If it is required, however, that a second or "control" measurement be possible, then a restriction must be imposed on the time needed for carrying out the experiment, and it will be shown that this in turn requires a modification of the whole reasoning since it brings in the possibility of pair formation.

Since for the *high frequencies* used, the lateral recoil velocity of the electron is of order $c\delta$, the accuracy Δx can be achieved only if the process takes a time τ smaller than $\Delta x/c\delta$. The frequency of the wave train will be defined only within a latitude $\Delta\nu \sim c\delta/\Delta x$. Since $\Delta\nu$ is larger than the maximum Compton shift for the aperture used, it is obvious that this shift will be of no significance in the present arrangement. But in addition to this, we shall have to use an intensity in the primary radiation which makes it certain that *at least* one photon will be scattered into the spherical angle $\Omega \sim \epsilon^2$ during the time τ. Neglecting factors of the order unity, and remembering that the differential cross section for sufficiently small angles takes on the Thomson value, we obtain the following relation

$$cE^2\epsilon^2(e^4/m^2c^4)\cdot(\Delta x/c\delta) \sim hc/\lambda_0 \tag{6}$$

in which E is the field strength in the incident wave. Making use of Eqs. (2), (4) and (5) we obtain

$$E^2 \sim (m^4c^8/e^6)\alpha(1/\epsilon^3\delta), \tag{7}$$

α being the fine-structure constant.

We learn from Eq. (7) that for measurements of this type with an accuracy exceeding the Compton wave-length it is necessary to use field strengths exceeding the "critical value" which enters into the new tentative formulation of quantum electrodynamics. The square root of the first factor on the right side of (7) can be interpreted as "the field strength of the electronic field at the electron's surface." It is known that for values of the field strength larger than this critical value, the phenomena cannot be described, even approximately, by older electrodynamic theories. At present we do not have a satisfactory substitute and it does not seem worth while, even if feasible, to attempt any-

thing like a quantitative discussion. We shall limit ourselves to the statement that the (extremely strong) production of (virtual) pairs will extend over a distance from the electron which will certainly equal a Compton wave-length, and that these virtual pairs will in turn take part in the scattering of the primary radiation. Even from a purely qualitative standpoint it seems hardly possible that the electron should act like a point source of scattered radiation, a condition which is necessary for the efficacy of the microscope arrangement.

3. Measurement of Field Strength

Field strengths are measured by determination of the ponderomotive action on a charge, q. We therefore have to discuss the measurement of the changes of momentum imparted to a test body. In the discussion presented in this paragraph we shall follow in all general assumptions the discussion of Bohr and Rosenfeld.[2] We shall not be concerned with a renewed discussion of certain fine points presented in their investigation, but shall attempt to show that accepting the results there obtained we shall have to modify them on account of the new electrodynamics. We shall furthermore limit our discussion to the simple case of the measurement of a component of the electric field strength.

The experimental arrangement shall be as follows: A test body of mass M occupying a volume V shall carry a uniformly distributed charge q. *No atomistic restrictions shall be made concerning any property of the test body.* We measure with the aid of the Doppler effect the velocity of the test body at the time t_1; it is assumed that the time of measurement does not exceed τ.

During the following time interval T we let the body be exposed to the action of the electric field E_x which we want to measure. At the time $t_1+\tau+T$ we carry out a second determination of the velocity as we did previously with the aid of the Doppler effect, during the time interval τ. From these measurements we deduce the average field strength $\langle E_x\rangle_{Av}$ which is defined by the relation

$$\langle E_x\rangle_{Av}=(1/TV)\int E_x dt dV$$

with the aid of the formula

$$q\langle E_x\rangle_{Av}=\frac{M(v_2-v_1)}{T}. \tag{8}$$

Following the discussion of Bohr and Rosenfeld we also shall only be concerned with statements about $\langle E_x\rangle_{Av}$ and not about any instantaneous point values of E_x.

We now have to discuss the possible accuracy which can be obtained from (8) for $\langle E_x\rangle_{Av}$. Bohr and Rosenfeld have discussed in detail why τ must always be taken very small compared to T. The question of the relative magnitude of cT and $V^{\frac{1}{3}}$ which, for other reasons, was of great importance in the paper of Bohr and Rosenfeld does not concern us here; we shall assume that we are dealing with the physically most important case of

$$cT\sim V^{\frac{1}{3}}.$$

The inaccuracy in the determination of $\langle E_x\rangle_{Av}$ is now mainly determined by the inaccuracy of the measurements of v_1 and v_2. Since we want the test body to be localized in a region of the approximate size of $V\sim L^3$ the uncertainty principle gives us for the inaccuracy in the measurement of Mv_1 and Mv_2 the approximate values

$$M\Delta v_1\sim M\Delta v_2\sim h/L.$$

We can therefore say that $\langle E_x\rangle_{Av}$ could be measured with an inaccuracy determined by

$$\Delta\langle E_x\rangle_{Av}\sim h/qTL. \tag{9}$$

If we measure the field strength of a light wave of the wave-length λ it will be reasonable to assume the spatial domain L and the time interval T which is connected with it by $L\sim ct$ in such a way that L is only a fraction of λ. Only then can we be certain that a value obtained for our average field strength has something to do with the primitive concept of a field strength as referring to a point, i.e., an arbitrarily small domain in space; otherwise the actions of a field will be averaged to zero when taken over a domain comprising many wave-lengths. For the same reason we have chosen $L\sim ct$. Inserting these relations into (9) we obtain for the inaccuracy in the measurement of an average field strength

$$\langle\Delta E_x\rangle_{Av}\sim hc/q\lambda^2. \tag{10}$$

Assuming that we express the wave-length in units of the Compton wave-length of the electron

$$\lambda = \delta(h/mc) = \delta\Lambda$$

and the charge carried by the test body in units of the electron charge $q = ze$ we can write (10)

$$\langle \Delta E_x \rangle_{Av} \sim \frac{1}{\delta^2 z} \frac{e}{\Lambda^2} \cdot \left(\frac{hc}{e^2}\right). \tag{11}$$

From (11) Bohr and Rosenfeld have concluded that $\langle E_x \rangle_{Av}$ can be measured with an arbitrary accuracy as long as we do not impose any atomistic restrictions upon the test body. By assuming z suitably large, the expression for $\langle \Delta E_x \rangle_{Av}$ can obviously be made arbitrarily small.

It is to be admitted that it is, logically, fully consistent to use such an idealized test body. Quantum mechanics in its present stage takes into account only the finiteness of h and not the atomistic structure of the charge e. Whatever the future theory may be which will *combine* the finiteness of h with the atomistic structure of e it seems at present undoubtedly of great importance to test the internal consistency of a theory which admittedly gives a correct picture of only part of our knowledge of nature.

But quantum mechanics on the other hand has in a certain way already exceeded its own limits through the discovery of the phenomena of pair production and the changes in electrodynamics which though only incompletely formulated, have thereby become necessary. An atomistic concept has crept in concerning the mass and charge of the particles created out of the vacuum and we shall see immediately that this phenomenon of pair creation destroys the possibility of an arbitrarily accurate measurement of the average field strength.

Let us inquire into the order of magnitude of z which is necessary to make the right side of (11) a small number. Assuming mainly for the sake of illustration that we are dealing with an incident wave-length equal to the Compton wave-length of the electron we then find that $\langle \Delta E_x \rangle_{Av}$ will be small compared to 1 if $z \gg 10^{12}$. Even admitting in the sense of the hypothesis underlying the whole argument, that a test body carrying a charge of 10^{12} in a volume smaller than Λ^3 can be constructed, we must not forget that such a test body will not retain its charge permanently even in a vacuum. There will be a leakage due to pair production and though we do not feel that the present state of theory allows us to make any reliable quantitative estimate we can be sure that this leakage will be a rapid process. It can be easily visualized as being due to a production of pairs of which one member will be drawn towards the test body and diminish its total charge while the other will go off to infinity. The energy necessary for the creation of a pair will be supplied by the gain in potential energy, which is due to the partial neutralization of the test body. The process mentioned is an illustration of the well-known mathematical fact that in the presence of an external field, states of positive and negative energy of the electron get mixed up with each other. The process quite obviously will continue until the gain in potential energy due to adding a charge to the test body will have become smaller than $2mc^2$. We so arrive at the concept of a limiting charge which cannot permanently be exceeded on a body of given radius.

A very crude estimate of the order of magnitude of this limiting charge can be obtained as follows: The gain in potential energy obviously equals ze^2/L while the energy which is necessary for the creation of a pair exceeds $2mc^2$. Equating these two expressions we obtain for the limiting charge

$$z_0 = 2mc^2 L/e^2 \tag{12}$$

or with $a = e^2/mc^2$ (a = electron radius)

$$z_0 = 2L/a. \tag{13}$$

The relation (13) seems to lead to absurd results if applied to the case of nuclei which carry a charge larger than the limiting z_0. This contradiction is only apparent since in the deliberations leading to (13) we had failed to include the kinetic energy of the particles into the energy necessary for the creation of a pair. This was approximately justified as long as the wave-length of a particle exceeded the Compton wave-length and the radius L of the test body was sufficiently large. If the test body (nucleus) becomes too small the kinetic energy must be taken into account and the gain in potential energy diminishes. The whole argument obvi-

ously is closely related to the fact that there do not exist stationary states for a Dirac electron under the influence of a charge $z>118$.

This phenomenon of leakage makes it impossible for us to use a test body which carries an arbitrarily large charge. We see from (11) and (13) that the limit is reached long before z has taken on a sufficiently large value. Inserting for a moment the limiting value z_0 into (11) we obtain for the maximum accuracy (minimum error) of $\langle \Delta E_x \rangle_M$ the relation

$$\langle \Delta E_x \rangle_M \sim eh/L^3 mc. \tag{14}$$

Field measurements therefore can be carried out with great accuracy for long wave-lengths and large time intervals; they become increasingly and finally absurdly inaccurate if we pass to small wave-lengths and short time limits. This production of momentum during pair production and its reaction on the momentum of the test body accounts for the impossibility of measuring accurately the momentum change produced in the test body by the field.

If one wants to visualize other disturbances which arise through pair production it can, perhaps, be done as follows: The high frequency radiation which is incident upon the body at the time t_1 during a time interval of τ will create pairs under the influence of the large electrostatic field of the test body. These pairs together with the pairs created by the test body itself will exert forces upon the test body. If the particles are created in a distance of the order of magnitude L the momentum due to these forces created during the time L/c will be of the order of magnitude of

$$e^2 z/Lc.$$

We will therefore obtain, per pair, an inaccuracy in the field strength of an order of magnitude of

$$\langle \Delta E_x \rangle_M \sim \frac{e^2 z}{Lc} \frac{c}{ezL} \sim \frac{e}{L^2}.$$

Not too much weight should be given to these deliberations because they probably are too "classical" and because we have no exact way of predicting the completely different phenomena which will occur in such excessively large fields.

Letters to the Editor

PROMPT publication of brief reports of important discoveries in physics may be secured by addressing them to this department. Closing dates for this department are, for the first issue of the month, the eighteenth of the preceding month, for the second issue, the third of the month. Because of the late closing dates for the section no proof can be shown to authors. The Board of Editors does not hold itself responsible for the opinions expressed by the correspondents.

Communications should not in general exceed 600 words in length.

Radioactive Rb from Deuteron Bombardment of Sr

A. C. HELMHOLZ, *Department of Physics, Radiation Laboratory, University of California;*

CHARLES PECHER, *Fellow of the Belgian-American Education Foundation, Radiation Laboratory, University of California;*

AND

PERRY R. STOUT, *Department of Plant Nutrition, University of California, Berkeley, California*

May 12, 1941

ONE of us[1] has reported the production in large quantities of a long-lived radioactive Y from the bombardment of Sr with 16-Mev deuterons. At this bombarding energy one would expect an appreciable amount of Rb to be produced by the (d, α) reaction. We have found a radioactive Rb of half-life 19.5 ± 1 days, produced from this reaction in sufficient quantities for tracer work and with the added advantage of high specific activity.

To prove that the activity was Rb the following procedure was adopted. The filtrate remaining after Y and Sr had been precipitated as $Y(OH)_3$ and $SrCO_3$ was evaporated to dryness and the ammonium salts driven off. Fe, as carrier for the Y, and Sr were again added along with 10 mg of K. Fe and Sr were precipitated in alkaline Na_2CO_3 solution. After filtration, K and Rb were precipitated from the filtrate with $Na_3Co(NO_2)_6$. If the active material had been Na it would have remained largely in solution, but over 99 percent was precipitated. The precipitate was dissolved in HCl, 4 mg of Rb added, and Rb_2SnCl_6 precipitated. All the activity came with the precipitate. Sn was then removed as sulfide, and the whole activity of, in this case, 400 μC remained in 4 mg of RbCl. Subsequent experiments showed that the activity could be separated quantitatively with Rb from equal molar mixtures of K, Sr, Ca and Mg. The activity must come from the Sr (d, α) Rb reaction since the Rb contamination of the target was negligible.

There are two "stable" isotopes of Rb, Rb^{85} and Rb^{87}. Snell[2] found an 18-min. and an 18-day period by the slow neutron bombardment of Rb. Our activity is undoubtedly his 18-day activity. The half-life of 19.5 days was obtained by following several samples over from one to four half-lives. However, there is some evidence for a weak longer period activity, so that the half-life may be somewhat shorter. Of the two slow neutron activities, only that of Rb^{86} can be produced by the Sr (d, α) Rb reaction, since Sr^{88} is the heaviest stable isotope of Sr. Therefore this 19.5-day period can definitely be assigned to Rb^{86}. This agrees with the assignment of the 18-min. period to Rb^{88} on the basis of Th fission experiments.[3,4]

Rb^{86} emits negative electrons and no strong γ-rays. From absorption measurements, the spectrum has an upper limit of 1.56 ± 0.05 Mev calculated from Feather's rule.

The yield of Rb^{86} from a 2000-microampere hour bombardment of Sr was 0.4 mC, as compared with 17 mC of the 55-day Sr^{89} from Sr^{88} (d, p) Sr^{89}, and 35 mC of the 100-day Y from Sr $(d, 2n)$ Y. The isotope responsible for the production of Y is uncertain, but if we assume that all the products come from Sr^{88}, the ratio of the cross sections for the $(d, 2n)$, (d, p), and (d, α) reactions at 16 Mev is 29 : 10 : 0.1. Dr. Martin Kamen has kindly supplied us with yield data for Fe and Mg bombarded with deuterons. In Fe the reactions are Fe^{56} $(d, 2n)$ Co^{56},[5] Fe^{58} (d, p) Fe^{59}, and Fe^{56} (d, α) Mn^{54}, and correcting for the reduced abundance of Fe^{58}, the ratio is 7 : 10 : 1.7. The Fe data are for 16-Mev deuterons. For Mg at 8 Mev the reactions are Mg^{26} (d, p) Mg^{27} and Mg^{24} (d, α) Na^{22}. The ratio here is ? : 10 : 200. We see that with increasing atomic number the (d, α) reaction drops off markedly as one would expect from the increase in the Coulomb barrier height. It is interesting to note that at 16 Mev, the $(d, 2n)$ reaction is one of the most probable, if not the most probable, reaction.

We wish to express our thanks to Professor E. O. Lawrence for his interest in this work and to the Research Corporation for financial support.

[1] Charles Pecher, Phys. Rev. **58**, 843 (1940).
[2] A. H. Snell, Phys. Rev. **52**, 1007 (1937).
[3] A. Langsdorf, Jr., Phys. Rev. **56**, 205 (1939).
[4] A. H. Aten, Jr., C. J. Bakker and F. A. Heyn, Nature **143**, 679 (1939).
[5] The measured Co consists of two long-life activities, and since the assignment of these activities is uncertain, our estimate of the yield may be in error by a factor of 2 or 3.

Showers of Penetrating Particles

M. DAMY DE SOUZA SANTOS, P. A. POMPEIA AND G. WATAGHIN
Department of Physics, São Paulo University, São Paulo, Brazil

December 17, 1940

IN previous papers[1,2] a report was given of measurements which gave evidence for the existence of showers of at least two particles of a range not smaller than 17 cm of lead and the size of the penetrating core of which is of the order of 0.2 sq. m.

In this paper we report further measurements made with a sixfold coincidence set with a resolving time of 1.8×10^{-6} sec. and with the multivibrator circuit developed by one of us.[3] Some of the arrangements used (Fig. 1) were chosen in order to avoid knock-on showers and the secondary effects of the soft radiation which usually accompanies the penetrating rays.

First, we have tried to get evidence of a possible association of the observed showers with the extensive showers discovered by Auger and his co-workers. A fivefold coincidence set was used: Four counters were arranged in two telescopes at a distance of 30 cm from each other and surrounded by lead (arrangement I of reference 1); the fifth counter being placed at a distance of 280 cm from the others. The observed frequency was of 8×10^{-4} min.$^{-1}$, showing that some soft radiation is associated with the penetrating core. We can therefore conclude that meson showers are responsible for some of the extensive showers.

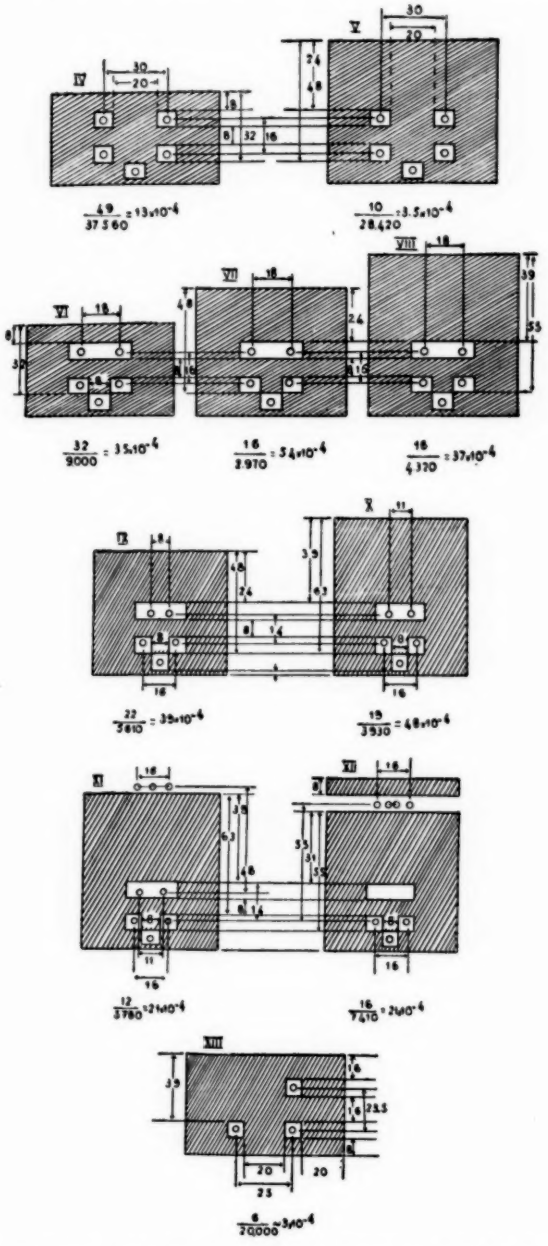

FIG. 1. Arrangements IV–XIII. The linear dimensions of the drawings are indicated in cm. The average frequency is given in min.$^{-1}$.

Other experiments on the nature of the penetrating showers are given in Fig. 1. The results of measurements IV and V show that a part of the rays responsible for the fivefold coincidences at a distance of 30 cm between the two telescopes, is absorbed by 24 cm of lead. By a narrower arrangement of type VI–X, there is no noticeable absorption and the observed frequency is about three times greater than the frequency of the fivefold coincidences in IV (and more than ten times greater than those in V) where 20 cm of Pb are placed between the telescopes. It might be objected that showers originated by a mesotron going through the lead sheet above the counters can produce such coincidences; especially if we take into account the experimentally established absorption coefficient of soft gamma-rays in lead [a sensible number of such rays are found in the cosmic rays][4] and the, experimentally as yet unverified, theoretical results of the meson theory[5] which predict high radiation losses for high energy mesons. We are very indebted to Professor G. Occhialini for having called our attention to this point. This assumption might also explain the differences in absorption effect observed in the arrangements IV–V and in VI–X. Such phenomena could be responsible for a part of the experimental results reported by Jánossy and Ingleby,[6] Froman, Josephson and Stearns[7] and Rossi and Regener.[8] Definite evidence for an association of at least two penetrating particles is given by arrangements of type V or of I, II, III of our previous paper, where the distance between two telescopes, each shielded from all the sides with at least 20 cm of lead, was increased to 120 cm.

It seems noteworthy that in experiments X, XI, XII the observed frequencies do not differ greatly, so that it is very probable that the observed showers are produced by vertical rays and contain several penetrating particles.

Other experiments are being carried out under 30 m of clay (about 50 m water equiv.). One of these is illustrated in Fig. 1—XIII. In a similar arrangement of threefold coincidences with a smaller distance between the two lower counters (only 8 cm Pb interposed) we have observed 13 coincidences in 14,500 min. We can therefore conclude that there is evidence for the existence underground (under 60 m water equiv.) of showers containing at least two particles penetrating more than 20 cm Pb. A simple calculation shows that it is highly improbable that soft radiation, which always accompanies the penetrating component underground, can be responsible for these showers. Further studies concerning the nature of the shower-producing rays is in progress.

[1] G. Wataghin, M. D. de Souza Santos and P. A. Pompeia, Annaes da Acad. Bras. de Sciencias, **11**, page 1. G. Wataghin, M. D. de Souza Santos and P. A. Pompeia, Phys. Rev. **57**, 61 (L) (1940). G. Wataghin, M. D. de Souza Santos and P. A. Pompeia, Phys. Rev. **57**, 339 (L) (1940).
[2] P. A. Pompeia, M. D. de Souza Santos and G. Wataghin, Annaes da Acad. Bras. de Sciencias, **12**, 229 (1940).
[3] M. D. de Souza Santos, Annaes da Acad. Bras. de Sciencias, **12**, No. 3, 179 (1940).
[4] G. Occhialini and M. Schönberg, Annaes da Acad. Bras. de Sciencias, **11**, No. 4; **12**, No. 3.
[5] H. C. Corbeu and H. S. W. Corbeu, Proc. Camb. Phil. Soc. **35**, 84 (1939). F. Booth and A. H. Wilson, Proc. Roy. Soc. **175**, 483 (1940).
[6] P. Ingleby and L. Jánossy, Nature **145**, 511 (1940).
[7] D. K. Froman, V. Josephson and J. C. Stearns, Phys. Rev. **57**, 335 (L) (1940).
[8] B. Rossi and V. H. Regener, Phys. Rev. **58**, 837 (1940).

Radioactivity Produced in Germanium*

R. SAGANE, G. MIYAMOTO AND M. IKAWA
Physics Department, Chemistry Department, Imperial University of Tokyo, Tokyo, Japan
April 23, 1941

IN continuing the study of the radioactivities produced in germanium,[1] we have checked most of the previous assignments of the isotopes after chemical separation. Four gallium and three arsenic isotopes were also produced from germanium. Seaborg and others[2] have reported recently on the same subject. They agree in general with our former assignments, but there remain some points which are not in accord with our present results. A further study is being carried out to make clear the discrepancy and some ambiguities.

Ge^{77} (8∼12 hr. e^-; 1.92 Mev). As has been suggested by one of the authors, this period was found in the germanium fraction of the Ge+SN sample and also in the Ge+D (3 Mev) sample. The results are in accord with Seaborg, although we are not quite certain whether the period should be 12 hours or shorter.

Ge^{75} (82±2 min. e^-; 1.10 Mev). In agreement with the former assignment done by one of us, the 82-min. period is produced by Ge (d, p), Ge (n, γ), Ge $(n, 2n)$, As (n, p) and Se (n, α). The results were checked by Seaborg and others.

Ge^{71} (30±4 hr. e^+; 1.15 Mev). In accord with the former results, a positron emitting period of about 30 hours was produced by Ge (n, γ), Ge $(n, 2n)$, Ge (d, p) and Se (n, α). Although the former value of 26 hours should be revised to be a little longer, yet the discrepancy between the result obtained by Seaborg (40 hours) is beyond the accuracy of the experiment. They also reported the 11-day period to be Ge^{71}, but we have not been able to find this period in the germanium fraction. Instead we found the 9-day period in the gallium fraction.

Ge^{69} 30-minute period reported by one of the authors has not been observed in Tokyo. We had accounted for the fact by the lack of energy in producing the $(n, 2n)$ reaction, but according to Seaborg and others they failed also. It might be an error due to the misinterpretation of the combined effect of gallium components (20 min. and 66 min.) produced in an appreciable amount.

Production of Ga^{68}, Ga^{70} and Ga^{72} in Ge+D and Ga^{70} and Ga^{72} in Ge+FN was chemically proved. One more long period of about 9 days (0.8 Mev) was found in the gallium fraction of the Ge+D sample, which is identical with the former suggestion. Probably this period is due to Ga^{74}.

We have reported[3] previously on the chemical identification of the 16-day and the 90-day periods as As^{74} and As^{77}, respectively. In addition to these a 50-hour period (e^+; 0.6 Mev) was also identified as an arsenic isotope. By making two successive chemical separations between germanium and arsenic fractions, it has been found that this isotope does not disintegrate successively. The fact shows that this period should be assigned to As^{73}. We failed to find the 88-minute (e^+) period in arsenic fraction. The former result[1] is probably due to the error of misinterpretation of the combined effect of the 66-min. and 30-hr. periods.

A more detailed report will be published shortly in the *Proceedings of the Physico-Mathematical Society of Japan.*

The authors are very grateful to Dr. Y. Nishina and Professor K. Kimura for their valuable help and discussions. The experiment has been aided by grants given by Hattori Hokokai and the Department of Education of the Government as the expenditure for the Scientific Researches.

The installation of the cyclotron has been aided by the Japan Society for the Promotion of Scientific Research, Mitsui Hoonkai Foundation, Tokyo Electric Light Company, Japan Wireless Telegraph Company and K. Hattori and Company.

* These results were reported at the meeting of the Phys.-Math. Soc. Japan held January 18, 1941.

[1] R. Sagane, Phys. Rev. **55**, 31 (1939).
[2] Seaborg, Livingood and Friedlander, Phys. Rev. **59**, 320 (1941).
[3] Sagane, Kojima, Miyamoto and Ikawa, Proc. Phys.-Math. Soc. Japan **21**, 660 (1939).

High Energy Gamma-Ray from Li+D

W. E. BENNETT, T. W. BONNER, H. T. RICHARDS AND B. E. WATT
Rice Institute, Houston, Texas
May 2, 1941

A 440-KEV gamma-ray is the only one reported to have been observed when lithium is bombarded by deuterons.[1] We have observed gamma-rays from this reaction which are more energetic and more intense than the 440-kev gamma-rays. The latter have not been observed in our experiments.

An absorption curve in lead of the gamma-radiation showed that its energy was considerably greater than 440 kev. The energy was measured more accurately by using coincidence counters to find the maximum range of the Compton electrons in aluminum.[2] The maximum range was 8.7 mm corresponding to a gamma-ray energy of 4.9±0.3 Mev. Effects from the nuclear beta-rays from Li^8 were avoided by using 7.2 g/cm² of carbon as an absorber between the target and the Geiger counters.

To get the absolute yield of gamma-rays a thin target of LiOH (13.4 kev thick) was bombarded by 770-kev deuterons and the gamma-rays were counted by a single Geiger counter, assumed to be 2 percent efficient in counting gamma-rays of these energies. From the number of gamma-rays produced in this thin target, the number produced in a thick target of lithium was calculated for 770-kev deuterons from an excitation curve for the gamma-radiation which we had taken. The intensity of the gamma-radiation was found to be 3.0×10^6 quanta per microcoulomb. The yield of neutrons for this reaction is known,[3] and we find the ratio of gamma-rays to neutrons to be 3.3 percent.

The gamma-rays were observed from thick and thin targets of LiCl and thin targets of LiOH deposited on copper and on silver. This makes it fairly certain that the gamma-rays were not produced by bombardment of any other material. Furthermore the excitation curve for the gamma-rays was similar to that for the neutrons from Li^7 and for the beta-rays from Li^8 formed by the bombardment of lithium by deuterons. All three excitation curves showed resonances at about 700 and 1000 kev of deuteron energy.

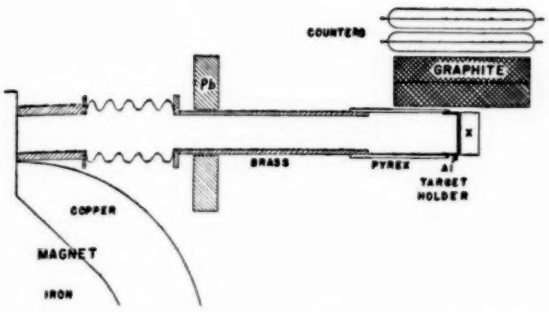

FIG. 1. Diagram of the experimental arrangement used to test whether the gamma-ray could be from inelastic scattering of the neutrons. X is the material under test.

It still seemed possible that the observed gamma-ray might have been produced by inelastic scattering of the neutrons or beta-rays (bremsstrahlung) from lithium in neighboring materials. We first verified that the gamma-rays originated in the immediate neighborhood of the target by moving the counters to different distances and comparing the change in counting rate with the inverse square law. We found that, at 10 cm from the target, 80 percent of the gamma-radiation and 97 percent of the harder components in it originated at the target. The materials near the target (brass, aluminum, Pyrex glass) were tested by placing additional amounts in front of the target (Fig. 1) and measuring the increase in the gamma-ray intensity at the side. Effects were found for all materials, but calculations showed that the amounts normally present were enough to increase the intensity of gamma-radiation by only 9 percent. Similarly the gamma-rays produced by neutrons and beta-rays in the carbon blocks used to absorb the beta-rays amounted to 10 percent at most. To check whether the neutrons were counted in any manner by the Geiger counter, the carbon blocks were replaced by a block of paraffin of equal absorbing power for gamma-radiation. The neutron intensity behind the paraffin was 0.48 of its value behind the graphite blocks, the ratio being measured by using an electroscope filled with methane at high pressure. The counting rate was the same whether the Geiger counters were shielded by carbon or by paraffin, and we conclude that the neutrons were not affecting the counting rate in any way. If the beta-rays from Li^8 had affected the counters either directly or indirectly the gamma-effect would have decayed with a period of 0.9 second when the bombardment was stopped. We found that at least 90 percent of the gamma-effect stopped immediately when the beam was cut off by a shutter. There were longer period activities induced in the counters by neutron bombardment, but these effects were always subtracted as part of the background count.

It is fairly certain that the 4.9-Mev gamma-ray is produced by the bombardment of Li^7 and not of Li^6 because the excitation curve (unpublished) is typical of Be^9 as the intermediate nucleus. The gamma-ray might indicate an excited level of either He^5 or Be^8 from energy considerations alone, but no group of alpha-particles has been observed which would correspond with the formation of He^5 in an excited state. There is some evidence[4] of a neutron group which corresponds to the formation of Be^8 in an excited state at 4 to 5 Mev so we take the existence of this gamma-ray as further evidence of an excited state in Be^8 which emits a gamma-ray before breaking up into two alpha-particles.

[1] J. H. Williams, W. G. Shepherd and R. O. Haxby, Phys. Rev. **52**, 390 (1937).
[2] The experimental arrangement is described by Bennett, Bonner and Watt, Phys. Rev. **59**, 793 (1941).
[3] Amaldi, Hafstad and Tuve, Phys. Rev. **51**, 896 (1937).
[4] H. T. Richards, Phys. Rev. **59**, 796 (1941).

A High Magnetic Saturation Value for the Copper-Manganese-Tin Heusler Alloy, Cu_2MnSn

LOUIS A. CARAPELLA AND RALPH R. HULTGREN
Department of Physical Metallurgy, Graduate School of Engineering, Harvard University, Cambridge, Massachusetts
May 5, 1941

THE Heusler alloy of the composition, Cu_2MnAl, has long been thought to be the most ferromagnetic of this famous series.[1] However, in the course of an extensive investigation of the magnetic nature of beta-copper-manganese-tin alloys, it was found that the Cu_2MnSn alloy is considerably more magnetic, both on a volume and an atomic basis. The alloy has been shown to be a body-centered-cubic superlattice of the Cu_2MnAl type[2] with $a_0=6.1608$A at 25°C. A high temperature x-ray diffraction pattern showed that ordering had not been destroyed at 630°C.

A maximum saturation value $\sigma_0=76.65$ ergs/gauss/gram at liquid-nitrogen temperature was found at the composition Cu_2MnSn. This equals $I_0=660$ ergs/gauss/cc or 4.14 Bohr magnetons per Cu_2MnSn group. The corresponding value which has been published[3] for the Cu_2MnAl alloy is $I_0=555$ or 3.15 Bohr units per group of four atoms. The substitution of tin for aluminum has increased the lattice constant (and, consequently, the corresponding atomic spacings) by about 4 percent and the magnetizability by 19 percent.

The high value is difficult to explain. If manganese is the sole source of magnetism, at least some of the atoms must have two 4s (valence) electrons, whereas transition elements are supposed usually to have zero valence[4] in the metallic state. Copper may be divalent and act as a ferromagnetic transition atom in these alloys.[5] Whatever the explanation, the alloy apparently has on the average nearly 8 valence electrons per 4 atoms in contradiction to the 3 : 2 electron-atom ratio predicted by the Hume-Rothery[6] rule for body-centered-cubic structures. (If normal valences are assigned to atoms, the Hume-Rothery rule is satisfied.)

A complete account of the research on the copper-manganese-tin system will be published in the near future.

[1] F. Heusler, W. Starck and E. Haupt, Verh. d. D. phys. Ges. **5**, 219–232 (1903).
[2] A. J. Bradley and J. W. Rodgers, Proc. Roy. Soc. **144**, 340–359 (1934).
[3] O. Heusler, Ann. d. Physik **19**, 155–201 (1934).
[4] N. F. Mott and H. Jones, *The Theory of the Properties of Metals and Alloys* (Clarendon Press, Oxford, 1936), Chapter V, pp. 150–174.
[5] J. C. Slater, Phys. Rev. **36**, 57–64 (1930).
[6] W. Hume-Rothery, J. Inst. Metals **35**, 295–361 (1926).

On the Virial Theorem in the Theory of Metals

R. LANDSHOFF
College of St. Thomas, St. Paul, Minnesota
May 15, 1941

IN the discussion of the many electron problem the virial theorem may frequently be used to great advantage. It has been shown by Fock[1] that not only the kinetic and potential energy of the correct but also of any approximate quantum-mechanical electron configuration will satisfy the virial theorem, provided only that the wave function of the approximate configuration has been determined by a variational method. The proof consists of a discussion of the effect of an infinitesimal uniform dilation of the entire system on the wave function of the electrons. In contrast to the very general method of this proof it is of interest to establish the theorem in a typical example by a direct calculation of the kinetic energy. The variational method has been used with great success in the theory of metals to consider the correlation between electrons with opposite spin[2,3] and we shall carry the demonstration through for this particular case.

The calculation of Wigner applies to the case where the positive ions are replaced by a uniformly distributed space charge. In the Hartree-Fock approximation this leads to products of free electron wave functions, that is plane waves, and both the total energy and the kinetic energy are easily calculated. They come out to be:[4]

$$E=(2.21Ry/r_s^2)-(0.916Ry/r_s) \tag{1}$$

and

$$K=2.21Ry/r_s^2. \tag{2}$$

The virial theorem in the form

$$K=-(d/dr_s)(r_sE) \tag{3}$$

can be easily demonstrated from these formulas. In addition to the energy calculated in the above approximation Wigner obtained the "correlation" correction.

$$E_1=\frac{1}{n!}\int dy|y|^2\Sigma_\nu\epsilon_\nu \tag{4}$$

with

$$\epsilon_\nu(y_1\cdots y_n)=\int\psi_\nu(y;x)^* \times\{V-(h^2/m)(\Delta_x-(2\pi i\nu/L)\mathrm{grad}_x)\}\psi_\nu(y;x)dx \tag{5}$$

[Eqs. (3), (3b) of reference 3]. $\psi_\nu(y;x)$ are the modified wave functions* (reference 3, Eq. (9)). It can be easily seen that

$$\kappa_\nu(y_1\cdots y_n)=-(h^2/m)\int\psi_\nu(y;x)^* \times(\Delta_x-(2\pi i\nu/L)\mathrm{grad}_x)\psi_\nu(y;x)dx \tag{6}$$

is that part of ϵ_ν which represents the additional kinetic energy. From the form of $\psi_\nu(y;x)$ one obtains

$$\kappa_\nu=\Sigma_\mu|\alpha_{\nu\mu}|^2t_{\nu\mu}. \tag{7}$$

By solving the minimum problem Wigner finds the coefficients $\alpha_{\nu\mu}$ (reference 3, Eqs. (17a) (17b)). We substitute them in Eq. (7) and obtain

$$\kappa_\nu=\sum_{\substack{2\nu-\mu\\ 0<c<c}}\frac{|V_{\nu\mu}|^2t_{\nu\mu}}{(t_{\nu\mu}+t'_{\nu\mu})^2}+\Sigma\frac{|V_{\nu\mu}|^2t_{\nu\mu}t^2_{\nu,2\nu-\mu}}{[(t_{\nu\mu}+t'_{\nu\mu})t_{\nu,2\nu-\mu}+t_{\nu\mu}t'_{\nu\mu}]^2}, \tag{8}$$

the corresponding formula for the total energy (reference 3, Eq. (19)) looks somewhat simpler than this one. Since the t do not depend on the y we compute with the help of (reference 3, Eq. (20))

$$K_\nu=\frac{1}{n!}\int dy|y|^2\kappa_\nu=\frac{2Ry}{3\pi^3}\int_{\substack{|\sigma+\rho|>1\\ |\sigma-\rho|<1}}\frac{\eta(\sigma)(\sigma^2+\sigma\cdot\rho)d\sigma}{\sigma^4[\sigma^2+\sigma\cdot\rho+c\epsilon'(\sigma)]^2} +\frac{2Ry}{3\pi^3}\int_{\substack{|\sigma+\rho|>1\\ |\sigma-\rho|<1}}\frac{\eta(\sigma)(\sigma^2+\sigma\cdot\rho)(\sigma^2-\sigma\cdot\rho)d\sigma}{\sigma^2[\sigma^4-(\sigma\cdot\rho)^2+2c\epsilon'(\sigma)]^2}. \tag{9}$$

By comparing this with the equivalent formula for the total energy (reference 3, Eq. (22)) we see that it can be written as

$$K_\nu=-F_\nu-c(d/dc)F_\nu. \tag{10}$$

The parameter c is proportional to r_s (reference 3, Eq. (22a)) and we can therefore write

$$K_\nu=-(d/dr_s)(r_sF_\nu). \tag{11}$$

By summing this over all the states ν we obtain for the total kinetic energy the relation

$$K_1=-(d/dr_s)(r_sE_1), \tag{12}$$

which is demanded by the virial theorem.

[1] V. Fock, Zeits. f. Physik **63**, 855 (1930).
[2] E. Wigner and F. Seitz, Phys. Rev. **46**, 509 (1934).
[3] E. Wigner, Phys. Rev. **46**, 1002 (1934).
[4] E. Wigner, Trans. Faraday Soc. **34**, 678 (1938).
* The notation which is employed hereafter is that of Wigner's paper and as it is fully explained there such explanation is omitted in this paper.

Remarks on Energy Losses Attending Thermionic Emission of Electrons from Metals

W. B. NOTTINGHAM
George Eastman Laboratory of Physics, Massachusetts Institute of Technology, Cambridge, Massachusetts
November 30, 1940

THE recent publication of a paper on "The energy losses attending field current and thermionic emission of electrons from metals" by Dr. Gertrude M. Fleming and Professor Joseph E. Henderson[1] presents the results of a very valuable experimental study of this subject but, in the opinion of the writer, an error has been made in the assumed physical processes involved. If one considers that the free electrons in a metal can be described as having a Fermi distribution characterized by the thermodynamic potential μ, then at any temperature T the "random" current flow in the positive x direction across any boundary can be calculated. As far as the flow of heat energy is concerned this may be calculated by determining how many electrons with energy greater than μ cross the boundary in a given time and multiplying this by the *average* energy carried by each electron. In addition to this one may consider that there is a "current" of "holes" in the Fermi band crossing the same boundary and that energy is carried by these and may be computed by multiplying the number of holes crossing in a given time by the *average* energy carried by each hole. Fleming and Henderson compute this average energy associated with the current flow of holes and

find $\bar{\epsilon}_0=\mu-1.2kT$. The determination of the 1.2 is necessarily an approximation but is good to better than four percent. They then proceed to compute the heat carried away by electrons emitted in an accelerating field as though the emission current were supplied at the cool part of the filament at the level $\bar{\epsilon}_0$ instead of μ. This leads to the result $\bar{w}=\phi+3.2kT$ for the average energy carried away per electron when emitted thermionically. Here ϕ is the work function $(C-\mu)$ and C is essentially the potential energy of an electron just outside of the emitter relative to the bottom of the Fermi band as zero.

Consider the receiving plate of a tube for studying thermionic emission to be at 0°K. Then the electrons in the emission current cannot fall into quantum states lower than μ upon being received because all of those states are filled. The electric current flows around the circuit at the level μ (except for batteries) and flows into the emitter at this level. Richardson[2] visualized a situation essentially no different from this and showed that the true heat loss per electron attending thermionic emission is $\bar{w}=\phi+2kT$. A reflection effect, or a transmission coefficient $D(W)$ which is constant and therefore independent of W for all values of $W>C$, does not alter $\bar{w}$ where W is the energy associated with the motion normal to the surface. Thermionic studies[3] indicate that $D(W)=1-\exp(W-C)/R$ represents the experimentally determined energy distributions accurately where R is an empirical constant equal to 0.191 electron volt. A paper is being prepared which shows that with this transmission coefficient, $\bar{w}=\phi+kT[2+1/(1+kT/R)]$. For the temperature range 1500°K to 2200°K this coefficient of kT varies from 2.6 to 2.5 as compared with 2 for non-selective transmission.

The possibility that there are misprints on page 893 of Fleming and Henderson makes a detailed checking of their results difficult since three of the integrations have limits μ to ∞ instead of those expected of 0 to ∞ and the brackets are not completed in front of the exponentials as it seems they should be. Although the writer has not yet been able to duplicate the final equation giving $\bar{w}$ as computed for the case of field emission using the indicated limits of μ to ∞, there can be no doubt concerning the final result that an inappreciable heat loss is to be expected for the electrons emitted even though the temperature of the emitter is fairly high. In fact it seems likely that one would find a detectable heating effect when a strong emission takes place from a very sharp point. If one uses integration limits 0 to ∞ and assumes that the electrons enter the emitter at the μ level, the calculation of such heating, if it exists, is straightforward.

It should be clear that the above criticisms apply to aspects of the theory which are on the borderline of the experimental accuracy that one may hope to attain. The main general conclusions, that in the case of thermionic emission the heat loss is largely dominated by an energy very nearly $\phi+2kT$, and that very little heat loss is to be expected in the case of field emission, are well borne out by the experiments.

[1] G. M. Fleming and J. E. Henderson, Phys. Rev. **58**, 887 (1940).
[2] O. W. Richardson, Phil. Trans. **A201**, 497 (1903).
[3] W. B. Nottingham, Phys. Rev. **49**, 78 (1936).

On the Energy Losses Attending Thermionic and Field Emission

GERTRUDE M. FLEMING
Russell Sage College, Troy, New York
AND J. E. HENDERSON
University of Washington, Seattle, Washington
May 15, 1941

IN the preceding letter Professor Nottingham is concerned about a calculation performed in a paper[1] by us to evaluate the energy loss in thermionic emission. The essential difference in viewpoint, as Professor Nottingham chooses to discuss it, depends upon whether the electrical conduction in a metal can occur at levels lower than μ, the Fermi parameter; Professor Nottingham's contention being that conduction physically occurs only at the level μ.

Other than the experimental results themselves, the most important conclusion to be drawn from the paper[1] under discussion is that conduction can occur at levels below μ. This conclusion rests upon the validity of two experimental results: first, the conclusion of the paper in question that there is no measurable temperature change of a field current emitter, and second, that there exists an energy distribution[2] for the electrons involved in field emission, which exhibits a maximum often two volts below the maximum energy corresponding to μ.

To make this conclusion more evident, consider a piece of metal with electrons being emitted at one end and supplied by conduction at the other end. Let $N(E)$ be the rate at which electrons of energy E are emitted, and let the average energy in the current of electrons entering the metal be E_1. Then the rate at which energy is acquired during emission by the metal is $\int_0^\infty(E_1-E)N(E)dE$. Since the experimentally determined energy distribution for field electrons emitted near room temperature shows that $N(E)$ has a maximum for an energy, E, of the order[2] of a volt or more below μ, if E equals μ the integral is essentially positive and equal to at least one electron volt/electron. The temperature change of any point in the emitter depends on the degree of concentration of energy released in the vicinity of the point. For field emission at room temperature an average energy transfer of 0.002 electron volts per electron would, if concentrated at the emitting surface, have been detectable. Thus the experiments[1] show that not more than 1/500 of the energy release is concentrated at the emitting surface. Therefore, either the electrons in the net current are not supplied at the level μ, or their transition from higher to lower levels occurs on the average at a large distance from the emitting surface.

The usual perturbation methods used in the kinetic theory evaluation of conduction take into account three kinds of perturbations (density, temperature and potential variations). It is further required that these perturbations be small. The condition in the vicinity of a boundary may be regarded as a perturbation of another kind and in this case the perturbation is not necessarily small. In view of the deficiency of the theory for this kind of problem, the calculation in the paper[1] is necessarily a rough estimate of the phenomena occurring in the neighborhood of the boundary.

The three integration lower limits, μ, on page 893 are not misprints. However, the brackets should be closed in front of the exponential factor in the second equation for w, and the last equation on page 894 should read $w=\phi+3.2kT$.

[1] G. M. Fleming and J. E. Henderson, Phys. Rev. **58**, 887 (1940).
[2] J. E. Henderson and R. K. Dahlstrom, Phys. Rev. **55**, 473 (1939).

On the Selection Rules in Beta-Decay

J. R. OPPENHEIMER
Physics Department, University of California, Berkeley, California
April 25, 1941

THE rapid decay of a presumably largely ^1S He^6 to a $^3S+^3D$ Li^6 has always been regarded as strong evidence for the Gamow-Teller selection rules in beta-decay. The analogous disintegration $C^{10}\rightarrow B^{10}$ is also rapid and obviously allowed. However the three further at first sight similar disintegrations

$$(S) \qquad H+H\rightarrow D; \quad Be^{10}\rightarrow B^{10}; \quad C^{14}\rightarrow N^{14},$$

where in every case the parent nucleus would be expected to be largely ^1S, and the product nuclei are known to be predominantly $^3S+^3D$, are slower than would be expected for allowed transitions of the observed energy by factors of the order 10^4-10^7. The activity $O^{14}\rightarrow N^{14}$, homologous to that of C^{14}, is not known; the activity of F^{18}, where normal states can perhaps be less unambiguously assigned, is allowed.

The assumption that the initial states in the disintegrations (S) have been incorrectly assigned is very unsatisfactory. For the reaction $H+H\rightarrow D$ there can be no question that the initial state is ^1S; and the astrophysical evidence that this reaction is slow seems excellent. For Be^{10} and C^{14} states of very high angular momentum (^1G) would be required to account, with Gamow-Teller selection rules, for their extremely long life; this is not only highly implausible on the basis of any known nuclear theory, but in gross contradiction with the expected proton-neutron symmetry of the nuclei C^{10} and Be^{10}. Almost equally unsatisfactory is the assumption that He^6 and C^{10} are ^3S or ^3D, and the Gamow-Teller selection rules wrong; for this too, in addition to leaving unexplained the many less direct evidences for spin change in allowed transitions, would grossly violate theoretical expectations on the symmetry of normal states and on the proton-neutron symmetry in C^{10} and Be^{10}.

The fast reactions

$$(F) \qquad He^6\rightarrow Li^6; \quad C^{10}\rightarrow B^{10}$$

differ from the slow reactions (S) systematically, in that for (F) energies of over 3 Mev are available, whereas for (S) the energies are 350 kev, 550 kev, and 150 kev, respectively. This suggests that the Gamow-Teller selection rules have a "threshold," such as would be involved if the corresponding neutrino had a rest mass. This rest mass would have to be at least of the order of that of an electron, and might for instance characterize a neutrino of spin $\frac{3}{2}$. On this theory the reactions (S) would be governed by Fermi selection rules, and there would then be no difficulty, on taking into account the small amount of ^3P to be expected in the initial states, and of ^1P in B^{10} and N^{14}, in accounting for their very long lifetimes. The reactions (F) on the other hand would involve the emission of a heavy neutrino and be allowed by Gamow-Teller selection rules.

This suggestion has three simple consequences: (I) There should be a discrepancy, given by the mass of the heavy neutrino, in the energy balance of the reactions (F).[1] (II) The shape of the upper end of the He^6 and C^{10} spectra should correspond to a finite neutrino mass. (III) The disintegration $O^{14}\rightarrow N^{14}$, that has an estimated upper limit 3.8 Mev$-\mu c^2$, with μ the heavy neutrino mass, should decay rapidly. If we take N^{14} as 15 percent ^3S, and $\mu c^2\sim\frac{1}{2}$ Mev, the lifetime should be about 20''.[2]

It would appear that published evidence was neither sufficient to check nor disprove these expectations. If we suggest the *a priori*, highly improbable existence of the heavy neutrino, it is in part because these three points can so readily be settled, but even more again to call attention to the very puzzling difficulties that have arisen in interpreting these activities.

[1] The Wigner and Hartree estimates of the $C^{10}-Be^{10}$ Coulomb difference themselves differ by several hundred kilovolts, and are presumably of insufficient accuracy to afford a test of the C^{10} energy balance.
[2] The bombardment of C with alpha-particles, of N with deuterons, both lead to strong O^{15} activity; the bombardment of N with protons leads to a strong C^{11}. All these reactions have been tried in Berkeley, by Dr. Kamen, Dr. Segrè, and Mr. Wright, as sources for O^{14}; in every case the results of a preliminary survey were negative. These investigations are not yet concluded, and I am grateful to these workers for telling me of their findings.

Non-Laue Diffraction Maxima from Rocksalt—Non-Equatorial Maxima

G. E. M. JAUNCEY, O. J. BALTZER, AND D. C. MILLER
Washington University, St. Louis, Missouri
May 15, 1941

PROFESSOR W. H. Zachariasen has been kind enough to send the senior author a copy of his Letter to the Editor which appears in this issue of *The Physical Review*. Non-equatorial associated Bragg spots appeared on the films which were used in Jauncey and Baltzer's paper.[1] A correction for the position of these spots on the film must be made if the l axis of the crystal and the axis of the cylinder of photographic film are not parallel. Making this correction, which will be described later, we find the experimental shifts, $2\theta_m-2\theta_B$, shown in the second column of Table I. The shifts are for the 402 associated Bragg spots

TABLE I. *Values of* $2\theta_m-2\theta_B$.

		FORMULA	
Δ	EXP.	ORIG.	REV.
$-3°20'$	$-1°19'$	$-2°29'$	$-1°37'$
$-2°25'$	$-0°55'$	$-1°48'$	$-1°10'$
$-1°39'$	$-0°47'$	$-1°14'$	$-0°48'$
$-0°44'$	$-0°09'$	$-0°33'$	$-0°21'$
$+0°12'$	$-0°00'$	$+0°09'$	$+0°06'$
$+1°01'$	$-0°28'$	$+0°45'$	$+0°29'$
$+1°49'$	$-0°45'$	$+1°21'$	$+0°52'$

produced by Cu $K\alpha$ radiation. In his first paper on the theory of non-Laue maxima, Zachariasen[2] gave $2\theta_m - 2\theta_B = 2\Delta \sin^2\theta_B$. In his letter, he gives a revised formula $2\theta_m - 2\theta_B = 2\Delta/(1+\cot\theta_B \cot\phi_m)$. The shifts calculated from these formulas are shown in the third and fourth columns, respectively. The revised formula agrees much better with the experimental results than the original formula. The shifts for the non-equatorial spots are somewhat difficult to measure and we do not attach any significance to the discrepancies between the second and fourth columns.

[1] G. E. M. Jauncey and O. J. Baltzer, Phys. Rev. **59**, 699 (1941).
[2] W. H. Zachariasen, Phys. Rev. **57**, 597 (1940).

The Temperature Diffuse Scattering Maxima for Rocksalt

W. H. ZACHARIASEN
Ryerson Physical Laboratory, University of Chicago, Chicago, Illinois
May 13, 1941

THE current issue of *The Physical Review* contains an article by Jauncey and Baltzer[1] dealing with the positions of temperature diffuse scattering maxima observed for rocksalt. The authors state that the observed shifts from the Bragg positions are considerably smaller than predicted by the theory due to the present writer[2] and they suggest that the theory may be valid only in a limited range not covered by their experiments.

Jauncey and Baltzer compare their observations with the formula given as Eq. (23) of reference 2. This formula is obtained from the simplified intensity expression [Eq. (18)] which—as clearly stated by the writer—is but a crude approximation to the rigorous expression [Eq. (17)]. The failure of Eq. (23) to provide a quantitative explanation of the experimental data accordingly does not imply that the theory needs revision. It can be shown[3] that Eq. (17) in the case of rocksalt leads to the following formula for the position of a diffuse maximum:

$$2\theta_m = 2\theta_B + 2\Delta/(1+\cot\theta_B \cot\varphi_m)$$

where $$\varphi_m = 0.600\theta_B + 0.017\theta_B^4.$$

Table I contains the shift from the Bragg positions as calculated from this formula and as observed by Jauncey and Baltzer. The two sets of values agree within the experimental error. Thus the experiments of Jauncey and Baltzer far from throwing any doubt on the validity of the theory actually represent convincing evidence in its support.

TABLE I. *Observed and calculated shifts.*

	400 $2\theta_m - 2\theta_B$			620 $2\theta_m - 2\theta_B$	
Δ	OBS.	CALC.	Δ	OBS.	CALC.
7.0°	2.4°	2.7°	3.87°	4.5°	4.4°
6.0	2.4	2.3	2.87	3.2	3.2
5.0	2.1	1.9	1.87	1.8	2.1
4.0	1.6	1.5	0.87	0.9	1.0
3.0	1.3	1.2	−0.13	0	−0.1
2.0	0.8	0.8	−1.13	−1.2	−1.3
1.0	0.6	0.4	−2.13	−2.3	−2.4
0	0	0	−3.13	−3.6	−3.5
−1.0	−0.4	−0.4	−4.13	−4.5	−4.7
−2.0	−0.6	−0.8	−5.13	−5.4	−5.8
−3.0	−1.2	−1.2			
−4.0	−1.8	−1.5			
−5.0	−1.8	−1.9			

[1] G. E. M. Jauncey and O. J. Baltzer, Phys. Rev. **59**, 699 (1941).
[2] W. H. Zachariasen, Phys. Rev. **57**, 597 (1940).
[3] W. H. Zachariasen, Phys. Rev. **59**, 860 (1941), (this issue).

Geomagnetic Character and Cosmic-Ray Intensity Pulses

JAMES W. BROXON
Department of Physics, University of Colorado, Boulder, Colorado
May 13, 1941

UNFORTUNATELY and inadvertently, in a Letter to the Editor under the above title in the April 15 number of *The Physical Review* there was not included a reference to a paper by S. E. Forbush (Bull. Int. Union Geod. and Geophys. No. 11, pp. 438–452 (1940)) in which he arrived at about the same conclusions by a different method. Employing Bartels' harmonic dial method of harmonic analysis, he showed the existence of quasi-persistent 27-day waves (and also 13.5-day waves) in the cosmic-ray intensity at Huancayo, Peru, and Christchurch, N. Z., with amplitudes of 0.22 and 0.14 percent, respectively. He also showed the cosmic-ray variations were approximately opposite in phase to similar variations in the American magnetic character-figures, and concluded they were not due to a solar magnetic moment inclined to the rotation axis of the sun.

Proceedings of the Southeastern Section of the American Physical Society

Minutes of the Nashville, Tennessee, Meeting

April 4–5, 1941

THE seventh annual meeting of the Southeastern Section of the American Physical Society was held at Vanderbilt University, Nashville, Tennessee, on Friday and Saturday, April 4–5, 1941. Approximately one hundred and sixty members and guests attended the meeting. Local arrangements were made by a committee headed by F. G. Slack.

The regular program consisted of twenty papers, abstracts for thirteen of which are appended hereto. Abstracts for other papers will be found in the June issue of the *American Journal of Physics*. There was a special symposium of invited papers on molecular structure as follows:

Use of Isotopes in Molecular Spectra. Edward Teller, *George Washington University.*

Absorption Spectra of Substituted Benzenes. Hertha D. E. Sponer, *Duke University.*

Interaction Theory and Anomalies in the Infra-red Spectra of Polyatomic Molecules. Harald H. Nielsen, *Ohio State University.*

The Structure Determination of Molecules and Groups in Crystals by Means of X-Ray Diffraction. Rose C. L. Mooney, *Sophie Newcomb College, Tulane University.*

At the business meeting the election of the following officers for the year 1941–42 was announced: Chairman, Fred Allison; Vice Chairman, W. S. Nelms; Secretary, E. S. Barr; Treasurer, C. B. Crawley; Members of the Executive Committee, F. G. Slack (4 years) and R. S. Williamson (1 year).

The invitation extended by the University of Mississippi to hold the 1942 annual meeting at Oxford, Mississippi, was accepted.

E. S. Barr, *Secretary*

Abstracts

1. Optimum Liquid Combinations in Cloud Chambers. Clifford Beck, *University of North Carolina.*—Combinations of liquids were studied to find mixtures giving good electron tracks and minimum fog at low expansion ratios. A seven-inch, rubber-diaphragm chamber was used; observations were visual. 40–60 percent ethyl alcohol-water mixtures gave a minimum expansion ratio in semiquantitative agreement with published values. A similar ratio was obtained with 40–60 percent *n*-butyl-water, but this caused extensive fog. Isopropyl or *n*-propyl with water gave still lower minimum expansion ratios. No alcohol-alcohol combination gave a lower ratio than one of the alcohols involved. Acetone (25 percent) with ethyl or *n*-propyl gave excellent conditions but high expansion ratios; addition of water lowered them. The best mixture found was approximately 50–25–25 percent ethyl or normal propyl, water, and acetone, respectively. Brief irradiation with a Labarc before expansion caused general fog. Effects of such irradiation disappear in 3 to 6 minutes. Acetone increased fog due to ultraviolet, but hastened subsequent clean-up of neutral condensation nuclei; hence its general favorable effect. Photoflood lamps used for illumination also produced fog. Pressure increase (2 pounds/square inch) affected background fog and necessitated lower expansion ratios.

2. Differential Measurement of the Meson Lifetime. W. M. Nielsen, C. M. Ryerson, L. W. Nordheim, *Duke University*, and K. Z. Morgan, *Lenoir Rhyne College.*—Measurements of the meson lifetime were made by comparing the lead absorption curves of the cosmic radiation at two different elevations, and by compensating the air column at the higher level by a layer of graphite placed on top of the counter telescope. The method does not require any knowledge of the energy distribution or of the height of the producing layer of the mesons. All systematic errors are greatly reduced by the differential method used and can be shown to be insignificant. The value of the lifetime comes out to be appreciably shorter than in previous determinations, viz. $(1.25\pm0.3)(\mu c^2/10^8$ e.v.$)\times10^{-6}$ sec.

3. Decay Radiation and Nature of the Meson. L. W. Nordheim, *Duke University.*—Knowledge of the lifetime of the meson and of the intensity of the soft component produced by its decay would make it possible to determine the fraction of the meson energy which in the decay process is given to electrons and photons. A knowledge of this fraction α would allow important conclusions regarding the nature and the spin of the mesons. An analysis of the available data shows that α is definitely less than 1, which

means that part of the energy is converted into an inobservable form, i.e., into neutrinos. It is not even certain that α can be as large as 1/2 which value corresponds to the usual hypothesis that a meson with spin 1 decays into a single electron and a single neutrino.

4. A Van de Graaff Pressure Type Electrostatic Generator. G. T. HUNTER AND D. C. SWANSON, *University of Florida.*—A Van de Graaff electrostatic generator designed to operate at potentials as high as a million volts is being developed at the University of Florida. This generator is enclosed in a steel tank eight feet long and four feet in diameter and is to be operated at pressures up to 100 pounds per square inch. The tank is mounted horizontally, one end of which is firmly attached to a concrete pier. The rest of the tank is supported by an undercarriage on rails and can be unbolted from the rigid end and rolled back out of the way. The high potential electrode, 28 inches in diameter, is suspended from the fixed end of the tank by a horizontal textolite tripod. An endless belt 128 inches in length and 13 inches wide carries the electric charge to the high potential electrode. Other descriptive details and operating characteristics are also given.

5. Some New Measurements on ν_3 and $\nu_4+\nu_5$ of C_2H_2. ALVIN H. NIELSEN[1] AND DUDLEY WILLIAMS,[2] *Ohio State University.*—Because individual lines in the infra-red spectrum of the deutero-acetylenes[3] exhibit fine-structure it was considered of value to re-investigate the spectrum of C_2H_2.[4] A report can be made at this time on ν_3 at 3.0μ and $\nu_4+\nu_5$ at 7.5μ. Many of the lines in ν_3 (3288 cm^{-1}) are found to be complex. Though some of this complexity may be due to overlapping with the parallel vibration $\nu_1+\nu_4+\nu_5$ it seems difficult to ascribe it all to this cause. $\nu_4+\nu_5$ (1328 cm^{-1}) does not overlap any other band, but most of its lines exhibit fine-structure. Its appearance is similar to that of $\nu_4+\nu_5$ for C_2HD and C_2D_2. The existence of a weak Q branch, doubted by Hedfeld and Mecke,[5] is verified. Observations on ν_3 were made with slits 0.8 cm^{-1} and at intervals of both 0.50 cm^{-1} and 0.25 cm^{-1}. On $\nu_4+\nu_5$ observations were made with slits 0.47 cm^{-1} and at intervals of 0.20 cm^{-1} and 0.10 cm^{-1}. The importance of utilizing the full resolution of the spectrometer by observing galvanometer deflections at as small intervals as possible is evident from the increase in detail observed in the second run on each band.

[1] University of Tennessee.
[2] University of Florida.
[3] Alvin H. Nielsen, Phys. Rev. **57**, 346A (1940).
[4] Levin and Meyer, J. Opt. Soc. Am. **16**, 137 (1928).
[5] Hedfield and Mecke, Zeit. f. Phys. **64**, 151 (1930).

6. A Wadsworth-Littrow Spectrometer for the Near Infra-red. DUDLEY WILLIAMS, WALTER MILLETT, AND ALVIN COHEN, *University of Florida.*—A recently constructed prism spectrometer is described. The instrument is so arranged that it may be used with a single glass prism in the region between the visible and 2.2μ and with a train of two rocksalt prisms in the region between 2μ and 10μ. Test runs indicate that the results in the range 1μ to 2.2μ compare favorably with the results obtained with prism and grating spectrometers in operation in other laboratories. Transmission curves for several materials will be shown and compared with other previously published curves.

7. New Measurements on Some Infra-Red Bands of Methyl Iodide. R. T. LAGEMANN, *Marshall College.*—The infra-red absorption of CH_3I vapor near 3.3μ, 6.9μ and 8.0μ has been re-measured by means of a prism-grating spectrometer of high resolving power. In each of the three regions the high resolution obtained has resulted in the finding of new lines and more detail. The region near 3.36μ is revealed to consist in part of what appears to be a perpendicular band of average Q branch separation of 4.9 cm^{-1}. The Q branches of the 6.9μ band (ν_4) are each split into several components, probably due to centrifugal distortion. The parallel band (ν_3) at 8.0μ has been partially resolved and appears more complex than any previously measured band of the methyl halides.

8. Structure of the (0,4) Angstrom Band of CO for High Rotational States. MYRON S. MCCAY, *Virginia Polytechnic Institute.*—The rotational structure of the P, Q and R branches of the Angstrom band at λ6080 has been extended to higher rotational terms by analysis of spectrograms of the band made in the first order of a 21-foot concave grating. A re-determination of the initial lines of the series shows essential agreement with the results of previous investigators. The new region affords a check on a perturbation in the final ($A'\pi$) level which has been reported from analyses of the Fourth Positive bands of CO. A marked decrease in intensity of the band-lines sets in near the region of $Q(20)$, a possible indication of molecular predissociation in these states.

9. The Correlation between Cochlear Microphonics and Stapes Motion. OTTO STUHLMAN, JR., *University of North Carolina.* (*Read by title.*)—Davis has shown that an inward movement of the stapes produces a positive potential at the apex of the cochlea. This led Wiggers to follow experimentally the changes in potential at the apex as the motion of the footplate executed a complete cycle. These data will be shown to correlate with the mechanical motions that the footplate undergoes as it moves in the fenestra ovalis, deduced from a 20× model constructed for the purpose.

10. A Study of the Gaseous Exchange between the Circulatory System and the Lungs. N. UNDERWOOD AND J. T. DIAZ, *Vanderbilt University.*—Radon dissolved in normal saline was injected into a vein in the leg of a dog. The dog's breath was collected in successive intervals of time and its radon content determined by a Geiger counter. Five dogs were studied over a period of time and under varying conditions. It was found that the radon was eliminated exponentially, and that the elimination constant was primarily dependent on the ventilation of the lungs, and was independent of a 63 percent change in heart rate. About one-half of the radon is eliminated in 1 minute.

11. The Measurement of the S_{13} Elastic Constant of Zinc. ALVIN W. HANSON, *The Citadel.*—A direct method was used to measure the S_{13} elastic constant of zinc. The accuracy was about one percent. The crystals were 2 cm cubes, requiring the measurement of a strain of about 10^{-5} cm for the maximum stress. The strain gauge was a mechanical optical lever having a magnification of about 10^5. The stress was applied to the specimen by lowering lead weights on to it by means of a screw.

12. Alpha-Particle Range in and Relative Stopping Powers of Some Gases. T. N. HATFIELD, *Louisiana State University*, AND R. C. SMITH, *University of Texas.*—The results are given for some measurements made with the Hatfield-Colby[1] ionization apparatus, using Polonium as a source. The additive law of molecular stopping powers is verified for several gases including the isomers propylene and cyclopropane, and the law is used in calculating the stopping powers of carbon and sulfur with measurements on gases containing these elements. The use of the apparatus in range measurements and in a modern physics experiment is discussed.

[1] M. Y. Colby and T. N. Hatfield, Rev. Sci. Instr. **12**, 62 (1941).

13. Note on the D.C. Characteristics of the String Galvanometer.* F. T. ROGERS, JR., *University of North Carolina.* (Introduced by A. E. Ruark.)—The steady deflection D of the mid-point of an elastic conductor of length L, which is supported between two fixed points a distance l apart and which carries a steady direct current i, in a unidirectional magnetic field symmetric about the mid-point is given by the fifth-degree equation,

$$\Delta\gamma^2D^5+3\beta^2\gamma\delta lD^3/8+9\beta^4l^2tD/64=9\alpha\beta^5l^4i/512.$$

The magnetic field direction is taken to be perpendicular to the line joining the fixed points; the strength is taken to be zero for distances less than $bl/2$ and greater than $cl/2$ from the mid-point, and to be a in between; α, β, and γ are then defined as $a(c-b)$, $2-c-b$, and $3-2c-b$ respectively. The quantities t, δ, and Δ are the coefficients in the expression $T=t+\delta(L-l)+\Delta(L-l)^2$ for the elastic tension in the conductor. This equation is useful in the practical study of departures of a string galvanometer's deflection-*vs.*-current curves from strict linearity, particularly when such departures are large.

* This work was begun as a part of a (1940) summer research program of The General Geophysical Company, of Houston, Texas, and was completed while the author was in residence at the University of Houston.

Proceedings of the American Physical Society

MINUTES OF THE WASHINGTON, D. C., MEETING

May 1–3, 1941

THE Spring Meeting or Washington Meeting of 1941, being the 241st regular meeting of the American Physical Society, was held at Washington on the first three days of May—at the National Bureau of Standards on the first two of these days, at the National Academy of Sciences on the last. This was one of the best-attended of all our meetings, there being no fewer than eight hundred and eighty-six registrations.

One hundred and fifty ten-minute papers were presented before the Society, extending over fourteen sessions. The abstracts of these are printed hereinafter; also included are eleven other abstracts (Nos. 30, 45, 53, 57, 74, 79, 136, 157, 159, 160, 161) which were submitted though the corresponding papers were not presented. An author index will be found at the end.

A symposium on "The Nuclear Energy Sources in Stars" was held on Saturday afternoon in the Auditorium of the National Academy of Sciences, under the sponsorship of Professor G. Gamow of George Washington University. Professor Gamow opened the session with a talk on "Stellar Classification" and ended it with one on "Stellar Explosions." The other speakers were H. Bethe, Cornell University, on "Energy Sources of Main Sequence Stars"; E. Teller, George Washington University on "Reactions of Light Elements in Red Giants"; R. Marshak, University of Rochester, and Charles L. Critchfield, Princeton University and Institute for Advanced Study, on "The Problem of White Dwarfs." The Chairman was Dean George B. Pegram, Columbia University. Several hundred attended.

At the dinner of the American Physical Society which was held on the evening of May 2nd at the Wardman Park Hotel, the President of the Society, Dean George B. Pegram, presided. More than three hundred and fifty attended. After-dinner speeches were delivered by Dr. Charles Darwin, Director of the National Physical Laboratory, and by Sir Lawrence Bragg, Director of the Cavendish Laboratory, both now associated with scientific missions to this country and to Canada; by Dean Pegram, speaking in memory of Dayton C. Miller; by the Director of the National Bureau of Standards (Dr. Lyman J. Briggs); by the head of the Local Committee responsible for the arrangements for the meeting (Dr. F. G. Brickwedde); and by the Secretary of the Society.

The Council met on Thursday, May the first, and elected eight members to the rank of Fellow: these are Herbert L. Anderson, Eugene T. Booth, Paul L. Copeland, G. Norris Glasoe, Ralph P. Johnson, Ralph B. Kennard, Dana P. Mitchell and David Sinclair. Eighty-nine candidates were elected to the rank of Member: these are Charles B. Aiken, Ray S. Alleman, Daniel Alpert, Stephen J. Angello, Dolores Bandini, Carl Beckman, Hugh Bradner, Frank W. Brown, III, Erastus H. Butler, Jr., Robert C. Byers, Edward E. Caldwell, Jack A. Campbell, H. Reed Christensen, Dayton H. Clewell, Densil Cooper, John H. Daniel, Sergio De Benedetti, Richard L. Dolecek, Richard J. Duffin, Raymond B. Dull, Henry F. Dunlap, Marshall D. Earle, Theodore Enns, George A. Espersen, Kasimir Fajans, David Fidelman, Leon H. Fisher, R. G. Fowler, Joseph E. Fox, David H. Frisch, Herbert Fusfeld, O. Bruce Goldsmith, Serge Gorodetsky, Gilbert Halverson, Harry E. Heskett, Francis M. Hesling, John Hornbostel, Eldred Hough, Donald Hughes, Joseph L. Hunter, Frank E. Jablonski, Robert B. Jacques, Aelfric James, Jr., Frederic B. Jennings, Arthur Kantrowitz, Albert R. Kaufmann, N. B. Keevil, Takasi Kituregawa, Vernon M. Korty, William Krasny-Ergen, Robert W. Krueger, Harry Krutter, Theodore W. Lashof, Arnold J. Lincoln, Waldo K. Lyon, Dan McLachlan, Jr., Robert C. McReynolds, J. S. Meares, Otto M. Miller, Thomas D. Morgan, Joseph F. Mullaney, George Nordquist, Harper Q. North, Atuyosi Okazaki, Sidney M. Ostrow, Dwight M. Pasek, Rex B. Pontius, Dorr C. Ralph, Robert E. Reed-Hill, W. A. Rense, Eric M. Rogers, Fred T. Rogers, Jr., Samuel Seely,

Simon S. Share, Chaloner B. Slade, R. Ellis Smith, Roland W. Smith, Jr., William V. Smith, Leo J. Sullivan, Charles D. Swartz, Robert W. Swain, Liston Tatum, Jr., David Telfair, Robert S. Wehner, Alvin M. Weinberg, Van Zandt Williams, J. Edmund Woods, Robert C. Woods, and Hughes M. Zenor.

Word was received by the Council of the death of two fellows (Frederick C. Fowle and Dayton C. Miller) and one member (R. E. Nyswander).

KARL K. DARROW, *Secretary*
Columbia University, New York

ABSTRACTS

1. Measurements of Some Optical Properties of Atmospheric Maze. E. O. HULBURT, *Naval Research Laboratory.*—By means of a telescopic photometer measurements were made in daylight of b, the brightness of a large approximately blackbody at a distance $d=3.2$ km, and of h, the brightness of the sky just above the blackbody. For visual ranges v from 3.2 to 15 km the measurements agreed with the theoretical relation

$$v/d=[\log 1/\eta]/[\log 1/(1-b/h)],$$

where $\eta=0.02$. This led to values of the attenuation of daylight in a hazy atmosphere for values of v in the above range, and to the ratio of the attenuation to that of pure air. The angular distribution of light scattered by haze was determined in two ways (1) by measuring the brightness at various angles of a searchlight beam at night, and (2) by measuring the brightness of the horizon sky at various azimuths for a moderately low sun and a cloudless sky. The distribution was much the same for haze ranging from thin to thick. It showed pronounced forward scattering as may be expected for haze particles of dimensions greater than the wave-lengths of white light.

2. Angular Distribution of Light Scattered in Liquids. L. H. DAWSON AND E. O. HULBURT, *Naval Research Laboratory.*—According to the theory of the scattering of light by an isotropic particles that are small with respect to the wave-length of light, the scattered intensity at angle θ to the direction of propagation of the incident light varies as $1+\alpha\cos^2\theta$. Measurements were made for θ from about 22° to 168° for wave-lengths in the visible and near ultraviolet regions of the spectrum. For benzene, carbon disulphide and carbon tetrachloride, which were practically dust free, the theory was found to be approximately true. Complete success in removing all optical impurities from water was not achieved. The purest water obtained was prepared by slow distillation in quartz and was nearly as dust free as any reported by others. It showed considerable forward scattering which was obviously due in large part to the motes. Indeed, the angular scattering distribution curve was a very sensitive indicator of the optical purity of the water.

3. Far Ultraviolet Absorption Coefficients. W. M. PRESTON, *Harvard University.*—Between 900 and 1300 angstroms there are regions where both nitrogen and oxygen are comparatively transparent to ultraviolet light. Low absorption coefficients, particularly for the lines of the Lyman series of hydrogen, are of interest in connection with the formation of the ionosphere and the origin of radio fade-outs.[1] Schneider[2] has measured the absorption of a large number of lines in air, but was limited with his apparatus to coefficients of the order of 25 cm^{-1}. In the present work it has been possible to measure coefficients one hundred times smaller by using a fast pump to evacuate a chamber separating the discharge tube and the spectrograph into which the absorbing gas was introduced. Values have been obtained for some 75 hydrogen molecular lines, and for several members of the atomic series.

[1] W. M. Preston, Phys. Rev. **57**, 887 (1940).
[2] E. C. Schneider, J. Opt. Soc. Am. **30**, 128 (1940).

4. Reflectivity of Thin Al and Cu Films in the Ultraviolet. MARY BANNING, *Johns Hopkins University.*—The reflectivity of thin films of aluminum and copper have been studied in the ultraviolet between 1000 and 2000A. The films were evaporated on glass plates in a large bell jar which also contained an open end discharge tube and which was connected through a valve to a vacuum spectrometer. After evaporation a few millimeters of H_2 or CO_2 were let into the system, and exposures taken of both the reflected and direct light from the discharge tube. Aluminum films showed a marked increase in reflectivity over previous measurements, in which the films had been exposed to air. Copper films also reflected more, and showed some structure between 1300 and 1600A. The thickness of the films did not appreciably affect the reflectivity unless the films were made very transparent.

5. Quenching and Depolarization of Mercury Resonance Radiation by Helium, Neon and Argon. LEONARD O. OLSEN, *Case School of Applied Science.*—The polarization of mercury resonance radiation excited by plane polarized light from a water-cooled d.c. mercury arc has been determined experimentally at pressures ranging from 0.1 mm to 10 mm of mercury for the rare gases listed above. The polarization as a function of applied magnetic field has

RESULTS

GAS	QUENCHING CROSS SECTION	DEPOLARIZATION CROSS SECTIONS NON-ADIABATIC	ADIABATIC
Helium	Negligible	10.6×10^{-16} cm²	2.66×10^{-16} cm²
Neon	0.328×10^{-16} cm²	13.0×10^{-16} cm²	1.97×10^{-16} cm²
Argon	0.222×10^{-16} cm²	22.8×10^{-16} cm²	1.55×10^{-16} cm²

been measured at several pressures for each gas and the angle of rotation of the plane of maximum polarization as a function of magnetic field intensity has also been observed for these pressures. These data have been used to calculate quenching and depolarizing efficiencies and cross sections for helium, neon and argon. In order to represent satisfactorily the data it is necessary to assume that the total depolarizing cross section results from adiabatic as well as non-adiabatic depolarizing collisions.

6. Lifetime of Fluorescence by an Electronic Method. R. D. RAWCLIFFE, *University of Illinois.*—An apparatus has been constructed which gives directly on a cathode-ray tube screen a decay curve of fluorescence. Incident light from a mercury arc is interrupted by a Kerr cell or a rotating slotted disk so that "square" pulses of light enter the fluorescence cell. The fluorescent light falls on an electron multiplier tube which is connected to one pair of deflecting plates of the cathode-ray tube. A sweep circuit connected to the other pair is so arranged that the electron beam is held at one side while the incident light is shining, and then sweeps linearly across the tube while the light is off, tracing the decay curve. The sweep circuit also controls the Kerr cell. Measurements on diacetyl give a mean lifetime of fluorescence of 1.47×10^{-3} sec. ± 3 percent as compared with 1.65×10^{-3} sec. ± 10 percent, as given by Almy and Anderson.[1] The apparatus in its present form is probably limited to measurements of lifetimes longer than 10^{-6} sec.

[1] G. M. Almy and S. Anderson, J. Chem. Phys. **8**, 805 (1940).

7. A Grating Map of the Infra-red Solar Spectrum: 14 mu to 2 mu. ARTHUR ADEL, *Lowell Observatory.*—In 1935 the infra-red solar spectrum was examined with an echelette grating at the University of Michigan by Adel, Slipher and Fouts, who mapped 101 solar and terrestrial lines between 11.0 mu and 7.7 mu.[1] Continuing this work, the author has set up a Pfund type spectrometer and a Firestone Periodic Radiometer. The spectrometer is equipped with a vacuum thermopile, supplied by C. O. Lampland, and with a 2400-line echelette grating, ruled at the University of Michigan. The solar spectrum has been mapped from 14 mu to 2 mu. The atmospheric bands of carbon dioxide, ozone, nitrous oxide and water vapor have been resolved. Many solar lines appear in the new map; for example, the compound doublets $3D$-$4P$ of Na I and $6P$-$5D$ of K I. The satellite lines provide the splitting of the D terms, 1.74 cm^{-1} and 0.70 cm^{-1}, respectively. I wish to record my gratitude to Profsesors H. M. Randall and E. F. Barker, of the University of Michigan, for the grating, without which this work could not have been done.

[1] A. Adel, V. M. Slipher and O. Fouts, Phys. Rev. **49**, 288 (1936); A. Adel and V. M. Slipher, Astrophys. J. **84**, 354 (1936).

8. Interference Between Quadrupole and Magnetic Dipole Radiation. F. A. JENKINS AND S. MROZOWSKI, *University of California.*—The forbidden line λ 7330 ($^1D_2 \rightarrow {}^3P_1$) of lead is composed of both magnetic dipole and electric quadrupole radiation. From the hyperfine structure Mrozowski has shown that less than 9 percent of quadrupole radiation is involved. We have investigated the Zeeman effect in order to evaluate the exact amount present. Measurements of the intensity ratio of the pure quadrupole components ($\Delta M = \pm 2$) to the pure magnetic dipole ones ($\Delta M = 0$) show that about 2 percent of the total radiation is quadrupole. When this figure is used to compute the relative intensities of the six mixed components ($\Delta M = \pm 1$), agreement with experiment is not obtained if one merely adds the intensities of a quadrupole pattern and of a magnetic dipole pattern in the indicated proportion. Interference between the two types of radiation must be taken into account. When this is done, using theoretical equations derived by Mr. E. Gerjuoy, the agreement with the intensities predicted for 2 percent of quadrupole radiation is satisfactory. The intensity measurements were made by photographic photometry of the Fabry-Perot patterns, integrating the intensity contours where necessary. Corrections for the overlapping hyperfine structure components had to be made. Including all sources of error, we find 2.0 ± 0.3 percent of quadrupole radiation present in this line.

9. Preliminary Study of the Doublet Structure of the Principal Series of Potassium. H. R. KRATZ AND J. E. MACK, *University of Wisconsin and Princeton University.*—A concave mirror (diameter 7.5 cm, curvature radius 4.1 m) and an especially designed prism, constituting an optical device for the production of a long absorbing path by repeated traversal[1] were mounted in a steel tube. The system was designed for, and works well with, 12 traversals (path = 50 m). With a General Electric H-6 lamp as a continuous source and with the tube filled with pure potassium plus an atmosphere of hydrogen, the absorption spectrum was studied on an E1 quartz prism spectrograph as a function of the temperature of the tube (but both ends were kept cool). Several hitherto unresolved lines were resolved into doublets, and incidentally the number of experimentally known series members was considerably extended. Quantitative studies are now being made with a 21-foot grating.

[1] H. R. Kratz and J. E. Mack, Phys. Rev. **57**, 1059A (1940).

10. The Spectra of the Rare Gases. J. B. GREEN, *Ohio State University.*—Configurations of high azimuthal quantum number in atoms with nearly closed shells have been shown theoretically by Shortley and Fried[1] to lead to levels with multiple J values in the limit, and such has been found to be true in the case of copper.[2] The rare gases show similar results in the p^5f configuration of Ne and A, but with Kr and Xe the degeneracy begins to disappear. Zeeman effects in Kr and Xe for the p^5f configurations yield g factors that indicate that the limiting type of coupling for p^5x configurations is one for which only one electrostatic and one electromagnetic parameter need be considered. There are still some anomalies in the Paschen-Back that cannot be explained by so simple a picture.

[1] G. H. Shortley and B. Fried, Phys. Rev. **54**, 739 (1938).
[2] A. G. Shenstone, Phil. Trans. Roy. Soc. **A235**, 195 (1936).

11. New Classifications in the Spectrum of Cs II. MARSHALL A. WHEATLEY* AND RALPH A. SAWYER, *University of Michigan.*—Previous work on the first spark spectrum of caesium by Sommer, by Laporte, Miller and Sawyer, and by Olthoff and Sawyer has resulted in the discovery of most of the low terms of the configurations $5p^5(^2P_{1\frac{1}{2}})5d$, $-6d$, $-7d$, $-6p$, $-6s$, $-7s$ and $-8s$, and $5p^5(^2P_{\frac{1}{2}})5d$, $-6p$, $-6d$, $-6s$ and $-7s$. In an attempt to find higher levels in this spectrum, the caesium spectrum has been rephotographed in the region from 2954A to 1857A, using as light source an electrodeless discharge in a quartz tube. Of the 850 lines measured, only 193 had previously been observed. With the aid of 36 newly established levels, 188 lines have been newly classified in the Cs II spectrum. In addition to supplying some missing members in the lower configurations, the new levels appear to belong to the $5p^5(^2P_{1\frac{1}{2}})8d$, $-7p$, $-9s$, $-10s$ and $-nf$, and $5p^5(^2P_{\frac{1}{2}})7d$, $-7p$ and $-8s$.

* Now at Wayne University.

12. New Classifications in Au I and Au II. JOHN R. PLATT* AND RALPH A. SAWYER, *University of Michigan.*—The gold spectrum emitted by a hollow cathode discharge in helium has been photographed from 600A to 10,000A. New classifications have been made in both Au I and Au II on the basis of the new lines found. In the arc spectrum, the *ns* and *nd* series discovered by Thorsen have been extended, giving for the series limit, $5d^{10}\,{}^1S_0$, a value of 74,410 cm^{-1} above the ground state of Au I. Most of the classifications of McLennan and McLay have been confirmed, and the $5d^9 6s 6p$ and $5d^9 6s 7s$ structures have been extended, while new levels of uncertain configuration have been found above the series limit. The lines assigned by McLennan and McLay to $5d^{10}5f$ transitions could not be found, and new terms have been suggested for this state. In the spark spectrum of gold, the six members of the $5d^9(^2D_{5/2})7p$ group were found, and the five missing terms were added to the $5d^9 6s^2$ structure whose lowest levels had been located by McLennan and McLay. The ground state, $5d^{10}\,{}^1S_0$, 15,039 cm^{-1} below $5d^9 6s\,{}^3D_3$, given by Sawyer and Thomson, was confirmed. In Au I, about 200 lines have been newly classified, and 38 new levels have been found. In Au II, the 82 new transitions found involve 12 new terms.

* Now at the University of Toledo.

13. The Scattering of High Energy Neutrons by Deuterons. JEROME ROTHSTEIN, *Columbia University,* AND LLOYD MOTZ, *The College of the City of New York and Columbia University.*—The neutron-deuteron elastic scattering cross section for 2.8-Mev neutrons has been calculated using the method employed by Motz and Schwinger[1] for thermal neutrons. We assumed the interaction between all particle pairs to be of the form

$$V_{ij} = -[(1-g-g_1-g_2)P_{ij} + gP_{ij}Q_{ij} + g_1 + g_2Q_{ij}]J_0 \times \exp(-r^2/a^2),$$

where the symbols have their usual meanings. We chose $g_1 = g_2 = 0$, $g = 0.22$, $J_0 = 91.8mc^2$, and $a^2 = 0.0463$ in units $\hbar^2/Mmc^2$. The range and depth values are those of Breit and collaborators.[2] Polarization effects and p and higher wave scattering were neglected. We obtained $\sigma = 1.32 \times 10^{-24}$ cm^2. The experimental value is $\sigma_{\text{total}} = 2.17 \times 10^{-24}$ cm^2.[3] Since polarization effects are probably unimportant at these energies, it seems that the p and higher waves may be responsible for the discrepancy.

[1] L. Motz and J. Schwinger, Phys. Rev. **58**, 26 (1940).
[2] Breit, Thaxton and Eisenbud, Phys. Rev. **55**, 1018 (1939).
[3] W. H. Zinn, S. Seely and V. W. Cohen, Phys. Rev. **56**, 260 (1939).

14. Production of Mono-Energetic Protons with the Cyclotron. EDWARD C. CREUTZ AND ROBERT R. WILSON, *Princeton University.*—The proton beam of a cyclotron is ordinarily unsuited for precision measurements such as proton-proton scattering because of the large inhomogeneity of the energy.[1] However, by placing three slits in the external fringing magnetic field of the Princeton cyclotron, we have been able to select an energy interval of less than one percent and with ample intensity for scattering experiments. The three-slit arrangement, which is almost one meter long, serves also as a vacuum connection between our scattering chamber and the cyclotron. Although it is possible to calculate the energy of the protons by measuring the fringing magnetic field and the position of the slits, we find it more convenient to place a simple magnetic analyzer so that the protons enter it after passing through the scattering chamber. The energy analyzer consists of an electromagnet which produces a field of about two thousand gauss over a distance of five inches. A fluorescent screen thirty cm beyond the magnet measures the ten-cm deflection obtained. The energy can then be evaluated by the use of a simple formula which has been checked to one-half of one percent by numerical calculation.

[1] R. R. Wilson, J. App. Phys. **11**, 781 (1940).

15. Proton-Proton Scattering at 8 Mev. ROBERT R. WILSON AND EDWARD C. CREUTZ, *Princeton University.*—The mono-energetic protons described in the accompanying abstract have been used to study proton-proton collisions. A coincidence method of counting the scattered protons is used to eliminate the neutron background due to the large internal current, impurity scattering, and slit scattering. Advantage is taken of the condition that the paths of the recoil and scattered proton are perpendicular by placing two proportional counters at a right angle to each other with a thin Cellophane target at the vertex so that only coincidences between scattered and recoil protons are registered. As the target is a thin foil, the geometry is somewhat better than when gas is used, and there is little difficulty in measuring the scattering current or in energy loss because the scattering chamber is highly evacuated. We have made an extensive study of the scattering yield as a function of the solid angle subtended by both counters and as a function of the Cellophane thickness. This indicates that multiple scattering influences the yield by a few percent if the target is thicker than 0.0005". Preliminary results indicate that the scattering yield at 8 Mev is isotropic to within two percent in the angle interval 35° to 55°.

16. Proton Recoils from High Energy Neutrons. H. TATEL, *University of Michigan.*—Two parallel plate Wynn-Williams type ionization chambers are arranged to count

coincidences. High energy protons may pass through both, but short recoils do not. This makes possible the counting of a very few recoil protons from a hydrogenous scatterer near a cyclotron. When tested with alpha-particles, the apparatus showed a resolving time of 1.2×10^{-4} second. Working near the cyclotron there is an additional coincident background giving one count per six hundred events. For measuring neutron-proton scattering the neutron beam is defined by a 15-cm hole in a waterwall. The scatterer is placed four meters from the thick Be target and the detector is placed at an angle of 16° or 45° with respect to the neutron beam. It is necessary to count all recoils at these angles due to neutrons with energies between 9 and 13 Mev. For a thin (to the proton, 9 air cm at 16° and 3 air cm at 45°) hydrogen gas scatterer subtending ±2° at the detector very small corrections are necessary as the actual counting rates show.

17. Inelastic Scattering of Protons. R. H. DICKE AND JOHN MARSHALL, *University of Rochester.*—The measurement of the energies of inelastically scattered protons enables one to determine the lower energy levels of the scattering nucleus. Using a proportional counter biased so as to count only slow protons, we have obtained curves of the range in aluminum of the protons scattered from thin foils of aluminum, magnesium and several other elements. In aluminum we have found four energy levels. In magnesium, up to 3 Mev, we find only one energy level, its value being 1.4 Mev. Our values for the energy levels in Al^{27} are: 0.92 Mev, 1.93 Mev, 2.8 Mev, 3.9 Mev. The value for the level at 3.9 Mev is probably not very accurate. Wilkins and Kuerti,[1] and Wilkins and Wrenshall[2] measuring ranges in photographic emulsions obtained a value of 1.3 Mev in magnesium and 0.9 Mev for the first aluminum level.

[1] T. R. Wilkins and G. Kuerti, Phys. Rev. **57**, 1082 (1940).
[2] T. R. Wilkins and G. Wrenshall, Phys. Rev. **58**, 758 (1940).

18. Elastic and Inelastic Scattering of 2.5-Mev Neutrons. H. H. BARSCHALL, R. LADENBURG AND C. C. VAN VOORHIS, *Princeton University.*—The scattering of the 2.5-Mev $d-d$ neutrons was investigated by analyzing the distribution in energy of recoil α-particles. Since the angular distribution of 2.5-Mev neutrons scattered by helium is known, the differential cross section for elastic scattering could be determined and the amount of inelastic scattering estimated. Neutrons losing less than 200 kev in the scattering process could not be distinguished from elastically scattered neutrons. The values of $4\pi\sigma(\vartheta)$, $\sigma(\vartheta)$ being the differential scattering cross section per unit solid angle, are given in Table I in units of 10^{-24} cm². These are compared with the corresponding values for the total scattering obtained by Kikuchi, Aoki and Wakatuki. The difference gives the cross section for inelastic scattering.

TABLE I.

	Elastic Scattering		Total Scattering	
	$\vartheta=100°\pm20°$	45°±10°	100°	45°
Al	1.1 ±0.2	3.4±0.5	1.9±0.1	3.4±0.2
Fe	0.57±0.15	1.7±0.3	2.0±0.4	4.3±0.3
Cu	0.36±0.1	1.4±0.3	2.2±0.2	3.5±0.3
Pb	2.5 ±0.4	5.0±0.6	2.8±1.3	9.2±0.6

The distribution in energy of the recoils shows also, independently of this comparison, that the ratio of "inelastic" to "elastic" scattering at these angles is considerably greater in Fe and Cu than in Al and Pb.

19. Total Cross Sections for 900-kev Neutrons. W. E. GOOD* AND G. SCHARFF-GOLDHABER, *University of Illinois.*—We have measured previously[1] the total cross sections of hydrogen and carbon for Rd Th+Be neutrons. In this experiment the neutrons were detected by a hydrogen-filled ionization chamber. In the same way we have now determined the total cross sections of various elements with widely differing atomic number. Leipunsky and his collaborators[2] have studied the cross sections of a large number of elements for neutrons from Rd Th+Be with a different method. After having passed through the absorber the neutrons were slowed down in a paraffin sphere and then detected through the activation of a dysprosium target in its center. In Table I our results are compared with Leipunsky's:

TABLE I.

			σ_{tot} for 900 kev Neutrons in 10^{-24} cm²	
Element	Absorber	λ(g/cm²)	Authors	Leipunsky
$_1$H	C_nH_{2n+2}	2.43	3.70±0.35	5.5±1.1
$_4$Be	Be	5.30	2.82±0.20	1.7± .2
$_6$C	C	7.42	2.66±0.20	3.3± .4
$_{13}$Al	Al	13.10	3.39±0.25	3.1± .4
$_{29}$Cu	Cu	37.9	2.78±0.15	2.5± .4
$_{82}$Pb	Pb	50.0	6.83±0.40	5.1± .6
$_{92}$U	U	48.1	8.00±0.40	

* Now at the Westinghouse Research Laboratories.
[1] W. E. Good and G. Scharff-Goldhaber, Phys. Rev. **58**, 89 (1940).
[2] A. I. Leipunsky, J. Phys. U.S.S.R. **3**, 231 (1940).

20. Capture Cross Sections for Slow Neutrons. JOHN W. COLTMAN, *University of Illinois.*—In order to fill in the gaps in our knowledge of slow neutron capture cross sections a systematic investigation of various elements is being carried out. The cross sections of the elements have been compared with that of boron, using for the boron capture cross section a value of 600×10^{-24} cm². Any change in the measured cross section of boron will affect the results given below proportionately:

Element	$_{16}$S	$_{20}$Ca	$_{26}$Fe	$_{28}$Ni
$\sigma_{capt}\times10^{24}$ cm^{-2}	0.44±0.03	0.50±0.04	2.1±0.2	6.2±50.
Element	$_{29}$Cu	$_{30}$Zn	$_{51}$Sb	
$\sigma_{capt}\times10^{24}$ cm^{-2}	4.3±0.3	1.0±0.06	5.3±0.3	

In the cases where a calculation from the difference between the total and scattering cross sections is possible, the values check within probable errors with those given by Goldhaber and Briggs. The values for antimony and copper are higher than those obtained by the method of induced radioactivity.[1,2] This method would give too low values for the cross sections if K-capture activity were present, as is to be expected for these cases.

[1] R. D. O'Neal and M. Goldhaber, Phys. Rev. **59**, 102 (1941).
[2] F. Rasetti, Phys. Rev. **58**, 869 (1940).

21. Velocity Dependence of Slow Neutron Capture Cross Section of Boron. E. A. LUEBKE, J. H. MANLEY AND L. J. HAWORTH, *University of Illinois.*—The absorption of slow neutrons in boron as a function of neutron velocity has been investigated, using a modulated source of neutrons from the Illinois linear accelerator and special circuits[1] for making velocity measurements. The detector is a parallel plate BF_3 ionization chamber with a sensitive volume of 1100 cm³. A source-detector distance of 250 cm was used with a neutron pulse width of 150 microseconds. Observations were made in a velocity range 1 to 10 km/sec. with time scale of 150 microsecond intervals. Within the limits of error, the data obtained indicate the velocity dependence of the slow neutron capture cross section of boron to be $1/v$. This is in agreement with the experimental results of Alvarez[2] and differs from those of Fertel, Gibbs, Moon, Thomson and Wynn-Williams.[3]

[1] L. J. Haworth, J. H. Manley, M. P. Vore and E. A. Luebke, Phys. Rev. **57**, 1075 (1940).
[2] L. W. Alvarez, Phys. Rev. **54**, 609 (1938).
[3] G. E. F. Fertel, D. F. Gibbs, P. B. Moon, G. P. Thomson and C. E. Wynn-Williams, Proc. Roy. Soc. **175**, 316 (1940).

22. Inflation of Heavy Nuclei. R. D. PRESENT, *Harvard University.*—Deviations from the law that the nuclear volume is propotironal to the number of particles ($R=r_0A^{\frac{1}{3}}$) occur when the Coulomb repulsion, the surface tension pressure and the neutron excess are considered in addition to the usual exchange forces for $N=Z$. These effects are estimated from Euler's statistical treatment[1] which gives an inverse compressibility for nuclear matter $A^{-1}R^2(d^2E/dR^2)=70$ Mev. The corrections to the nuclear radius are proportional to the compressibility and (assuming constant thickness of the surface layer) all three corrections tend to increase r_0 with increasing A. The particle radius beneath the surface layer is given by:

$$r_0=\mathring{r}_0\{1+0.010Z^2/A^{4/3}-0.3A^{-1/3}+0.8[(N-Z)/A]^2\}.$$

r_0 increases by 9 percent from Fe^{56} to Pb^{207}. For light nuclei where the surface correction is made differently,[2] r_0 increases with decreasing A, by 5 percent from Fe^{56} to O^{16}. Nuclear radii determined from elastic scattering of fast neutrons are expected to be 2×10^{-13} cm larger than the statistical radii R. Experiments of Wakatuki,[3] interpreted by the Placzek-Bethe shadow formula, show a 12 percent increase of r_0 from Fe^{56} to Pb^{207}. The Barkas-Bethe radii for light positron emitters, Weisskopf-Ewing radii for intermediate nuclei and Gamow radii for radioactive nuclei are consistent with the calculated corrections ($\mathring{r}_0=1.4\times10^{-13}$ cm).

[1] H. Euler, Zeits. f. Physik **105**, 553 (1937).
[2] S. Flügge, Zeits. f. Physik **96**, 459 (1935).
[3] T. Wakatuki, Phys.-Math. Soc. Japan **22**, 430 (1940).

23. The Nuclear Radii of Light Elements. D. R. ELLIOTT, *Purdue University.*—The differences in mass defects between isobaric pairs of nuclei of the type $Z=N\pm1$ (N the number of neutrons) have been measured by various workers.[1] It is generally assumed that these differences are due only to the change in Coulomb energy when the extra proton is replaced by a neutron. Under this assumption, the radii of these nuclei can be calculated with the help of specific nuclear models. If the nucleus is considered as a homogeneous sphere with a uniform charge distribution, the difference in Coulomb emergy is

$$E_C=\frac{6}{5}\frac{Z-1}{R_0}e^2.$$

On the other hand if a slightly modified form of Bethe's[2] central core nucleus, which includes a correction for the extension of the wave function of the "extra" neutron, is used, one obtains the formula

$$E_C=3\frac{(Z-1)e^2}{R_0}f(1/\epsilon R_0).$$

The radii of the nuclei between $Z=2$ and $Z=21$ have been calculated on the basis of these formulae. For the first model, the volume per particle turns out to be larger for low atomic numbers, but has many local variations. The second model yields a volume per particle which is constant within a given Hartree shell, but changes slightly from one shell to the next.

[1] White, Creutz, Delssaso and Wilson, Phys. Rev. **59**, 63 (1941); D. R. Elliott and L. D. P. King, Phys. Rev. **59**, 403 (1941); G. T. Seaborg, Chem. Rev. **27**, 199 (1940).
[2] H. A. Bethe, Phys. Rev. **54**, 436 (1938).

24. Neutron Shielding. M. STANLEY LIVINGSTON, *Massachusetts Institute of Technology.*—Neutron absorption coefficients in paraffin obtained from unpublished data of Aebersold are used to determine the attenuation in water tanks, now generally used for cyclotron shielding. Production and absorption in the tanks of the 2.2-Mev gamma-radiation from the $H(n,\gamma)$ reaction is calculated from the absorption coefficients. The ionization behind the tanks resulting from this secondary gamma-radiation is found to be much greater than from the residual fast neutrons. Concentrations of borate materials required to reduce the slow neutron and hence the gamma-ray intensity to a few percent are determined. The scattering of neutrons around the shielding tanks is considered and overhead and side tank requirements are estimated. The accepted safe dose rates of 0.1 roentgen per day for gammas and 0.01 roentgen per day for neutrons are reduced to number of quanta per second and used as intensity units. Using the reported neutron yields from cyclotrons the intensity behind the shields due to each component of the radiation can be determined. Gamma-rays produced by neutrons scattered around the tanks or escaping through apertures are shown to contribute the most ionization.

25. An Automatic Frequency Control for Cyclotron R.F. Power Supply. R. B. JACQUES, *Ohio State University.* (*Introduced by M. L. Pool.*)—A control device has been constructed to correct automatically for the drift in frequency of a power oscillator due to changes in the capacitive and inductive load reactances. These changes are a result of load heating effects encountered in using the power oscillator to provide driving power for a cyclotron. The control unit consists of a local electron coupled oscillator circuit, tuned to a frequency 5000 cycles below the fundamental frequency of the power oscillator. This

provides a heterodyne signal of 5000 cycles, which is amplified through a conventional high gain audio-amplifier. This amplified signal is fed into a balanced bridge circuit, consisting of capacitive and inductive reactances resonated at 5000 cycles. If the frequency of the power oscillator varies due to load reactance changes, the heterodyne signal frequency will also vary in frequency in direct proportion, and the bridge circuit will become unbalanced. This unbalanced voltage is applied through two diodes across a load resistor in the grid circuits of two relay vacuum tubes, normally biased to cut-off. These relay tubes operate a reversible motor, through power relays, driving a load correction capacitor in the proper direction to compensate for the frequency change.

26. Flow of a Radioactive Gas Through a Tube. W. H. FURRY, *Harvard University.*—If a gas carrying a radioactive substance of long life flows at a uniform rate through a tube of small radius, the activity per unit length varies as $e^{-s/l}$, with $l=V/\pi a^2\lambda$; here V is volume per second, a is radius, and λ is decay constant. This law is never exact for nonturbulent flow, because the speed of flow is not everywhere equal to $V/\pi a^2$, but varies from $2V/\pi a^2$ along the axis to zero at the wall. The simple exponential law holds only in the limit $a^2\lambda/D=S\to 0$, where D is the diffusion coefficient. In general, the activity varies as $\Sigma A_j e^{-s/b_j}$, where the A_j depend on the precise way in which the gas entered the tube. For small S, $b_0/l=1-S/48+\cdots$, $b_1/b_0\sim 0.1S$, and $|A_1|/A_0\sim 0.02S$. For larger values of S the b's become comparable in magnitude, and so do the A's; the situation is then decidedly complicated. In experimental practice the reasonable procedure is to keep S small. This can always be done very easily if the lifetime is longer than a few seconds.

27. Isolation of Pure Radioactive Strontium and Barium. J. D. KURBATOV, M. L. POOL AND H. B. LAW, *Ohio State University.*—In previous work radium and thorium X were isolated from mother elements without addition of carriers.[1] In this investigation radioactive strontium and barium were obtained in pure state. Strontium oxide was activated with deuterons. Yttrium isotopes were separated as radiocolloids from strontium without the addition of rare earths as carriers. Adsorption isotherms of strontium by ferric hydroxide at different pH's were obtained, using $_{38}Sr^{89}$ of known activity diluted with stable strontium. The number of strontium atoms adsorbed by unit weight of precipitated iron was established. Yttrium active isotopes were precipitated in the presence of ferric chloride, and $_{38}Sr^{87}$ was isolated in pure state at pH 6.8. After determination of the decay period, $_{38}Sr^{87}$ was quantitatively adsorbed from solution by new portions of ferric hydroxide at pH 9. Radioactive barium ($_{56}Ba^{139}$) was similarly isolated in pure state from activated lanthanum. The adsorption process is offered (1) for quantitative separation of radioelements in pure state, without addition of carriers, and (2) as a means of obtaining radioelements in concentrated form, rather than the method of recrystallization of isomorphic systems based on the Berthelot-Nernst law of distribution. A new formulation of the adsorption law of radioelements is suggested.

[1] J. Kurbatov, "Adsorption of thorium X by ferric hydroxide at different pH." Am. J. Phys. Chem. **36**, 1241 (1932).

28. Magnetic Beta-Ray Spectrometer. RALPH L. MCCREARY, *University of Rochester.*—A beta-ray spectrometer has been constructed which is especially adapted for the study of nuclear beta-rays and internal conversion electrons. It is of the 90° focusing type and employs a thin window counter as a detector. The counter forms a separate unit and is held in place by the vacuum seal. The chamber contains an adjustable slit system for defining the electron beam. Because of the leakage flux at the physical boundary of the magnetic field, the source holder and counter are arranged so that they may be moved to the position of best focus for the particular magnetic field used. The source holder is so arranged that short-lived activities may be studied by successive replacement with new samples. Results obtained will be discussed.

29. Range of Intermediate Ions. J. H. M. BRUNINGS AND J. K. KNIPP, *Purdue University.*—The velocity-range relation in air of neon ions has been calculated by assuming the effective charge of the ion for a given velocity to be determined by the relation $V_e=\gamma V$, where V_e is the velocity of the electron which is being captured and lost, V is the particle velocity and γ is a parameter which in principle might be determined from the cross sections for capture and loss but which actually is determined from experiment.[1] The curves obtained are compared with experimental data on neon ions produced in recoil from alpha-particles.[2] These data are represented very well up to $V=4\times 10^8$ cm/sec. by a single value of the parameter ($\gamma=1.15$). However, above this velocity a somewhat smaller value of the parameter is required. The value $\gamma=1.15$ is approximately correct for the first few p-electrons of all the intermediate ions for which data exist (C^{12}, N^{14}, O^{16}, F^{19}, Ne^{20}). Data at higher degrees of ionization are incomplete but they seem to indicate throughout the necessity of a smaller average value of γ for the inner electrons.

[1] Knipp and Teller, Phys. Rev. **59**, 659 (1941).
[2] W. W. Eaton, Phys. Rev. **48**, 921 (1935); J. T. McCarthy, Phys. Rev. **53**, 30 (1938).

30. Comparative Study of Photo-Neutron Sources. R. D. O'NEAL, *University of Illinois.*—The slowing down of the photo-neutrons from 100 mg Ra+Be, 100 mg Ra+D_2O, 10 mg Rd Th+D_2O, and Y+Be were studied by the method of Amaldi and Fermi, using an indium detector. An intense yttrium gamma-ray source was very kindly loaned by Dr. Pecher. The number of neutrons from this source surrounded by beryllium as measured by the integral under the Amaldi-Fermi curve was compared with the number of neutrons from Ra+Be measured in the same manner. This ratio was approximately equal to the ratio of the hard gamma-ray intensities of these sources (as measured through 6 mm of lead). This is in agreement with the result that the energy of the yttrium gamma-rays, 1.87±.05 Mev,[1] is intermediate between the energy

of the radium gamma-rays responsible for photo-neutrons. An attempt was made to determine whether the 2.2-Mev gamma-ray of radium gives any appreciable contribution to the neutrons from Ra+D_2O. A comparison was made between the curves for Ra+D_2O and Rd Th+D_2O and between Ra+D_2O and Ra+Be. Curves for both C and D neutrons were studied but no evidence was found for low energy neutrons produced by the 2.2-Mev gamma-rays.

[1] See abstract by Scharff-Goldhaber.

31. Partial Separation of the Oxygen Isotopes by Thermal Diffusion. S. B. WELLES, *Yale University.*—With an eighteen-meter column, O^{18} has been enriched from the ordinary concentration of 0.2 percent to 14 percent and O^{17} from 0.04 percent to 0.8 percent. The former increase was determined by the mass spectrometer, the latter by the increased activity of F^{18} produced in the nuclear reaction $O^{17}(d, n)F^{18}$. The time rate of increase of the concentration of O^{18} was characterized by a step-wise nature, which arises from the staggering of the six three-meter tubes convectively coupled in series. The theory of "staggering" will be discussed. An investigation is being made of the proton groups from the enriched oxygen under deuteron bombardment.

32. Improved Counting Rate Meter for Radioactivity Detection. ARTHUR F. KIP AND ROBLEY D. EVANS, *Massachusetts Institute of Technology.*—The design of the counting rate meter[1] has been improved to give greater ease of operation, stability, range and linearity. The output current, which is proportional to the average counting rate of the radioactive sample being measured, is fed through a vacuum tube voltmeter, whose maximum output is 5 ma. This increased output current allows replacement of photographic recording, with its inherent delays, by a commercial 5-ma pen and ink recorder, which is very easy to monitor visually. Use of the vacuum tube voltmeter in the output circuit permits reduction of the integrating condenser from 100 μf to 2 μf. Time constants of 15, 30 and 60 seconds are now used for the high, medium and low counting rate ranges. Seven output ranges are provided, varying from 200 to 20,000 counts per minute for full scale deflection, and the amplifier is linear over the entire range. Continuously variable high voltage, from 500 to 2000 volts, is provided by a thermionic stabilizer. The amplifier is entirely a.c. operated.

[1] Evans and Alder, Rev. Sci. Inst. **10**, 332 (1939).

33. Radioactivity of Rocks. ROBLEY D. EVANS AND CLARK GOODMAN, *Massachusetts Institute of Technology.*—Although numerous previous measurements of the radioactivity of terrestrial materials have been made, most of these researches are of qualitative value only in their applications to geology, geophysics, and cosmology because of inadequate recognition of the analytical care necessary in order to obtain reliable results. In recent studies of the radioactivity of terrestrial materials, a systematic program of standardization, calibration, and interchecking has been followed throughout. By combining our newer measurements with the limited number of well-authenticated earlier analyses available, average values have been obtained as follows: $1.37\pm0.17\times10^{-12}$ g Ra/g for 43 acidic igneous rocks, $0.51\pm0.05\times10^{-12}$ g Ra/g for 7 intermediate igneous rocks, $0.38\pm0.03\times10^{-12}$ g Ra/g for 54 basic igneous rocks, and $0.57\pm0.08\times10^{-12}$ g Ra/g for 28 sedimentary rocks; $3.0\pm0.3\times10^{-6}$ g U/g, $13.\pm2.0\times10^{-6}$ g Th/g, and a Th/U ratio of 5.0 for 26 acidic igneous rocks; $1.4\pm0.2\times10^{-6}$ g U/g, $4.4\pm1.2\times10^{-6}$ g Th/g, and a Th/U ratio of 2.6 for 6 intermediate igneous rocks; $0.96\pm0.11\times10^{-6}$ g U/g, $3.9\pm0.6\times10^{-6}$ g Th/g, and a Th/U ratio of 4.0 for 34 basic igneous rocks. The Th and U values are substantially lower and the Th/U ratios are higher than those obtained by Jeffreys[1] in a compilation of most of the measurements reported prior to 1936. Estimates are made of the rate of production of heat by radioactive decay based on the above average values for the different rock types.

[1] H. Jeffreys, Gerlands Beit. zur Geophysik **47**, 149–170 (1936).

34. Helium Age Measurements. CLARK GOODMAN, ROBLEY D. EVANS AND PATRICK M. HURLEY, *Massachusetts Institute of Technology.*—Following discard of the previous helium time scale because of invalidation of the radioactivity measurements,[1] an attempt was made to establish a new scale from alpha-helium age determinations on a variety of rocks. Substantially lower helium age-ratios were obtained for acidic rocks than for corresponding basic rocks and both types gave values considerably lower than the equivalent lead age-ratios for radioactive minerals. Mean age-ratios of 103 million years for pyroxene separates and 36 million years for feldspar separates were obtained for six samples of Triassic diabase. This discrepancy between age-ratios for geologically contemporaneous materials appears to be due to a difference in helium retentivity. Six samples of late Triassic magnetite from ore occurrences in West Virginia, Pennsylvania, and Nova Scotia gave age-ratios closely grouped about a mean value of 134 million years. The constant age-ratio, despite widely varying contents of radium and thorium, suggests that magnetite retains essentially all of its radiogenic helium. Additional evidence on the high helium retentivity of magnetite is provided by specimens of differing geological ages. Age-ratios on some 30 magnetites show a sequence and spacing compatible with geological knowledge, and the results are in fair agreement with corresponding lead age-ratios.

[1] R. D. Evans, C. Goodman, N. B. Keevil, A. C. Lane, and W. D. Urry, Phys. Rev. **55**, 931–946 (1939).

35. An Analysis of the Amplification of Exponential Pulses. CHESTER H. PAGE, *Lafayette College*—A counter-pulse amplifier with fixed bias on the tube grids has the disadvantage of changing its gain noticeably as the tubes and batteries grow old. Self-bias obtained from a resistor in the cathode circuit gives a much stabler arrangement; one whose characteristics are little affected by tube replacements. A study is made of the pulse shape amplification characteristics of a self-biased stage, which is in-

herently degenerative by virtue of the cathode network, and it is shown that an unconventional cathode network has advantages. By proper adjustment of the time constant of the cathode network, backlash may be reduced and the time resolution greatly increased without appreciable loss in gain as compared with a fixed bias stage.

36. Apparatus for Studying Surface Tension at High Pressures. LAURENCE B. HEILPRIN, *Harvard University.*—A high-pressure bomb has been constructed for visual or photographic study of surface tension in a two-phase liquid-liquid system. Mercury and a lighter, transparent liquid are sealed in a glass capillometer in such a way that hydrostatic pressure is transmitted inside and out. The capillometer consists of two vertical glass capillary tubes of different internal radii, with a scale mounted parallel between them. Tubes and scale are photographed through glass windows. Difference in height, and shape of meniscus of the two mercury columns are measured as a function of pressure. The thermodynamic relation

$$(\partial\gamma/\partial p)_{T,A}=(\partial V/\partial A)_{T,p},$$

where γ is surface tension, p pressure, T temperature, V volume of a mass of liquid, and A its area, indicates difference of molecular volume in the interior and at the surface of a liquid. The system mercury-water has been investigated over a range of 2500 atmospheres at room temperature. Preliminary results indicate a decrease with pressure, in mercury-water interfacial surface tension.

37. Electrical Conduction in the Glass Insulation of Resistance Thermometers. HAROLD J. HOGE, *National Bureau of Standards.*—The platinum leads of many resistance thermometers pass through a soft glass seal, which during measurements is subjected to an e.m.f. of the order of 0.1 volt. Above 300°C, conduction in the glass becomes noticeable and increases rapidly with the temperature. The effect was studied in similar seals with the thermometer coil omitted. The apparent conduction consists of a displacement current and probably also of an ionic current. Application of a constant potential causes a large current to flow, which decreases rapidly for several minutes and is still measurable after an hour or more. Upon removal of the e.m.f. and substitution of a resistance, the discharge current varies with time in much the same way. Similar behavior has long been observed in the case of Leyden jars. The rate of discharge is greatly increased by heating above the charging temperature. Two simple precautions are recommended when thermometers of this type are calibrated at the sulfur point: (a) always to apply the e.m.f. in the same direction, and (b) to allow the current to flow for several minutes before taking the first measurement, so that the displacement current will have fallen to a relatively low value.

38. A Method of Making Direct Measurements of the Thermal Coefficient of the Index of Refraction, with Some Results for Distilled Water. JOHN B. HAWKES, *Stevens Institute of Technology.*—An interferometer of the Jamin type is used to measure directly the thermal coefficient of the index of refraction of distilled water. The chief advantage of this method, in addition to a high precision, is its great sensitivity to anomalies in the index-temperature relation. The method is particularly adaptable to measurements at temperatures below the dew point, for which fogging of the windows is a serious problem in the conventional refractometers. The refractive index of water was measured between 40°C and 0°C. The refractive index above the temperature of maximum density is in complete agreement with established values. The behavior below 4°C shows peculiarities of sufficient magnitude to warrant further investigation.

39. Characteristics of Two New Photoflash Lamps. W. E. FORSYTHE AND M. ADELAIDE EASLEY, *Lamp Department, General Electric Company.*—Two new types of photoflash lamps have been developed. In the first of these new lamps, the foil or wire filling has been replaced with shredded foil. This newer type of filling is not only shredded and put into the bulb automatically, but the resulting lamps are an improvement over the older types. The second of these new lamps is the all primer photoflash lamp in which all the light is produced by the new type of primer. This lamp has a very short time to peak and a short duration which gives it some advantages for certain types of synchronization. Data on some of these newer lamps are given in the table.

No. and Bulb Size	Total Light Lum. Sec.	Maximum Flux Lumens	Time to Peak	Effective Duration	Color Temp.
SM–B11	3,500	$0.6\ 10^6$	5 ms.	4 ms.	3550°K
5–B11	18,000	$1.2\ 10^6$	20 ms.	10 ms.	3800
16A–A17	45,000	$2.5\ 10^6$	20 ms.	14 ms.	3800
50–A21	100,000	$6.0\ 10^6$	30 ms.	14 ms.	3800
6–B11	18,000	$0.6\ 10^6$	—	30 ms.	3800

40. Bridge Method for Specific Heat of Wire Samples. B. KURRELMEYER, W. H. MAIS, AND E. H. GREEN, *Brooklyn College.*—A metal wire, of 2 to 4 mil diameter, enclosed in an evacuated bulb, is placed in one arm of a Wheatstone bridge and brought to the temperature at which its heat capacity is to be determined. With the bridge balanced, galvanometer key closed, and battery key open, a charged condenser is connected across the battery terminals of the bridge. The heat capacity is evaluated from the resulting ballistic deflection. In an alternative procedure, the bridge is initially unbalanced so that discharge of the condenser gives zero deflection. The resistance of the wire must be known as a function of temperature, and this will in general be the most severe limitation on the accuracy of the method. The thermal time constant of the wire and the time constant of the condenser discharge are such that heat losses are negligible at ordinary temperatures. The method has been tested on pure platinum, tungsten, and iron in the neighborhood of room temperature. So far an accuracy of 0.5 percent has been obtained. The internal consistency appears to be much better. The method will be applied to the study of iron in magnetic fields.

41. A Large Recording Spectrograph for the Infra-Red to 15μ. E. D. McAlister,[1] G. L. Matheson, and W. J. Sweeney, *Standard Oil Development Company.*—An infra-red spectrograph that will be of most practical value in industrial work must provide the highest resolution consistent with a wide wave-length range. These considerations led to the construction of a Littrow instrument employing a large prism of "artificial" rocksalt (base dimension equivalent to 30 centimeters). A resolving power equal to the theoretical limit of the prism was achieved for all wave-lengths greater than 2.5μ (6 cm^{-1}, 1 cm^{-1} and 0.3 cm^{-1} at 2.7, 6, and 14μ, respectively). The improvements in detail necessary for this practical balance between prism size, aperture and sensitivity of detection are described. The instrument is very useful in the visible and ultraviolet regions, although a perceptible inhomogeneity in refractive index of the prism material (probably due to strain) prevents attainment of the theoretical resolution here.

[1] Consultant from the Smithsonian Institution.

42. Radiant Energy Measurements with Thermopiles. N. C. Beese, *Westinghouse Lamp Division.*—The ultra-violet energy from several mercury vapor lamps was measured by the use of thermopiles and filters. It was discovered that lower values were always obtained when the thermopiles were evacuated than when they were filled with air. The difference was of the order of 20 to 40 percent. A possible explanation is that the carbon coating on the thermopile surface passes the radiations from the Standard lamp, chiefly infra-red, to the thermal junctions whether the thermopile is evacuated or filled with air. Ultraviolet radiations on the other hand are absorbed by the outer surface layers and the energy is transmitted to the active thermal junctions by conduction through the lower layers of carbon particles and by the gas molecules in the porous layer of soot. When evacuated, the effect of the gas molecules in transferring energy through the coating is lost, and so causes a reading that is too low.

43. Dielectric Constant of a Space Charge Rotating in a Magnetic Field. John P. Blewett and Simon Ramo, *General Electric Company.*—In a recent paper in the Physical Review,[1] the authors presented a theoretical discussion of the behavior of a space charge of uniform density rotating under the influence of a uniform magnetic field. The solutions of the field and force equations were found to be somewhat similar to the free space wave guide solutions. In particular, it was noted that the space charge behaves toward an E_0 type wave as though it were a medium whose dielectric constant is less than unity by an amount depending on magnetic field and frequency. For convenient values of magnetic field and frequency, this dielectric constant may easily become zero, or even attain negative values. An experimental study of this phenomenon for a frequency of 470 Mc and magnetic fields of a few hundred gauss gives results in agreement with the theoretical predictions.

[1] Phys. Rev. 57, 635 (1940).

44. Determination of Diffusion Coefficients. R. T. Ellickson and B. Serin, *Polytechnic Institute of Brooklyn.*—In a paper presented elsewhere[1] the following equation was derived from Fick's law and shown to apply to diffusion in a slab of thickness L:

$$1-\alpha=8/\pi^2 \sum_{n \text{ odd}} (1/n^2) \exp\left[-n^2\pi^2 Dt/L^2\right],$$

where α is the fraction of the diffusion process completed at time t and D the diffusion coefficient. It is clear that for large values of t all terms in the sum are negligible compared with the first, and a plot of log $(1-\alpha)$ against t yields a straight line with slope proportional to D. The higher terms can be neglected for values of t corresponding to $\alpha \geqslant 0.3$. However, many experiments do not yield values of α greater than 0.3. A method will be described which gives a value of D for each experimentally determined value of α, regardless of the magnitude of α. The method will be applied to various diffusion data.

[1] R. Ellickson and R. Ward, St. Louis Meeting of Am. Chem. Soc., April, 1941.

45. Molybdenite as a New Lubricant. M. E. Bell and J. H. Findlay, *Westinghouse Lamp Division, Westinghouse Electric & Manufacturing Company.*—In designing a bearing for a rotating anode x-ray tube, oils and greases were discarded on account of their high vapor pressures. All tubes containing these substances ultimately became gassy. Unlubricated ball bearings made of tool steel were tried with only fair results. Experiments indicated that when metal bearing surfaces are thoroughly cleaned, outgassed and used in a vacuum, welding action occurs between adjacent rolling or sliding surfaces. Successive welds and breaks roughen the surfaces and soon create high friction. The need for a good lubricant with a low vapor pressure and high chemical stability became apparent. Molybdenite was chosen for tests because of its laminar crystal structure. Each lamina consists of a layer of molybdenum atoms with a layer of sulphur atoms on each side. One of these lamina adheres strongly to a metallic surface because of a strong metal-sulphur bond. Lamina on adjacent metal surfaces slip easily over each other because of the weakness of the sulphur to sulphur bond. Bearings in a vacuum coated with molybdenite have operated extremely well. The use of molybdenite as a lubricant is not necessarily restricted to a vacuum.

46. On the Silicon Oxide Bands. L. H. Woods, *University of Chicago.* (*Introduced by S. Mrozowski.*)—Pankhurst[1] has described shortly a band spectrum believed by him to belong to an oxide of silicon, possibly SiO_2. A better excitation of the same bands has been obtained from a similar source (a high voltage uncondensed discharge through a constriction in a quartz tube), but in an atmosphere of helium instead of hydrogen. These bands have been photographed on the 30-foot, 30,000 lines/inch grating spectrograph. A band around λ3840 has been resolved in the first and second order and found to be a (0,0) transition (overlapped by a weak 1,1 band) of the type $^2\Sigma \rightarrow {}^2\Sigma$ with

the values $\nu_0 = 26{,}015.05$ cm, $B' = 0.7180$, $B'' = 0.7253$. The coefficients of the spin doubling for the two states are $\gamma' = \pm 0.005$, $\gamma'' = \mp 0.006$. The difference in sign indicates the presence of a perturbing $^2\Pi$ state lying between the upper and lower levels. The doublet structure and the B values prove that the emitter is SiO^+. A less intense group of bands λ4270 has also been resolved but not yet analyzed. The relative intensities in hydrogen and in helium of both groups of bands indicate that the group λ4270 is not emitted by an ionized molecule. Of the two remaining possibilities, neutral SiO and SiO_2, the distance of the lines and the excitation conditions indicate that neutral SiO is much more probable.

[1] R. C. Pankhurst, Proc. Phys. Soc. **52**, 707 (1940).

47. Rotational Analysis of a System of CO_2 Bands. S. MROZOWSKI, *University of Chicago.*—The band spectrum of CO_2 has been investigated in the second order of the 30-foot Chicago grating, with a practical resolving power of 350,000. Nearly all the bands previously reported by Smyth,[1] and in addition a few new ones, were obtained. A partial vibrational analysis shows that more than forty of these belong to an extended system of the type $^2\Pi \rightarrow {}^2\Pi$. Of these, three pairs of bands (previously investigated with lower resolving power by Schmid in this laboratory) have been analyzed so far. The analysis, thanks to the complete resolution, now leaves no doubts about the numbering of the lines. The lower $^2\Pi$ appears to be the ground state $^2\Pi_g$ of the molecule CO_2^+, the upper $^2\Pi$ is the first excited state $^2\Pi_u$ of this molecule predicted by Mulliken. The λ-doubling in $^2\Pi_u$ is bigger than in $^2\Pi_g$ and increases fast with the vibrational energy. The results of the analysis are: $\nu_0^{0,0} = 28{,}532.59$ cm^{-1}, $\nu_0^{1,0} = 29{,}659.28$, $\nu_0^{2,0} = 30{,}781.96$ (all $^2\Pi_{3/2} \rightarrow {}^2\Pi_{3/2}$); and $\nu_0^{0,0} = 28{,}468.51$, $\nu_0^{1,0} = 29{,}594.28$, $\nu_0^{2,0} = 30715.22$ (all $^2\Pi_{1/2} \rightarrow {}^2\Pi_{1/2}$), the upper indices indicating the quantum numbers of the symmetrical vibration. Further for $^2\Pi_{3/2g}$, $B_0 = 0.3795$; $^2\Pi_{1/2g}$, $B_0 = 0.3809$; $^2\Pi_{3/2u}$, $B_0 = 0.3486$, $B_1 = 0.3475$, $B_2 = 0.3463$; $^2\Pi_{1/2u}$, $B_0 = 0.3501$, $B_1 = 0.3489$, $B_2 = 0.3476$.

[1] H. D. Smyth, Phys. Rev. **38**, 2000 (1931).

48. Rotational Analysis of the CO_2^+ Band near 2900A. F. BUESO-SANLLEHÍ, *University of Chicao.*—A rotational analysis of the CO_2^+ doublet band near λ2896 and λ2882 has been made. The band was photographed in the third order of the 30-ft. grating spectrograph in Ryerson Laboratory with a dispersion of 0.22 A/mm. The structure is explained by a $^2\Sigma_u^+ \rightarrow {}^2\Pi_g$ transition, where the latter is the ground state of CO_2^+. The close agreement of the $\Delta F'''$s with Mrozowski's (see preceding abstract) proves that the bands have the same lower state. In addition there are much weaker bands superposed which may be ascribed to transitions between higher vibrational states. Alternate lines are missing as expected for $^2\Sigma$ and the zero spin of the oxygen nuclei. A number of perturbations are observed, showing displacements and weakenings of lines. These are probably caused by higher vibrational levels of the $^2\Pi_u$ state (see preceding abstract) which lies immediately below the $^2\Sigma_u^+$. The weakness of some of the perturbed lines suggests that the perturbation is sometimes accompanied by predissociation. A tentative value of the spin doubling in the upper $^2\Sigma_u^+$ state has been obtained ($\Delta\nu = 0.020$ $(K + \frac{1}{2})$). The B values of the upper and lower states are very nearly equal, B' being slightly smaller.

49. Vibrational Analysis of the Absorption System of Sulphur Dioxide at λ3400–2900. N. METROPOLIS, *University of Chicago.*—Photographs of the bands of sulphur dioxide in the region of λ3400–2900 have been taken under low, medium and high dispersion, both at room temperature and at 200°K; the pressure of the absorbing gas was varied from 0.3 mm to 480 mm. Thirty bands can be represented by the formula

$$\nu = 29622 + 770v_1 + 320v_2 + 813v_3 - 6v_1^2 - 2.5v_2^2 - 20v_1v_2 - 25v_2v_3 - 15v_1v_3,$$

where v_1, v_2, v_3, are the quantum numbers of the symmetric valence, the deformation and the antisymmetric vibrations, respectively. The three fundamental frequencies for infinitesimal vibrations are $\nu_1 = 794$, $\nu_2 = 345$ and $\nu_3 = 833$ cm^{-1}. In addition, twelve bands have been identified that correspond to transitions from excited vibrational levels in the normal state. The relatively long v_1 and v_2 progressions indicate that both the bond distance and angle have changed considerably in the transition to the excited electronic state. The vibrationless transition at 29,622 cm^{-1} is weak, as one would have expected from considerations of the Franck-Condon principle. Substituting the three fundamental frequencies in the valence force potential, one obtains a value of 100° for the apex angle in the upper state, as compared with 120° in the normal state. The absence of any regularity in the rotational structure supports the conclusion that the molecule has become a more asymmetrical top.

50. Species Classification and Rotational Energy Level Patterns of Triatomic Molecules. ROBERT S. MULLIKEN, *University of Chicago.*—The quantized energy levels of symmetrical and asymmetrical tops are discussed from the viewpoint of their classification into species defined by symmetry operations. These are then used in a discussion of the rotational levels of symmetrical nonlinear triatomic molecules AB_2. Using SO_2 as an example, the pattern of rotational levels is studied as a function of the apex angle 2α (near-prolate-symmetrical case for large α, oblate or near-oblate case for intermediate α, second near-prolate case for small α). The classification of the *over-all* wave functions of the levels with respect to exchange of equal nuclei and for inversion is then considered. This gives rise to level-patterns like those of diatomic and linear molecules in the first near-prolate case, but of interesting unfamiliar types (expected also in molecules such as BCl_3 or NH_3) in the oblate case, and of relatively unfamiliar types (known for the molecule H_2CO) in the second near-prolate case. The concept of gyrovibronic species, and a corresponding nomenclature, are then introduced. Finally, the problem of the correlation between states of linear and nonlinear AB_2 molecules is considered, and a correlation diagram relating the sets of gyrovibronic levels of the two cases is obtained.

51. Absorption Spectrum of Fluorobenzene in the Near Ultraviolet. H. SPONER AND S. H. WOLLMAN, *Duke University.*—The absorption spectrum of C_6H_5F at 2750–2380A was photographed in the first order of a 3-m grating spectrograph. As in monochlorobenzene the band system corresponds to an electronic transition $A_1 \rightarrow B_1$. In agreement with this assignment to an allowed transition the 0,0 band appears strongly at 37,818 cm^{-1}. Several progressions of totally symmetrical vibrations occur involving particularly frequencies of 913, 966 and 1228 cm^{-1}. Probably all three, but surely the first two, belong to totally symmetrical carbon vibrations in the upper state. In contrast to C_6H_5Cl the carbon-halogen frequency appears strongly in C_6H_5F. On the other hand, the vibration whose excitation brings the benzene spectrum into appearance and which shows up relatively intensely also in C_6H_5Cl, is of no prominence in the C_6H_5F spectrum. Bands appearing on the red side of the main bands with intervals of 67 and 206 cm^{-1} are considered as due to $v-v$ transitions of nontotally symmetrical vibrations. As in monochlorobenzene the structure of the spectrum becomes more complicated toward the ultraviolet because of the increasing number of possible combinations of totally symmetrical vibrations.

52. Raman Spectra of Alkyl Acetylenes. FORREST F. CLEVELAND AND M. J. MURRAY, *Illinois Institute of Technology.*—Investigations directed toward a better understanding of the reasons for the occurrence of more lines for disubstituted than for monosubstituted acetylenes in the 2200 cm^{-1} region of the Raman spectrum have been extended to include 1-heptyne, 4-methoxy-1-butyne, 2-octyne, 3-octyne, 5-decyne, 7-tetradecyne and 9-octadecyne (all kindly supplied by Dr. G. F. Hennion of the University of Notre Dame). The monosubstituted acetylenes, 1-heptyne and 4-methoxy-1-butyne, gave only a single strong line at 2118 cm^{-1} and faint lines at 2064 and 2097 for the former, 2064 and 2094 for the latter. These weak lines may be attributed to the isotopic molecules, $R-C^{13}\equiv C^{12}-H$ and $R-C^{12}\equiv C^{13}-H$, respectively. The faint line at 2198 in the spectra of the disubstituted acetylenes may be ascribed to the isotopic molecule, $R-C^{13}\equiv C^{13}-R'$. If Fermi resonance is to account for the remainder of the lines, it seems probable that at least one fundamental in addition to the infra-red active $C-C\equiv C-C$ frequency (at 1126 in dimethylacetylene) must be involved. This may be an inner frequency (near 1100) of the $-CH_2$-group, since a line at 2245 is observed in the Raman spectrum of diethylacetylene in addition to the two strong lines near 2230 and 2300 which constitute the well-known resonance doublet of dimethylacetylene.

53. Absorption Spectrum of Monobromobenzene. I. WALERSTEIN, *Purdue University.*—The absorption spectrum of monobromobenzene in the region 2750–2400A was photographed with an E-1 spectrograph. An analysis of the bands shows that the spectrum is a combination of the allowed transitions due to the C_{2v} symmetry of C_6H_5Br and of the forbidden transitions of the benzene structure. The 0,0 band is located at 36,996 in the vapor and around 36,670 in the solid. Combinations of the totally symmetrical carbon vibrations of 933, 963, and 1020 cm^{-1} in the upper state account for one group of intense bands. This group also contains may bands spaced 60 (or 2×60) cm^{-1} away. This frequency difference is interpreted as the decrease in the upper state of the totally symmetrical ground vibration of 185 cm^{-1}. The excitation of an E_g^+ vibration which makes the forbidden transition of benzene partly allowed is evident in the C_6H_5Br spectrum by the presence of a second group of intense bands displaced 525 cm^{-1} from the first, This frequency corresponds to the nontotally symmetrical vibration of 616 in the ground state. Several of the Raman frequencies are observed in the weaker preposed bands. Further combinations occur with 242 and 2563 cm^{-1} corresponding to the totally symmetrical 317 and 3063 ground levels.

54. High Resolution Study of the Infra-Red Bands of Cyclopropane. LINCOLN G. SMITH, *Princeton University.*—At 3.3μ the fundamental bands of C_3H_6 due to C–H valence vibrations have been observed as follows: a perpendicular-type band at 3024.4 cm^{-1} whose fine structure was not resolved; and a parallel-type band with origin at 3103.0 cm^{-1} for which rotational structure has been measured. From these measurements the value 41.87 $\times10^{-40}$ g cm^2 is obtained for the moment of inertia A'' in the ground state. From this, if one assumed C–H = 1.09A as in methane, one obtains values of the H–C–H angle from 126° to 146° for values of C–C between 1.52A and 1.54A. The most reasonable values appear to be C–H = 1.09A, C–C = 1.53A, H–C–H = 136°. The latter angle corresponds to a tetrahedral C–C–H angle. At 9.6μ a single perpendicular band has been found. The fine structure near the center of this band has been partially resolved, the average spacing of the pQ and rQ branches being 0.5 cm^{-1}. The origin of the band is at 1027.6 cm^{-1}. At 11.5μ there appear to be two bands very nearly coincident, the centers of each being within ±4 cm^{-1} of 870 cm^{-1}. Though the interpretation is not yet completely certain, it is practically certain that one of these bands is of the parallel type very similar to that at 3103 cm^{-1}. It thus appears that Linnett's[1] assignment of the low frequency fundamentals is incorrect. The correct assignment seems to be: The parallel band in the symmetry class A_2'' lies at about 872 cm^{-1} while the two degenerate perpendicular bands in the symmetry class E' lie at 1027.6 cm^{-1} and about 868 cm^{-1}. This assignment is in accord with the fact that Raman lines are observed at 1022 cm^{-1} and 863 cm^{-1} and with the selection rule that the E' vibration should appear in both Raman and infra-red spectra.

[1] J. W. Linnett, J. Chem. Phys. 6, 692 (1938).

55. Association of Alcohol Studied by Infra-Red Spectroscopy. H. S. SACK† AND J. PRIGOGINE, *University of Brussels.*—The association of alcohol molecules with alcohol molecules and with a series of other molecules is studied by the observation of the intensities of the infra-red absorption bands of binary and ternary solutions of alcohol at different temperatures. The results of these measurements may be represented by the law of Guldberg-Waage, and "association energies" can be calculated for the dif-

ferent complexes formed (e.g. ~5 kcal./mol. for double molecules). It is made probable that this association, often assigned to an O—H bond, is of electrostatic nature.

† Now at Cornell University.

56. On the Mechanism of the Nitrogen Afterglow. M. H. HEBB AND H. SPONER, *Duke University.*—The theory of active nitrogen proposed by Cario and Kaplan has been critically examined in the light of recent experimental and theoretical results. The theory is shown to be untenable since it requires transitions in violation of the Franck-Condon principle to be produced in collisions of the second kind. A new theory which is a modification of the old triple collision hypothesis is proposed. The energy of the afterglow (up to 5 hours) is stored partly as the energy of dissociation of the nitrogen into normal atoms and partly as the excitation energy of metastable ^2D atoms. A ^2D atom recombines with a normal atom in the presence of a third body directly into the $B^3\Pi$ state, which is the upper state of the afterglow bands.

57. Rotational Magnetic Moments of H_2, HD, and D_2. HARVEY BROOKS, *Harvard University.*—The formula for the rotational moment is, in atomic units

$$\mu=\frac{M_1+M_2}{2M_1M_2}M\left\{1-\frac{2}{R^2}\frac{\langle L^2\rangle_{Av}}{\langle E_{ON}\rangle_{Av}}\right\}J,$$

where M_1, M_2 are the nuclear masses, R the internuclear distance, $\langle L^2\rangle_{Av}$ the mean square electronic angular momentum, $\langle E_{ON}\rangle_{Av}$ a mean absorption frequency which we shall call the "downstairs centroid of angular momentum." Witmer has calculated the quantity $\langle L^2\rangle_{Av}$ with Coolidge-James functions, but no reliable theoretical estimate of $\langle E_{ON}\rangle_{Av}$ exists. However, it is possible to calculate an "upstairs centroid" for angular momentum, and both an "upstairs" and "downstairs" centroid for kinetic energy, and by taking the ratio of upstairs to downstairs centroids the same in both cases we obtained the value 1.97 atomic units for the downstairs centroid of angular momentum. With $\langle L^2\rangle_{Av}=0.222$ this gives a rotational moment of 0.885 nuclear magneton in good agreement with the measurements of Ramsey. With Witmer's value of 0.195 estimated with 11-term Coolidge-James functions, the calculated rotational moment is 0.91 nuclear magneton in less good agreement.

58. Note on the Indexing of Powder Diffraction Patterns. LUDO K. FREVEL, *The Dow Chemical Company. (Introduced by J. D. Hanawalt.)*—Solutions for the quadratic form of Debye-Scherrer-Hull patterns have been limited in practice to cubic crystals and to the simpler substances with tetragonal or hexagonal symmetry. However, by supplementing the normal powder pattern by other physical data such as a temperature shift of the interference maxima,[1] it is possible to index more complicated cases. Another method of classifying the various reflections of a powder diagram is to produce a preferred alignment of crystallites in the specimen. An expedient technique for producing preferred orientation in a crystalline powder is to compound the powder with an amorphous plastic such as polystyrene and severly work the compounded material in its thermoplastic state. The fiber diagram obtained from the worked specimen can then be indexed by the standard methods applicable to complete rotation diagrams of single crystals. The method will be illustrated on the orthorhombic system.

[1] L. K. Frevel, Jr. App. Phys. **8**, 553 (1937).

59. X-Ray Structure Analysis of Polyvinyl Alcohol. ROSE C. L. MOONEY, *Newcomb College, Tulane University.*—The polymer is fibrous, showing good orientation about the fiber axis, and random orientation perpendicular to this direction. The experimental data consist of x-ray photographs taken with copper radiation filtered through nickel. There are about thirty measureable spots on the fiber diagram, which can be indexed with reference to a psuedo-orthorhombic cell of the following dimensions: $a=7.80$ A.U.; $b=2.52$ A.U.; $c=5.60$ A.U. The periodicity along the fiber axis, namely, 2.52 A.U., points to a planar zig-zag configuration for the carbon chain. There are two segments of $-CH_2CHOH-$ chains in the unit cell, giving a calculated density of 1.31. The reported value is 1.293. A study of the data leads to a structure having the symmetry of $C^2_{2h}-P2_1/m$. Positions have been found for the carbons and oxygens such that the calculated intensities are in good agreement with the limited number of observed intensities. The structure consists of long chain molecules so oriented that pairs of chains are linked through hydroxyl bonds between oxygens. The O—H—O distance is 2.7 A.U.

60. The Random Structure of Chrysotile Asbestos. B. E. WARREN AND K. W. HERING, *Massachusetts Institute of Technology.*—The present x-ray study of chrysotile indicates that a layer structure is in better agreement with the composition and the diffraction pattern than the previously proposed chain structure. The layers are built up in the sequence 3 O, 2 Si, 20 OH, 3 Mg, 3 OH. The diffraction pattern can be indexed in terms of monoclinic axes $a=7.33$A, $b=9.24$A, $c=5.33$A, $\beta=93°16'$. Nearly all reflections are of the type *hOl* or *Okl*. All *hOl* reflections are of the sharp crystalline type, most of the *Okl* reflections are smeared out along the layer lines resembling two-dimensional lattice reflections (*kl*). The diffuse reflections are due to a randomness in the stacking together of successive layers. The effects on the diffraction pattern of various kinds of randomness will be discussed.

61. Twinning in Nesquehonite, $MgCO_3\cdot 3H_2O$. R. PEPINSKY,* *University of Chicago.*—Earlier investigators[1] have assigned nesquehonite, $MgCO_3\cdot 3H_2O$, to the orthorhombic system, and from x-ray data Fenoglio[2] has placed it in space group D_{2h}^1-Pmmm, with $a=7.68$, $b=11.93$, $c=5.39$, and $Z=4$. Improbability of this space group prompted re-examination of the crystal, revealing that in terms of the orthorhombic cell *hkO* reflections are absent for $h+k$ odd, indicating a net plane parallel to (001) and the space group $D_{2h}^{13}-Pmmn$ or subgroup C_{2v}^7-Pmn. Despite optical data, certain systematic variations in diffracted intensities, and Patterson and Harker projections based on intensities, it was not possible to derive a structure

in the orthorhombic cell. The failure is apparently associated with close doubling of many maxima on Laue, a and c axis oscillation diagrams, which persists in both natural and artificial crystals and suggests that the crystals are built of repeated twins of lower symmetry. This is in accord with conclusions of Cesaro,[3] based on cleavage properties and strongly-striped prism faces, and perhaps accounts for the doubled reflections from the basal plane reported by Penfield.[1] Further support is given the twinning hypothesis by observations of Rogers[4] on related hydromagnesite, $3MgCO_3 \cdot Mg(OH)_2 \cdot 3H_2O$, which is pseudo-orthorhombic due to polysynthetic twinning of monoclinic lamellae.

* Now at U. S. Rubber Co., Providence, Rhode Island.
[1] Genth and Penfield, Am. J. Sci. [3] **39**, 121 (1890).
[2] Fenoglio, Atti Acad. Lincei **24**, 219 (1936).
[3] Cesaro, Bull. Cl. d. Sc. Akad. Roy. Belgique (1910), 751.
[4] Rogers, Am. J. Sci. [5] **6**, 37 (1923).

62. The Structure of Stretched Rubber. C. M. PARSHALL AND K. LARK-HOROVITZ, *Purdue University.*—X-ray diffraction patterns of evaporated latex (sheets, 1.5, to 2.0 mm thick) at various elongations have been obtained and Fourier-analyzed. 100 percent, 200 percent, 250 percent stretching produces patterns similar in appearance to the pattern of the unstretched material; at 275 percent elongation crystal structure is definitely indicated. Three rings have been observed in the amorphous pattern at $\sin \theta/\lambda$, values of 0.1047–0.1055; 0.210–0.220; 0.411–0.418. The half-breadth value of the first peak remains essentially the same for all elongations but its height and the appearance of the outer rings is changed. The distribution curves from the Fourier analyses show 1.9 first neighbors at 1.52A; 2.6–2.9 second neighbors at 2.48–2.54A. With increasing elongation the definition of the second peak increases and it appears completely resolved at 250 percent. A further concentration appears in all distribution curves at 5A; with increasing elongation concentrations at 3.5A and 4.2A, barely visible in the distribution curve of the unstretched latex, become strongly pronounced, comparable with the peak at 5A.

63. A New Electron Diffraction Camera for Molecular Structure Investigation. H. J. YEARIAN, *Purdue University.*—The electron diffraction method of molecular structure determination has a twofold limitation when applied to materials of low molecular weight. The total diffracted intensity is small since it is essentially proportional to the square of the molecular weight, and the useful diffraction pattern is one of low contrast superimposed on a very steep background. In the camera to be described, the over-all intensity has been raised by using electrostatic focusing to obtain 1–2-μa beams of 40-kv electrons. The second difficulty is reduced by incorporating a rotating sector in front of the plate which gives an exposure proportional to r^3, as introduced by P. P. Debye.[1] Check measurements with CCl_4 and N_2, and preliminary results on C_2H_2 will be given, together with a description of a simple mechanical device for calculation of the intensities to be expected from assumed molecular models.

[1] P. P. Debye, Physik. Zeits. **40**, 60 (1939).

64. The Structure of Black Carbon. ADDISON H. WHITE AND LESTER H. GERMER, *Bell Telephone Laboratories.*—Carbon films deposited upon silica surfaces by thermal decomposition of methane are of importance because of their microphonic properties. This paper is concerned with the results of determinations of the structure of more than 100 such films by means of electron diffraction, in some cases by the reflection method and in others by transmission through films after removal from their supports with hydrofluoric acid. In some of the specimens the individual crystallites are strongly oriented, and reflection patterns obtained from these are approximations to rotation patterns from single crystals. From these patterns one can conclude that the films consist of pseudo-crystals in each of which the carbon atoms are arranged in hexagonal planes as they are in graphite, but the successive parallel atomic layers are laterally displaced so that no regularities exist other than the uniform separation of the hexagonal planes and the regular arrangement of atoms in each of them. Determinations have been made of five structural parameters of the films,—average dimensions of crystallites parallel and normal to the planes of carbon atoms, mean separation of the planes and mean spacing in the planes, and degree of preferential orientation of the individual crystallites.

65. Crystal Structure and Surface Flow of Thin Evaporated Antimony Films. J. E. RUEDY, *RCA Manufacturing Co.*—When antimony is evaporated in vacuum onto a surface which is near room temperature, the resulting layer exhibits a flow phenomenon if the thickness is greater than a certain critical value, which is geometrically calculated on the basis of bulk density as being about 85A. If the evaporation of the antimony is done quickly and then stopped, the coating on a flat glass plate at first has a normal continuous gradation of light transmission about the projection of the source. Within a few seconds, however, many pin points of greater opacity appear in the denser region and then grow and spread until they run together, finally forming a quite regular circular region of greater opacity with a sharp boundary. When studied by means of electron diffraction, the thicker type films yield sharp patterns which indicate the presence of well-developed crystallites with their 111 faces parallel to the base material, but otherwise randomly oriented. The thinner-type films give two diffuse rings which coincide with those due to reflections from the 110 and 221 planes, with no indication of orientation. The widths of these rings correspond to an average grating extension of about 10 atoms or 25A. Photographs of these films were taken with the electron microscope at a magnification of 13,000 diameters. Both types show a mosaic structure composed of irregular chains of about 150A in width, but with strikingly different density distributions.

66. Atomic Distributions in Liquid Aluminum and Lithium. CARL GAMERTSFELDER, *University of Missouri.*—The diffraction patterns of liquid aluminum and lithium have been obtained using Mo $K\alpha$ radiation, and the atomic distribution curves have been determined from them by

means of a Fourier analysis. The diffraction pattern of aluminum at about 700°C has four maxima. In terms of $\sin\theta/\lambda$ units the first peak is at 0.10, the second peak, which is the most pronounced, is at 0.210, the third is at 0.36, and the fourth is at 0.55. The distribution curve shows that each atom in liquid aluminum has, on the average, 10.6 nearest neighbors at 2.96A. Each atom in crystalline aluminum has 12 nearest neighbors at 2.86A. The diffraction pattern for liquid lithium at 200°C has three maxima, located in terms of $\sin\theta/\lambda$ units, the first and strongest is at 0.195, the second at 0.340 and the third at 0.55. Each atom in liquid lithium has, on the average, 9.8 nearest neighbors at 3.24A. Each atom in the crystal has 8 nearest neighbors at 3.03A. In order to complete this analysis the density of liquid lithium had to be determined. The value of the density of liquid lithium at 195°C is 0.46 ± 0.01 g/cm^3.

67. Atomic Distribution Curve for Liquid Argon. C. N. WALL, *North Central College.*—Rushbrooke[1] has given a theoretical atomic distribution curve for liquid argon at 90°K based on Lennard-Jones and Devonshire's model ($N_1=12$, $R_1=4.077$A). His $4\pi r\rho_1(r)$ function for the first peak, obtained by numerical calculation, is compared with Wall's[2] simplified function. The two are found to agree closely when the parameter σ in the simplified function is chosen to make the maxima of the two functions coincide. This agreement is not accidental since σ can be calculated directly from the Lennard-Jones and Devonshire potential function for an argon atom in its cell and is found to be $0.140R_1$. This compares favorably with the value $0.141R_1$ given by Rushbrooke. Unfortunately, Rushbrooke's function does not agree with the experimental distribution curve for liquid argon given by Gingrich and Eisenstein.[3] A much better fit could be expected by choosing $N_1=7$ and $R_1=3.86$A. In this case the calculated value of σ is 0.48A whereas the value obtained from the experimental curve is 0.50A. These latter values of σ give satisfactory results for the entropy of liquid argon.

[1] G. S. Rushbrooke, Proc. Roy. Soc. Edinburgh **60**, 182 (1940).
[2] C. N. Wall, Phys. Rev. **54**, 1062 (1938).
[3] A. Eisenstein and N. S. Gingrich, Phys. Rev. **58**, 307 (1940).

68. Structure of Liquid Helium. L. I. SCHIFF, *University of Pennsylvania.*—The weak forces that exist between helium atoms and the large zero-point kinetic energy of their motion in liquid helium make the usual theory of liquids inapplicable to this substance. However, x-ray data indicate the regular distribution of nearest neighbors that is characteristic of normal liquids. From the point of view of the one-particle model, this suggests that at moderate temperatures each atom moves throughout the whole volume in the approximately periodic field of the other atoms, this periodic field being produced by correlations between positions of the atoms. At absolute zero we assume that each atom is in a semi-bound state in the field of its neighbors, in which it may diffract over several atom distances; while there may be one such state for each atom, the large zero-point energy and weak forces preclude the existence of more than one. The phase transition then consists of the "condensation" of atoms from excited gas-like states to the lowest liquid-like states. The resulting specific heat curve resembles, but is less steep, than that found experimentally. Arguments will be presented that indicate that the liquid-like states contribute a negligible amount to the viscosity.

69. On the λ Transition in Liquid Helium. W. E. LAMB, JR. AND A. NORDSIECK, *Columbia University.*—In the previous attempts to relate the transition between liquid helium I and II to the condensation of a Bose-Einstein gas, one has not been able to obtain a discontinuity of the specific heat curve at the transition temperature, without *ad hoc* assumptions about the distribution of energy levels for the motion of single atoms. We have obtained an expression for the energy levels of the system as a function of the numbers N_i of atoms in the various states, which is strictly valid only for low densities, i.e., in the uncondensed gas. The calculation is similar to that of the correlation energy in the theory of metallic binding, except that use is made of the fact that the range of the forces is small compared to the wave-length. The energy contains quadratic terms in N_i as well as the usual $\Sigma_i N_i E_i$. If there is no bound level in the intermolecular potential, the quadratic terms favor condensation. We have calculated the partition function with the above energy expression and find, apart from a latent heat, a specific heat curve of the observed form.

70. Finite Electromagnetic Self-Energies and Nuclear Electric Forces. ALFRED LANDE, *Ohio State University.*—When monochromatic radiation is scattered by an electric particle, a pulsating energy amount is retained by the particle according to the classical theory. For very high frequencies this energy is reduced in its amplitude and retarded in its phase. The "mutual energy" in Fermi's radiation theory corresponds to this pulsating energy, without the reduction for high frequencies, however, thereby leading to infinite self-energies. Correcting this deficiency we arrive at a "cutting-off method" made invariant by the Doppler effect for particles in motion through the radiation field. The electromagnetic self-energy becomes $\frac{3}{4}$ of mc^2, if m is the total inertia, leaving the possibility of neutral particles having a rest mass, too. The Coulomb potential changes to $(e^2/r)[1-\exp(-r/r_0)]$ where $r_0=2e^2/3mc^2$, for particles of equal masses. A more complicated formula with applications to nuclear physics results for the potential between masses m and M. Whereas the force of one charge on another of equal mass remains finite even for $r=0$, the force on a test charge $M=\infty$ becomes infinite for $r=0$, similar to the distinction between E and D in Born-Infeld's theory. For an electron and a proton at the distance $r=0$ the mass defect is only a few electronic mass units. For electrostatic reasons alone, electrons and positrons could exist as such inside the nucleus. The appearance of an electromagnetic "radius" is the result of radiation damping, rather than of any change of the basic field equations as proposed.

71. The Gravitational Field in Special Relativity. N. ROSEN, *Black Mountain College.*—Although previous attempts to describe gravitation in the special theory of

relativity have not been successful, one can do this satisfactorily provided one uses for the potential of the gravitational field a symmetrical tensor of rank two. However, if such a description is used, it turns out that reasonable assumptions lead to field equations and equations of motion which are formally the same as the ones in the general theory of relativity.

72. On Relativistic Thermodynamics. PETER G. BERGMANN, *Institute for Advanced Study.*—A relativistic treatment of thermodynamics has been proposed by several authors[1] and lately by Eckart[2] for a continuous medium. The entropy of a system is an invariant, as shown by a statistical or a purely thermodynamical argument. The temperature has to be replaced by a world vector, β_ρ. Its scalar product by the four-velocity is equal to $1/T_0$ (T_0 being the proper temperature), while its fourth component is $1/T$ (T being the relativistic temperature). Contrary to the usual assumption, β_ρ need not be $1/T_0$ times the four-velocity of the system, particularly when the "system" is an infinitesimal amount of matter in a fluid. Eckart's resolution of the energy-momentum tensor into proper components and his formulation of the first and the second laws will be discussed.

[1] A. Einstein, *Jahrbuch der Radioaktivität und Elektronik* (1907), Vol. 4, p. 411; M. Planck, Berl. Ber. p. 542 (1907); Ann. d. Physik **26**, 1 (1908); Van Dantzig, Physica **6**, 673 (1939).
[2] C. Eckart, Phys. Rev. **58**, 919 (1940).

73. Theory of Superconductivity. J. BARDEEN, *University of Minnesota.*—It is assumed that in the superconducting state there is a small periodic distortion of the lattice yielding a unit cell containing $\sim 10^6$ atoms. This gives rise to a fine grained zone structure in k space. Electrons which have energies within $\sim kT_c$ of the energy surface lie near the boundaries of $\sim 10^4$ zones and some of these have a very small effective mass ($\sim 10^{-4}m$). A small fraction of the electrons have a very high diamagnetic effect, sufficient to make the metal a perfect diamagnetic. Although about one electron in 10^4 lies in the surface zones, only about one in 10^6 is a superconducting electron. The energy discontinuities produced by the zone structure yield a decrease in the energy of the electrons at the expense of the increase in energy of the lattice resulting from the distortion. A rough estimate of the interaction between the electrons and the lattice obtained from the electrical conductivity in the normal state indicates that the superconducting state may be stable at low temperatures. The most favorable metals are those which have a high density of valence electrons in a wide energy band and which have a large interaction between electrons and lattice (low conductivity).

74. Attractive Forces Between Ions and Neutral Molecules. H. MARGENAU, *Yale University.*—In theories of ionic mobility the attractive potential between an ion and a neutral molecule is usually taken to be $\frac{1}{2}e^2\alpha R^{-4}$, α being the polarizability of the molecule and R the internuclear distance. This represents only the long range attraction. At closer range, terms proportional to R^{-6} appear. The present note examines their magnitude. They are due to two causes: (a) the inhomogeneity of the ion field; (b) mutual polarization of the two structures (dispersion forces). The latter are well known. The former yields a contribution approximately given by $(e^4/5R^6)(r^4)_{00}$, where $(r^4)_{00}$ is the fourth moment of the charge distribution of the neutral molecule. When computed for He, this term adds about 5 percent to the usual attraction at minimum separation between ion and atom. Estimates of the term have been made for molecules satisfying a one-term dispersion formula. It is generally small enough to be neglected in cruder theories of mobility, but should be included in quantitative considerations. Cause (b) contributes a somewhat larger attraction; both causes may increase the attraction by about 30 or 40 percent at closest separation. A list of computed values of the terms proportional to R^{-6} for different gases will be presented.

75. Action at a Distance between Simple Atoms. JOHN A. WHEELER, *Princeton University.*—The mutual energy of two atoms in S states varies in a complicated way for small internuclear separations but for larger distances approaches van der Waals' $1/r^6$ law. In quantum mechanics this result receives a simple interpretation. The instantaneous energy of interaction of two dipoles varies as $1/r^3$; the dipole moments of the two atoms vanish, however, in the first approximation; and the second approximation leads to van der Waals' law. At distances outside the so-called wave zone of the oscillating dipoles, however, the field falls off more slowly than $1/r^3$. Consequently, van der Waals' force assumes a dependence upon distance different from $1/r^6$ for separations greater than the wave-length associated with the resonance radiation of the atoms in question.

76. The Energy of Dissociation of Water Vapor. ROBERT J. DWYER,* *Harvard University.*—A precise determination of the energy of dissociation of water vapor in the reaction $H+OH=H_2O$ was undertaken following the method of Bonhoeffer and Reichardt.[1] This consists essentially in applying the integrated form of the van't Hoff isochore to the measurement of the heat of reaction for $H_2O+O_2=4OH$ by observing the OH absorption spectrum under different conditions of temperature and oxygen-water vapor mixture. This heat of reaction, when reduced to absolute zero and combined with two accurately known reaction energies, gives the dissociation energy of H_2O into H and OH. The uncertainty introduced into the work of Bonhoeffer and Reichardt by their failure to resolve the individual lines of the absorption spectrum was avoided by the use of the second order of a 21-foot grating. The oven temperature was controlled automatically to a fraction of a degree, and the temperature distribution was measured by a platinum, platinum-rhodium thermocouple which could be adjusted to different positions along the length of the oven. The principal result was

$$H+OH=H_2O-117.6\pm0.5 \text{ kilo-calories.}$$

* Charles A. Coffin Foundation Research Fellow.
[1] K. F. Bonhoeffer and H. Reichardt, Zeits. f. physik. Chemie **A139**, 75 (1928).

77. Electron Microscopical Determination of Object Thickness. L. MARTON, *Collingswood, New Jersey.*—The usual methods of light optics for measuring the thickness of a specimen cannot be applied in electron microscopy. In case of thin objects, however, the measured intensity distribution of the micrographs permits the calculation of the thickness in first approximation. The first of several necessary assumptions is that only single scattering occurs. The classical Rutherford formula is applied for obtaining numerical values. The results are represented in the form of a nomogram with aperture ratio of the microscope, electron speed, blackening of the micrograph, and mass thickness of the object as variables. The limitations of the method are indicated and a few practical examples given.

78. A Magnetic Electron Microscope. G. G. HARVEY AND L. J. SULLIVAN, *Massachusetts Institute of Technology.*—A two-stage high magnification magnetic electron microscope has been constructed. A flexible design has been adhered to throughout so that the instrument may be easily disassembled for modification of the lens properties. An object stage similar to that of Ruska permits changing of specimens without breaking the vacuum. Provision is made for transverse and vertical adjustment of the object as well as a means of tilting the object for the purpose of taking stereoscopic pictures. The camera is provided with air-locks and external controls so that the plates may be changed without breaking the vacuum; several exposures may be made on the same plate. The pole piece design of the objective and the projection lens permits of ready removal and substitution of different shapes. The requirement of complete axial symmetry in these pole pieces is met by using the Prebus one-piece type of construction. Adjustments are provided in each of these lenses to bring the aperture into coincidence with the axis of the field. The condensing lens is fitted with apertures and stops of various sizes, providing for both bright and dark field illumination.

79. The Apsidal Motion in Binary Stars for a Point Source Convective Core Model with Varying Guillotine Factor. LLOYD MOTZ, *The College of the City of New York and Columbia University.*—Since investigations of the energy source in stars depend upon a definite stellar model, it is important to obtain independent verification of the density distribution yielded by such a model. The equation[1] which gives the distortion of components of a binary system was integrated numerically[2] for the second and third harmonics, using the values of the density and mass distributions for a polytrope of index 1.5 inside the convective core and the values given by "The project for the computation of mathematical tables"[3] for a point-convective solar model in the external region. The ratio of the orbital to the apsidal period is given as an expansion in k_2, k_3, etc., which are related to the harmonics. For the point-convective model k_2 and k_3 are 0.00616 and 0.00155 respectively. These values are to be compared with the values 0.0144 and 0.00368 for a polytrope of index 3 and 0.00134 and 0.00024 for a polytrope of index 4. For the binaries for which observations are available,[1] the observed apsidal motion corresponds to polytropes with indices between 3 and 4 and is therefore in qualitative agreement with the point-convective model.

[1] T. E. Sterne, M.N.R.A.S. **99**, 451 (1939); **99**, 662 (1939).
[2] Most of the numerical work was done by the Astronomical Computing Bureau at Columbia University.
[3] H. A. Bethe, G. Blanch, A. N. Lowan and R. E. Marshak, Phys. Rev. **59**, 467 (1941).

80. Formation of Multiple Stars by Fission and Simultaneous Capture. ROSS GUNN, *U. S. Naval Research Laboratory.*—The zone of gravitational instability surrounding a star is found to extend indefinitely as the rotational velocity of a visiting star approaches its critical fission value. Further, fission may occur at angular velocities notably below the critical value if the approach of two stars is close. Thus rapidly rotating stars divide by fission, preferentially in the vicinity of another star. In a close approach some orbital energy is used to separate the components of the visiting star and to change its axial rotation by tidal action. Upon determining graphically the orbits of the resulting three bodies it is found that various natural initial conditions permit: (a) the passage of the stars without effect, (b) the simple fission of either star producing either a close or a moderately separated pair, (c) the fission of one star, one component returning to infinity and the other being captured, (d) the fission of one star with the capture of both components by the other, usually forming a spectroscopic pair accompanied by a remote companion. These are in agreement with observed multiple star systems. However, because present data suggest that the close approach of two stars is not common it seems necessary to conclude that most binary systems evolve from *single* stars, probably in a manner much like that described in the author's "binary star fission theory" of the origin of the solar system.[1]

[1] R. Gunn, Phys. Rev. **39**, 130, 311 (1932).

81. The Lateral Extension of Cosmic-Ray Showers. L. W. NORDHEIM, *Duke University.*—The problem of angular scattering and lateral extension of showers can be solved completely if their longitudinal extension is known, i.e., the function $f(E_0, E, x)$ giving the number of electrons of energy E produced at the distance x by a primary E_0. For energies above the ionization limit the mean square deviation of electrons or quanta can be expressed by a rapidly convergent series showing the contributions of parent quanta, grandparent electrons and so on. For low energies a good approximation can be obtained by decomposing the electron distribution into two parts, the electrons which have been slowed down from high energies and those which have been created with low energies by quanta. The theoretical spread is much larger than estimated by Euler and Wergeland. It is fully sufficient, for instance, to explain the observations by Auger on large air showers, our value for the root mean square deviation being ~90 meters in agreement with a figure given by Bethe.[1]

[1] H. A. Bethe, Bull. Am. Phys. Soc. **16**, 7 (1941).

82. On the Theory of Cosmic-Ray Showers Including Ionization Loss. BRUNO ROSSI, *Cornell University.*—It is known that, neglecting ionization, the energy distribution of shower electrons at a thickness t and in the neighborhood

of the energy E can be approximated by a power spectrum const$\times dE/E^{s+1}$. s is a function of the ratio $t/\ln(E_0/E)$, where E_0 is the primary energy. It is shown that, if the ionization loss is taken into account, the expression of the energy spectrum becomes const$\times dE/(E\eta)^{s+1}$. η is a function of s and ϵ/E (ϵ being the ionization loss per radiation unit) which can be conveniently calculated in the form of a series $\eta=1+a_1(s)(\epsilon/E)+a_2(s)(\epsilon/E)^2+\cdots$ for energies in the neighborhood of ϵ.

83. A Cosmic-Ray Radio-Sonde. H. V. NEHER AND W. H. PICKERING, *California Institute of Technology.*—The cosmic-ray radio-sonde described in this paper was used for observations in the stratosphere near the magnetic equator. The instrument can be used for single counters or coincidences up to fourfold. It includes the necessary amplifiers and scaling circuits to operate a relay which keys the radio-transmitter. High voltage for the counters is provided by a buzzer and transformer unit. Small storage batteries are used for power to operate the unit for about three hours. Pressure and temperature signals are sent at eight-minute intervals. The complete instrument ready for flight weighs about 3300 grams. The receiving equipment consists of a super-regenerative receiver with the signal output recorded on a paper tape.

84. Results of a High Altitude Cosmic-Ray Survey Near the Magnetic Equator. W. H. PICKERING AND H. V. NEHER, *California Institute of Technology.*—Electroscope and Geiger counter observations have been taken with free balloons at geomagnetic latitudes of 3°, 17°, and 25°N. The most important results are as follows: (1) The Geiger counter technique using a single counter will give results very close to those obtained with the electroscope and of comparable accuracy. (2) Vertical coincidence measurements give rise to markedly different values for the relative amounts of incident energy at various latitudes, as compared with the electroscope or single counter data. (3) Within the experimental error, no difference was obtained between the vertical coincidence curves at 3° and 17°, and thus no new energy lies in the primary energy spectrum between the limits of 17 and 14 Bev. (4) This is direct evidence for a banded structure in the primary cosmic-ray spectrum. (5) Flights made with triple and quadruple coincidences, and also with counters arranged to record showers, showed that showers do not significantly affect the vertical coincidence measurements.

85. The Experimental Testing of a Hypothetical Distribution of Energy in the Cosmic-Ray Spectrum. ROBERT A. MILLIKAN, *California Institute of Technology.*—From a previously reported theory of the origin of cosmic rays it is possible to predict the existence of definite cosmic-ray bands and plateaus of unchanging cosmic-ray intensities as a function of latitude. In this paper these predictions are compared with already existing data and it is shown from them why the recent exploratory work in India was done at the chosen latitudes, the results of which are reported in the accompanying papers by Neher and Pickering.

86. The Vertical Intensity and the Latitude Effect of the Hard Component at High Altitudes. WILLIAM P. JESSE, E. O. WOLLAN AND MARCEL SCHEIN, *University of Chicago.*—Further measurements[1] of the intensity of the hard component have been carried out up to altitudes corresponding to about 3 cm Hg both at Chicago ($\lambda=51°$N) and at Waco, Texas ($\lambda=40°$N). The vertical intensity for various lead thicknesses between the counters increases continuously up to the highest altitudes reached (1.8 cm). The value at this point at Chicago is about 13 times that at sea level. At 3-cm pressure the latitude effect for the hard component between 51° and 40° was found to be about 15 percent for lead thicknesses of 8 and 10 cm. No maximum in the intensity curves was observed in any of these later experiments.

[1] Marcel Schein, William P. Jesse and E. O. Wollan, Phys. Rev. **57** 847 (1940).

87. The Production of Mesotrons by Ionizing Cosmic Rays. MARCEL SCHEIN, WILLIAM P. JESSE AND E. O. WOLLAN, *University of Chicago.*—An experiment designed to investigate the possibility that ionizing particles may produce mesotrons has been carried out at high altitudes. Four fourfold coincidence counter sets were used. Two of these sets, each covering the solid angle of the other, were used to measure the vertical intensity through 18 cm of lead. A third counter set was arranged to measure below the total lead the emergence of one or more particles accompanying a particle traversing the set. The fourth counter set similarly registered the ejection in the first four centimeters of lead of two or more particles coincident with the traversing particle. At altitudes corresponding to a pressure of 3 cm Hg 46 percent of the vertical coincidences registered in set 1 and 2 were accompanied by coincidences in set 3 and 15 percent were accompanied by coincidences in set 4. The fact that set 4 records only 15 percent of the vertical particles indicates that at least 85 percent of the mesotrons at 3 cm pressure are not produced by the soft component. The large proportion of counts (46 percent) recorded by set 3 seems best explained by assuming that one traversing ionizing particle which is probably a proton produces a number of mesotrons in the lead.

88. The Nature of the Primary Cosmic Radiation. E. O. WOLLAN, MARCEL SCHEIN AND WILLIAM P. JESSE, *University of Chicago.*—Seven balloon flights with counter arrangements similar to those used before have been made with lead between the counters of thickness 4, 6, 8, 10, 12 and 18 cm. The vertical intensity *vs.* altitude curves were found to be nearly the same for all of these thicknesses at the highest altitudes reached (less than 1 radiation unit from the top of the atmosphere). This fact is not in agreement with the assumption that electrons between 10^9 and 10^{12} ev enter the earth's atmosphere. Further evidence as to the nature of the particles was obtained by side counters arranged to register any showers which accompany a particle traversing the apparatus. The number of counts in the side counters was in no case more than a few percent of the number of traversing particles. Within one radiation unit of the top of the atmosphere a large proportion of the

particles entering the apparatus should be of primary origin. Since electrons ($10^9 < E < 10^{12}$ ev) are not observed at these altitudes they must constitute at most a very small fraction of the primary radiation. The incoming radiation, according to our experiments, must be ionizing, penetrating and non-shower-producing and hence consists probably of protons.

89. The Effect of External Temperature on Cosmic-Ray Intensity. NIEL F. BEARDSLEY, *University of Chicago.*—A considerable diversity of opinion seems to exist as to the importance and magnitude, even of the sign, of the effect of external temperature on the ionization due to cosmic rays as observed at the surface of the earth. A study of cosmic-ray intensities, the temperatures and the pressures at Cheltenham indicates that the difference in the results of different observers is caused by different methods of computation. Using each available day for one year (A); the average result of using monthly periods (B); and the results of using the monthly averages of the variables (C); (δP in millibars, δT in degrees C, δI in percent of variation from the annual mean)

(A) $$\delta I = -0.161\delta P - 0.132\delta T$$

Contribution to the variance of I;

P : 27 percent T : 33 percent

(B) $$\delta I = -0.134\delta P - 0.065\delta T$$

P : 56 percent T : 3 percent

(C) $$\delta I = -0.205\delta P - 0.154\delta T$$

P : 0 percent T : 69 percent

indicate that daily changes in temperature are, as some have reported, not important; however the seasonal changes in temperature are extremely important. Other correlation results will also be discussed.

90. Cloud Chamber and Counter Tube Cosmic-Ray Studies Under Ground. DONALD J. HUGHES AND VOLNEY C. WILSON, *University of Chicago.*—At the Cosmic-Ray Symposium held at Chicago in June, 1939, it became evident that several different types of cosmic rays may be present below ground. To identify some of these rays, the following experiments were performed in the Isle Royal Copper Mine at Houghton, Michigan. An eight-inch cloud chamber in a 1230 oersted magnetic field was set up at a depth of 70 meters water equivalent. Abundant evidence is present for penetrating ionizing rays accompanied by secondary negative electrons. A few large showers were observed. Attempts to detect secondaries produced by penetrating non-ionizing rays gave negative results. Counter tube absorption experiments were performed at 70 meters and 630 meters. Within the experimental errors, the relative number of soft secondaries to the penetrating rays is the same at the two depths. At various depths counter tube measurements were made of showers produced in a 15-cm lead block. At moderate depths, but not at the greater depths, there is some evidence that a small percent of the showers are produced by non-ionizing rays. The relative number of large showers increases greatly with depth. These experiments indicate that the large majority of the penetrating rays underground are ionizing, probably mesotrons and/or protons.

91. The Latitude Effects of the Hard and Soft Components of Cosmic Rays. V. C. WILSON AND R. N. TURNER, *University of Chicago and Canadian-Australasian Line.*—Two threefold Geiger-Mueller tube telescopes were mounted upon the *R.M.M.S. Aorangi*, which plies between Vancouver, Canada, and Sydney, Australia. The telescopes subtended identical solid angles. One recorded both the soft and the hard cosmic rays, whereas the other, which contained 11 cm of lead as an absorber, recorded only the hard rays. The difference between the two counting rates represents the intensity of the soft rays. Data were taken during four round trips. The latitude effect for the soft rays is slightly greater than for the hard rays. If the soft component is produced by the hard component, one should expect the latitude effect of the soft rays at sea level to equal that of the hard rays at the altitude where the hard rays produce the observed soft rays. At an altitude above sea level the latitude effect of the hard rays is greater than at sea level; so, also, the latitude effect for the soft rays at sea level should be slightly greater than for the hard rays at sea level. Since this agrees with the observations, one may conclude that the soft cosmic rays at sea level are secondaries produced by the penetrating rays.

92. Further Experiments on Mesotron Showers. W. F. G. SWANN AND W. E. RAMSEY, *Bartol Research Foundation of the Franklin Institute.*—A quintuple coincidence set of Geiger counter sensitive areas, with a large thickness of metal below the upper area, was used as in the case of observations formerly reported. The block of metal was of tin and each of the four lower trays was covered with a slab of lead 1 cm thick. 11,000 "events," corresponding to the passage of at least one ray through the whole apparatus, gave two cases in which one counter discharged in the upper tray and two counters discharged in each of the four lower trays, and thirteen cases in which two counters discharged in the upper tray and two discharged in each of the lower trays. The absence of multiplicative effects arising in the lead slab suggests that the pairs in each case were mesotron pairs. The characteristics of the apparatus are such that the thirteen observations above referred to represent 12,000 times the value which would be calculated from accidental coincidences of the individual counters conspiring to produce these events, and 2600 times the number which would be obtained by the accidental passage of two mesotrons through the apparatus within its resolving time. The directions of the rays as defined by the geometry of the counters is in harmony with the supposition of mesotron pairs.

93. Rest Mass and Lifetime of the Mesotron as Found from Cosmic-Ray Measurements. PAUL WEISZ, *Bartol Research Foundation of the Franklin Institute.*—The values for the lifetime of the cosmic-ray mesotron obtained experimentally by various authors show considerable disagreement even after recalculation on the basis of equiva-

lent conditions. However, these values show a marked relation to the average path length of the radiation in each experiment. Since experimental determinations of the mesotron rest mass have yielded values from below 100 to over 500 times the electronic mass, a distribution in rest masses is assumed rather than a single rest mass, and with this postulate it is shown that a relation between measured "pseudo-lifetime" and path length must be expected of the sort actually found regardless what form the distribution may possess. The deviation of the pseudo from the real lifetime becomes smaller with decreasing path length. An extrapolation towards zero path length leads to a real lifetime of the order of 5×10^{-7} sec. consistent with Yukawa's original prediction. Other experimental findings, as the increasing frequency of heavily ionizing tracks with altitude, the secondary peak of the Rossi curve, and possibly others may also be explained on the basis of a distribution in rest mass.

94. Multiple Values of the Specific Ionization Produced by Cosmic-Ray Entities. W. E. RAMSEY, W. F. G. SWANN, AND PAUL WEISZ, *Bartol Research Foundation of the Franklin Institute.*—Some years ago two of us reported measurements of the ionization per centimeter of path in argon, and we recorded two primary values, one about double the other. The experiments have now been repeated with improved resolving time, using a proportional counter system in place of the ionization chamber formerly used. Again the results indicate two primary values for the ionization, occurring with comparable frequency, and multiple values occurring with much smaller frequency and corresponding to each of these primary values. The proportional counter was operated by the assistance of other ordinary Geiger counters in such a manner as to define a unique path length within the proportional counter itself. The procedure of measurement involved a collection of charge corresponding to the ionization along the fixed path length, and the time of collection was of the order of 10^{-4} second. The control counter system also limited the sensitive time of the apparatus to 10^{-4} second, and the net result was that in the measurements there was only one chance in a thousand of more than one ray participating in the charge measured in any particular case, unless more than one ray participates as part of a simultaneous multiple event.

95. The Initial Avalanche in Discharge Counter Breakdown. SANBORN C. BROWN AND W. P. ALLIS, *Massachusetts Institute of Technology.*—A theoretical study of the initial avalanche in discharge counter breakdown has been undertaken. In the most general case three regions exist within the counter: (1) the region in which no multiplication takes place, (2) the region in which the avalanche multiples, (3) the region in which the multiplication is reduced by the space charge of the avalanche. Graphical integration of the multiplication as a function of the position in the counter shows that the form of the function is quite independent of the particular space charge model assumed. In region 2 the field is inversely proportional to the distance from the anode and the total number of ions produced can be computed from a single function. This function has been tested experimentally for helium and found to be valid over the pressure range from 5 mm to 7 atmospheres and a ratio of cathode to anode radii from 250 to 1.4. In region 3 the assumption that the ionization is constant can be shown to be satisfactory and the total multiplication can again be computed from a single function. The relation of these functions to the counter breakdown voltage is discussed.

96. Time Lags in Geiger-Müller Counter Discharges. C. G. MONTGOMERY AND D. D. MONTGOMERY, *Yale University.*—A spark produced simultaneously a burst of ultraviolet light and an electrical pulse. The ultraviolet light ejected photoelectrons from a counter cathode and started a discharge. The electrical pulse was delayed a known time by a vacuum-tube circuit which was also energized by the pulse from the counter wire. The number of counts from the counter and the number with lags greater than a given time were recorded. Knowing the average number of photoelectrons formed by a burst of photons, the probability that an electron would be captured to form a negative molecular ion could be determined. In a counter, 18 mm in diameter, filled with a mixture of argon with 6 percent oxygen, the probability of capture in such a way as to produce a lag of more than 1.4 microseconds increased with pressure, attaining a value of 0.48 at 19 cm of mercury. From the known breakdown characteristics of argon-oxygen counters, the mean cross section for capture by an oxygen atom was found to be about 10^{-18} cm^2 in agreement with previous measurements. In a counter in which the primary ions are produced in the gas, the fraction of delayed counts at first increases with pressure, reaches a maximum, and falls again at higher pressures.

97. A Precision Method of Measuring Geiger Counter Resolving Times. YARDLEY BEERS, *New York University.*—An improved method for measuring resolving times of Geiger counters has been devised for use in some recent work on the measurement of the charge of the β-particle.[1] The counting rates of two constant β-ray sources, first separately and then together, are measured. Because of the finite resolving time the sum of the counting rates due to the separate sources exceeds that due to the combined source. By application of formulae which have been derived the resolving time and error involved are calculated from these quantities. Relatively high accuracy can be obtained without excessive expenditure of time upon the measurements and without the use of high counting rates for which the validity of correction formulae is questionable or which damage the counter. For example, for a determination of a resolving time of about 10^{-4} second lasting one hour, the probable error in the corrected counting rate at 300 counts per second is only one half of a percent.

* This work was done at Princeton University, Princeton, New Jersey.

[1] R. Ladenburg and Y. Beers, Phys. Rev. **58**, 757 (1940).

98. Forms of Discharge in Micro-Gaps. R. W. JONES, *Central Y.M.C.A. College,* AND W. S. HUXFORD, *Northwestern University.*—Hobbs[1] and others have shown that

significant departures from Paschen's law occur in the low voltage spark breakdown across gaps of the order of 10^{-4} cm at atmospheric pressure. More recently Pearson[2] has measured the field currents prior to breakdown. In the present report it is shown that transient discharges occur between polished silver electrodes at atmospheric pressure before arcing sets in. These discharges are faintly audible and luminous when observed in a darkened room. They produce markings on the electrode surfaces which are different from those formed in the usual spark discharge. Four types of patterns are noted: (1) A "bird-shot" pattern of small spots clustered in an irregular manner about a central circular area devoid of spots; (2) Multicolored rings enclosing a clear central area; (3) Rings as in (2) in which the central area contains a "bird-shot" pattern; (4) Circular patterns similar to (2) except that the colored rings completely fill the area. Cathodes and anodes exhibit differences which are consistent in all types of markings. Evidence is found that these discharges are initiated by field electrons as previously observed in reignition of arcs across switch contacts.[3]

[1] G. M. Hobbs, Phil. Mag. [6] **10**, 617 (1905).
[2] G. L. Pearson, Phys. Rev. **56**, 471 (1939).
[3] W. S. Huxford, S. G. Eskin and R. W. Jones, Phys. Rev. **55**, 1146(A) (1939).

99. The Colinear Emission of Annihilation Quanta. ROBERT BERINGER AND C. G. MONTGOMERY, *Yale University*.—The distribution in angle between the two oppositely directed quanta resulting from the annihilation of a Cu^{64} positron has been studied with coincidence counters. Two counters were placed at equal distances on opposite sides of a small pellet of activated copper foil wrapped in lead foil slightly thicker than the positron range, each counter subtending 0.0133 steradian. The ratio of the number of coincidences to the number of counts in a single counter was determined for various displacements of one counter from the position in line with the source and second counter. For the in-line position, this ratio represents the efficiency of one counter for 0.51 Mev photons and was about 10^{-3}, in agreement with the accepted value for similar counters. The observed variation of this ratio with displacement agreed closely with that calculated from the geometry for quanta emitted in exactly opposite directions. The results indicated that the two quanta are oppositely directed to within one degree.

100. Measurement of the Electron-Electron Cross Section at Energies from 1.3 to 2.6 Mev. PAUL E. SHEARIN AND T. EUGENE PARDUE, *University of North Carolina*.—Until recently experimental values of the electron-electron cross section covered a restricted range of energies. The results of some experimenters disagree with Möller's relativistic theory. The situation was clarified by Howell and Hornbeck (Proc. Am. Phil. Soc.) who measured 190 meters of track in nitrogen (primary energy, 1.3–2.6 Mev), finding 107 secondaries with energies greater than 20 Kev. This investigation extends their work, with objects of increasing the accuracy of measurement and decreasing statistical error. We employed 343 meters of track. Letting R equal observed cross section over calculated cross section, the results were these:

OBSERVER	LOWER LIMIT OF SECONDARY ENERGY	NUMBER OF SECONDARIES	R
H. and H.	20 Kev	107	1.21 ± 0.12
	30	63	1.12 ± 0.14
	40	35	0.86 ± 0.15
S. and P.	20	180	1.11 ± 0.07
	30	105	1.02 ± 0.10
	40	81	1.07 ± 0.11

101. The Growth of Drops in a Wilson Cloud Chamber. WAYNE E. HAZEN, *University of California*. (*Introduced by Robert B. Brode.*)—The rate of growth of ethyl alcohol drops in nitrogen, helium, and hydrogen was measured by photographing the drops in a cloud chamber with intermittent illumination of known frequency. Measurements of the separations of successive images on the film gave data for calculating the velocity as a function of time and hence, from Stokes' law, the radius as a function of time. The square of the radius increased linearly with the time in all cases, the slopes being about 6×10^{-6} cm²/sec. for nitrogen and 18×10^{-6} cm²/sec. for hydrogen. The rate of growth was found to increase linearly with expansion ratio from the ion threshold to the fog threshold. The temperature of the drop was calculated from the rate of growth. From the drop temperature and its rate of growth and the vapor pressure of ethyl alcohol as a function of temperature the diffusion coefficients for ethyl alcohol vapor in nitrogen, helium and hydrogen were calculated. Reasonable agreement with other measured values of the diffusion coefficients was obtained.

102. The K-Absorption Edges of Metal Ions in Solution. W. W. BEEMAN* AND J. A. BEARDEN, *The Johns Hopkins University*.—A double crystal spectrometer has been used to measure the K-absorption edge structure of Ni^{++}, Cu^{++}, Zn^{++}, $Cu(NH_3)_4^{++}$, and $Cu_2(CN)_4^{--}$ in aqueous solution. It was found that Ni^{++}, Cu^{++} and Zn^{++} have similar edges whose main features may be understood on the assumption that the ions absorb as if they were in vacuum. In each of the three edges two absorption lines have been resolved. Their positions indicate that they are due to excitation of a K electron into the $4p$ and $5p$ orbits of the ion. The solvent does not measurably displace the absorption maxima from the positions calculated for an ion in vacuum but there is considerable broadening of the maxima which must be due to the fields of the coordinated water molecules. The complex ions have quite different absorption edge structures which it is suggested arise from the scattering of the photoelectron by the other atoms of the ion. The same process takes place in the absorption of x-rays in a polyatomic gas.

*Now at the General Motors Research Laboratories, Detroit, Michigan.

103. Radiations from the Induction Accelerator. D. W. KERST, *General Electric Company*.—Since the x-ray yield from the induction accelerator is now approximately

equivalent to that from one gram of radium, it has been possible to take radiographs. The results show that the beam as it impinges on the edge of the target is less than ½ mm in width. Cathode rays coming through the glass walls of the acceleration chamber have also been photographed. X-ray absorption curves in copper and lead will be shown for comparison with Van Atta and Northrup's absorption curve for x-rays produced by two million volt electrons.[1] The absorption coefficient for lead is 0.62 cm^{-1} giving a monochromatic equivalent of 1.4 Mev for the x-rays, and for copper the absorption coefficient is 0.454 cm^{-1} which gives a monochromatic equivalent of about 1.35 Mev. The absorption curve indicates that the radiation is thin target radiation. This is to be expected since the electron orbits shrink toward the target and impinge on its outermost edge. Consequently a lower limit can be estimated for the beam current by comparison with thick target yields.[1] This estimate is 0.02 microampere.

[1] Van Atta and Northrup, Am. J. Roent. and Rad. Therapy, April 1939.

104. Characteristic X-Rays Produced by Deuteron Bombardment. J. M. CORK, *University of Michigan.*—An investigation has been made of the nature and yield of x-rays produced when thin targets of various elements are bombarded with deuterons of energy up to 10 Mev. The total radiation from the bombarded target is collimated at right angles to the deuteron beam. The scattered and disintegration particles are deflected out by the strong magnetic field of the cyclotron augmented with a magnetic shunt. At 10 Mev, x-rays shown to be characteristic K radiation, are observed for elements of atomic number less than 39. An apparent maximum occurs for elements of atomic number about 28, due to absorption. The yield of x-rays as a function of the energy of the incident deuteron was observed for a copper target. The results including an estimate of the cross section are compared with the theoretical calculations of W. Henneberg.[1]

[1] W. Henneberg, Zeits. f. Physik **86**, 592 (1933).

105. A New Evaluation of h/e. J. A. BEARDEN AND G. SCHWARZ, *The Johns Hopkins University.*—Two methods have been used: (1) the high frequency limit of the continuous spectrum with gold and copper targets, (2) x-ray excitation potentials for $K\alpha_1$ lines of nickel, copper, zinc, gallium and the $L\alpha_1$ line of tungsten.

Twenty-eight runs for method (1) and a gold target yield $h/e=1.3772\cdot10^{-17}$ e.s.u. Five similar runs with a copper target give 1.3777. The limit obtained with the copper target is practically as intense as with gold but much sharper. The intensity and sharpness are probably due to the thin layer of tungsten, which deposits by evaporation from the filament. The probable error is about 2 in the last figure and hence we believe the difference between the values for gold and copper is real. The values for h/e obtained with the second method depend greatly upon the target used. For nickel, copper, and tungsten the accuracy of the measurements is better than above and gives $h/e=1.3793$, 1.3789, and 1.3773, respectively. Differences in the width of the absorption limits may introduce corrections in the last figure. The results for zinc and gallium are less reliable but indicate a value of about 1.3775. These differences within each method and between them, which we believe to be real, indicate that some modification of the simple theory is necessary.

106. The Velocity of Sound in Air. H. C. HARDY AND W. H. PIELEMEIER, *Pennsylvania State College.*—The velocity of sound has been accurately measured by at least fifteen workers since 1900. The values they obtain range from 330.77 to 331.92 meter $sec.^{-1}$ at 0°C. A survey of these values has been made and an attempt will be made to explain this discrepancy. Assuming the experimental technique is correct, the following corrections must be set up in every experiment in order that the values may be compared: (1) The H_2O and CO_2 content must be specified and *properly* corrected for. (2) Correction for temperature and pressure must be accurately made from a dependable equation of state. *In this correction the change of C_v with temperature cannot be neglected.* (3) A dispersion correction must be made for measurements at high frequencies. (4) *The composition* (O_2 and N_2 content) *of the air should be known at the time and place of the measurement.* A calculation of the velocity of sound from known spectrographic data, the Beattie-Bridgman equation of state, and the latest values of the fundamental constants have been made. Assuming a mean density of 1.2930 g $liter^{-1}$ and a mean composition given by Humphreys,* this value is 331.447 ±0.010 meter $sec.^{-1}$. Due to the variation in the composition of the air, this value should probably be written as 331.45 ± 0.05 meter $sec.^{-1}$.

* W. J. Humphreys, *Physics of the Air* (McGraw-Hill) third edition, p. 67.

107. Supersonic Measurements with a New Apparatus. D. TELFAIR AND W. H. PIELEMEIER, *Pennsylvania State College.*—The region of acoustical dispersion in a polytomic gas may be explored in three ways besides that of varying the frequency. By varying the density, the temperature, or the foreign gas concentration the acoustical relaxation time may be altered, thus shifting the region of dispersion to a different frequency. An apparatus has been constructed which makes possible a variation of these controlling factors over relatively wide ranges. The gas density and foreign gas concentration may be regulated by using high vacuum technique. The temperature is regulated by means of a thermocouple-controlled photoelectric relay. The sound chamber is made of stainless steel, and by means of a specially designed vacuum-tight joint may be easily opened to insert a quartz plate of the desired frequency. Measurements have been made on velocity in air and velocity and absorption in methane and propylene with interesting results.

108. The Temperature Effect on Ultrasonic Velocities in Carbon Dioxide. C. J. OVERBECK AND H. C. KENDALL, *Northwestern University.*—Ultrasonic velocity measurements in pure carbon dioxide gas were made at temperatures ranging from 25° to 530°C with frequencies from 50 to 147 kilocycles. A sonic interferometer similar to

Pierce's employing quartz crystals was used. The interferometer chamber was built of chromium plated brass, glass and quartz to avoid gas contamination at high temperatures. Two sources of carbon dioxide were used: a specially prepared high purity tank of gas, and gas from sublimated dry ice. Traces of water vapor were removed by either dry ice or long phorphorous pentoxide traps. Temperature measurements were made by placing a thermojunction in the middle of the gas space between the crystal and reflector. Frequencies were determined by beating harmonics of the crystal driving oscillator against harmonics of a calibrated standard oscillator. The curves plotted—reduced velocity *vs.* temperature—do not show the irregularities found in published work. Earlier work in this laboratory[1] has shown the effect of gas contamination as a partial explanation of conflicting published results. Recent work has shown that a temperature discrepancy will account for the balance of the variations.

[1] C. J. Overbeck and E. Wiler, Phys. Rev. **55**, 1127 (1939).

109. Sound Velocity and Absorption by Ultrasonic Interferometry. J. C. HUBBARD, *The Johns Hopkins University.*—Half-wave-length spacings for determining sound velocity and decrement of corresponding galvanometer or other readings for determining absorption by the methods of acoustic interferometry are both highly sensitive to boundary conditions. Such data are particularly misleading if there is a periodic error in the screw, if there is a systematic departure from parallelism between source and reflector as distance apart is changed, or if there are measurable diffraction effects. The requirements of design for acoustic interferometry are fully as rigorous as those for optical interferometry and have seldom been met in practice. It is because of this that many have favored optical or other methods of securing acoustic data, but such methods have been used with sound intensities now known to be high enough to account for the great confusion and discord among values found by different observers. The much discussed dispersion of sound in liquids has as yet no basis in experimental measurement.[1] Data are presented showing types of errors encountered and methods of estimating them. Specific application is made to the calibration of screws by ultrasonics.

[1] J. C. Hubbard, Am. J. Phys. **8**, 219 (1940).

110. Friction Phenomena and the Stick-Slip Process. F. MORGAN, M. MUSKAT AND D. W. REED, *Gulf Research & Development Company.*—Further studies* have been made of the stick-slip phenomenon recently investigated by Bowden and collaborators. The apparatus has been modified so as to eliminate radial motion between the slider and rotating table. This change has removed spurious indications of slipping during the stick phase, although under certain conditions some degree of slip appears to be inherent in the process. This aspect of the problem has been studied by quantitative measurements on motion pictures of the slider during stick-slip. Temperature records of the stick-slip cycle confirm previous observations that the temperature flash is confined exclusively to the slip phase and in no case studied exceeds 50°C above ambient. Traces made of the slip phase with very high camera speeds permit an analysis of the variation of the kinetic friction with velocity. Thus both static and kinetic friction data can be obtained from a single stick-slip cycle. Motion pictures of the stick-slip process both for dry and lubricated surfaces will be shown.

* F. Morgan, M. Muskat and D. W. Reed, Phys. Rev. **58**, 205 (1940).

111. Relaxation Time of Colloidal Particles from Measurements of the Electro-optical Effect. B. W. SAKMANN, *Massachusetts Institute of Technology.* (*Introduced by H. Mueller.*)—The electro-optical effect furnishes a method for the determination of the relaxation time of colloidal particles and, hence, of their size and shape. If the frequency of the electric field is larger than the relaxation frequency, the electric birefringence is steady. For low frequencies the double refraction consists of a steady and a vibrating part; the latter oscillates with twice the frequency of the applied field and lags behind the field. Both parts have been measured in bentonite sols by using a photoelectric method. Measurements of the phase-shift and of the frequency dependence of the alternating part confirm Tummers' theory. The size of the miscelles found by this method shows good agreement with the values determined by the ultracentrifuge.

112. The Velocity of Radio-Waves over Short Distances. R. C. COLWELL, H. ATWOOD, JR., J. E. BAILEY AND C. O. MARSH, *West Virginia University.*—A fixed station at Morgantown sends out sixty pulses per second, each pulse lasting for ten microseconds on a frequency of 3492.5 kc. This signal is received on a portable station so constructed that a thyratron sets off a return pulse with a frequency of 2398 kc. The two pulses appear upon the screen of an oscilloscope at the fixed station with a sweep of 22,800 inches per second. The distance between the two pulses gives the total time taken for the radio-pulse to travel twice the distance between the stations and to pass through the receivers. The portable station then moves to a new place and similar readings are taken. The difference in time for the two positions is the time taken for the radio-pulse to travel twice the distance between the two positions of the portable station. The measured radio-velocity in the line of sight is practically the velocity of light.

113. Transient Current in Dielectrics. KENNETH S. COLE, *Columbia University,* AND ROBERT H. COLE, *Harvard University.*—The complex dielectric constant, ϵ^*, of many liquids and solids is given by[1]

$$\epsilon^* - \epsilon_\infty = (\epsilon_0 - \epsilon_\infty)/[1 + (i\omega\tau)^{1-\alpha}],$$

where ω is the angular frequency, ϵ_0 and ϵ_∞ are the "static" and "infinite frequency" dielectric constants, respectively, τ is a generalized relaxation time and α is a constant, $0<\alpha<1$. The transient current, I, at a time, t, after the application of a unit constant potential difference has been calculated from the above expression in series form. For $t \ll \tau$

$$I = (\epsilon_0 - \epsilon_\infty)(t/\tau)^{-\alpha}/\tau\Gamma(1-\alpha)$$

and for $t \gg \tau$

$$I = (\epsilon_0 - \epsilon_\infty)(1-\alpha)(t/\tau)^{-(2-\alpha)}/\tau\Gamma(\alpha).$$

The center of the transition region between these extremes is near $t=\tau$, and the total charge remains finite as $t \to \infty$. Many data in the literature are of this form although the range of times has not included the entire transition region in any case.

[1] K. S. Cole and R. H. Cole, J. Chem. Phys. **9**, 341 (1941).

114. Small-Ion Content of Air in a Closed Room Occupied by People. G. R. WAIT, *Department of Terrestrial Magnetism, Carnegie Institution of Washington.*—The number of small ions in the air of a closed room diminishes when people occupy the room and rapidly recovers when it is vacated. To understand the cause it is necessary to examine the rate of production and destruction of these ions. The rate of production, as measured with a thin-walled ionization chamber, diminishes when the room is occupied and tends to recover after it is vacated. The cause for this is not fully understood. The rate of destruction is due principally to combination with large ions and varies with their number and size. The number and size of large ions increase when the room is occupied by people and rapidly recovers when vacated. The increase in number and size of large ions, when the room becomes occupied, appears to be due to an introduction into the room of particles, larger than the ordinary condensation nuclei. These particles are given off by people, principally in their breath.

115. Radiations from Radioactive Cobalt. ARTHUR S. JENSEN, *University of Pennsylvania.*—Energy measurements have been made in a cloud chamber in a magnetic field on the particles emitted by radioactive cobalt produced by deuteron bombardment of iron. The sample was separated chemically, and the measurements were made about five months after the activation of the sample so that presumably only the 72-day (Co^{58}) and the 270-day (Co^{56}) isotopes were present. A total of 1410 tracks in helium near atmospheric pressure were measured and the momentum distribution curves plotted. These showed a positron spectrum with an upper energy limit at 1.36 $\pm$0.10 Mev. The spectrum of the negative electrons suggests the internal conversion of a γ-ray line near 0.1 Mev; this is confirmed by measurements made with a magnetic spectrograph and reported in another abstract. A few negative electrons of energies up to 0.9 Mev are observed, suggesting the possibility of a feebly converted γ-ray of higher energy.

116. Radioactive Isotopes of Nd, Il and Sm. H. B. LAW, M. L. POOL, J. D. KURBATOV AND L. L. QUILL, *Ohio State University.*—Pr, Nd and Sm have been bombarded with 10-Mev deuterons, 5-Mev protons, neutrons and gammas from deuterons and protons on lithium metal, respectively. Several new periods were found, tentative values of which are listed.

	Pr	Nd	Sm
α	(3.7 hr., 17 hr., 108 days)	(2.3 hr., 10 days)	
d		(2.3 hr., 47 hr., 10 days, 108 days)	(21 min., 9 hr., 47 hr., 60 days)
n		(2.3 hr., 47 hr., 10 days)	(21 min., 47 hr.)
p		(2.3 hr., 6 days)	
γ		(2.3 hr., 10 days)	(21 min., 47 hr.)

In all cases chemical separations were performed to eliminate isotopes that do not follow the rare earths. Since the 108-day period occurs with Pr+α and Nd+α it may be ascribed to $_{61}I^{144}$. The 3.7-hr. and 17-hr. periods found with Pr+α can be analyzed as isotopes which are rare earth group elements after bombardment. The 2.3 hr. may be either $_{61}Il^{147}$ or $_{61}Il^{149}$ if one postulates a fast period for $_{60}Nd^{147-9}$ which decays by electron emission to Il.

117. Radioactive Isotopes of Iodine. A. ROBERTS AND JOHN W. IRVINE, JR., *Massachusetts Institute of Technology.*—Tellurium bombarded by 11.5-Mev deuterons shows no iodine β or γ activities other than those observed by Livingood and Seaborg.[1] Positron emission is not observed, and constitutes less than 3 percent of the negatron activity 5 days after bombardment. Thus no appreciable I^{124} is formed. We find that a weak iodine activity of half-period about 9 days can be repeatedly extracted from deuteron activated Te targets many months after bombardment. Absorption measurements indicate a spectrum very little different from that of the 8-day I^{131}. The latter grows[1] from isomers of Te^{131} with half-periods 1.2 days and 25 minutes. Other negatron-emitting Te activities are $_{52}Te^{129}$ (32 days), whose daughter has not been previously observed, and $_{52}Te^{127}$ (90 days), which might give a radioactive isomer of the only stable isotope $_{53}I^{127}$. A bombardment of 500 cc ethyl iodide with 70,000 r/cc of 2.0-Mev x-rays gave a chemically concentrated activity of *ca.* 10 counts per minute of half-period >1 day. Assignment of the 9-day activity to I^{129} seems doubtful from total yield considerations. Identification with I^{131} involves the assumption of a third long-lived isomeric state in Te^{131}.

[1] J. J. Livingood and G. T. Seaborg, Phys. Rev. **54**, 775 (1938).

118. Studies with a Permanent-Magnet β-Ray Spectrograph.* ERNST H. PLESSET, *University of Pennsylvania.*—A large permanent magnet β-ray spectrograph has been constructed. For the purpose of checking the absolute calibration of the magnetic field, the β-ray spectrum of RaB has been examined and the measured momentum values compared with those given by Ellis.[1] The agreement is within $\frac{1}{2}$ percent for 10 measured lines. The conversion electrons emitted by a sample of radioactive Co containing the 72-day and 270-day periods indicate γ-ray energies of 119 kev and 132 kev, correct to about 1 percent. A sample of gold bombarded with deuterons shows definite lines corresponding to a 400-kev γ-ray which is doubtless that reported by Lawson and Cork.[2] There is evidence for other lines in this spectrum. The investigation is being continued.

* This research was assisted by a grant-in-aid from the Penrose Fund of the American Philosophical Society.

[1] C. D. Ellis, Proc. Roy. Soc. **A143**, 352 (1934).

[2] J. L. Lawson and J. M. Cork, Phys. Rev. **58**, 580 (1940).

119. Energy of the Hard Gamma-Rays of Radio-Yttrium (100 days). G. SCHARFF-GOLDHABER, *University of Illinois. (Introduced by W. E. Good.)*—A source of radio-yttrium[1] of about 30 milligrams radium equivalent in penetrating gamma-rays (generated in the Berkeley cyclotron by deuteron bombardment of strontium) was kindly loaned to us by Dr. Pecher for a study of the neutrons emitted from beryllium under the action of these gamma-rays. In order to determine the neutron energy the photo-neutrons were detected by proton recoils which were produced in a hydrogen filled ionization chamber connected to a linear amplifier. The energy distribution of the recoil protons was found to be very similar to that obtained from the 220-kev neutrons of a Rd Th+D_2O source. From this it was concluded that the photo-neutrons from Rd Y+Be have an energy of 220±20 kev. If the binding energy of the neutron in Be is assumed to be 1.62±0.02 Mev[2], this leads to an energy of 1.87±0.05 Mev for the hard gamma-ray emitted by radio-yttrium. Because of its simplicity this method may prove to be of value for measuring energies of hard gamma-rays.

[1] C. Pecher, Phys. Rev. **58**, 843 (1940).
[2] L. S. Skaggs, Phys. Rev. **56**, 24 (1939).

120. Radioactive Barium from Cesium. H. W. COLLAR, J. M. CORK AND G. P. SMITH, *University of Michigan.*—Radioactivity in cesium and barium has been studied by D. C. Kalbfell and R. A. Cooley.[1] In carrying out a more detailed investigation, two strong activities are observed in the barium separation from cesium bombarded by deuterons. One of these is of particular interest. Cesium has a single isotope of mass 133, so that a (D, n) reaction would give Ba^{134} and a $(D, 2n)$ reaction would result in Ba^{133}. Since Ba^{134} exists in nature, any radioactivity attributed to this isotope can be due only to an excited state of the stable nucleus. This is undoubtedly the case for a barium activity of half-life 39.5 hrs. The radiation is found to consist of gamma-rays and certain groups of beta-particles due to high internal conversion. The peaks corresponding to the ejection of K, L, and M electrons are resolved in the magnetic spectrometer giving for the gamma-ray an energy of 272 kev. The value for the ratio of the K to L, M conversion is about 2.6. The second barium activity has a half-life of 340 hrs. and emits a gamma ray of energy 17 kev and is attributable to Ba^{133} or Ba^{134}.

[1] D. C. Kalbfell and R. A. Cooley, Phys. Rev. **58**, 91 (1940).

121. Beta-Ray Spectra of Scandium. G. P. SMITH, *University of Michigan.*—Calcium metal and calcium oxide have been irradiated with 10-Mev deuterons in the University of Michigan cyclotron. Samples were bombarded for about ten hours, at average beam currents of 9–10 microamperes. The active scandium formed was separated out chemically as the hydroxide. The spectra were measured in a magnetic beta-ray spectrometer of high resolving power, described by Lawson and Tyler.[1] The following spectra have been observed:

β^- 640±7 kev, 44±2 hr. half-life
γ 268±5 kev, 52±4 hr. half-life
β^+ 1.45±0.02 Mev, 4.0±0.1 hr.; 52±3 hr.

The 4 hr. and 52 hr. positrons have the same energy spectrum; the 4 hr. activity can thus be produced either directly from calcium, or by a 52 hr. γ-transition from an excited level in scandium.

[1] J. L. Lawson and A. W. Tyler, Rev. Sci. Inst. **11**, 6 (1940).

122. Transmutation of Mercury by Fast Neutrons. R. SHERR AND K. T. BAINBRIDGE, *Harvard University.*—Ten radioactive nuclei have been observed in mercury irradiated with fast neutrons obtained by bombarding lithium with 11.5-Mev deuterons. A trace of gold is amalgamated with several hundred grams of irradiated mercury and recovered by distillation in vacuum. The gold is then dissolved in acid and a Pt-Au chemical separation made. The gold precipitate yields a new period of 48±1 min. and the well-known 65-hr. Au^{198} and 78-hr. Au^{199} periods.[1] The latter can be formed by $n-p$ reactions from Hg^{198} and Hg^{199}. The mercury decay curve shows a feeble activity with period >30 days, in addition to the well-known 43-min. and 25-hr. periods.[1] The platinum precipitate gives: 27±5 min., 85±10 min., 19±2 hr., and >2 days. The first and third are in approximate agreement with the known 31-min. Pt^{199} and the 18-hr. Pt^{197} activities. They can be formed by $n-\alpha$ reactions from Hg^{202} and Hg^{200}. The relative probabilities for $n-\alpha$, $n-p$, and $n-2n$ reactions in mercury are of the order of magnitude of 1, 10, and 10,000.

[1] McMillan, Kamen and Ruben, Phys. Rev. **52**, 375 (1937).

123. Excitation of Nuclei by X-Rays. J. R. FELDMEIER AND GEORGE B. COLLINS, *University of Notre Dame.*—The technique employed by Waldman and Collins[1] in observing the nuclear excitation of lead and indium by x-rays has been used in a search for other nuclei that have low lying metastable levels with activation levels between 0.5 to 1.5 Mev. Counters were constructed with the metal under investigation forming the cylindrical cathode, in order to detect low energy, internally converted electrons that might be emitted by an excited nucleus. The counters were irradiated by placing them directly behind a lead target which was bombarded with electrons from the electrostatic generator. Silver counters showed a 40-second period, which agrees with that observed by Alvarez, Helmholz and Nelson[2] who found isomeric silver formed during the Ag$(d, 2n)$Cd reaction. Cadmium counters gave evidence of a one-hour period which probably corresponds to the 50-minute period observed by Dode and Pontecorvo.[3] Gold, tellurium and tantalum counters were irradiated with x-rays up to 1.5 Mev, but showed no activity. Metastable levels higher than 50 kev with periods between 20 seconds and five hours could have been detected.

[1] B. Waldman and G. B. Collins, Phys. Rev. **57**, 338 (1940).
[2] Alvarez, Helmholz and Nelson, Phys. Rev. **57**, 660 (1940).
[3] Dode and Pontecorvo, Comptes rendus **207**, 287 (1938).

124. Highly Forbidden Transitions in Beta-Decay. R. E. MARSHAK, *University of Rochester.*—There are several beta-emitting nuclei having extremely long half-lives and which therefore undergo large changes of angular momentum. This information may help to decide among

various possible theories of beta-decay which do not involve derivatives of the light particle wave functions. For a given spin change, the vector interaction (Fermi) gives a lifetime $(c/v)^2$ (v is the velocity *change* of the nuclear particle) longer than the pseudovector interaction (Gamow-Teller) whereas the scalar theory gives a lifetime $(\lambda\!\!\!^{-}/R)^2$ (R is the nuclear radius, $\lambda\!\!\!^{-}$ an average wave-length of the electron) longer than the pseudovector theory. A calculation has been performed for K^{40} which has a maximum electron energy of 0.7 Mev and a half-life of $1.4 \cdot 10^9$ years.[1] The only possible spin changes are 3 or 4. *The second choice is probably correct*[2] *and* the Gamow-Teller theory would *then* just agree with the observed lifetime—somewhat longer—the Fermi theory would give a *thousand* times longer lifetime while the scalar theory would give a *ten* times still longer lifetime. The experimental material *is somewhat* uncertain *but would seem to decide for the Gamow-Teller against the Fermi and scalar interactions.*

[1] A. Bramley and A. K. Brewer, Phys. Rev. **53**, 502 (1938).
[2] J. R. Zacharias (unpublished) has found a spin of 4 for K^{40}.

125. Ferromagnetic Impurities in Copper, Brass and Silver. F. W. CONSTANT AND R. E. FAIRES, *Duke University.*—As previously reported, small amounts of ferromagnetic impurities have been found in copper wire, commercial brass and C. P. silver which could not be attributed to surface effects. Further study has been made to determine whether such impurities might be rendered nonmagnetic through heat treatment. In the case of copper and brass, heating for several hours at 900°C and 800°C, respectively, in a hydrogen atmosphere and then quenching completely removed all trace of magnetism (although most of the disappearance occurred around 700° and 500°). But in the case of silver heat treatment had comparatively little effect. This seems understandable if the magnetic impurity is chiefly iron, which at high temperatures can change from a body-centered to a face-centered lattice and so dissolve in the copper lattice in a metastable state, while for silver this is impossible since the metals do not form solid solutions. Heat treatments at intermediate temperatures in various atmospheres have shown that the ferromagnetism may be strongly accentuated. Hysteresis loops were taken before and after treatment.

126. Measurement of the Magnetic Susceptibility of Vapors. R. K. REBER AND G. F. BOEKER, *The City College of New York.**—An apparatus has been developed to measure the magnetic susceptibilities of vapors of substances which are liquids or even solids at room temperatures. The design of the apparatus makes it possible to make measurements at temperatures up to 300°C and at independently controlled pressures of one atmosphere and less. The measurements consist of compensating the twist produced by a test body in a nonhomogeneous magnetic field by the rotation of the suspension support. The temperature is controlled by the circulation of liquid from a thermostatically controlled bath through a jacket which completely surrounds the test unit. The pressure control consists of a tube which dips into a reservoir of the liquid and which is non-uniformly heated so as to get progressively hotter towards the top. The upper end of the tube leads to the apparatus. An external gas pressure on the liquid in the reservoir forces it up the tube until an equal vapor pressure is established. This arrangement permits the pressure to be read externally on a manometer. Measurements on several diamagnetic vapors at 110°C have shown that results can be duplicated to within one percent.

* Research done in laboratories of Columbia University.

127. Paramagnetic Dispersion. C. STARR, *Massachusetts Institute of Technology.*—The dispersion at radiofrequencies of the paramagnetic susceptibility of several salts of the iron group has been measured at liquid nitrogen and room temperatures. An improved beat frequency method was used to determine the high frequency susceptibility. At any frequency, the dependence of this susceptibility upon the value of the applied constant magnetic field was determined from the change in the audiofrequency beat note. The measurements were made at various frequencies up to 10 megacycles and at constant magnetic field strengths up to 50,000 gauss. The results at 77°K and 10 megacycles for ferric alum, when compared with the results of du Pre[1] at liquid helium temperatures and 60 cycles, indicate that the thermodynamic theory of Casimir and du Pre[2] is valid over this temperature range. This agrees with the recent results of Teunissen and Gorter[3] at 7 megacycles which indicated that previous experimental deviations from the thermodynamic theory resulted from erroneous absorption measurements and the use of frequencies not sufficiently high. The effect predicted by Kronig and Bouwkamp[4] for large values of the applied field was not found.

[1] du Pre, Physica **7**, 79 (1940).
[2] Casimir and du Pre, Physica **5**, 507 (1938).
[3] Teunissen and Gorter, Physica **6**, 1113 (1939).
[4] Kronig and Bouwkamp, Physica **6**, 290 (1939).

128. On the Mechanism of Paramagnetic Relaxation at Helium Temperatures. J. H. VAN VLECK, *Harvard University.*—I have shown elsewhere[1] that the conductivity of lattice oscillators at helium temperatures is insufficient to make them serve as a thermostat in the way ordinarily assumed in the theory of paramagnetic relaxation. Consequently, it is not surprising that calculations based on the usual assumptions fail completely in the helium domain. The following substitute mechanism is now suggested. When a paramagnetic ion reverses its spin, it emits a virtual vibrational quantum, which is absorbed in the surrounding liquid helium in virtue of the latter's anharmonic terms. Thus, the conductivity takes place via virtual rather than real lattice waves, and the coupling between the spins and the helium bath is reminiscent of the interaction formalism in nuclear field theories except that the ghost lattice waves replace the transient particle (e.g., mesotron) as the intermediary. With this model, Casimir and du Pre's thermodynamic formulas preserve their validity. In addition, the new theory appears to give correct relative magnitudes of the relaxation time τ for the different alums, and also the proper dependence of τ on the applied magnetic field and on the temperature.

[1] J. H. Van Vleck, Phys. Rev. **59**, May 1, 1941.

129. Magnetic Properties of Antimony-Tin Crystals at Low Temperatures. S. H. BROWNE AND C. T. LANE, *Yale University.*—Temperature dependence of the magnetic susceptibility in monocrystals of pure antimony and antimony alloyed with small percentages of tin has been investigated in the range from 295°K to 77°K. The measurements were made with a Sucksmith balance modified to allow the use of crystals in the form of long cylindrical rods. Results are given for the temperature dependence of both the susceptibility parallel to the principal axis of the crystal (χ_{II}) and also perpendicular thereto ($\chi_{\perp}$). For antimony and antimony-tin solid solutions (0.48, 1.05, 2.24, 4.10 atomic percent Sn), $\chi_{\perp}$ is sensibly independent of temperature and diamagnetic. However χ_{II} is temperature dependent. For pure antimony and up to about 1 percent Sn the diamagnetism was found to increase with decreasing temperature. Above 1 percent Sn χ_{II} becomes paramagnetic and this paramagnetism increases as the temperature falls. A plot of χ_{II} *versus* $1/T$ gives a curve which, in all cases, is in close agreement with that predicted by the Bloch theory. In consequence it is possible to estimate the degeneracy temperature of electrons in antimony as approximately 600°K. Essentially the same value was found for all percentages of tin. Further it is shown that the amount of overlap into the second zone in antimony (approximately 10^{-2} electrons per atom) is closely temperature independent in the range of temperature studied.

130. Magnetic Domain Size Determined from Measurements of Damping in 68 Permalloy. H. J. WILLIAMS AND R. M. BOZORTH, *Bell Telephone Laboratories.*—When a ferromagnetic material is subjected to small periodic stresses there are energy losses due to eddy currents and magnetomechanical hysteresis, and these are generally large compared to the losses in nonferromagnetic materials subjected to similar stresses. In theory the losses in ferromagnetic materials have been put into three classifications by Becker and Döring:[1] macro-eddy-current, micro-eddy-current, and magnetomechanical hysteresis. When the material is unmagnetized, the macro-eddies will be zero; that part of the logarithmic decrement that is due to micro-eddies is proportional to frequency and depends on domain size; that due to magnetomechanical hysteresis is independent of frequency. The decrement has been determined for an 80-cm bar of unmagnetized 68 Permalloy and plotted as a function of frequency. A straight line is obtained and from its slope the size of the domains (assumed cubic in form) is found to be 10^{-8} cm³, a value agreeing closely with that obtained previously from Barkhausen experiments.[2]

[1] R. Becker and W. Döring, *Ferromagnetismus* (Springer, Berlin, 1939).
[2] R. M. Bozorth and J. Dillinger, Phys. Rev. **35**, 733 (1930).

131. Transitions in Alloys of Cobalt Nickel and Iron by the Hydrogen Diffusion Method. W. R. HAM AND F. D. BENNETT, *The Pennsylvania State College.*—The measurement of the rate of hydrogen diffusion through metals provides a sensitive and accurate method of detecting transition points in the metal lattice. For a homogeneous metal or alloy the diffusion rate is given by

$$R = \text{const. } p^{z} \cdot \epsilon^{-b/T},$$

where z is usually $\frac{1}{2}$. An examination of two Ni-Co alloys shows that while the physical magnetic change occurs at 600° and 910°, respectively, the Curie point break for Ni is still present in the diffusion curve. This fact indicates a fundamental electronic transition in Ni at 360° not necessarily associated with any magnetic change in the alloy. An Fe-Ni alloy in which the magnetic transition is depressed to 340° shows a marked discontinuity at 768°, the temperature at which the magnetic change in pure Fe takes place. The magnetic transitions of pure Ni and Fe appear to take place in two distinct steps. From the straightness of the diffusion curve one may also infer that no electronic rearrangement is associated with the phase changes in pure Fe or Co, at 910°C and 440°C, respectively.

132. The Thermal Expansion of Pure Metals: Iron, Nickel, Copper, Gold and Aluminum. F. C. NIX AND D. MACNAIR, *Bell Telephone Laboratories.*—Extremely accurate determinations of the linear thermal expansions have been made interferometrically[1] from −196°C to temperatures about +400°C for Al and +700°C for Fe, Ni, Cu and Au. The relationship between true thermal coefficient of expansion and temperature conforms very well to the Grueneisen-Debye theory when values are chosen for the Debye characteristic temperatures which turn out to agree well with those chosen to achieve agreement with the Debye theory of specific heats. Our values for these characteristic temperatures are: 410°K for Ni, 420°K for Fe, 400°K for Al, 325°K for Cu and 190°K for Au. The magnetic Curie temperature for Ni is found to be 352°C. In plotting true coefficient of thermal expansion *versus* temperature Simon and Bergmann[2] found a horizontal plateau at *ca.* −50°C to −100°C for Ni and Fe; but we do not confirm this.

[1] F. C. Nix and D. MacNair, Rev. Sci. Inst. **12**, 66 (1941).
[2] F. Simon and R. Bergmann, Zeits. f. physik. Chemie **8B**, 255 (1930).

133. Elasticity in Order-Disorder Transformations. H. F. LUDLOFF, *Cornell University.*—It was suggested by the author that the temperature curve of an isothermal and corresponding adiabatic elastic modulus through the temperature region of order-disorder transformations might be measured by determining there two proper-frequencies of an appropriate vibrating sample of the alloy considered. To find appropriate conditions for such a method, the temperature distribution in such a sample has been computed for different vibration types and sample forms, since the value of the amplitude of the temperature fluctuation indicates the isothermal or adiabatic character of the vibration. One finds that for plates, reeds, roads, loops there is a set of antisymmetrical (bending) vibrations which for appropriate sample dimensions contains an isothermal ground tone and an adiabatic overtone. In the low frequency range the variation of Young's modulus E is:

$$|E(\omega)| - E_{is} \sim (E_{ad} - E_{is})\omega \left\{ \frac{1}{(\omega^2 + (\pi^4/a^4) \cdot D^2)^{\frac{1}{2}}} + \cdots \right\},$$

ω frequency, a thickness, D thermal conductivity. The

$E(\omega, T)$-curves through the transition region can be illustrated by means of available experimental data.

134. Some Measurements of the Temperature Dependence of Young's Modulus of β-brass and Certain Other Metals. P. G. BOHLKE, T. R. CUYKENDALL AND H. S. SACK, *Cornell University.*—For the study of certain elastic properties of solids, an apparatus has been constructed which employs a vibrating reed of the solid in question. The reed vibrates transversely at a medium frequency, 90 to 6000 c.p.s. These vibrations, excited by electrostatic forces, modulate a beam of light and thereby allow their study with a photo-cell and a linear amplifier. The sensitivity of the arrangement is such that amplitudes of vibration of the order of 0.01 mm may be measured. The reed, placed in a temperature controlled furnace, exhibits vibration resonance phenomena and the resonance frequencies occuring up to 700°C have been measured. From these data, the temperature dependence of Young's modulus of polycrystalline β-brass in the phase transition region has been calculated.

135. The Evaporation of Molten Metals from Hot Filaments. WALLACE C. CALDWELL, *Iowa State College.* (*Introduced by Percy H. Carr.*)—Several investigators have used the evaporation technique for making surface mirrors, thermocouples, high resistances, and other devices. The method usually used involves attaching the metal to be evaporated to a refractory filament that is heated electrically. Tungsten was nearly always used as the filament until recently other filament materials have been found preferable. In the present investigation a determination of the best filament to be used with each metal was made. In order that a metal evaporate from a filament satisfactorily the metal must adhere to the filament, must have sufficient vapor pressure to evaporate while still at a temperature below the melting point of the filament material, and must not form with the filament an alloy which has a melting point below the temperature at which evaporation will ensue. Acquiring a knowledge of the degree to which the filament material meets these requirements has made possible the selection of the filaments most suitable for the evaporation of each of the metals investigated.

136. On the Theory of Secondary Emission. H. A. BETHE, *at present at Columbia University.*—The secondary electron emission (SE) from solids is proportional to the ratio of the rates of energy loss (REL) of primary particle and secondary electron, the number of secondaries per primary being about $\frac{1}{10}$ to $\frac{1}{4}$ of that ratio. This is demonstrated by the large SE produced by protons and especially He^+.[1] From the known REL of protons ($\approx$30 ev/A in Cu at 200 kv) and the measured SE (3 electrons/proton) the REL of the secondaries is calculated $\approx$1.5 ev/A. From measurements with primary electrons, we find the REL to increase with energy up to about 500 ev where REL $\approx$10 ev/A. In insulators, the REL of the secondaries is extremely small because they cannot give energy to electrons in the filled bands; hence the large SE of insulators.[2] In alkalies, the conduction electrons are nearly free and are therefore ejected mostly at right angles to the primary; therefore the SE increases strongly with the angle of incidence θ of the primary and is very low for $\theta = 0$. Experiments with primary protons would give most information.

[1] A. G. Hill, W. W. Buechner, J. S. Clark and J. B. Fisk, Phys. Rev. **55**, 463 (1939).
[2] H. Bruining and J. H. de Boer, Physica **5**, 17, 901, 913 (1938); **6**, 823, 834, 941 (1939).

137. Radiations from $I^{131} \rightarrow Xe^{131}$. MARTIN DEUTSCH, *Massachusetts Institute of Technology.*—Radiations emitted in the disintegration $I^{131} \rightarrow Xe^{131}$ (8 day) have been studied by means of a magnetic lens beta-ray spectrometer.[1] I^{131} was grown from Te^{131} formed by a Te (d, p) reaction. The maximum energy of the beta-rays was found to be 0.595 ± 0.015 Mev as compared with 0.687 Mev found by Tape[2] in a cloud chamber. One gamma-ray was found to have an energy of 0.364 ± 0.02 Mev from the energy of internal conversion electrons. It is estimated that the conversion coefficient for this gamma-ray is about 1 percent with conversion in the K shell at least five times as probable as in the L shell. By studying coincidences between beta-rays focused in the spectrometer and gamma-rays it was found that no transitions take place to the ground state of Xe^{131}. Coincidences between conversion electrons and beta-rays indicate that the most energetic beta-rays are probably emitted in transitions to a level 0.364 Mev above the ground state of Xe^{131}. The presence of a soft component of maximum energy less than 0.3 Mev is also indicated by the coincidence spectrum.

[1] M. Deutsch, Bull. Am. Phys. Soc. **16**, No. 1, 7 (1941).
[2] G. F. Tape, Phys. Rev. **56**, 965 (1939).

138. Coincidence Study of the Decay of Br^{82}. J. R. DOWNING AND A. ROBERTS, *Massachusetts Institute of Technology.*—$\beta\gamma$ and $\gamma\gamma$ coincidences are observed in the radiations from Br^{82}. The number of $\beta\gamma$ coincidences per 1000 β-rays is independent of absorber thickness. Thus the β spectrum is simple. The γ-ray absorption curve indicates an energy of about 1.0 Mev. and remains a simple exponential over an intensity range of at least 30. We estimate not more than 10 percent higher energy radiation present. No x-rays were found; thus internal conversion or K capture takes place in less than 5 percent of the disintegrations. The ratio of $\beta\gamma$ coincidences per 1000 β's to $\gamma\gamma$ coincidences per 1000 γ's is 1.53 ± 0.06, indicating 3 quanta per disintegration. The γ-counter efficiency for quanta in this energy range was determined with Mn^{56} assuming the levels reported by Langer, Mitchell and McDaniel.[1] The high energy portion of this spectrum yielded 1.07 ± 0.03 $\beta\gamma$ coincidences per 1000 β's as compared with 3.44 ± 0.06 in Br^{82}. The Br γ-ray, being slightly more energetic, has a somewhat higher efficiency for detection than 0.107 percent, giving excellent agreement with the assignment of 3 quanta per Br^{82} disintegration. An estimate of the spins of the Kr^{82} levels has been made.

[1] Langer, Mitchell and McDaniel, Phys. Rev. **56**, 422 (1939).

139. Proton-Induced Fission. G. DESSAUER AND E. M. HAFNER, *University of Rochester.*—The 6.9-Mev beam of the Rochester cyclotron was employed in looking for

proton-induced fission. Our method of detection is similar to that of Gant.[1] With a thorium target and a bombardment of 25 μ Ah within 8 hours, radioactivity was observed on an aluminum catching foil whose decay could be followed for over 60 hours. The decay curve showed the curvature characteristic of a mixture. After a check bombardment with identical geometry with respect to the catcher, but with the proton beam striking the other side of the thorium sheet, no activity was observed. This rules out fission due to the neutron background, and to neutrons produced by protons in the target itself. The threshold for proton-induced fission of the compound nucleus in question, namely Pa^{233}, is below 5.8 Mev, as indicated by excitation data. The range of the fission fragments lies below 0.7 mil of aluminum.

[1] D. H. T. Gant, Nature **144**, 707 (1939).

140. Fission Tracks on the Photographic Plate. K. LARK-HOROVITZ AND W. A. MILLER,* *Purdue University.*—Photographic plates (Eastman fine-grain α, Ilford R_2), bathed in alcoholic solutions of uranium nitrate and thorium nitrate have been exposed to slow and fast neutrons and the resulting tracks have been measured microscopically with a filar micrometer. With fast neutrons new types of tracks besides the ordinary alpha-particle tracks have been observed on both the U and Th treated plates; with slow neutrons these tracks have been found only on the U plate. We conclude that these tracks are due to fission fragments because: (a) Their range is different from the range of the U α-particles. (b) The reciprocal grain spacing decreases toward both ends of the track, in contrast to the appearance of α-tracks. (c) Distribution curves of the observed grain spacings show a minimum distance far more frequently than with α-tracks. (d) Recoil protons issuing from the track are frequently found; and from stereoscopic projection their energy can be estimated and related to the energy of the fission product at this point of the path in good agreement with the calculation of Knipp and Teller.[1] Most of the tracks are assymetric but some symmetric tracks have been observed. To study fission processes due to cosmic radiation, U and Th treated plates as well as plates treated with thallium iodide solution have been sent into the stratosphere reaching a height of about 30 km. Fission tracks like the ones observed in the laboratory were obtained only on the U plate but not on the Th plate indicating that most of the neutrons in the cosmic radiation even at this altitude are too slow to produce the fission.

* Purdue Research Foundation Fellow.
[1] J. Knipp and E. Teller, Phys. Rev. to be published.

141. Deuteron-Tritium Reaction in Nitrogen. LYLE B. BORST, *University of Chicago. (Introduced by H. W. Newson.)*—The reaction Be^9 (d, H^3) Be^8 has been established[1] and there are indications of similar reactions[2] in Cu^{63} and Ag^{107}. It therefore seemed desirable to look for other examples of this reaction. The reaction N^{14} (d, H^3) N^{13} has been established and its excitation function measured. The threshold was found to be 6.8 ± 0.1 Mv. Calculations from the masses give $Q=-4.54$ Mv, so that the H^3 nucleus emerges with an energy of 2.2 Mv. The value of the potential barrier involved is 2.6 Mv. Aluminum was similarly studied, but no indication of the reaction was found with 8.2 Mv deuterons. In this case $Q=-5$ Mv, and the potential barrier, 3.4 Mv, so that by analogy the threshold should be about 8 Mv, and consequently difficult to observe at the energy used.

[1] R. D. O'Neal and M. Goldhaber, Phys. Rev. **57**, 1086A (1940).
[2] Krishman and Gant, Nature **144**, 547 (1939); Krishman and Banks, Nature **145**, 777 (1940).

142. The Determination of Nuclear Reaction Energies for a Mixture of Copper Isotopes. HENRY W. NEWSON AND LYLE B. BORST, *University of Chicago.*—The ranges of four groups of protons from Cu (d, p) have been measured by Davidson[1] who found Q's of 6.35, 5.70, 4.35 and 3.54 Mv. We have measured the angular distribution of the radioactive recoil atoms in an attempt to assign each of the above groups to the proper isotope of copper. The results are definite to the extent that the cut-off angle for Cu^{66} is decidedly higher than that for Cu^{64}; the first group must therefore be assigned to Cu^{66}. The distribution of Cu^{64} shows little curvature at large angles, and indicates a single group with $Q=5.6$ Mv. This value agrees with the second of the above groups; the same assignment was made by Davidson because of the relative intensities. The shape of the Cu^{66} distribution shows a decided curvature which indicates the presence of at least two groups: the first and third. The fourth group is uncertain, but it seems most likely that it belongs to Cu^{66}.

[1] W. L. Davidson, Phys. Rev. **56**, 1062 (1939).

143. Distribution with Angle of Protons from D-D Reaction. H. P. MANNING, C. M. CRENSHAW AND V. J. YOUNG, *New York University.*—A thin D_2O vapor target was bombarded with deuterons. Following previous investigators,[1] the distribution of protons in the center of mass coordinate system was found to be well represented by $1+A\cos^2\theta$ where A is a function of bombarding energy. The following values of A and their probable errors were obtained:

kv	A	kv	A
100	0.49 ± 0.09	180	0.80 ± 0.08
110	$.50\pm.04$	183	$.86\pm.04$
125	$.51\pm.12$	190	$.76\pm.07$
140	$.58\pm.05$	200	$.87\pm.03$
150	$.72\pm.02$	220	$.90\pm.06$
160	$.66\pm.05$	240	$1.00\pm.11$
167	$.75\pm.06$	250	$0.98\pm.09$
175	$.70\pm.03$		

These A values may be represented by $A=a+bE$ where $a=0.11\pm0.05$ and $b=.0037\pm.0003$. Energy measurements are good to better than 5 percent.

[1] R. D. Huntoon, A. Ellett, D. S. Bayley and J. A. Van Allen; Phys. Rev. **58**, 97 (1940).

144. Disintegration of Nitrogen and Oxygen by Neutrons. W. HANSEN, *Yale University. (Introduced by A. F. Kovarik.)*—An amplifier employing inverse feedback and which satisfies the conditions of Johnson and Johnson[1] has been constructed and used with a parallel-plate ionization chamber to study the reactions

$$N^{14}+n^1\rightarrow B^{11}+He^4,$$
$$N^{14}+n^1\rightarrow C^{14}+H^1,$$
$$O^{16}+n^1\rightarrow C^{13}+He^4.$$

Neutrons from the bombardment of Be and Li by deuterons in a cyclotron were used. The pulses on a cathode-ray oscilloscope screen were photographed and the distributions of number of pulses *versus* energy were plotted. The distributions for nitrogen showed numerous peaks separated by about 0.2 Mev, in agreement with the work of Thibaud and Comparat.[2] A larger average spacing at higher energies is indicated. The interpretation of these results is uncertain, but it is likely that they are correlated with the energy levels of the compound nucleus.

[1] Johnson and Johnson, Phys. Rev. **50**, 170 (1936).
[2] Thibaud and Comparat, J. de phys. et rad. **10**, 161 (1939).

145. Alpha-Proton Reactions of Sodium and Aluminum. RICHARD F. HUMPHREYS AND ERNEST POLLARD, *Yale University.*—To investigate the possibility of the operation of selection rules in transitions from the compound nucleus to energy levels near the ground state it is necessary to observe the energy levels found in different reactions which give the same final nucleus. We have previously reported levels in Mg^{26} and Si^{30} formed by deuteron bombardment of magnesium and silicon, and compared the results with the known results of alpha-particle bombardment of sodium and aluminum, in which natural sources were used. We have now repeated these experiments with alpha-particles of 7.4 Mev from a cyclotron with much better angular conditions and find that the older work is not complete. In the case of aluminum we find, in addition to the well-known groups corresponding to two states of excitation, some nine groups. These are found when a thin layer is bombarded by reasonably homogeneous particles whose energy, moreover, is in excess of the barrier height and so the groups are not due to resonance. If it is assumed that all the previously assumed resonance levels are in reality true levels in the Si^{30} nucleus then the present measurements are in good agreement with older work. Excited states of the Mg^{26} nucleus were found at 0.23, 0.60, 1.18, 1.92, and 2.75 Mev. The complete level scheme for Si^{30} is not yet determined, but the spacing of the groups is definitely less than 1 Mev in place of greater than 2 Mev as formerly thought. It seems likely that the level spacing in the moderately light nuclei is much smaller than the generally published figures.

146. Energy Levels of S^{33} by Deuteron Bombardment of S^{32}. E. SMITH AND ERNEST POLLARD, *Yale University.*—Measurements of the yields of protons from the deuteron bombardment of sulphur indicate that there are six definitely resolved groups due to transitions to the ground and five excited states. The energy change values we find are as follows: 6.62, 5.57, 4.45, 3.40, 2.29 and 1.30 Mev. The yields of the groups are roughly in the ratios 1 : 1 : 1 : 3; 3 : 6. The average spacing is therefore about 0.9 Mev which is of the same size as found for other neighboring nuclei.

147. The Electrical Properties of Zinc Oxide. PARK H. MILLER, JR., *University of Pennsylvania.*—The electrical conductivity of zinc oxide is found to obey the usual law for semi-conductors $\sigma = Ae^{-E/kT}$ for temperatures below 100°C, where the activation energy E varies between 0.01 and 0.1 volt depending on the past history of the sample. When kT vecomes the same order of magnitude as E this equation is no longer valid because most of the electrons have left the bound levels. However, this same type of equation does hold in the temperature range of 450°C to 700°C with E having a value between 0.5 and 1.0 volts. The conductivity changes because the effective number of interstitial zinc atoms increases and not because a second electron is being evaporated into the conduction band. The conductivity is oxygen pressure dependent obeying the law $\sigma = cp^{-\frac{1}{4}}$. This activation energy of 0.5 to 1.0 volt is not the energy required to evaporate oxygen atoms from the lattice because we would expect this energy to be about 5 volts and the time required to reach oxygen equilibrium with well centered samples is of the order of days and these measurements required only several hours. This indicates there is probably a "coagulation" of the interstitial zinc atoms with their electrons and the activation energy associated with this process is about one volt. The activation energy for the diffusion of zinc atoms in the lattice is 2.2 volts as measured by a sectioning method employing radioactive Zn^{65} as a tracer. The ionic conductivity calculated from the measured diffusion constant is 10^{-4} times the observed conductivity at 900°C.

148. The Electrical Conductivity of Titanium Dioxide. MARSHALL D. EARLE, *University of Pennsylvania.*—Detailed studies were made of the electrical conductivity of titanium dioxide as a function of the oxygen pressure surrounding the sample and also as a function of the temperature between 500 and 1000°C. Both the rutile and anatase modifications of titanium dioxide were studied, most of the work being done on rutile. In the range of temperature investigated it was found that the variation of conductivity with temperature is well represented by the equation $\sigma = Ae^{-\epsilon/kT}$ for both porous and well sintered samples, the value of ϵ, the activation energy, in both cases being approximately 1.7 ev. The variation of conductivity with oxygen pressure obeys very closely the formula $\sigma = Pe^{-1/n}$ (where n is a constant), for the pressure range of 30 to 800 mm of mercury. The agreement below 30 mm was poorer, the slope being too steep, indicating a greater conductivity than that predicted, which is probably due to small impurities in the samples used. Transport measurements were made on well-sintered samples of rutile. The results showed the ionic conductivity to be negligible. In the measurement of the Hall effect it was found that the Hall constant was very small being of the order of -10^{-7} volt-cm/amp.-gauss. Indicating that the mean free path of the conduction electrons is probably very small. These experiments indicate that titanium dioxide is a reduction semi-conductor of the same type as zinc oxide.

149. Dislocations in NaCl. H. B. HUNTINGTON, *University of Pennsylvania.*—Much of the observed behavior of plastic flow has been explained by the theory of linear dislocations as developed by Taylor and others. The stress energy of such a dislocation can, at large distances, be

treated by the standard methods of elasticity. Inside a cylinder, with radius of atomic dimensions about the dislocation line, the strains can no longer be treated as small. A detailed calculation of the energy in this region has been carried through for an alkali-halide, NaCl, making use of short range repulsive and electrostatic forces between rows of ions. The dislocation has been orientated so that slip occurs in the (110) direction along the (110) slip plane to agree with observation. Qualitative reasons will be presented to show why this orientation would be expected. The stress energy in the immediate neighborhood of the dislocation is less than 1 ev per atomic plane, as compared with about 2.5 ev per atomic plane found for the region of elastic strain.

150. The Energy Stored During Work Hardening. J. S. KOEHLER,* *University of Pennsylvania.*—A calculation of the energy which is stored in a solid when it undergoes work hardening has been made using the theory of dislocations. Following Taylor[1] a work-hardened material is assumed to contain many dislocations arranged in a regular two-dimensional lattice. The energy required to produce a dislocation pair in such a lattice is the energy required to form an isolated dislocation pair minus the binding energy of a dislocation pair in the lattice. The energy required to produce an isolated dislocation pair is found to be about 3.16 ev per atomic plane in copper. Taking the density of dislocations to be 10^{12} per cc,[2] the binding energy of a dislocation in a lattice is found to be 0.43 ev per atomic plane in copper. The energy stored in the process of work hardening in copper thus becomes 0.42 cal. per gram. The experimental value is 0.5 cal. per gram.[3]

* Rackham Postdoctoral Fellow of the University of Michigan.
[1] G. I. Taylor, Proc. Roy. Soc. **A145**, 362 (1934).
[2] W. F. Brown, Jr. Phys. Rev. **59**, 528 (1941); F. Seitz and T. Read, J. App. Phys. **12**, 178 (1941).
[3] G. I. Taylor and H. Quinney, Proc. Roy. Soc. **A143**, 307 (1934); *ibid.* **A163**, 157 (1937).

151. The Generation of Dislocations in Polycrystalline Copper. A. W. LAWSON, *University of Pennsylvania.*—The internal friction of oxygen-free polycrystalline copper has been studied as a function of applied compressive stress. It is found that the internal friction increases to a maximum and then decreases somewhat as the stress increases. The maximum increase in internal friction is approximately 100 percent. Corresponding to the maximum in internal friction, a minimum in Young's modulus occurs. The maximum decrease in the latter quantity is about 6 percent. This effect seems to be nearly temperature independent from the temperature of liquid nitrogen up to the recrystallisation temperature of copper. Although the Taylor dislocation model of plasticity seems capable of explaining qualitatively the form of the curves at any given temperature, it seems incapable of explaining, at least at the present stage of its development, the temperature independence of the observed effect.

152. Electron Emission from Surfaces Subject to Periodic Fluctuations in Work Function. A. T. WATERMAN, *Yale University.*—The usual calculation of the electron current density from a metallic surface assumes a potential barrier or work function which is uniform over the surface and invariable with time. This approximation implies that the use of a mean work function is legitimate and is justified by the degree of agreement between theory and experiment. With increasing study of local differences in work function from a given surface it is a matter of interest to know what sort of mean the observed work function represents and what its expected properties may be. To examine this matter briefly and simply, the thermionic current density is calculated from a plane emitter of the usual idealized variety except that small perturbations, which take the form of standing waves, occur in its work function. If χ is the amplitude of such a wave, then the perturbation contributes an effective work function which is less than the unperturbed one by an amount χ^2/kT. The possible consequences of this result are discussed in their application to thermionic and photoelectric emission and the temperature dependence of the work function.

153. The Measurement of Self-Diffusion in Zinc Single Crystals. FLOYD R. BANKS, *Morgan State College,* AND PARK H. MILLER, JR., *University of Pennsylvania.*—Radioactive Zn^{65} was electroplated on the plane and parallel ends of single crystals of pure zinc (1 cm diameter, 2 cm long). The crystals were annealed at several different temperatures for predetermined periods, sectioned in a lathe, and the diffusion coefficient D determined as in the previous work of Banks.[1] The orientation of the c axis with respect to the plane end of the crystals was determined after heat treatment from a back-reflection Laue photograph .The diffusion coefficient perpendicular to the c-axis, D_2, was calculated for each crystal, using the value of the diffusion coefficient parallel to the c axis (D_1) previously determined, and the value for D obtained in this experiment. The preliminary value of the activation energy Q_2 perpendicular to the c axis, obtained from the temperature dependence of D ($D=Ae^{-Q/RT}$) is 28,600 cal. per mole, a value approximately fifty percent larger than that of Q_1 (19,600 cal. per mole) previously reported[1] for the activation energy parallel to the c axis. Surprisingly, however, A_2 is about 10^3 times larger than A_1.

[1] F. R. Banks, Phys. Rev. **59**, 376 (1941).

154. Field Dependence of the Surface Photo-Effect. CHARLES J. MULLIN AND EUGENE GUTH, *University of Notre Dame.*—The photoelectric current emitted under the influence of an applied electric field is found to contain a term analogous to the Schottky term for thermionic emission and also a term periodic in the field intensity similar to that recently found and explained for thermionic emission.[1] If frequencies near the threshold are used, then for fields of 3×10^5 volts cm^{-1} the periodic term has a magnitude of about four percent of the nonperiodic part of the current. If the photoelectric threshold frequency for zero field is used to eject the electrons, the resultant plot of the nonperiodic part of the photo-current against the field is a straight line for high field intensities. This line gives the most convenient reference system for observing

the periodic term; in addition, the use of the zero field threshold gives the fractional magnitude of the periodic term a relatively large value.

[1] E. Guth and C. J. Mullin, Phys. Rev. **59**, 575 (1941).

155. Average Thermionic Constants for Single Crystal Tungsten Wire. MYRON H. NICHOLS, *Princeton University.*—Experimental data have clearly demonstrated that different crystal surfaces of the same metal have different work functions. Consider a thermionic emitter whose surface is made up of different crystal surfaces or patches having different work functions. Group these patches according to their work functions. For sufficiently large collecting field strengths, the total emission is

$$i=\sum_n i_n=\sum_n A_n^* T^2 \exp\left(-e\varphi_{0n}/kT\right),$$

where i_n is the emission from the nth group of patches whose thermionic constants are φ_{0n} and A_n^*. Using values of φ_{0n} taken from experiments on single crystal tungsten wires[1] and 120 amp./cm² T^2 for A_n^*, it can be shown that the average thermionic constants φ_0' and $A^{*\prime}$ for such wire should be close to 4.40 volts and 40 amp./cm² T^2. This is not in agreement with the accepted values of 4.50 and 60 for pure tungsten wire retaining the drawing die marks. To test this result, the average thermionic constants of a G. E. type 218 tungsten wire, polished and recrystallized to give large crystals, were measured and turned out to be 4.40 volts and 30 amp./cm² T^2, in agreement with the above theory.

[1] M. H. Nichols, Phys. Rev. **57**, 297 (1940).

156. The Contamination of Incandescent Molybdenum Filaments in a Vacuum Obtained by an Oil Diffusion Pump. FRANCIS T. WORRELL AND S. S. SIDHU, *University of Pittsburgh.*—Molybdenum filaments, heated to incandescence in a vacuum obtained by a diffusion pump using Octoil-S, were found to be contaminated by the oil when the vacuum was maintained at about 10^{-6} mm Hg. Microphotographs of the contaminated filaments show roughened surfaces with deep, sharp-edged cracks such as might be expected of a contaminated surface layer of different expansivity than molybdenum. X-ray diffraction analyses of the contaminated filaments reveal the formation of (1) molybdenum carbide (Mo_2C), (2) solid solution of carbon in molybdenum, (3) graphite, and (4) an unknown substance.

157. New Absorption Bands in Colored Alkali-Halide Crystals. JULIUS P. MOLNAR, *Massachusetts Institute of Technology.*—The coloration produced by x-rays in crystals of the alkali-halides has been shown[1] to be due to a single absorption band which for most of the salts lies in the visible part of the spectrum. The absorption band is commonly attributed to the presence of color centers (sometimes referred to as Farb- or F-centers), the nature of which being not yet definitely established. A re-investigation of the absorption spectra of colored alkali-halide crystals indicates the presence of other weaker bands besides the main band. In the case of KCl, the new bands consist of three peaks on the long wave-length side of the main band. Their position and breadth depend on the temperature in a manner similar to that of the main band, indicating that their origin is probably due to trapped electrons and not colloidal particles. One of the new bands is of particular interest since it appears simultaneously with the main band in x-rayed crystals, and can be bleached. The other two bands appear only after long exposures and do not seem to bleach. The new absorption bands suggest the possibility of several trapping modes for free electrons in the alkali-halide lattices. Several trapping processes have been proposed in explanation of F centers, and it may be that more than one of these actually exist. Two of them seem especially likely processes, the trapping of electrons on cations[2] and in vacant holes left by missing anions.[3]

[1] E. Mollwo, Zeits. f. Physik **85**, 56 (1933).
[2] N. F. Mott, Proc. Phys. Soc. **49**, 32 (1937).
[3] A. von Hippel, J. Chem. Phys. **8**, 605 (1940).

158. Work Function and Double Layer. R. SMOLUCHOWSKI, *Princeton University.*—Work function is experimentally known to be different for different faces of a crystal. For tungsten the faces can be arranged according to decreasing work function as follows: 110, 211, 100, and 111. The differences are of the order of several tenths of a volt. The explanations suggested so far give either an incorrect sequence or a wrong order of magnitude for the observed differences. The author uses the theory of Wigner and Bardeen according to which the work function is a sum of a volume contribution and a double layer on the surface of the metal. The latter is due to the shift and rearrangement of the electron cloud on the surface. The calculation of the value of the double layer shows that it is strongly dependent on the orientation of the surface and gives the right order of magnitude of the differences of the work function for different faces. The sequence of the faces appears to depend mainly upon the type of crystal lattice and to a certain extent also upon the tendency exhibited by the electrons to form a smooth surface. Under reasonable assumptions the calculated sequence of the faces agrees with the experimental data for tungsten which were mentioned above.

159. Equivalent Thickness of the Atmospheric Nitrous Oxide Layer. ARTHUR ADEL, *Lowell Observatory.*—The existence of a nitrous oxide layer in the earth's atmosphere was established by Adel in 1939.[1] The gas is presumably at a high level and of photochemical origin; and its infra-red bands appear to remain of nearly uniform strength throughout the seasons. The fine structure of the ν_1 band of atmospheric nitrous oxide at 7.78 mu has now been obtained with a 2400-line echelette grating ruled at the University of Michigan. The rotational structure is clearly distinguishable from the complex of atmospheric absorption upon which it is superimposed. From a comparison of the atmospheric absorption with the controlled absorption by nitrous oxide in the laboratory it appears that 3 mm of the gas (NTP) exercises as much absorption in ν_1 as does the atmospheric layer. However, since the infra-red absorption of N_2O is undoubtedly pressure sensitive this figure provides only a lower limit; for at the reduced pressures to

which the layer is probably subject far more gas would be required to have the same effect. Nitrous oxide exercises both continuous and band absorption in the ultraviolet.[2]

[1] Arthur Adel, Astrophys. J. **88**, 186 (1938); **90**, 627 (1939).
[2] J. Nicolle and B. Vodar, Comptes rendus **210**, 142 (1940).

160. Phase Shifts in the Scattering of 100-Mev Protons by Protons. H. M. THAXTON AND S. H. MILES, *Agricultural and Technical College of North Carolina.*—The presence of s, p and d wave anomalies in the scattering of 100-Mev protons by protons has been investigated for the Gaussian potential well. The phase shift (K_0) due to the presence of an s wave anomaly is 24.5°; the phase shift (K_1) due to attractive p and repulsive p wave anomalies is 3.5° and 2.8°, respectively. The phase shift due to the d wave anomaly (K_2) is 1.5°. The calculations are performed by numerical integration of the wave equation and the subsequent adjunction of coulomb functions at $r=3e^2/mc^2$. These computations have been checked by the integral $\tan K_L=\int(V/E')F_L^2 d\rho$. The Coulomb functions used in these calculations are computed by series expansions and by integration of the differential equation,[1]

$$d^2u/d\rho^2+(1/\log_{10}e)^2[\rho^2+2\eta\rho+(L+\tfrac{1}{2})^2]u=0.$$

The series expansions converge only after thirty-five terms for Φ^* and thirty terms in Ψ are computed. For this energy the Mott ratio has been calculated for the scattering angle $\Theta=30°$. The s wave anomaly gives a contribution of 79.5 percent to the scattering cross-section, the attractive p anomaly a contribution of 21.9 percent and the d wave anomaly 3.6 percent. These results confirm the prediction[2] that the scattering cross section at high energies is influenced by the presence of p and d wave anomalies.

[1] E. R. Wicher, Terr. Mag. (Dec. 1936).
[2] H. M. Thaxton and L. E. Hoisington, Phys. Rev. **56**, 1194 (1939); G. Breit, H. M. Thaxton and L. E. Eisenbud, Phys. Rev. **55**, 1018 (1939).

161. Note on the Energy-Range Relations.* F. T. ROGERS, JR., *University of North Carolina.*—Let V_x be the energy of Mev. of an x-particle ($x=D$ or P for deuterons or protons) having a range of r_x cm in air at 760 mm Hg and 15°C. Let p_x represent r_x in all cases except for α-particles with ranges greater than 0.6, in which case let it be $r_\alpha-0.3$. Then the energy-range relations are approximated by

$$\log_{10}V_x=A_x+B_x\log_{10}p_x, \tag{1}$$

and

$$\log_{10}p_x=C_x+D_x\log_{10}V_x; \tag{2}$$

the constants A_x, B_x, C_x, and D_x are given in Table I, together with the average percent deviations (e) of these equations from the accepted relations.

TABLE I.

x	EQ.	DOMAIN	A_x, C_x	B_x, D_x	e
D	1	r_D: 0–12	−0.076	0.590	1
D	2	V_D: 0–3.6	0.129	1.695	2
P	1	r_P: 0–236	−0.170	0.567	1
P	2	V_P: 0–15	0.300	1.763	2
α	1	r_α: 0–0.6	0.391	1.453	4
α	2	V_α: 0–1.1	−0.269	0.688	3
α	1	r_α: 0.6–20.8	0.391	0.599	2
α	2	V_α: 1.1–15	−0.653	1.670	3

* This work was completed while the author was in residence at The University of Houston.

AUTHOR INDEX TO ABSTRACTS OF PAPERS PRESENTED AT THE WASHINGTON MEETING

Adel, Arthur—Nos. 7 and 159
Allis, W. P.—see Brown, Sanborn C.
Atwood, H., Jr.—see Colwell, R. C.

Bailey, J. E.—see Colwell, R. C.
Bainbridge, K. T.—see Sherr, R.
Banks, Floyd R. and Park H. Miller, Jr.—No. 153
Banning, Mary—No. 4
Bardeen, J.—No. 73
Barschall, H. H., R. Ladenburg and C. C. Van Voorhis—No. 18
Bearden, J. A. and G. Schwarz—No. 105
—— see Beeman, W. W.
Beardsley, Niel F.—No. 89
Beeman, W. W. and J. A. Bearden—No. 102
Beers, Yardley—No. 97
Beese, N. C.—No. 42
Bell, M. E. and J. H. Findlay—No. 45
Bennett, F. D.—see Ham, W. R.
Bergmann, Peter G.—No. 72
Beringer, Robert and C. G. Montgomery—No. 99
Bethe, H. A.—No. 136
Blewett, John P. and Simon Ramo—No. 43
Boeker, G. F.—see Reber, R. K.
Bohlke, P. G., T. R. Cuykendall and H. S. Sack—No. 134
Borst, Lyle B.—No. 141
—— see Newson, Henry W.
Bozorth, R. M.—see Williams, H. J.
Brooks, Harvey—No. 57
Brown, Sanborn C. and W. P. Allis—No. 95
Browne, S. H. and C. T. Lane—No. 129
Brunings, J. H. M. and J. K. Knipp—No. 29
Bueso-Sanllehí, F.—No. 48

Caldwell, Wallace C.—No. 135
Cleveland, Forrest F. and M. J. Murray—No. 52
Cole, Kenneth S. and Robert H. Cole—No. 113
Cole, Robert H.—see Cole, Kenneth S.
Collar, H. W., J. M. Cork and G. P. Smith—No. 120
Collins, George B.—see Feldmeier, J. R.
Coltman, John W.—No. 20
Colwell, R. C., H. Atwood, Jr., J. E. Bailey and C. O. Marsh—No. 112
Constant, F. W. and R. E. Faries—No. 125

Cork, J. M.—No. 104
—— see Collar, H. W.
Crenshaw, C. M.—see Manning, H. P.
Creutz, Edward C. and Robert R. Wilson—No. 14
—— see Wilson, Robert R.
Cuykendall, T. R.—see Bohlke, P. G.

Dawson, L. H. and E. O. Hulburt—No. 2
Dessauer, G. and E. M. Hafner—No. 139
Deutsch, Martin—No. 137
Dicke, R. H. and John Marshall—No. 17
Downing, J. R. and A. Roberts—No. 138
Dwyer, Robert J.—No. 76

Earle, Marshall D.—No. 148
Easley, M. Adelaide—see Forsythe, W. E.
Ellickson, R. T. and B. Serin—No. 44
Elliott, D. R.—No. 23
Evans, Robley D. and Clark Goodman—No. 33
—— see Goodman, Clark
—— see Kip, Arthur F.

Faires, R. E.—see Constant, F. W.
Feldmeier, J. R. and George B. Collins—No. 123
Findlay, J. H.—see Bell, M. E.
Forsythe, W. E. and M. Adelaide Easley—No. 39
Frevel, Ludo K.—No. 58
Furry, W. H.—No. 26

Gamertsfelder, Carl—No. 66
Germer, Lester H.—see White, Addison H.
Good, W. E. and G. Scharff-Goldhaber—No. 19
Goodman, Clark, Robley D. Evans and Patrick M. Hurley—No. 34
—— see Evans, Robley D.
Green, E. H.—see Kurrelmeyer, B.
Green, J. B.—No. 10
Gunn, Ross—No. 80
Guth, Eugene—see Mullin, Charles J.

Hafner, E. M.—see Dessauer, G.
Ham, W. R. and F. D. Bennett—No. 131
Hansen, W.—No. 144
Hardy, H. C. and W. H. Pielemeier—No. 106
Harvey, G. G. and L. J. Sullivan—No. 78
Hawkes, John B.—No. 38
Haworth, L. J.—see Luebke, E. A.
Hazen, Wayne E.—No. 101
Hebb, M. H. and H. Sponer—No. 56
Heilprin, Laurence B.—No. 36
Hering, K. W.—see Warren, B. E.
Hoge, Harold J.—No. 37
Hubbard, J. C.—No. 109
Hughes, Donald J. and Volney C. Wilson—No. 90
Hulburt, E. O.—No. 1
—— see Dawson, L. H.
Humphreys, Richard F. and Ernest Pollard—No. 145
Huntington, H. B.—No. 149
Hurley, Patrick M.—see Goodman, Clark
Huxford, W. S.—see Jones, R. W.

Irvine, John W.—see Roberts, A.

Jacques, R. B.—No. 25
Jenkins, F. A. and S. Mrozowski—No. 8
Jensen, Arthur S.—No. 115
Jesse, William P., E. O. Wollan and Marcel Schein—No. 86
—— see Schein, Marcel
—— see Wollan, E. O.
Jones, R. W. and Huxford, W. S.—No. 98

Kendall, H. C.—see Overbeck, C. J.
Kerst, D. W.—No. 103
Kip, Arthur F. and Robley D. Evans—No. 32
Knipp, J. K.—see Brunings, J. H. M.
Koehler, J. S.—No. 150
Kratz, H. R. and J. E. Mack—No. 9
Kurbatov, J. D., M. L. Pool and H. B. Law—No. 27
—— see Law, H. B.
Kurrelmeyer, B., W. H. Mais and E. H. Green—No. 40

Ladenburg, R.—see Barschall, H. H.
Lamb, W. E., Jr. and A. Nordsieck—No. 69
Landé, Alfred—No. 70
Lane, C. T.—see Browne, S. H.
Lark-Horovitz, K. and W. A. Miller—No. 140
—— see Parshall, C. M.
Law, H. B., M. L. Pool, J. D. Kurbatov and L. L. Quill—No. 116
—— see Kurbatov, J. D.
Lawson, A. W.—No. 151
Livingston, M. Stanley—No. 24
Ludloff, H. F.—No. 133
Luebke, E. A., J. H. Manley and L. J. Haworth—No. 21

Mack, J. E.—see Kratz, H. R.
MacNair, D.—see Nix, F. C.
Mais, W. H.—see Kurrelmeyer, B.
Manley, J. H.—see Luebke, E. A.
Manning, H. P., C. M. Crenshaw and V. J. Young—No. 143
Margenau, H.—No. 74
Marsh, C. O.—see Colwell, R. C.
Marshak, R. E.—No. 124
Marshall, John—see Dicke, R. H.
Marton, L.—No. 77
Matheson, G. L.—see McAllister, E. D.
McAlister, E. D., G. L. Matheson and W. J. Sweeney—No. 41
McCreary, Ralph L.—No. 28
Metropolis, N.—No. 49
Miles, S. H.—see Thaxton, H. M.
Miller, Park H., Jr.—No. 147
—— see Banks, Floyd R.
Miller, W. A.—see Lark-Horovitz, K.
Millikan, R. A.—No. 85
Molnar, Julius P.—No. 157
Montgomery, C. G. and D. D. Montgomery—No. 96
—— see Beringer, Robert
Montgomery, D. D.—see Montgomery, C. G.

Mooney, Rose C. L.—No. 59
Morgan, F., M. Muskat and D. W. Reed—No. 110
Motz, Lloyd—No. 79
—— see Rothstein, Jacob
Mrozowski, S.—No. 47
—— see Jenkins, F. A.
Mulliken, Robert S.—No. 50
Mullin, Charles J. and Eugene Guth—No. 154
Murray, M. J.—see Cleveland, Forrest F.
Muskat, M.—see Morgan, F.

Neher, H. V. and W. H. Pickering—No. 83
—— see Pickering, W. H.
Newson, Henry W. and Lyle B. Borst—No. 142
Nichols, Myron H.—No. 155
Nix, F. C. and D. MacNair—No. 132
Nordheim, L. W.—No. 81
Nordsieck, A.—see Lamb, W. E., Jr.

Olsen, Leonard O.—No. 5
O'Neal, R. D.—No. 30
Overbeck, C. J. and H. C. Kendall—No. 108

Page, Chester H.—No. 35
Pardue, T. Eugene—see Shearin, Paul E.
Parshall, C. M. and K. Lark-Horovitz—No. 62
Pepinsky, R.—No. 61
Pickering, W. H. and H. V. Neher—No. 84
—— see Neher, H. V.
Pielemeier, W. H.—see Hardy, H. C.
—— see Telfair, D.
Platt, John R. and Ralph A. Sawyer—No. 12
Plesset, Ernst H.—No. 118
Pollard, Ernest—see Humphreys, Richard F.
—— see Smith, E.
Pool, M. L.—see Kurbatov, J. D.
—— see Law, H. B.
Present, R. D.—No. 22
Preston, W. M.—No. 3
Prigogine, J.—see Sack, H. S.

Quill, L. L.—see Law, H. B.

Ramo, Simon—see Blewett, John P.
Ramsey, W. E., W. F. G. Swann and Paul Weisz—No. 94
—— see Swann, W. F. G.
Rawcliffe, R. D.—No. 6
Reber, R. K. and G. F. Boeker—No. 126
Reed, D. W.—see Morgan, F.
Roberts, A. and John W. Irvine, Jr.—No. 117
—— see Downing, J. R.
Rogers, F. T., Jr.—No. 161
Rosen, N.—No. 71
Rossi, Bruno—No. 82
Rothstein, Jerome and Lloyd Motz—No. 13
Ruedy, J. E.—No. 65

Sack, H. S. and J. Prigogine—No. 55
—— see Bohlke, P. G.
Sakmann, B. W.—No. 111
Sawyer, Ralph A.—see Platt, John R.
—— see Wheatley, Marshall A.
Scharff-Goldhaber, G.—No. 119
—— see Good, W. E.
Schein, Marcel, William P. Jesse and E. O. Wollan—No. 87
—— see Jesse, William P.
—— see Wollan, E. O.
Schiff, L. I.—No. 68
Schwarz, G.—see Bearden, J. A.
Serin, B.—see Ellickson, R. T.
Shearin, Paul E. and T. Eugene Pardue—No. 100
Sherr, R. and K. T. Bainbridge—No. 122
Sidhu, S. S.—see Worrell, Francis T.
Smith, E. and Ernest Pollard—No. 146
Smith, G. P.—No. 121
—— see Collar, H. W.
Smith, Lincoln G.—No. 54
Smoluchowski, R.—No. 158
Sponer, H. and S. H. Wollman—No. 51
—— see Hebb, M. H.
Starr, C.—No. 127
Sullivan, L. J.—see Harvey, G. G.
Swann, W. F. G. and W. E. Ramsey—No. 92
—— see Ramsey, W. E.
Sweeney, W. J.—see McAlister, E. D.

Tatel, H.—No. 16
Telfair, D. and W. H. Pielemeier—No. 107
Thaxton, H. M. and S. H. Miles—No. 160
Turner, R. N.—see Wilson, V. C.

Van Vleck, J. H.—No. 128
Van Voorhis, C. C.—see Barschall, H. H.

Wait, G. R.—No. 114
Walerstein, I.—No. 53
Wall, C. N.—No. 67
Warren, B. E. and K. W. Hering—No. 60
Waterman, A. T.—No. 152
Weisz, Paul—No. 93
—— see Ramsey, W. E.
Welles, S. B.—No. 31
Wheatley, Marshall A. and Ralph A. Sawyer—No. 11
Wheeler, John A.—No. 75
White, Addison H. and Lester H. Germer—No. 64
Williams, H. J. and R. M. Bozorth—No. 130
Wilson, Robert R. and Edward C. Creutz—No. 15
—— see Creutz, Edward C.
Wilson, V. C. and R. N. Turner—No. 91
—— see Hughes, Donald J.
Wollan, E. O., Marcel Schein and William P. Jesse—No. 88
—— see Jesse, William P.
—— see Schein, Marcel
Wollman, S. H.—see Sponer, H.
Woods, L. H.—No. 46
Worrell, Francis T. and S. S. Sidhu—No. 156

Yearian, H. J.—No. 63
Young, V. J.—see Manning, H. P.